69-8019

BLAKE, J. Roger, 1936-

THE INFLUENCE OF COASTAL AND SEA FLOOR GEOMETRY ON NATURAL ELECTROMAGNETIC VARIATIONS OF 10^{-4} TO 10^{3} HZ.

University of Alaska, Ph.D., 1968
Physics, general

University Microfilms, Inc., Ann Arbor, Michigan

THE INFLUENCE OF COASTAL AND SEA FLOOR GEOMETRY ON NATURAL ELECTROMAGNETIC VARIATIONS OF 10^{-4} TO 10^{3} HZ

A

DISSERTATION

Presented to the Faculty of the

University of Alaska in Partial Fulfillment

of the Requirements

for the Degree of

DOCTOR OF PHILOSOPHY

by

J. Roger Blake, B.Sc.

College, Alaska

May 1968

THE INFLUENCE OF COASTAL AND SEA FLOOR GEOMETRY

ON NATURAL ELECTROMAGNETIC VARIATIONS OF 10^{-4} TO 10^{3} HZ

APPROVED:

Charles R. Wilson

Daniel W. Swift

Daniel B. Hawkins

Sydney Chapman
Chairman

Roger Sheridan
Department Head

APPROVED: C. Bilecki DATE: Apr. 17, 1968
Dean of the College of Mathematics, Physical Sciences and Engineering

Vice President for Research and Advanced Study

ABSTRACT

Plane electromagnetic waves, originating from a source external to the earth, are assumed to be normally incident on the earth's surface. The field within the earth is modified by the geometry of the earth's conducting layers; the total field satisfies not only Helmholtz' equation but also the boundary conditions imposed on the fields at the interfaces between regions of different conductivity. In particular, electric and magnetic fields measured at the surface of the earth vary markedly near a sharp change in conductivity such as occurs across a shoreline. Several theoretical models have been analyzed mathematically to determine the influence of coastal geometry on the fields. The frequency limits are determined by the neglect of induction in the mantle (periods less than 1 hour) and the neglect of displacement currents in Maxwell's equations (frequency less than 10^3 Hz).

The models studied fall into three classes: those resembling a vertical geological "fault" (i.e. a continental shoreline), a vertical "dyke" (i.e. a long promontory), or an "inclined fault" (i.e. a sloping ocean floor). In the first two classes, the fault and dyke are assumed to be either infinitely deep or of finite depth so that the effect due to the basement may be determined.

Maxwell's equations are solved for the vertical fault and dyke models, using a Fourier transform technique. The horizontal surface magnetic field is very insensitive to conductivity changes when the

media are horizontally stratified, and this fact is used to establish an approximate boundary condition.

The "coast effect" near an infinitely deep, vertical continental shoreline (fault) comprises a substantial enhancement of variations in the vertical component of the magnetic field, and a marked linear polarization of the electric field--normal to the coastline on land and parallel to the coast offshore. The presence of a horizontal non-conducting basement increases the enhancement of the vertical magnetic component and causes the electric field to become more linearly oriented; the effect on the electric field is more pronounced to seawards.

If, instead of a continental coast, a dyke or long promontory is present, the coastal enhancement of the vertical magnetic field is suppressed. The linearity of the electric field polarization is more pronounced than for the fault model, especially on the landward side of the shore, and the preferred orientation of the polarization is more evident in both media. The presence of a non-conducting basement again increases the coastal enhancement of the vertical magnetic field. The effect on the electric field polarization at sea is dependent on the depth of the sea floor, but on land the polarization is more linear than for a deep basement.

Specific examples of the frequency responses for the E_x, E_y, and H_z components are compared for sites over land and ocean, near both a continent and a promontory, over either a deep or a shallow basement.

The influence of a sloping sea floor on the electric and magnetic fields at the ocean surface is calculated for various basement conductivities. The calculations refer to sites remote from a coastline and are applied to observations on ice-islands in the Arctic Ocean. The vertical magnetic field is enhanced over the shallower depths, while the electric field polarization shows a transition from the behavior on the landward side of a continental shore to that on the seaward side. The width of the transition region is approximately ten times the oceanic penetration depth. The fields are computed for slopes of 3° and 10° and compared with those over an ocean with horizontal floor.

ACKNOWLEDGEMENTS

I wish first to thank my wife, Bronwyn, for her patience and understanding during the preparation of this thesis, for her considerable practical help in the tedious tasks of proof-reading, typing and editing, and for her organization of a large portion of the bibliography from my rough notes.

To Dr. Russell E. Carr, previously Head of the Department of Mathematics, and now at the University of Wyoming, I extend my very grateful appreciation for his generous assistance to me during my sojourn in Alaska. His discussions and suggestions, and his comments on certain of the mathematical and numerical sections of this work were most helpful.

The subject of electric and magnetic variations near conductivity anomalies was first suggested to me, in another context from that treated here, by Professor Sydney Chapman. To him and to Dr. A. A. Ashour of the Applied Mathematics Department, University of Cairo, with whom I also discussed Professor Chapman's suggestion, I extend my thanks and appreciation. I am also indebted to Professor Chapman for the time and trouble he took in reading this work and for his suggestions.

The present study of the transient variations in the electromagnetic field at micropulsation and magnetotelluric frequencies developed from the interest and contractual support of Mr. D. Swift. I thank him for his assistance, for his comments and suggestions on the manuscript, and for providing certain of the computations used in §4.1 (see §4.1.4).

The programming of the computations in Chapter IV could not have been accomplished without the very able assitance of Mrs. Carol Echols, now of the Mathematics Department. While the program remains my own, it was she who circumvented many of the stumbling blocks and traps I encountered in programming the computations in FORTRAN II for the IBM 1620 and 7094 computers. I extend to her my very grateful appreciation.

Additional programming and computer assistance was rendered by Helen Henris, Bob and Eve Porter, Doug Smith and Bruce Morton; I acknowledge their help with thanks. Bruce Morton of the Geophysical Institute Computer Group also provided considerable assistance in programming the formulae of Chapter VI in FORTRAN IV for use with the IBM 7094 and System 360 computers, and in debugging the programs sent to WDPC, University of California.

I acknowledge Western Data Processing Center, University of California for the use of their IBM 7094 and system 360/75 computers and thank Mr. D. Swift and Dr. R. E. Carr for their assistance in arranging to use this facility.

I am grateful to Ed Gauss (Head) and Dennis Ruff of the University of Alaska Computer Center for running the unfunded program of Ch. VI, free of charge, during and subsequent to the installation of the IBM 360/44 Program System FORTRAN G compiler with this University's System 360/40 computer.

I thank Drs. Syun Akasofu, V. P. Hessler and Mr. R. R. Heacock for reading and constructively criticizing sections of this work and I am greatly indebted to Mrs. Carla Helfferich for her voluntary and critical

editorial comment on the entire text. I also thank Miss Janice Duncan for her assistance in compiling the bibliography.

The figures were prepared by Dan Wilder and Chris Anderson of the Institute Drafting Office and Frank Danels of the Data Processing and Photographic Section. The difficult job of typing the mathematical manuscript was admirably handled by the Stenographic Center under the supervision of Mrs. M. McCoy, and in particular by Mrs. Peggy Grafe. To these people I am also most grateful.

Parts of the work described here were supported by National Science Foundation Grants GP-4647 and GP-5540.

TABLE OF CONTENTS

LIST OF ILLUSTRATIONS

LIST OF APPENDIX ILLUSTRATIONS

LIST OF TABLES

LIST OF APPENDIX TABLES

CHAPTER I

INTRODUCTION

Although etymologically "geophysics" means "physics of the earth," the term now includes the study of the earth's spatial environment (the magnetosphere) and many aspects of solar-terrestrial relations, as well as the solid earth and its immediate atmosphere. Specifically, "solid-earth geophysics" refers to both "pure" geophysical studies such as volcanology and glaciology, and "applied" geophysics, such as exploration seismology. The other disciplines are branches of meteorology, aeronomy, or space geophysics; geomagnetism is interdisciplinary, involving processes deep within the earth and far out in space.

The branch of geomagnetism sometimes called magnetotellurics links the otherwise remotely connected fields of exploration geophysics and space geophysics; it deals with the behavior of the electromagnetic field observed at the earth's surface. The origin of most of the variations in the magnetic field is remote from the surface, but induction effects in the conducting earth can result in anomalies of interest to both solid earth and exploration geophysicists. The former study variations with periods of one hour or longer, to determine the electrical conductivity distribution deep within the earth. At shorter periods, localized conductivity anisotropies at shallow depths within the crust may be detected. In this case, simultaneous study of the electric field variations greatly simplifies the analysis.

Most electromagnetic and hydromagnetic phenomena within the magnetosphere influence the surface electric and magnetic fields. The space geophysicist is concerned with the sources of these magnetic field variations, and must record the magnetic field at the earth's surface as well as in space. Because of the earth's inhomogeneity these records show variation not directly related to the sources. Since some variations (eg. micropulsations) are monitored or recorded by observing the electric field, the space geophysicist is interested in the effect of local conductivity anomalies on both the electric and magnetic fields at the earth's surface.

To see the basic mechanism involved in the induction process, consider Fig. 1.1. Lenz's Law states that currents will be induced in a conductor located in a changing magnetic field; the magnetic fields produced by the currents will oppose the flux change which can be considered as a movement of the conductor relative to the source. Suppose the primary magnetic field H_p is harmonically varying in time with frequency ω, and is proportional to cos ωt. Assume that H_p arises from some source distribution of electric field E_p (Fig. 1.1 a). The initial decay of the field is equivalent to moving the conductor away from the source (b). The induced currents (c) oppose this "motion" (decay), and generate a secondary magnetic field H_i (d). This induced field is such that the horizontal component of primary magnetic field H_p is reinforced at the surface by the secondary component H_i, but the vertical component Z_p is opposed by Z_i (e). Thus the primary and secondary electric fields are 180° out of phase, while the horizontal and vertical induced magnetic

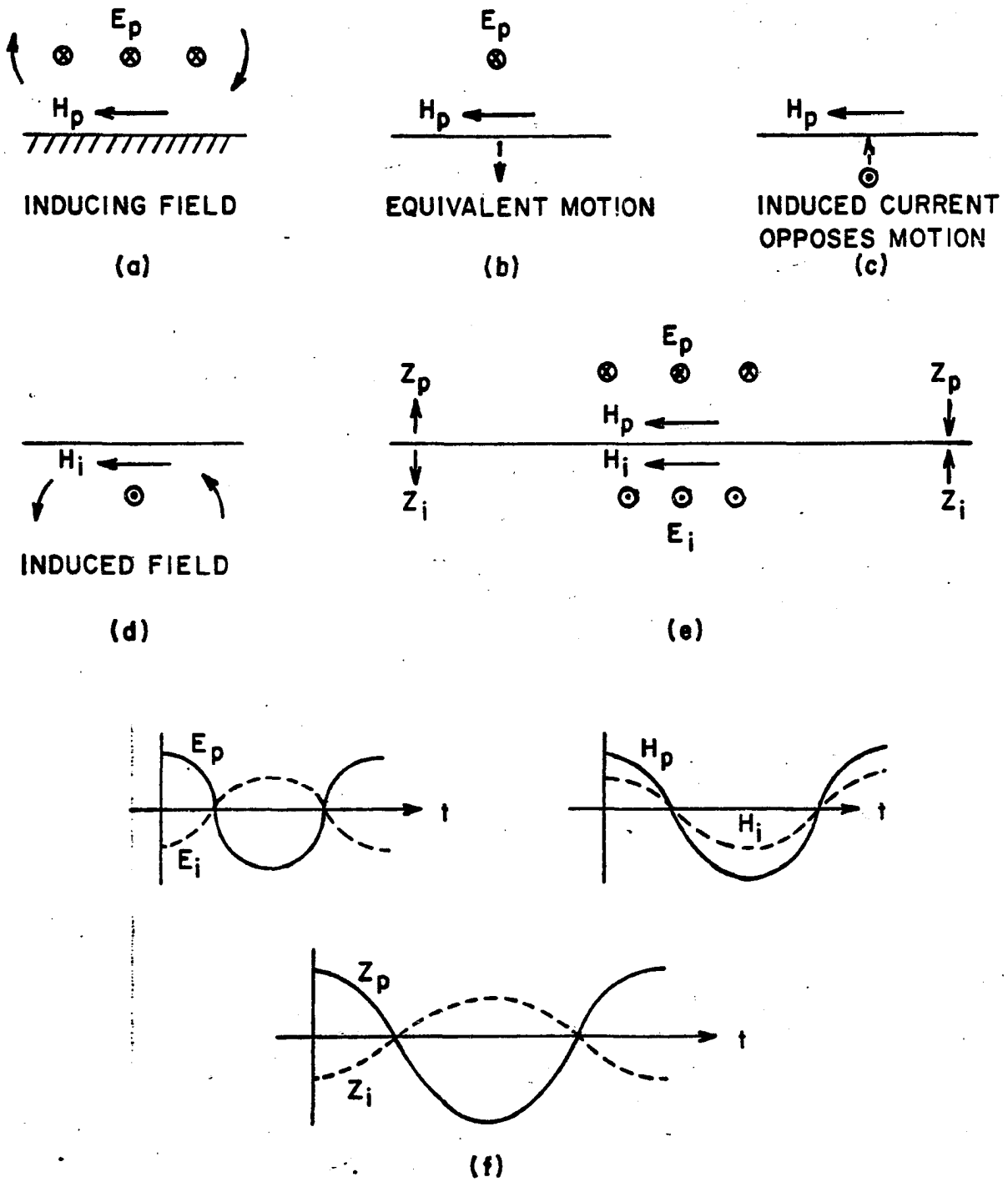

Fig. 1.1 Induction within the earth by a changing primary field.

fields are respectively in phase and out of phase with the primary components (f). Further properties of the induced fields are given in App. 4.

The ideal study of these fields at a given location would involve an extensive set of observations over the entire frequency range of interest, at a great number of sites, for several different source configurations. Such a study would not necessarily be helpful in determining the effects at a different site.

Observational studies, although dealing with realistic geometries, are usually limited by practical considerations. Thus a study of the frequency response at a given site requires a power spectral analysis of the records. This means an extensive set of observations, difficult to obtain without a permanent observatory. Such observations would be necessary at a number of field sites even if a permanent observatory were present, and the difficulties in obtaining adequate data would be enormous.

There are thus three possible approaches: firstly, an observational study of restricted scope; secondly, a model study, where a small scale model of the actual situation is studied in the laboratory; and thirdly, a mathematical approach, using a model which, though greatly simplified, reproduces the broad features of the actual geometry. These last two methods both involve simplifications, but can be expected to give the first-order behavior of the fields without the fine-structure due to the countless small variations occurring in nature.

In this work we apply the mathematical approach to several geometries and extend earlier studies. The geometries are interpreted in

terms of coastlines between sea and land, the most significant conductivity change which affects shorter-period variations (< 1 hour). At longer periods the influence of the conducting mantle becomes predominant; we do not consider this.

In Chapter II we first briefly summarize the background material necessary to understand the nature of the sources of the electric and magnetic fields. The observational evidence for the influence of oceans and coastlines on the electromagnetic fields is reviewed in the latter half of this chapter, and, as much of the earlier research was applied to geophysical prospecting, a short account is given of this subject also. Some observations of the possible influence of a coastline on the aurora are mentioned in conclusion.

In Chapter III the concepts of electromagnetic wave theory are presented in a manner pertinent to the theoretical discussion of coastal discontinuities. The background theory used in the later chapters is also developed. A review of the theoretical approaches to several geometries of conductivity distribution is given, including a summary of the controversy over the importance of the primary source distribution. This controversy was initiated when Cagniard published his papers (1953 a,b) applying magnetotelluric fields to geophysical prospecting.

Chapter IV deals with the effect of a straight coastline on the fields. From the geological analogy, we term it the "fault geometry." Previous work on an infinitely deep fault is compared with calculations for fields over a fault of finite depth. Comparison is also made with observations of the "coast effect."

In Chapter V the same techniques are used to study a long promontory--the model is termed the "dyke geometry." Again dykes of both infinite and finite depths are considered. The limiting cases for infinite depth and very shallow depth are computed and compared with the solutions for the fault. An application is made to a specific example, so as to examine the field behavior for all four geometries.

In Chapters IV and V the models for discontinuities of finite depth all assume a horizontal basement or sea floor. In Chapter VI we examine the case of a sloping basement. Mathematical difficulties prevent the solution from being obtained close to the shoreline, but a solution may be obtained which is valid at some distance seaward from the shore. Thus we are dealing with the "ocean effect". Application is made to the observations obtained on floating ice-islands over the Arctic Ocean.

Chapter VII summarizes the study and suggests further possible lines of research.

CHAPTER II

A REVIEW OF THE FUNDAMENTAL NATURE OF THE EARTH'S MAGNETIC AND ELECTRIC FIELDS

This chapter outlines the basic nature and properties of the magnetic and electric fields associated with our planet. It presents the fundamental background for the considerations set out in the later chapters. The treatment is necessarily cursory - greater detail would be superfluous here. No attempt is made to reference the enormous literature relating to this background material, but some basic, comprehensive references are given in §2.4.

2.1 The Geomagnetic Field

The total magnetic field of the earth may be said to comprise a steady component and a varying component. The varying component has two main parts. One consists of a very long term change originating in the earth's core, termed the "secular" variation, with a scale time of centuries and probably a very great change in magnitude as well as direction. The other part consists of much smaller and shorter term "transient" variations with scale times varying from seconds to days and originating primarily outside the solid earth. The steady state component and the secular variation component are generally termed the "main field", while the transient variations are subdivided into a number of component parts depending on their physical origin.

2.1.1 The Main Field and its Variation

If the main field of the earth is represented as a magnetostatic field generated from a potential V which satisfies Laplace's equation, the potential may be represented by a series of spherical harmonic functions, representing in turn external and internal contributions (Chapman and Bartels, 1940)

$$V = V^e + V^i \sim a \sum_{n=o}^{\infty} \left[\left(\frac{r}{a}\right)^n T_n^e + \left(\frac{a}{r}\right)^n T_n^i \right] .$$

Here a specifies the earth's radius, and the tesseral functions T_n are given by

$$T_n = \sum_{m=o}^{n} (g_n^m \cos m\phi + h_n^m \sin m\phi) P_n^m (\cos \theta)$$

The question of of units is omitted (hence the $\sim$ relationship above). The point in question has the spherical coordinates (r, θ, ϕ), the P_n^m are the partially normalized Associated Legendre Polynomials in the Schmidt form, and the functions g_n^m and h_n^m contain the source specification, differing for sources within or external to the earth. The coefficients g and h can be determined from the analysis of the surface field at a large number of stations, and it is found that, within the accuracy of the spherical harmonic analysis, the main field is entirely of internal origin.

Such analysis shows the main field to be predominantly dipolar (n=1) with its axis inclined to the rotation axis, and eccentrically situated with respect to the earth's center. There is a small

non-dipole contribution (n>1), and the coefficients g and h exhibit the long term secular variation, and must therefore be periodically redetermined.

The main field is of internal origin and must be maintained by some form of electrical dynamo action involving fluid-field interactions within the highly conducting liquid core (see for instance: Bullard and Gellman, 1954). The secular variation probably results from the changes of large scale eddies. Such dynamo models are extremely complicated to develop, but simplified investigations show that instabilities may develop which allow the main field to reverse itself, a behavior strongly suggested from palaeomagnetic observations.

An extensive review of these matters has been given by one of its foremost workers, Rikitake (1966).

2.1.2 The Transient Fields

The transient fields which contribute to the total geomagnetic field are further subdivided into the daily contributions from a magnetically quiet sun (Sq) and the moon (L), together with the disturbance field (D), this last resulting from several different physical sources during magnetically disturbed periods.

The Solar Daily Quiet Variation Field (Sq) may be regarded as essentially fixed with respect to the sun-earth line. It thus varies as a function of latitude and local time, as well as season and solar-cycle. Spherical harmonic analyses carried out along the lines indicated in the last section, but applied to the Sq fields only (Chapman and Bartels, 1940), indicate that perhaps 60% of the

field is of external origin (ionospheric current systems), the remainder being due to the induction of electrical currents in the outer layers of the earth. The external part is most likely to be caused by dynamo action of E-layer winds across the field lines, resulting from solar tidal and thermal effects.

The Lunar Daily Quiet Variation Field (L) is similarly produced by lunar tidal dynamo action at ionospheric heights (Chapman and Bartels, 1940), but,except along the dip equator, is very much weaker than (c. 10% of) the Sq variation. A spherical harmonic analysis indicates the external contribution to L is about two-thirds of the whole.

The disturbed field D has been subdivided in many different ways. Chapman resolved each element of the D-field for a given latitude by applying a Fourier analysis so that

$$D = a_o + \sum_{n=1}^{\infty} a_n \sin (n\lambda + \epsilon_n)$$

where λ specifies the longitude (Eastwards) relative to the midnight meridian. Then the coefficients a_o, a_n and phase ϵ_n are functions of both storm time and latitude. The initial constant a_o Chapman designated D_{st}, the storm-time field, while the summation term was collectively designated DS, the disturbed daily solar variation. Thus D_{st} represents the mean value of D around the particular latitude in question, while DS has zero mean around this latitude, and is a function of the station longitude relative to the midnight meridian. Chapman derived the equivalent current systems for both

the D_{st} and DS fields and combined them to give an equivalent D-field current system (see Chapman and Bartels, 1940, Sugiura and Chapman, 1960, Chapman, 1964, Akasofu, 1966a).

More recent knowledge of the behavior of the earth's field and of solar terrestrial relations has led to an additional subdivision based on the physical source of various parts of the disturbed field.

2.2 The Disturbance Field

Before describing the physical subdivisions of the D-field we outline the relationships of the earth's field with the sun and interplanetary matter. This clarifies the further subdivision of the disturbed part of the geomagnetic field.

2.2.1 Solar Terrestrial Relations and the Solar Wind

The disturbance component of the geomagnetic field variations has its origin ultimately in several events on the sun which have magnetic consequences at or near the earth. The disturbance field shows variations in close accord with the 11 year sunspot cycle, seasonal variations, and 27-day solar rotation period, in addition to such individual events as sunspots and solar flares.

It is known that there is a plasma flow outward from the sun, which has three different components:

(i) The quiet solar wind, an ever-present stream of particles (electrons and protons) with a velocity of 300-400 km sec^{-1}.

(ii) The solar plasma stream, originating in hypothetical M-regions of the sun, rotating with it and lasting for

perhaps several months. These streams are responsible for the 27-day recurrences in the disturbed geomagnetic field. Velocities of 300-800 km sec^{-1} occur, and weak magnetic fields (5-10γ) are present. The envelope of the particle trajectories is a spiral, and the stream has a limited cone of emission. This "garden hose" effect results from solar rotation, together with the outward motion of the solar wind and the "frozen-in" magnetic fields of the solar corona. Travel times to the earth are from 1 to 3 days.

(iii) The flare shells or clouds, wide-angle "pulse" emissions of particles at high velocities (1000-1500 km sec^{-1}) during solar flares, having travel times of a day or two. These emissions are followed by geomagnetic storms. In addition to the particle emissions, various electromagnetic emissions also occur. The Type IV emission usually associated with flares is a reliable predictor of geomagnetic storms.

The quiet-time interplanetary magnetic fields are very weak ($\leq 5\gamma$), approximately in the plane of the ecliptic, and very disordered.

2.2.2 The Magnetosphere and the Earth's Environment

In 1931 Chapman and Ferraro considered the effect of a neutral but ionized highly conducting plasma, free of magnetic fields, on

the geomagnetic field (taken as an axial dipole), if the plasma flow were initially assumed to maintain a plane front. They predicted that the plasma flow would compress the field inducing electric currents in the plasma. The plasma would continue its approach until the secondary magnetic fields established equilibrium with the primary geomagnetic field. The strongest interaction would be along the sun-earth line, and the interaction boundary would curve around the earth. Two neutral points (the foci of the current systems) would occur on the interface.

This prediction has since been confirmed by satellite measurements. More involved and precise determinations have also been made of the three-dimensional nature of the interface. The basic boundary condition at the interface is that the magnetic and plasma pressures must balance:

$$\frac{H^2}{2\mu_o} = 2\, n\, m\, v^2 \cos^2 \chi \qquad \text{(mks units)}$$

Here H is the total magnetic field, including the field of the magnetospheric surface current; n, m, v are the neutral ion-pair number density, mass and velocity respectively; and χ is the angle of obliquity relative to the boundary normal.

The boundary region is termed the "magnetopause" and the cavity formed around the earth is the "magnetosphere". Its shape is approximately hemispherical on the solar side but streams out into the magnetospheric "tail" on the night side, taking the geomagnetic field with it. The subsolar point of the magnetopause is about 8-10 earth radii (R_E) from the earth.

Since the solar wind velocity much exceeds the characteristic Alfvén velocity in a field-carrying plasma, and since the mean free path in the plasma is about 1 A.U., a collisionless, standing shock wave is set up on the sunward side of the magnetosphere, the stand-off distance at the stagnation point being some 3-4 R_E. Great turbulence in both particle velocities and magnetic fields occurs in the region between the shock front and the magnetopause. It has been termed the "magnetosheath". The lower latitude field lines reach the sunward side of the magnetosphere, while the higher latitude field lines sweep back into the magnetospheric tail. The field line reaching the neutral point of the magnetopause distinguishes the two regions.

Trapped bands of particles (electrons and protons) are located within the inner magnetosphere; they are popularly termed the Van Allen radiation belts. The particles in these belts spiral around the field lines. Their motion, associated with three adiabatic invariants related to their gyration, bounce and drift, produces a ring current around the earth at a distance of a few earth radii. Electrons in the "outer" belt are generally considered to be responsible for the aurora, but some kind of acceleration mechanism must be invoked to inject the particles to a sufficiently low altitude along the observed auroral oval.

The magnetic tail, first predicted in 1960 by Piddington, has since been detected as a permanent feature of the magnetosphere,

extending to at least 80 R_E, well beyond the moon's orbit (Ness Behannon, et al, 1967), and possibly to 1000 R_E or more (Ness, Scearce et al, 1967). The geomagnetic field lines are oppositely directed on either side of a thin equatorial, magnetically neutral region - the neutral sheet. There are probably daily and annual motions of the tail due to the obliquity of the earth's magnetic dipole axis relative to its spin axis, and its changing inclination to the ecliptic. Possibly the high energy auroral particles come from the solar plasma through the geomagnetic tail, but the acceleration mechanism is not yet understood.

2.2.3 Classification of the Disturbance Field According to its Physical Origins

In the above sketch, several physical mechanisms have been outlined which contribute to the disturbed geomagnetic field. These various contributions may be written as:

$$D = DCF + DR + DT + DP$$

Here DCF is the disturbed field generated at the magnetopause by the interaction between the geomagnetic field and the solar corpuscular flux with the consequent production of electric currents, as initially predicted by Chapman and Ferraro; DR is the disturbance generated by ring currents flowing around the earth in the radiation belts and inner magnetosphere; DT is the disturbance produced by the magnetospheric tail currents; and DP is due to ionospheric currents predominant over the polar cap.

Since there is always a quiet solar wind, there are always DCF and DT contributions from the magnetosphere; these portions are included in the Sq field and not the disturbed field. The DCF field is generally considered responsible for the "sudden commencement" and initial phase of magnetic storms, which Akasofu (1960) and Akasofu and Chapman (1963 a,b) pointed out were essentially independent of the "main phase" of magnetic storms, which result from the DR field. The duration of the DCF or initial phase may vary from 1/2 hour to about 10 hours, while the DR main phase is typically of the order of 10-12 hours in the growth phase, and one or more days in the recovery phase.

The DCF and DR contributions to the D field constitute almost all the D_{st} field at low and middle latitudes, but are dominated by the DP fields at high latitudes. The DT (tail) field is apparently modified during polar magnetic substorms, and the DP field is dominated by the auroral electrojet in auroral regions. The ionospheric currents are also enhanced over the daylight equator, because the ionospheric conductivity is increased by a polarization which suppresses the Hall current there. The polar substorms, concurrent with auroral substorms, correspond to "bays" in the magnetic field, which last for an hour or so.

2.2.4 A Summary of Solar Terrestrial Relations and Geophysical Disturbances

The effects of the various solar emissions at terrestrial observatories are summarized in Table 2.1. The effects not mentioned already are designated as follows:

PCA: Polar Cap Absorption (of cosmic rays)

SID: Sudden Ionospheric Disturbance (eg. radio fadeout)

The high energy (cosmic ray) particle events are mentioned here solely for completeness; they are irrelevant to this discussion.

Table 2.1

Summary of Solar Terrestrial Relations

Source	Conditions	Effect
Electromagnetic	UV ionization and heating	ionosphere formation and heating, atmospheric tide and dynamo action, Sq
	Flares: optical	monochromatic flare
	UV and soft X-rays	SID
	radio	radio bursts of all types
High Energy Particles	protons and heavier nuclei ($1\text{-}10^3$ MeV)	cosmic ray particle increases, PCA
Solar Corpuscular Flux	Quiet Solar Wind (Kev protons; ev electrons)	Quiet DCF, DR and DT, Formation of magnetosphere and shock. Daily cosmic ray variation.
	M-Region Streams	27-day recurrence in DCF, DR, DP, aurora, auroral absorption of cosmic radio waves, 27-day modulation of cosmic rays (solar diurnal variation, Forbush decrease)
	Flare Shells	Forbush decrease, auroral absorption, aurora, DCF, DR, DP.

2.2.5 Micropulsations

The geomagnetic and telluric fields vary with frequencies from 10^{-3} cps to 10 cps, and amplitudes of less than 10 γ. These variations

are collectively referred to as micropulsations; their origins are evidently complicated. Various classifications have been proposed for them, and three observational categories are given in Table 2.2 this table also includes the distinctive "pearls" separately.

Table 2.2

Classification of Micropulsations

Symbol	Name	Period	Amplitude	Duration	Occurrence
Pc	Continuous Pulsations	10-60 sec.	0.1 γ	many hours	morning hours, daytime
Pt	Pulsation trains	40 sec-mins.	0.5 γ (damped)	10-20 min. pulses 1 hour overall	before midnight, often associated with magnetic bays
Pg	Giant Pulsations	several mins.	$\sim$ 10 γ	1 hr. or more	in or near auroral zones, morning
Pp	"Pearls"	0.3-4 sec	0.1γ -1γ or more in auroral zones	10 min.-10 hrs. with 1-5 min spacing	all latitudes with latitude dependent peak

Each of these types has been further subdivided and various other classifications have been proposed to take into account the geographical distribution or physical causes of the suggested subdivisions. Much of this work has been initiated by Troitskaya. Comprehensive review articles have been given by Saito (1962), Jacobs and Westphal (1963), Troitskaya (1964), Tepley (1966), and Wentworth (1966).

The IAGA (Berkeley, 1963; Jacobs et al, 1964) proposed a classification of micropulsations in an attempt to establish some uniformity in the vast number of schemes previously used (Matsushita 1963). This classification is given in Table 2.3.

Table 2.3

Classification of Micropulsations

	New Terminology	Period Range	Old Terminology
Regular	pc 1	0.2-5 sec	PP (pearl)
	pc 2	5-10 sec	Pc
	pc 3	10-45 sec	
	pc 4	45-150 sec	Pg
	pc 5	150-600 sec	
Irregular			
	pi 1	1-40 sec	auroral and storm pulsations
	pi 2	40-150 sec	Pt

The Pc family of pulsations is thought to be due to poloidal and toroidal hydromagnetic waves generated in the magnetosphere by the solar corpuscular streams, the effects of which thus travel to the lower ionosphere. Here part of the hydromagnetic wave energy is expended in generating electric ionospheric currents. The latitude distribution of three suggested subgroups (Pc I: 10-40 sec.; Pc II: 1-2 min.; Pc III (or Pg): 2-7 min.) is consistent with these current systems and oscillations, and a relationship is found at least between Pc-I and upper atmospheric phenomena. The origin of some of these Pc ranges has also been explained in terms of hydromagnetic ionospheric resonances (Field and Greifinger, 1965).

The Pt pulsations are likewise thought to originate from either hydromagnetic waves developing in the equatorial plane of the night magnetosphere, or bursts of particles from the tail. They are closely related to high atmospheric phenomena and may be identified with poloidal oscillations of the highly asymmetrical magnetospheric cavity.

"Pearl" type micropulsations tend to occur during quiet states of the magnetosphere, although some are characteristic of some magnetic storms and sudden commencement types of disturbances. They were once thought to result from trapped bunches of monoenergetic particles bouncing along the field lines of the magnetosphere and drifting around the earth. The mirror points would be considerably above ionospheric levels and the disturbance would be propagated down as hydromagnetic waves. This theory has now been discarded in favor of a hydromagnetic wave packet bouncing along a magnetic field line. Such waves may be produced by proton beams with certain pitch angle anisotropies traveling faster than the Alfvén velocity (Cornwall, 1965). These pulsations are probably connected with characteristic regular ionospheric changes, and with the electron concentration there.

A further type of micropulsation not mentioned in the above table is the rapid irregular pulsation (SIP) characterized by periods of 6-10 sec., (and probably a part of pi 1), with amplitude maxima in the auroral zones on the night side of earth. They show connections with auroral zone phenomena, especially auroral intensity. It is thought that SIP s result from an interaction of the

corpuscular stream with the magnetosphere, which in some way causes symmetrical dumping of charged particles (auroral electrons) into the polar cap ionospheres, and leads to the development of pulsating currents in the lower ionosphere (E-layer). The magnetic field variations are observed as SIP s.

Jacobs and Sinno (1960) determined the overhead current systems arising with Pc and Pt micropulsations, and a few attempts have been made to associate ionospheric electric and magnetic dipole fields with micropulsations (Law and Fannin, 1961, Weaver, 1961, and Bomke, 1962).

Table 2.4 summarizes the micropulsation relations with other geophysical events; it is compiled from Troitskaya (1964); see also Saito (1963), and Campbell and Matsushita (1962).

2.3 Terrestial Induction by the Transient Magnetic Fields:

Harmonic analyses of world wide observations indicate internal contributions in many components of the transient geomagnetic field. These arise from the electric currents induced within the earth by the changing magnetic fields. The frequency of the variation governs the depth of penetration of these induced fields into the earth, and, as the conductivity of the earth is far from uniform, the fields will depend on the non-uniformities. We review here some of the pertinent points regarding the induced fields.

2.3.1 Long Period Induction and Investigation of the Earth's Interior

Following Gauss, Schuster (1889) harmonically analyzed the Sq data from four stations and discovered that part of the field

Table 2.4

Some Relations Between Geophysical Phenomena and Micropulsations

Type	Relationship Exists Between
Pc	Pc occurrence frequency and period with Kp; daily variations of Pc with f_0F2; Pc occurrence and storms with no main phase; Pc-III occurrence with intensification of long-period X-ray bursts; Pc-II and Pc-III with whistler dispersion.
Pt	Occurrence frequency and period with Kp; occurrence with onsets of magnetic bays. High peak occurrence at auroral zones of certain Pt.
Pp	Occurrence of most Pp at low Kp; some Pp during SSC and intense storms; some suggestion exists of Pp occurrence with X-ray bursts, solar proton bursts, low latitude red aurora, f_0F2 decrease, auroral form decay, pulsating aurorae and ionospheric diffusive spread; sudden large amplitude Pp possibly with cosmic noise absorption.
SIP	Occurrence with auroral intensity fluctuations, cosmic noise absorption and PCA, f_0F2, X-ray bursts, storm main phase, duration with Kp. A polar substorm phenomenon.

originates within the earth. He surmised that this contribution is an induction effect, and deduced that the outer part of the earth is relatively non-conducting compared to that at great depths. Chapman later extended this with more extensive data, and several other analyses have since been made.

These were the first attempts to use the daily variations of the geomagnetic field to determine the electrical conductivity (and hence the composition) of the earth at great depths. Any time-varying magnetic field induces an electric field, according to Faraday's Law, written in its differential (Maxwell equation) form as:

$$\text{curl } \underset{\sim}{E} = - \frac{\partial \underset{\sim}{B}}{\partial t} \quad ,$$

In principle it can be used to investigate the internal conductivity. Apart from the Sq (and also L) analyses, similar treatments have been made for the storm time variation (Dst: time scale $\sim$ days), bays ($\sim$ 1 hour), solar flare effect (sfe $\sim$ 30 min.), and storm sudden commencements (ssc $\sim$ minutes). Some attempts have also been made to use the much longer variations in the field (e.g. the 27-day variation with the solar rotation period) but here instrument instability becomes a significant matter to contend with. Rikitake (1966) has reviewed some of these investigations; he devoted several chapters to the interior conductivity. Earlier work, including the analytical procedures, is described in detail by Chapman and Bartels (1940).

The early model of the earth's interior was a uniformly conducting core surrounded by a concentric non-conducting shell. It

agreed well with the first four harmonics of the periodic Sq and L analyses, but such a model could not accurately allow for the effect of the highly conducting oceans. Chapman, Price and Lahiri used a 3-layer model to interpret the slower aperiodic Dst variations; they obtained a good fit by taking an initial decrease in interior conductivity (after the enhancement by the oceans) with a sharp rise at about 800 km depth. MacDonald (1957) and Yukutake (1959) obtained information about the conductivity at much greater depths, using the secular variation originating in disturbances in the highly conducting liquid core, and propagated dispersively outwards.

2.3.2 Earth Currents

The flow of electric currents in the immediate surface layers of the earth is well-known. Apparently it was first observed in British telegraph lines in the middle of the 19th century, at times of magnetic storms and aurorae. There are perhaps three basic mechanisms producing this current flow:

(i) Variations in the geomagnetic field.

(ii) Electrochemical potentials in the ground. These may vary seasonally with moisture content, freezing, permafrost, etc.

(iii) Artificial origins - induced from overhead lines, return currents from ground-earthed installations, etc.

We shall concern ourselves only with those arising from geomagnetic field variations. From the earliest observations it was evident that occurrence of telluric currents was closely associated with magnetic disturbances. Various statistical studies were made to show the variations with sunspot cycle, 27 day recurrence and so on. The daily behavior of the earth-current and magnetic field is also very similar. Correlations exist between earth current activity and ionospheric phenomena - auroral activity, radio transmission through the polar ionosphere and geomagnetic micropulsations. As geomagnetic field and ionospheric phenomena show this connection with earth-current activity, there is a strong suggestion that the currents originate from ionospheric disturbances through induction in the earth. When quantitative connections between the earth current and magnetic records are attempted, the situation becomes much more complicated; however, earth current amplitudes do show a high correlation with the amplitudes of magnetic variations.

Since the penetration of the induced currents depends on both frequency and conductivity, the local geological structure affects the earth currents. Such effects have been widely studied by geophysical prospectors to determine geological structure from earth current recordings. A study by Hessler and Wescott (1962) near College, Alaska, showed magnitude differences of more than 600% between stations a few km apart. The phase differences between orthogonal electric and magnetic fields are likewise complicated by the geological and physiographical surroundings.

Ivanov (1951) and Troitskaya (1953 a,b) first studied micropulsations in earth currents, and noted considerably more detail in the earth current records than on the rapid-run magnetograms. Earth current recording is an established technique of investigating micropulsation it has a special advantage in the considerably greater signal-to-noise ratio obtainable, and in the relative simplicity of the equipment.

2.3.3 The Influence of Currents Induced in a Conducting Ocean on the Magnetic Field

Since the ocean is a relatively good conductor, the penetration of electromagnetic fields into it is considerably less than into land. Thus the ocean shields the lower layers of the earth, especially for higher frequency magnetic variations (Lamb, 1883). Chapman and Whitehead (1923) anticipated considerable shielding of periods of even one day, so that the penetration of the Sq variation would be seriously influenced by a large ocean. This in turn would affect the internal contribution to Sq by induced currents and tend to reduce the observed vertical component of Sq over a large ocean. Rikitake (1961 a,b, 1962) pointed out that the effect would be lessened by a highly conducting mantle of a few hundred km depth.

Rikitake (1966) found that an ocean 1000 m. deep over the whole earth would completely shield the interior from magnetic variations with periods less than 1 minute. The conducting mantle would reduce the purely oceanic effect in this case also (Rikitake 1961a). Zhigalov (1960), using observations on a floating ice station on the Arctic

Ocean, concluded that the $\Delta Z/\Delta H$ ratio of fluctuations is severely attenuated in deep oceans, and that for periods less than ten minutes it becomes almost insignificant at depths of about 3000 m.

The influence of small oceans has been indicated by the work of Ashour (1950) in his treatment of induction in a circular disc. He showed that electric currents in a sea of radius less than 1000 km would have a decay time constant of only a few minutes. Hence geomagnetic variations of period 1 hour or more would not be greatly affected. The influence of a larger deep ocean is likely to be much more pronounced.

Rikitake has reviewed the studies so far made on this subject (1966, ch. 12). Clearly the electric currents induced in the ocean will to some extent affect the transient magnetic fields, especially the higher frequency components. However, the presence of the conducting mantle diminishes the ocean effect, and must be taken into account, especially at lower frequencies.

2.4 Bibliographic Notes

The literature relating to the subjects discussed so far is enormous and we have not attempted reference to original papers. Some of the books, review articles, and more comprehensive or pertinent papers are here briefly mentioned.

The great classical work on geomagnetism is of course the book of that title by Chapman and Bartels (1940, 1962), recently supplemented to some extent by Chapman (1964). Another general reference work in this field is by Mitra (1948).

Among the more recent books covering various aspects of solar-terrestial relations, either broadly or within a specific area, we mention Parker (1962b), de Witt et al. (1963), le Galley (1963), le Galley and Rosen (1964), Odishaw (1964), Hess (1965), Hines et al. (1965), Mackin and Neugebauer (1965), King and Newman (1967) and Matsushita and Campbell (1967). Comprehensive review articles in addition to those included in some of the above books, are given by Obayashi (1959, 1964), Parker (1962 a, 1965), de Jager (1963), Lüst (1963), Akasofu (1963, 1965, 1966 b), Akasofu, Chapman and Meinel (1964), Piddington (1964), Ohshio (1964), Hess et al. (1965), Ness (1966), and Cole (1966). An exhaustive bibliography of the literature between 1958 and 1966 on many aspects of solar-terrestial relations has been compiled by Hess and Mead (1966); see also the Japanese National Report (1967).

The literature on micropulsations is enormous, and we mention only the comprehensive reviews by Kato and Watanabe (1957), Saito (1962), Jacobs and Westphal (1964), Troitskaya (1964), Tepley (1966) and Wentworth (1966).

Various aspects of the main field and its secular variation have been summarized by Elsasser (1950, 1955), Jacobs (1956), Runcorn (1956), Hide (1956), Hide and Roberts (1961), Kern and Vestine (1963), Malkus (1963), Rikitake (1966), and Gaskell (1967), in addition to Chapman and Bartels (1940). The last two works also review the induction effects of the various magnetic field variations and their use in investigating the deep conductivity of the earth.

The properties of telluric currents have been discussed by Rooney (1939) and Chapman and Bartels (1940), and extensively by Cagniard (1956). A brief review of later work has been given by Hessler and Heacock (1962).

2.5 Geophysical Prospecting

Although we are not directly concerned with the field of applied geophysics, much of the work described in the next chapter arose in this connection. It is therefore of some interest to delve briefly into this sphere of man's study of the Earth's magnetic and electric fields.

Obviously a large deposit of magnetic material in the Earth affects the local magnetic fields, and, similarly, a deposit with a significantly different electrical conductivity affects the telluric currents. Field geophysicists use these facts to try to determine the nature and location of the deposits.

Three basic techniques employing electric and/or magnetic fields are used:

(i) Magnetic Prospecting

(ii) Electrical Prospecting

(iii) Electromagnetic Prospecting

The first involves the detection of static magnetic field anomalies around deposits whose permeability or susceptibility is appreciably different from that of their surroundings. The interpretation is ambiguous. It is aided by knowledge of the anomalies formed around mathematically idealized cases, together with the known geology

of the area. This technique is also used to detect undersea features (Bullard and Mason, 1963). Because we are not interested in media with large permeability anomalies, this technique will henceforth be ignored. A survey of some of the applications up to 1940 is given by Chapman and Bartels (1940). The behavior of oscillating magnetic fields, rather than static magnetic anomalies, is mentioned later.

Electrical prospecting methods fall into two classes, employing either introduced electric currents or the naturally varying telluric fields. A comprehensive review has been given by Cagniard (1956). Although some studies had been carried out early in this century, it was Schlumberger who, in the 1920's and 1930's, developed the former techniques into a useable field tool. The method requires the passage of electric current into the soil through a pair of electrodes; the potential distribution is then measured at various points of the surface with a second pair of detecting electrodes. At first, "potential maps" were prepared, but later it was found to be more practical to measure the current as well, and deduce maps of "apparent resistivity" of the region. This technique was developed into electrical "sounding", since the effect of greater sub-surface depths becomes more apparent with greater electrode separations. Both direct and, more usually, alternating currents are used. See Cagniard (1950), Griffiths and King (1965).

In the techniques that use the naturally induced telluric fields, the variations of the $\underset{\sim}{E}$-field in two orthogonal directions are measured at two localities. The amplitude ratios are compared at several

frequencies. The ratio of the apparent resistivities may then be obtained, assuming that the magnetic field is the same at both stations. The method has the advantage over the artificially introduced current technique of not requiring long electrode lines or cumbersome electrical power supplies, while still being able to penetrate high resistance layers. The literature on the subject is very extensive (Cagniard 1956, Berdichevskii, 1960, Fournier, 1966, and Van'yan, 1967).

The electromagnetic methods also fall into two groups depending on whether the fields are artificially introduced. The artificial electrical method requires a fairly close electrode separation in order to resolve localized regions of anomalous conductivity. To circumvent this difficulty alternating magnetic fields are produced by a transmitting coil in a low flying aircraft. These induce electric currents in the ground, and the resulting magnetic field is recorded.

In 1950 Tikhonov in the USSR, Kato and Kikuchi, and Rikitake in Japan all pointed out that the telluric method using the natural telluric fields could be augmented by simultaneously measuring both the magnetic and electric fields. None of these papers was developed from the point of view of the prospector, but Cagniard (1953 a,b) and Tikhonov and Shakhsuvarov (1956) developed the ideas extensively into what is now known as the magnetotelluric method. These papers are discussed further in §3.2.2. The ratio of orthogonal E and H components (the "impedance" - hence the Russian term "impedance method") is determined as a function of frequency, enabling the apparent resistivity to be determined (as opposed to the ratio, given by the

telluric method). The technique is now being used to an increasing degree, particularly in France and the USSR. (Berdichevskii, 1960, 1962, Bostick and Smith, 1961, 1962, Fournier, 1966).

Several other methods have been developed as modifications or extensions of those described above. A brief review is given by Vozoff et al. (1964); see also Yungul (1966).

2.6 Observations of Electromagnetic Fields Near and Over Oceans

Here we consider observations of fields over oceans, remote from the shore, and also over both land and sea, close to the shore.

2.6.1 The "Ocean Effect"

The influence of the ocean on the magnetic field at some observation point depends on the depth and area of the sea, and significantly on the frequency (cf. §2.3.3). At high frequencies (where the mantle can be disregarded), and for seas of limited size, the curvature of the earth may be neglected and a simple "skin" calculation suffices to indicate quantitatively the influence of the ocean (see §3.1.8 and Fig. 3.2); thus for periods of less than about an hour (frequency > 10^{-3} cps), any induction effect in the observed magnetic field is predominantly due to the electric currents induced in the ocean.

Perhaps the most elegant way to investigate such ocean effects is to establish a station on a floating ice-island, a technique used in recent years by a number of workers, particularly in the USSR. Zhigalov (1960) examined the magnetic data from such a station in the Arctic Ocean and found, in particular, that the short period

variations ($\lesssim$ 10 min) in the vertical magnetic field become less evident when the ocean depth exceeds 200 m., and are almost non-existent over depths of 2500 to 3000 m. He observed a similar, but less pronounced, effect in the mean of all frequencies. The H and D components were relatively unchanged. He also detected a high correlation between the $\Delta Z/\Delta H$ ratio and the ocean depth.

Fonarev (1961 a,b) estimated the telluric currents induced in the sea using the Tikhonov-Cagniard theory (see §3.2.2), and (1961c) obtained measurements in the Barents sea at a mean depth of 200 m, for periods of 1-30 minutes. His telluric current measurements were made from a moving ship and no simultaneously recorded magnetic measurements were available. Comparison with shore based magnetic records did, however, show a high correlation between the telluric current and magnetic H and D variations. He pointed out that this relationship (between ocean telluric and land magnetic fields) is complicated by the effect of the coast, and also that the telluric current intensities at sea depend greatly on the conductivity of the underlying rock [Fig. 2.1 a]. He was not able to determine the expected enhancement of telluric current variations at a given frequency as the ocean depth decreases.

Novysh and Fonarev (1963) continued this work from a floating ice station in the Arctic Ocean, over ocean depths of 80-260 m. For periods of 1-10 minutes, the records of the orthogonal horizontal electric and magnetic fields behaved almost identically. The electric field components in this period range showed elliptic polarization;

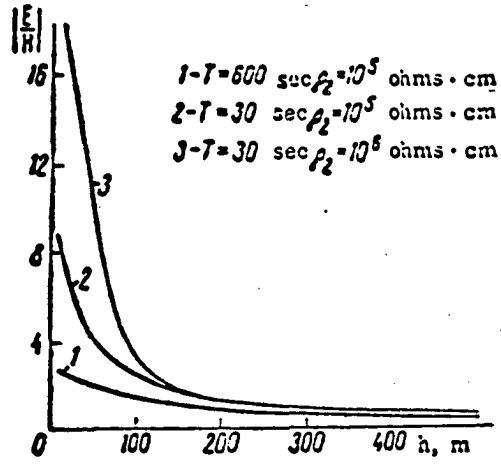

(a)

Fig. 2.1 (a) The ocean effect on telluric currents (Fonarev, 1961c).

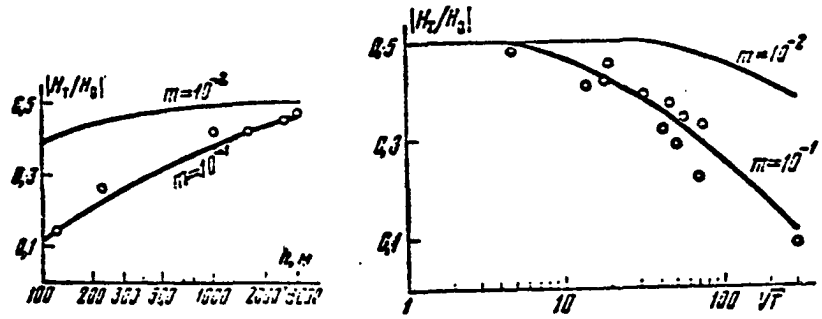

(b) (c)

Fig. 2.1 The contribution H_T of the ocean effect to the horizontal magnetic field, for different skin depth ratios m, as a function of (b) depth h, periods 3-6 min. (c) period $\sqrt{T}$, mean ocean depth 1750 m (except point at 24 hr. where h = 2700 m). (o represents observational values) (Fonarev and Ivanov, 1966).

it was never linear, but was sometimes nearly circular. The inclination of the ellipses was widely variable. The impedance (E_i/H_j ratio) was quite period dependent; it decreased with decreasing frequency, and showed a small depth dependence at short periods. The E/H ratio was enhanced somewhat at a shallower depth. This observation supports Zhigalov's result that magnetic variations with periods of less than ten minutes are suppressed over greater depths. Observations over a deeper ocean were however necessary to confirm this, as the penetration depth is considerably greater than the 260 m maximum depth of these observations. The electric currents were in fact measured at depths of both 6 m and 200 m and no significant difference was detected.

They calculated that the ocean effect on the horizontal magnetic field was 11-14% (130 m depth) and 16-19% (240 m depth) for periods of 2-15 minutes, but only 1-2% for diurnal and semidiurnal telluric variations.

Novysh and Fonarev (1966) and Fonarev and Ivanov (1966) continued these floating ice-island observations at much greater depths (1100-4000 m) with simultaneous magnetic and electric field measurements. They confirmed Zhigalov's (1960) observation that the vertical magnetic field variations with periods less than 10 minutes are damped out over these depths. Also the trend observed earlier was confirmed - the E/H ratio very definitely decreased with increasing depth (see Fig. 6.14). It was found however that, while agreement with the Cagniard-Tikhonov two-layer theory was good at great depths, this was not so at shallower depths; the explanation is probably connected

with the slope of the sea-bed, and the influence of the deeper water. Polarization of the E-field components (10-20 sec period, depth 2200 m) varied from linear to circular. However since the writers do not indicate the simultaneous H-field polarization, it is not possible to distinguish the effects due to induction from those due to the source.

In their second paper, the authors use the same observations to calculate the contribution to the horizontal magnetic field caused by the ocean. They give the results as a variation with depth for periods of 3-6 min., and as a variation with $\sqrt{T}$, over a depth of 1750 m (Fig. 2.1 b,c). For diurnal and semidiurnal variations the contribution is about 10%, but for short periods (< 1 min.) it is as much as 50% of the total field. The effect increases with the depth of the ocean, to a maximum of 50%.

Similar observations were made by Swift and Hessler (1964), also on an ice-island in the Arctic Ocean. Again the orthogonal electric and magnetic records were closely similar, but a comparison of the power spectra of the H/E ratios did not indicate any frequency dependence between periods of 1 minute and 1 hour. They suggest a possible explanation in terms of source size (Price, 1962). However, Fonarev (1961 a,c), Fonarev and Ivanov (1966) have indicated the significance of the basement conductivity in such observations, and this could be a contributing factor. Swift and Hessler, again like Novysh and Fonarev also find agreement with theory (that of Price (1962), cf. §3.2.3) as to the dependence of the $\Delta H/\Delta E$ ratio on

the ocean depth, at great depths (2300 m.), over a fairly even bottom. But they found a large discrepancy at shallower depths (400-450 m.), at the edge of a sharp increase in depth. This was probably due to the sloping basement.

Hessler (1962) attempted to measure the penetration of the telluric currents at a depth of 1370 m; he found no significant difference from the surface currents at periods of 2 to 5 mins. This distance is considerably less than the skin-depth at these frequencies. He calculated the contribution to the total magnetic field from the telluric currents to be about 30 to 50% at 2250 m depth, but did not state the frequency. Results for depths of 400 m indicated about 16% contribution.

Shand (1964) also observed the magnetic field at 6 cps on floating ice near Mould Bay, over a depth of 300 m,which corresponds to about 3 times the skin-depth. He expected the vertical component to be almost undetectable, but found it to be significant though small. The observations were preliminary, aimed at investigating ice-stability, and no further analysis was made. Heirtzler (1963, 1965) measured the total magnetic field variations at a depth of 306 m under an ice-island, over ocean depths of 3050-3300 m, between 70 and 400 sec. periods. He found an attenuation and phase shift relative to the surface field.

Hill and Mason (1962) observed the total magnetic field magnitude at longer periods over water of depth 450 to 2200 m. They appear to have detected some enhancement of the daily variation. The

observations, however, were complicated by effects which were apparently tidal and no frequency analysis was given.

Several attempts have been made to record the existence of vertical telluric current components in fresh water media. Vinogradov (1959) reported what appear to have been vertical telluric currents in the fresh water Lake Baikal, but could not conclude whether the short period oscillations in the total field resulted from phase shifts with depth, or vice versa.

Fonarev (1963) pointed out that these vertical currents probably resulted from conductivity inhomogeneities in the bottom. He calculated the approximate effect of a rectangular lake in producing a vertical current, and concluded that a shore effect exists, maximizing the vertical current inshore. He quoted results of Vinogradov (1963), showing a decrease in vertical electric current with increasing distance from the Lake Baikal shore.

Fonarev (1963) also reported that during strong electromagnetic disturbances, weak vertical telluric fields were observed from the ice-floe station in the Arctic Ocean, when this was over the sloping bottom near the continental shelf edge, at depths of 80 to 260 m. In contrast, Fonarev and Novysh (1965) and Hessler (1962), in similar circumstances but above ocean depths of 1120 to 4006 m and 1370 m respectively were unable to detect any vertical components.

A recent investigation (Jones and Geldart, 1967) of vertical earth currents on land in eastern Canada, found a great similarity with the horizontal fields, and a close relationship between vertical telluric fields at locations 160 km apart.

Thus we may conclude that electric currents induced in the ocean appreciably affect the magnetic field, particularly at short periods. This may be termed the "ocean effect". For periods of less than an hour the major modification to the magnetic field results from a pure ocean effect; at longer periods, however, the oceanic shielding of the high frequency variations from penetration to the mantle breaks down, and induction in the mantle becomes significant. In general, over deep oceans the high frequency variations in the vertical magnetic component are smoothed out, and the induced contribution to the horizontal magnetic field may be as high as 50%; the effects decrease with increasing ocean depth. The variations of the vertical magnetic component show a high correlation with the bathymetry. The influence of the ocean bed conductivity is appreciable, and in regions where the ocean is relatively shallow with a changing contour there is some evidence for the existence of vertical electric fields. These become less pronounced over greater depths. A high correlation between the orthogonal telluric and magnetic components is observed, and no particular polarization of the telluric field is found over great ocean depths, in contrast to that found from many land observations. Hessler (1962) noticed good correlation with auroral forms, however, based on visual observations during recording. Telluric current and active auroral arcs were always parallel. Theoretical $\Delta E/\Delta H$ ratios for a uniformly deep ocean agree with observations, provided the ocean is deep and the floor relatively flat. But observations show large discrepancies when applied to the shallower, steeply shelving edge of the continental shelf.

We have here dealt with the 'ocean effect'. Similar results have come from the many studies by geophysical prospectors of magnetotelluric fields in multilayered media based on the papers of Cagniard (1953) and Tikhonov and Shakhsuvarov (1956) (see §3.2).

2.6.2 The Effect of a Coastline

Vertical magnetic fields and electric currents are both significantly modified by a shelving ocean floor. Close to a shoreline, this behavior is usually termed the "coast effect".

Electromagnetic fields are affected over a very wide range of frequencies by large scale irregularities of conductivity such as occur at an ocean shore-line. At one extreme are the long-period daily variations in the earth's magnetic field; at the other we have radio propagation frequencies. We do not consider the latter (see, for example, the studies of Wait, 1963, and King and his co-workers, 1965, 1966a, b, and the bibliographies therein). "Coast effect" observations must be considered with respect to the type of variation.

Two New Zealand workers, Baird (1927), and Skey (1928) (see Lawrie, 1963), appear to have been among the earliest to investigate the coastal influence on magnetic observations. They found preferred directions of the disturbance[1] ratio $\Delta D/\Delta Z$ to incline upwards toward

[1] Lawrie (1963) does not state the disturbance periods which Baird and Skey used, and the original papers are not available to me.

the coast at Amberley, New Zealand and Watheroo, Western Australia. Several earlier workers had noted the connections between earth current and magnetic field disturbances (Chapman and Bartels, 1940, §13.15), and van Bemmelen (1908) suggested that telluric currents in the English Channel could account for the oppositely changing ΔZ variations at London and Paris during storm sudden commencements (see Barber, 1948).

Barber reported the results of three separate experiments, in an Icelandic fjord, in the Clyde Estuary in Scotland, and in the English Channel. These clearly showed that short period (10 sec - 10 min) variations in the vertical magnetic field at nearby magnetic observatories were produced by telluric currents in the confined sea configurations. He recommended that magnetic observatories be sited well inland to avoid the coast effect.

Rikitake and his co-workers have extensively studied the geomagnetic variations in Japan, both theoretically and observationally, from about 1951 to date. Summaries of their work are given in his papers (Rikitake and Yokoyama, 1955, Rikitake 1959, 1961a, 1964a, 1966). He has examined bay, ssc, sfe, Sq, and Dst disturbances, and finds greatly enhanced ΔZ variations, which some writers consider to be evidence of a coast effect. For variations of 1 hour or more the influence of the mantle becomes significant, and Rikitake has shown several times that at these periods the Japan anomaly is more likely to result predominantly from an anomalous mantle distribution than from the effect of the ocean. He pointed out (Rikitake, 1966, Ch. 19) that several similar anomalies are known in Europe, Canada, USA,

and Australia at these longer periods, and that many of them seem to require anomalous conductivity distributions at great depth to explain them. The Japan anomaly is also evident on Sakhalin (Van'yan and Marderfel'd, 1966).

Parkinson (1959, 1962a, b, 1964) developed a technique for representing the direction and magnitude of the tilt of a preferred plane of the magnetic vector. He applied it to bay-like disturbances (half-period 5 minutes to 1 hour) at Australasian observatories. Rikitake (1966, pp. 239-240) concisely summarized this technique and termed the resultant vector plots "Parkinson vectors". Parkinson found the magnetic disturbance vectors at coastal stations are always inclined upwards towards the deepest part of the ocean, while those at inland stations tend to be nearly horizontal. At first sight this appears to be a good example of the coast effect, but Parkinson (1963, 1964), on the basis of a model terrella experiment, concluded that a mantle effect was probably involved as well.

Schmucker (1964) observed enhanced ΔZ variations along the Californian coast, diminishing inland, for all periods from 7 1/2 min to 24 hours. He plotted the Parkinson vectors for bay disturbances of 1 hour and found that the coastal vectors always pointed out to sea. He concluded that the ocean was responsible for all of the anomalies, though he took account of the presence of the mantle.

Lawrie (1965) calculated similar Parkinson vectors for disturbance half periods of 1 min, at Apia, (Samoa), and Scott Base (Antarctica) and for 1 min, 12 min, 1 hr, and 6 hr half periods at Amberley, New Zealand. At the two shorter periods the vectors are oriented seawards

but the 1 hour vector is rather inconclusively oriented and the 6 hour vector is oriented directly inland. Undoubtedly the influence of the mantle currents is involved here also.

In 1957, while installing the magnetic observatory at Mirny, the major USSR Antarctic station for the IGY, Mansurov observed significant enhancements of disturbances in the Z and D components on the magnetograms. The effect fell off a few km inland from the shore or seawards, and the vertical magnetic field variations correlated well with the behavior of the ocean telluric currents immediately offshore, and strongly parallel to it (Mansurov, 1958, 1959, Sen'ko, 1958, 1959, Baranskii and Naumenkov, 1959, Rokityanskii, 1963, Rokityanskii et al., 1964). Telluric currents measured 10 km out to sea were similarly oriented, but were only some 15% of the magnitude of those recorded immediately offshore from Mirny. Baranskii and Naumenkov reported that the land telluric currents at Oasis station are approximately normal to the immediate coastline. Mansurov and his colleagues did not investigate the frequency dependence, but Rokityanskii quoted later studies referring to the period range 20 sec to 3 hours. Rokityanskii et al. gave the period of their results as 1-120 min. The conductivity ratio at Mirny is between perhaps 10^4 and 10^5, and the ocean floor slopes away very steeply from the shoreline, then becomes more gradual.

Duffus et al. (1959) investigated the spatial variation of micropulsations in the geomagnetic field, with periods between about 15 seconds and 10 minutes. They compared records at a coastal station

with those about 15 km inland, on Vancouver I., and found an appreciable difference at short periods (< 2 min), particularly in the X and Z components. The coastal Z component was always greater, the difference apparently becoming even more marked at periods < 20 sec. A factor of 3 to 1 or more was found at 20 sec periods. The X component was suppressed at the coastal station by about 70% at 20 sec and even more at shorter periods. The Y component showed a slight enhancement (20%) at 20 seconds, changing to a slight suppression (to about 80%) at periods of 5 minutes or more. The X and Y components were not resolved relative to the coastline but the writers regarded the ocean as contributing to the cause of this behavior.

The investigation was continued (Shand et al., 1959, Duffus et al., 1960 a,b) using for comparision a station 950 km inland. At periods of 20 seconds the ratio of Z at the coastal site was from 5 to 1 to 20 to 1 or more. Two coastal stations 7 km apart, facing the Juan de Fuca Strait (off southern Vancouver Island) in different directions, showed significantly different responses on occasions, particularly in X and Z. At the coastal stations a close relationship occurred between the X and Z records.

The coast effect at these micropulsation frequencies was further investigated in the area of the Fraser River delta (Western Canada), but the study was complicated by shallow mud banks and fresh water areas (Christoffel et al., 1961). However, it was concluded that the influence of the sea on the Z/H ratio for periods between 10 sec

and 10 min became insignificant at a distance 10 km inland from the shore in this region.

Duffus et al. (1962 b) summarized much of the Canadian work at micropulsation frequencies, and determined the spatial coherency of these variations. They found that the magnetic field gradients are too small to be detected at inland stations over a geologically homogeneous terrain (see also Duffus et al., 1962 a), but that, for periods between 2 sec and 10 min, the response of the various field components is frequency dependent, and influenced considerably by local geology. They concluded that an observatory sited at a coastal location is unsuitable as a base station for comparisons in the study of spatial coherence (and hence sources) of these magnetic fluctuations, because large perturbations can arise from the telluric currents induced in the seas.

Lambert and Caner (1965) also studied the coast effect in the magnetic field in Western Canada. They considered three separate frequency ranges in data at several stations on Vancouver Island and the associated mainland: low (6-24 hr); intermediate (20 min-3 hr); and high (20 sec-10 min). At Tofino, on the west side of Vancouver Island, they found a marked enhancement of the vertical component in the high and intermediate frequency ranges, peaking between 30 and 60 minutes in the latter case. The field was polarized roughly E-W, a direction not strictly normal to the edge of the continental shelf. However, the orientation at the higher frequency end of this range tended more towards perpendicular.

They concluded that, at periods of less than about 15 minutes, enhancement of the vertical magnetic field represented a true coast effect, due to the sea-land conductivity change. At periods greater than about 1 hour, any apparent "coast" effect was considered due to inhomogeneities in the upper mantle, apparently associated with the continental shelf. Some agreement with seismic studies was found.

Yoshimatsu (1957) summarized the effects at earth current observatories around the world. He classified three types of topographical response:

(i) Coast type: the principal direction of the earth currents generally tends towards the normal to the coastline.

(ii) Promontory type: the earth currents are oriented across the peninsula.

(iii) Inland type: the preferred directions of the earth currents depend on local topography. There is a trend for them to be parallel to river valleys or mountain regions.

Redding (1967), in a study of the diurnal variation of the telluric currents at Legon, Ghana, near the magnetic equator and 10 km from the coast, found their direction to be approximately normal to the coast. However, 450 km inland, there was apparently no preferred direction. The presence of the equatorial electrojet complicates the interpretation (see also Hutton, 1962). A study by Wescott and Hessler (1962) also emphasized the significance of local topography on telluric fields in both magnitude and direction.

Rokityanskii (1961, 1963), and Rokityanskii et al. (1964), discussed observations of telluric currents near the Black Sea, on the Crimean peninsula. For periods between 10 sec and 60 sec they found a definite increase in the amplitude of the telluric currents, as the coast was approached. The telluric fields were polarized almost linearly along a line approximately normal to the coast. The sea-land conductivity ratio was estimated as at least 100, but the geological structure is complicated.

At a different point on the Crimean peninsula, a shallow sea, shelving very slowly (5 m deep at 300 m, eventually reaching 10 m) abutted a homogeneous land mass with the very low conductivity ratio of 7 to 1. For all periods from 15 sec to 1 hour, it was found that the normal telluric field component increased to 15-20% within 1 km landwards and was 15% smaller 400 m seawards. The tangential field did not change more than 10% across the coastline, and the polarization was not greatly altered.

The effect of the shelving ocean floor on magnetotelluric observations has been studied on floating ice-stations over the Arctic Ocean. Zhigalov (1960) found a high correlation between the ocean depth and the $\Delta Z/\Delta H$ ratio for periods $\lesssim$ 10 min, while Fonarev and his colleagues found the telluric field/magnetic field disturbance ratio was quite depth dependent (see §2.6.1). Berdichevskii (1961) used the results of magnetotelluric sounding observations over a sloping igneous (non-conducting) basement in the Dnieper-Don basin to compare with his theoretical analysis. The basement depth varies from 500 m to

2000 m at an angle of 2-3° inclination and the observed telluric fields were linearly polarized parallel to the projected line of strike. The parallel telluric field component shows a close correlation with the basement depth, in agreement with his theory. He found that the phase relation between the telluric field and its asymptotic value increased from about -15° to +20° with increasing depth, a finding also in good agreement with the theory.

Berdichevskii also reports the results of a survey made in the Polish Litovsk depression, by the All-Union Scientific Research Institute of Geophysics, to compare the techniques of telluric, magnetotelluric and magneto-variational prospecting. The last named method uses the horizontal magnetic variations, and they are likewise found to depend on the basement depth, which slopes from 400 m to 2100 m. Similar results were also obtained in Eastern Siberia.

Recently Wescott (1967) made an observational study of magnetotelluric field variations across a coastal profile at Barrow on the Arctic Ocean. Here the sea floor shelves gradually while the adjacent land is flat and marshy, with many lakes, and permafrost extends to great depths (up to 1500 m). The land conductivity was estimated at between 0.1 to 1 mho m^{-1}, but the near surface layers probably have a much lower value due to the permafrost. Saline impregnated layers, with a conductivity approximating that of the ocean, exist in the first 30 m depth. The effective ocean-land conductivity ratio is probably quite small, in contrast to other stations where the coast effect has been studied. He found that, for general disturbances,

no significant coast effect occurs in either the vertical or horizontal magnetic field components. The electric field on land showed a preferred direction nearly normal to the shoreline, and this direction was maintained offshore at distances of 1-3 km (depth 35 m). This accounts for the lack of anomaly in the vertical magnetic field. The linear polarization of the telluric field became less marked at greater distances inland and was entirely absent 45 km from the coast. A decrease in the telluric field response to short period variations ($\sim$ 10 sec) was also found, but this may be due to the higher conducting surface saline layer, just as in the "ocean" effect. A visual analysis of the magnetic records indicated no consistently obvious frequency dependence.

Rokityanskii (1963) et al. (1964), gave excellent summaries of the effect of a coast for periods in the range 10 sec - several hours, based on observations at Mirny and the Crimea. Their interpretation is given in terms of the theoretical calculations of Ponomarev (1960) and Berdichevskii (1961), who discuss coastlines with a shelving floor under various approximations (see Chapter VI). Rokityanskii concluded that, in general, all components of the magnetotelluric fields will be affected by a coast, with the exception of the magnetic field parallel to the shoreline. The normal magnetic component is enhanced some 30% over the asymptotic values near Mirny; it peaks slightly to the seawards of the shore (see Fig. 2.2 a,b). The vertical magnetic field is also enhanced at the shore line, but falls to about

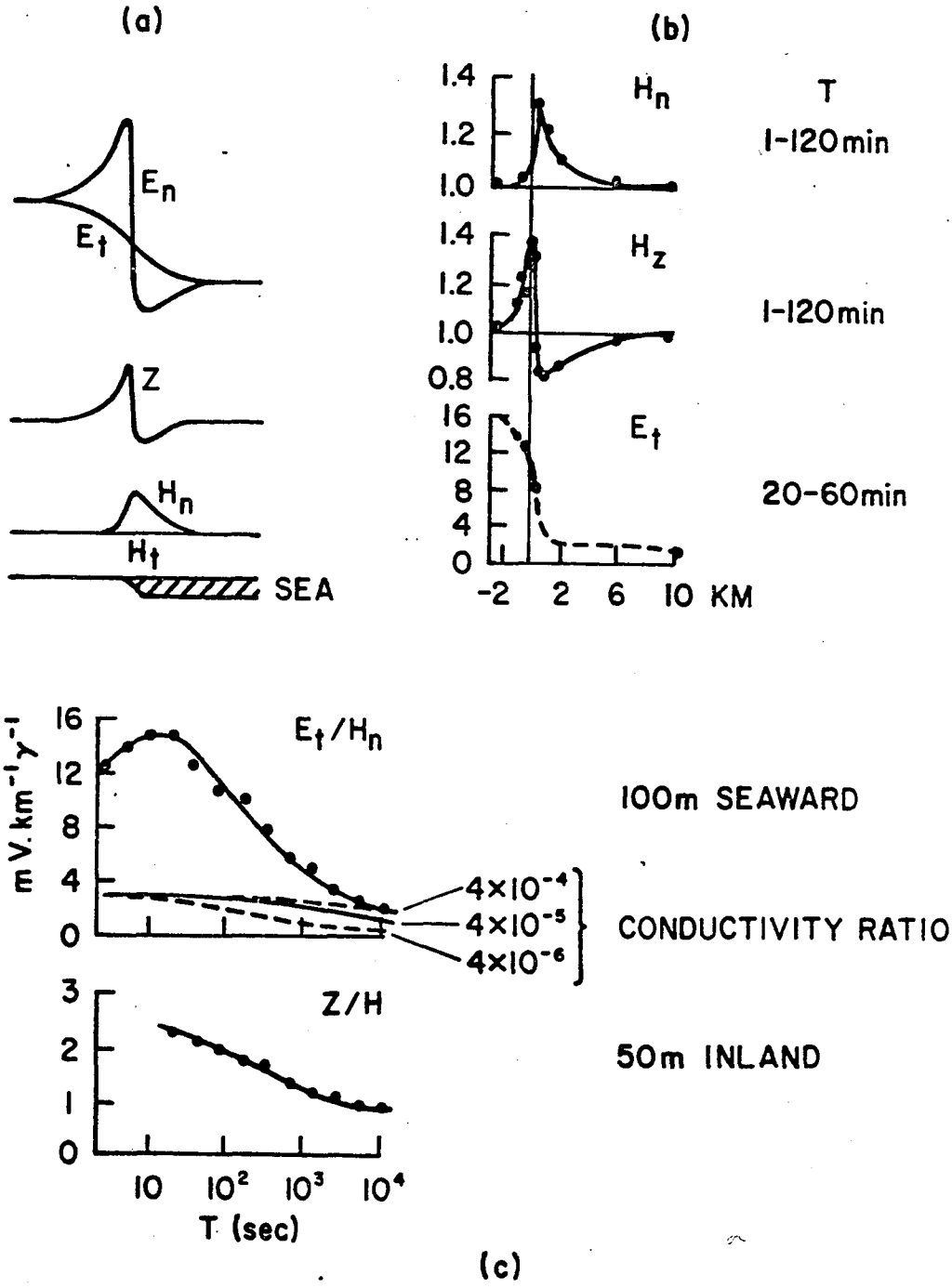

Fig. 2.2 The coast effect on the magnetic and electric field components (Rokityanskii, 1963: Rokityanskii et al., 1964).

85% of its asymptotic value about 1 km offshore, gradually recovering again at greater distances. The asymptotic values are recovered at distances of perhaps 8 km offshore and 3 km inland. These results refer to a period range of 1-120 minutes, with a conductivity ratio between land and sea, in the range 10^{-3} to 10^{-5}. The sea bed slopes steeply (from 50 m to 100 m depth within 100 m), becoming more gradual at greater distances.

The parallel electric field decreases very sharply by a factor of about 6 or 7 to 1 across the coastline, in the period range 20-60 min. It attains a steady value within about 2 km on either side of the coast. The normal electric field is sharply enhanced above its asymptotic (far inland) value immediately to the landward side, and is depressed somewhat below its oceanic asymptote just to seawards of the shoreline.

The penetration depths in the land and sea media are greatly different, (100 to 1 for conductivity ratio of 10^4), being larger in the relatively non-conducting land. It is perhaps surprising, therefore to find the field perturbations penetrating further on the ocean side of the coast. However, it should be remembered that the oceanic observations are complicated by the relatively shallow sea (400 m at 10 km) with a sloping bed.

The frequency responses of Z/H (where $H^2 = H_t^2 + H_n^2$) and E_t/H_n, at points 50 m landwards and 100 m oceanwards, are reproduced from Rokityanskii (1963) in Fig. 2.2c. For comparison the asymptotic response of the ocean (two parallel layers) is given in the second

case. It can be seen that the parallel telluric field falls off appreciably at both high and low frequencies.

2.6.3 The Island Effect

Since a large portion of the earth's surface is ocean covered, the need for island magnetic observatories is obvious. Nevertheless, the results described in the previous section cause some suspicion about records from islands, especially at shorter periods.

Parkinson (1962b) (see Rikitake 1966, ch. 17) investigated the $\Delta Z/\Delta H$ ratio at seven island observatories and found it ≤ 0.1 at S. Miguel (Azores), Guam, and Apia (Samoa). However, at the others - Honolulu (Hawaiian Is.), Koror (Caroline Is.), Heard I. and Macquarie I. - he sometimes found it relatively large (≥ 0.5). As the last three are in either equatorial or auroral electrojet regions, a source effect is undoubtedly involved. In the Hawaiian case this is not so, although there may be a mantle inhomogeneity as suggested by Parkinson.

Mason (1963a) examined the ΔZ variation at seven points on Oahu in the Hawaiian Is. and found large differences in stations only 20 km apart. A complete reversal in sign occurred for periods of 1 hour or less, and there was a 30° phase-difference in Sq. Small effects were also noticed on the horizontal component records. He concluded that the effects were caused by induced electric currents flowing around the island and suggested that island observatories should be centrally located.

Mason (1963 b,c) reported similar effects on Christmas I., and on Palmyra, Fanning and Jarvis Is. in the Line Is., all equatorial stations. Possibly some of this behavior may be explained by fluctuations in the location of the equatorial electrojet, as it is suspected to change by more than 100 km from day to day (Osborne, 1962). At Christmas I., ΔZ observations made at eight points changed by a factor of 5 or more in amplitude and 180° in phase from the values in the absence of the island, at periods of < 1 hour. A second order effect (a few percent) may also occur in the horizontal component. The 24 hour daily variation (Sq) showed phase differences of up to 70°. Mason also considered these ΔZ anomalies as due to the diversion of induced electric currents in the ocean around the island.

The short period magnetic disturbance vectors on several islands (see Parkinson 1962a, Lawrie 1965) are oriented upwards towards the ocean, in a way similar to those on continental coasts.

Swift and Wescott (1964) noticed that the telluric field at Macquarie I. was linearly polarized to a very high degree, and that its magnitude was increased tenfold over that observed elsewhere. The recording station is situated on a 250 m wide peninsula extending rather less than 2 km from the northern extremity of the 32 km long, 5 km wide island. The direction of polarization of the telluric field was normal to this peninsula. Good correlation exists between the telluric field and the orthogonally resolved magnetic field component, particularly for periods of 15 to 30 min. They considered

the presence of the island to have comparatively little effect on the frequency response, relative to the oceanic magnetic and electric fields (the surrounding ocean being some 3500 m or more in depth). The behavior of the telluric field was explained in terms of steady state current flow around a non-conducting island.

2.6.4 The Possible Effect of a Coastline on the Aurora

A coastal conductivity change of sufficient contrast causes a noticeable change in the magnetic and telluric fields. It is conceivable, therefore, that other geophysical phenomena may also be influenced by a coastline.

In 1961, two Russian workers published studies of the aurora in the Arctic (based on IGY data) in which a "coast effect" was noted. Nadubovich (1961) and Duma (1961) investigated homogeneous and rayed arcs in the Tiksi Bay area of Siberia, and noticed a tendency for the arcs to take the shape of the coastline for brief periods. This tendency had apparently been suggested much earlier by the explorer Wrangel (see Nadubovich, 1963). Nadubovich (1963) extended his observations by analyzing early auroral records. He found the frequency of occurrence of aurorae increased by about 10% over a coastline but an individual auroral form tended to orientate itself along a coastline for only a brief period - some tens of seconds. He concluded that sharply curved coastlines can possibly produce sharply curved auroral forms. Ponomarev and Rudenko (1963) studied various auroral forms in the Tiksi Bay area, and supported these observations. They concluded that the properties of the underlying

surface did seem to influence certain auroral forms and their development, particularly weak homogeneous arcs. Samsonov and Zaretskii (1963) also noted a possible effect on rayed forms by the Novosibirskiye Is., North of the Lena delta.

All of the above investigators studied the variation of the location of auroral forms near a coastline. Andriyenko (1965 a,b)[1] studied the height of the lower border of auroral arcs, with regard to a coastline. He again (1965a) used the Tiksi Bay records, for 1963 and 1964, and divided the data into two groups according to whether the height was $\leq$ 110 km or >110 km. This criterion was picked because a relative minimum occurs at 110 km in the height distribution of lower borders at Tiksi Bay. The height of the arcs falling in the second group showed no dependence on position relative to the coastline, but those with heights $\leq$ 110 km showed a distinct decrease in height with distance inland. The heights decreased linearly from approximately 110 km within the first 10 km out to sea, to about 100 km at some 25-30 km inland. Only one of the arcs measured actually followed the coastline, although it was typical of the first group.

In the (1965b) paper the height determinations of Vegard in Northern Norway in 1913-1914 were similarly analyzed. The lower borders of aurorae over shallow water tended to be lower than those elsewhere, but the complicated fjord-river coastline and the orientation of the auroral zone prevented any conclusion as to the existence of a coast effect. However, there was a minimum in auroral height

---

[1] I thank Mr. J. Boyd for drawing my attention to Andriyenko's papers.

at the effective coastline defined by Andriyenko. The "shallow water effect" was located some 100 km from the auroral zone, and he considered it to be real. It thus appears that there is some dependence of auroral height as well as position on the ground conductivity, particularly over oceans.

During his observations of the magnetotelluric field on an ice-island in the Arctic Ocean, Hessler (1962) also noted that active arcs with rapid longitudinal structural motion were aligned parallel to the telluric ocean currents. Swift and Hessler (1964) estimated that the scale size of the inducing field responsible for similar currents would have to be greater than 100 km in order to reach the ground without too great attenuation. Thus the tendency noted by the Russian observers may be connected with the enhanced electric current flow in the sea parallel to the coast, as was so clearly observed by Mansurov.

CHAPTER III

FUNDAMENTAL PRINCIPLES AND THEORETICAL TREATMENTS OF SHORT PERIOD INDUCTION

In this chapter, we will discuss the theoretical analyses of the effect of an ocean on the magnetic and telluric fields. A number of fundamental concepts are first outlined, with appropriate emphasis to establish a background for the later chapters.

3.1 Some Basic Concepts in Electromagnetic Theory as Applied to Interface Phenomena.

The contents of this section may be found in far more elaborate detail in any good text on electromagnetic theory - for instance, Stratton (1941), Sommerfeld (1948, 1952), Smythe (1950), Landau and Lifschitz (1959, 1960), Panofsky and Phillips (1955), Jackson (1962), Tralli (1963), Schelkunoff (1963), Clemmow (1966). Giorgi MKSQ rationalized units are used throughout, and time dependence is taken in the form $e^{-i\omega t}$.

3.1.1 Maxwell's Equations and Interface Conditions

In differential form, Maxwell's equations are written

$$\begin{aligned} \operatorname{curl} \underset{\sim}{H} &= \underset{\sim}{J} + \frac{\partial \underset{\sim}{D}}{\partial t} \quad ; \quad \operatorname{div} \underset{\sim}{B} = 0 \\ \operatorname{curl} \underset{\sim}{E} &= - \frac{\partial \underset{\sim}{B}}{\partial t} \quad ; \quad \operatorname{div} \underset{\sim}{D} = \rho \end{aligned} \tag{3.1}$$

where ρ, $\underset{\sim}{J}$ represent the free charge and current density. The field vectors $\underset{\sim}{B}$, $\underset{\sim}{H}$, $\underset{\sim}{D}$, and $\underset{\sim}{E}$ are related in an isotropic medium by:

$$\underset{\sim}{B} = \mu \underset{\sim}{H} \quad ; \quad \underset{\sim}{D} = \epsilon \underset{\sim}{E} \quad ; \quad \underset{\sim}{J} = \sigma \underset{\sim}{E}$$

Here μ, ϵ, and σ are respectively the permeability, permittivity and conductivity of the medium. We will assume that we always deal with non-permeable media so that the permeability $\mu = \mu_o$. This is true within 1% for most rocks and soils (Kato, 1938, 1940, 1941). We have

$$\mu_o \, \epsilon_o = c^{-2}$$

where c is the velocity of light. The free space values of μ_o and ϵ_o are:

$$\mu_o = 4\pi \, 10^{-7} \text{ henry } m^{-1}$$

$$\epsilon_o \approx 10^{-9} / 36 \, \pi \text{ farad } m^{-1}$$

Application of Maxwell's equations to an elementary section of an interface between two media yields the following conditions on the fields there:

B_{normal}, $E_{tangential}$: always continuous

$H_{tangential}$: continuous in the absence of free surface currents; otherwise the difference $[H_t]$ = free surface-current line density.

D_{normal}: continuous in the absence of free charge; otherwise $[D_n]$ = free charge surface-density.

Under steady state conditions we have

$$\nabla \cdot \underset{\sim}{J} = 0$$

so that J_{normal} is continuous across an interface. This is not necessarily true in time variant systems, since, in the presence of a changing charge density σ_s:

$$J_{normal} = - \partial\sigma_s/\partial t.$$

3.1.2 Low Frequency Condition

We are not interested in high frequencies (radio waves). We may therefore neglect the displacement current term in Maxwell's equations, in comparison with the conduction current, provided we are dealing with a conductor. For harmonic time dependence $e^{-i\omega t}$ of the fields, this is equivalent to assuming:

$$\omega << \frac{\sigma}{\varepsilon} \qquad (3.2)$$

and to neglecting the presence of free charges.

Certain metamorphic rocks, such as marble, have conductivities as low as 10^{-8} mho. m.$^{-1}$ while some granites have conductivities of 10^{-7} mho. m.$^{-1}$. However most sedimentary, metamorphic and igneous materials, as well as earth, have conductivities greater than 10^{-5} mho. m.$^{-1}$ (Hodgman, 1963). The conductivity of sea water is within 1 to 5 mho. m.$^{-1}$ (Thomas et al., 1934). Examples of conductivity and permittivity for various media are listed in Table 3.1. Since the values of the permittivity are rarely more than ten times ε_o, the neglect of displacement currents for angular frequencies $\omega << 100$ cps. is certainly valid even at these extremes, and in most media will be valid for $\omega << 10^5$ cps (see also §3.2.3, eq. 3.17).

Table 3.1

Some Values of Conductivity and Relative Permittivity for Common Natural Terrestrial Media

Medium	Conductivity[1] mho.m.$^{-1}$	Medium	Relative Permittivity[3] $\varepsilon' = \varepsilon/\varepsilon_0$
Sea Water	1 - 5		
Fresh Water	10^{-2} - 10^{-3}	Fresh water	78-81
Igneous Rock			
Granite	10^{-5} - 10^{-7}	Quartz	4.7-5.1
Basalt (lava)	10^{-4} - 10^{-5}	Marble	8.3
Quartz	$<10^{-4}$	Mica	5.6-6.0
		Slate	6.6-7.4
Metamorphic Rock		Sulphur	4.0-4.2
Marble	10^{-6} - 10^{-8}	Diamond	16.5
Mica Schist	10^{-5}	Asphalt	2.7
Shale	10^{-2} - 10^{-3}	Calcite	8.0-8.5
		Dolomite	6.8-8.0
Sedimentary Rock			
Limestone	10^{-2} - 10^{-3}		
Sandstone	10^{-1} - 10^{-3}		
Unconsolidated			
Clay	10^{-2} - 10^{-3}		
Gravel	10^{-3}		
Dry and moist sand	10^{-3} - 10^{-4}		
Flood plain alluvium[2] (silt, sand, river gravel)	10^{-2} - 10^{-4}		
Silt[2]	10^{-2} - 10^{-4}		
Permafrost-impregnated silt[2]	10^{-2} - 10^{-3}		

1. All values adapted from Hodgman (1963) except those marked: 2 and 3.

2. Adapted from Wescott (1960)

3. Adapted from Stratton (1941) and Hodgman (1963).

3.1.3 Static Cases

In the steady state limit when the fields are not varying with time, Maxwell's equations (3.1) reduce to

$$\text{curl } \underset{\sim}{H} = \underset{\sim}{J} \quad ; \quad \text{curl } \underset{\sim}{E} = 0$$

(a) Electric Field:

The electric field is therefore derivable from a scalar potential Φ

$$\underset{\sim}{E} = - \nabla\Phi$$

In the absence of free charge, this potential is a solution of Laplace's equation

$$\nabla^2 \Phi = 0$$

Solutions of this equation under various boundary conditions have been investigated extensively, and in two-dimensional applications conformal mapping may be used. Geophysical prospectors have employed this technique in investigating telluric current flow around non-conducting obstacles of various kinds (cf. §3.3.3).

The conjugate function to the potential leads to the concept of current function, originally introduced by Maxwell. This is a representation of the current flow-lines, as distinct from the equipotential surfaces. It has been employed by Ashour, Rikitake, Fonarev, and others, in their discussions of the electric and magnetic fields around islands and in ocean basins. The current function (often written Ψ) is analogous to the stream function of hydrodynamics: it is defined as the current flowing across any line joining two points. The conjugate functions Φ and Ψ/σ are related by the Cauchy-Riemann equations:

$$\frac{\partial \Phi}{\partial x} = \frac{1}{\sigma}\frac{\partial \Psi}{\partial y} \quad ; \quad \frac{\partial \Phi}{\partial y} = -\frac{1}{\sigma}\frac{\partial \Psi}{\partial x}$$

It is often more convenient mathematically to use the current function Ψ (or stream function) rather than the potential function Φ, since boundary conditions designate a value for Ψ itself, instead of the derivative of the potential $\partial\Phi/\partial n$, in a direction normal to the boundary.

(b) Magnetic Field:

In a non-conducting medium, the conduction current $\underset{\sim}{J}$ is zero, and the magnetic field may be described analogously by a magnetic potential usually written Ω, also a solution of Laplace's equation. Then:

$$\underset{\sim}{H} = -\nabla\Omega$$

Chapman and Price (1930), Lahiri and Price (1939), Rikitake (1950 a,b,c, 1951) and many others used this concept in their spherical harmonic investigations of the conductivity of the earth's deep interior. Price (1950), Ashour and Price (1948), and Ashour and Chapman (1965), also employed the idea of magnetic potential in the non-conducting atmosphere below the ionosphere, to determine the magnetic field resulting from current sheets. However, Nishida (1962, 1964), and Weaver (1963b) have pointed out the dangers of neglecting the displacement current in such situations (see §3.2.3).

The principle in the second application above is to calculate the current function for the steady state current flow in a thin sheet, and relate it, through Maxwell's relations, to the magnetic fields on either side of the sheet. A boundary condition is obtained

from the connection between the current function in the sheet and the magnetic potential Ω_o in the neutral medium immediately over it

$$\Omega_o = \tfrac{1}{2}\Psi$$

With this boundary condition, Laplace's equation may be solved to give Ω in the non-conducting region over the sheet.

3.1.4 General Wave Case

In the time dependent case (taken as $e^{-i\omega t}$), Maxwell's equations (3.1) reduce to

$$\nabla^2 \underset{\sim}{H} + i\omega\mu_o (\sigma - i\omega\varepsilon) \underset{\sim}{H} = 0$$

$$\nabla^2 \underset{\sim}{E} + i\omega\mu_o (\sigma - i\omega\varepsilon) \underset{\sim}{E} = 0$$

However, as we neglect the displacement current in comparison with the conduction current, the field vectors $\underset{\sim}{E}$ and $\underset{\sim}{H}$ are solutions of the complex vector Helmholtz equation:

$$(\nabla^2 + i\eta^2) \underset{\sim}{F} = 0 \qquad (3.3)$$

where

$$\eta^2 = \mu_o \omega\sigma \qquad (3.4)$$

The magnetic vector potential $\underset{\sim}{A}$ is defined by $\underset{\sim}{B}$ = curl $\underset{\sim}{A}$, so that, for the electric field, Maxwell's relation gives:

$$\underset{\sim}{E} = -\nabla\Phi - \frac{\partial \underset{\sim}{A}}{\partial t} = -\nabla\Phi + i\omega \underset{\sim}{A}$$

The first (frequency independent) term is the static solution. The frequency dependence at low frequencies thus appears as an additive "perturbation" to the static solution.

3.1.5 Plane Waves and Polarization

In a sourceless non-conducting medium, Maxwell's equations are homogeneous and the individual cartesian components F_j of $\underset{\sim}{E}$ and $\underset{\sim}{B}$ satisfy the wave equation:

$$(\nabla^2 - \frac{1}{\mu\varepsilon}\frac{\partial^2}{\partial t^2})\, F_j = 0$$

Separation of variables in the cartesian system leads to the plane-wave solutions:

$$F_j(k,\omega) = F_{jo}\, e^{i(\underset{\sim}{k}\cdot\underset{\sim}{r} - \omega t)} \quad ; \quad \frac{k}{\omega} = \sqrt{\mu\varepsilon}$$

with the general solution integrated over k and ω. The simple harmonic, uni-directional vector solutions for the fields are then

$$\underset{\sim}{E} = \hat{\underset{\sim}{\varepsilon}}_1\, E_o\, e^{i(\underset{\sim}{k}\cdot\underset{\sim}{r} - \omega t)}$$

$$\underset{\sim}{B} = \hat{\underset{\sim}{\varepsilon}}_2\, B_o\, e^{i(\underset{\sim}{k}\cdot\underset{\sim}{r} - \omega t)}$$

The solenoidal nature of the sourceless $\underset{\sim}{E}$ and $\underset{\sim}{B}$ fields in a homogeneous medium requires $(\hat{\underset{\sim}{\varepsilon}}_1, \hat{\underset{\sim}{\varepsilon}}_2, \underset{\sim}{k})$ to be mutually orthogonal, and a transverse wave is specified, with

$$\underset{\sim}{B} = \frac{1}{\omega}\,\underset{\sim}{k} \times \underset{\sim}{E}$$

The propagation constant k in a conducting medium is defined by

$$k^2 = \mu\varepsilon\omega^2 + i\mu\sigma\omega \qquad (3.5)$$

and under the low frequency or "good conductor" approximation implied by (3.2), only the second term is significant. Thus

$$k^2 = i\mu_o\sigma\omega \tag{3.6}$$

in the conductors we deal with here.

To allow for non-linear polarization, the general form of a plane wave may be written (using the $\underset{\sim}{E}$ vector):

$$\underset{\sim}{E} = (\hat{\underset{\sim}{\varepsilon}}_1 E_1 + \hat{\underset{\sim}{\varepsilon}}_2 E_2)\, e^{i(\underset{\sim}{k}\cdot\underset{\sim}{r} - \omega t)} \tag{3.7}$$

In general, the E_1 and E_2 are complex and the polarization is elliptic. If E_1 and E_2 are in phase, the wave is linearly polarized; if they are of equal magnitude but 90^o out of phase ($E_2 = \pm i E_1$) the wave is circularly polarized, left or right handedly.

The determination of the polarization characteristics of an arbitrarily polarized wave is described in more detail in App. 1.

3.1.6 The Impedance Concept

From an analogy with transmission line behavior, Schelkunoff, Stratton and others devised the concept of "intrinsic impedance" for plane wave propagation (Stratton, 1941). It is defined by the ratio

$$Z = E_x/H_y = -E_y/H_x$$

the sign being defined by the coordinate orientation and the requirement that $\underset{\sim}{H} \times \underset{\sim}{k}$ and $\underset{\sim}{E}$ be directed in the same sense. The boundary conditions on H and E require the impedance to be continuous across an interface; its value there is termed the "surface impedance".

The concept of impedance is used extensively by geophysical prospectors, particularly in Russia. Care must be taken with

anisotropic media, since the condition that $\underset{\sim}{E}$ and $\underset{\sim}{H}$ are orthogonal is no longer necessarily true. The same applies under certain source conditions (Price 1962).

3.1.7 Reflection and Refraction of a Plane Wave at a Plane Interface

Consider a low frequency plane wave in a double layered medium. Suppose the wave impinges normally at $z = 0$ on a medium of conductivity σ_1, depth h which is underlain by another conducting medium of conductivity σ_2 and infinite depth. If the z-axis is taken vertically downwards, and the incident wave is specified by (E_o, H_o) then (Stratton 1941) the total fields at the surface $z = 0$ are given by

$$E\Big|_{z=0} = \nu_E E_o$$

$$H\Big|_{z=0} = -\nu_H E_o$$

The coefficients are

$$\nu_E = 2\left\{(1+Z_{12}) + (1-Z_{12})\, e^{2ik_1h}\right\}/D$$

$$\nu_H = 2\left\{(1+Z_{12}) - (1-Z_{12})\, e^{2ik_1h}\right\}/Z_1 D$$

$$D = (1+Z_{o1})(1+Z_{12}) + (1-Z_{o1})(1-Z_{12})\, e^{2ik_1h}$$

Here $Z_{o1} = Z_o/Z_1 = k_1/k_o$

$Z_{12} = Z_1/Z_2 = k_2/k_1$

where Z_j specifies the impedance of the j^{th} medium ($j = 0$ referring to the atmosphere $z < 0$) and k_j represents the propagation constant in that medium.

Under the approximation made in §3.1.2, relation (3.6) applies and the two media may both be considered "good conductors" at low frequencies. Then the propagation constants may be written:

$$k_o = \omega/c$$

$$k_1^2 = i\omega\mu_o\sigma_1$$

$$k_2^2 = i\omega\mu_o\sigma_2$$

so that $Z_{o1} = c\sqrt{\frac{i\mu_o\sigma_1}{\omega}}$; $Z_{12} \approx \sqrt{\frac{\sigma_2}{\sigma_1}}$

with $|Z_{o1}| >> 1$.

The second coefficient above reduces to

$$\nu_H \approx \frac{2}{\mu_o c}$$

i.e., the magnetic field at the surface of the upper layer is independent of the underground conductivity structure, at least if it is horizontally layered.

Weaver (1963 a) similarly deduced this important point for a single layered homogenous medium where the above coefficients reduce to

$$\nu_E = \frac{2k_o}{k_o + k_1}$$

$$\nu_H = \frac{k_1}{\mu_o\omega} \cdot \frac{2k_o}{k_o + k_1}$$

Again, v_H becomes independent of the conductivity under the good conductor approximation $k_o << |k_1|$.

The essential constancy of the horizontal magnetic field at the surface implies that there are no vertical electric field components (or currents) near the surface. Such a condition would be expected when horizontal layering is involved, but would not be expected to hold up over a sloping bedding-plane or sea-bed. In fact, vertical telluric currents have been observed under just these conditions in relatively shallow lakes and seas (§2.6.1).

3.1.8 Skin Depth

Since the $\underset{\sim}{E}$ and $\underset{\sim}{H}$ waves are proportional to the factor $e^{i(kr-\omega t)}$, then, under conditions (3.2) for a good conductor where $k \approx \sqrt{i\omega\mu_o\sigma}$, there will be an exponential damping of the wave by a factor $e^{-r/\delta}$, where

$$\delta = \sqrt{\frac{2}{\mu_o \omega \sigma}} \tag{3.8}$$

The parameter δ has the dimensions of length and is called the skin-depth, it represents the spatial rate of decay of an electromagnetic wave within a conductor.

In many applications it is a nuisance to include the 2 in relation (3.8). The physical behavior is governed by the term

$$\eta = \sqrt{\mu_o \omega \sigma} = \sqrt{2}/\delta \tag{3.9}$$

and in this work we use η rather than δ. We call the parameter η^{-1} the "penetration depth".

In Fig. 3.1, values of η^{-1}, or D, are given in km for various values of the product $f\sigma$. In particular the penetration depths for an ocean of conductivity 3 mho m^{-1} are shown for the relevant frequencies.

Relation (3.8) is based on the solution of the diffusion equation (3.3) under the assumptions that the medium is a homogeneous half-space and that the induced currents are uniformly distributed in any horizontal plane. Price (1950, 1962, 1965, see also McCann and Price, 1965) has considered the modification to this type of decay when these assumptions are relaxed. He finds that the penetration will be reduced. The horizontal magnetic component attenuates more rapidly, for instance, in an ocean of finite depth, than do the similarly behaving vertical component and the induced currents. The more rapid decay results from the interaction of the multiply reflected waves at the surface and basement interfaces. This effect diminishes as the depth becomes greater and the E, H, and Z fields attenuate similarly.

Price's work is discussed in §3.2.3.

3.1.9 A Plane Wave at Non-normal Incidence

We have assumed that the incoming plane wave impinged normally on the surface under consideration. This is not very realistic, but it turns out that the angle of incidence is not usually a very significant parameter as far as the refracted wave is concerned.

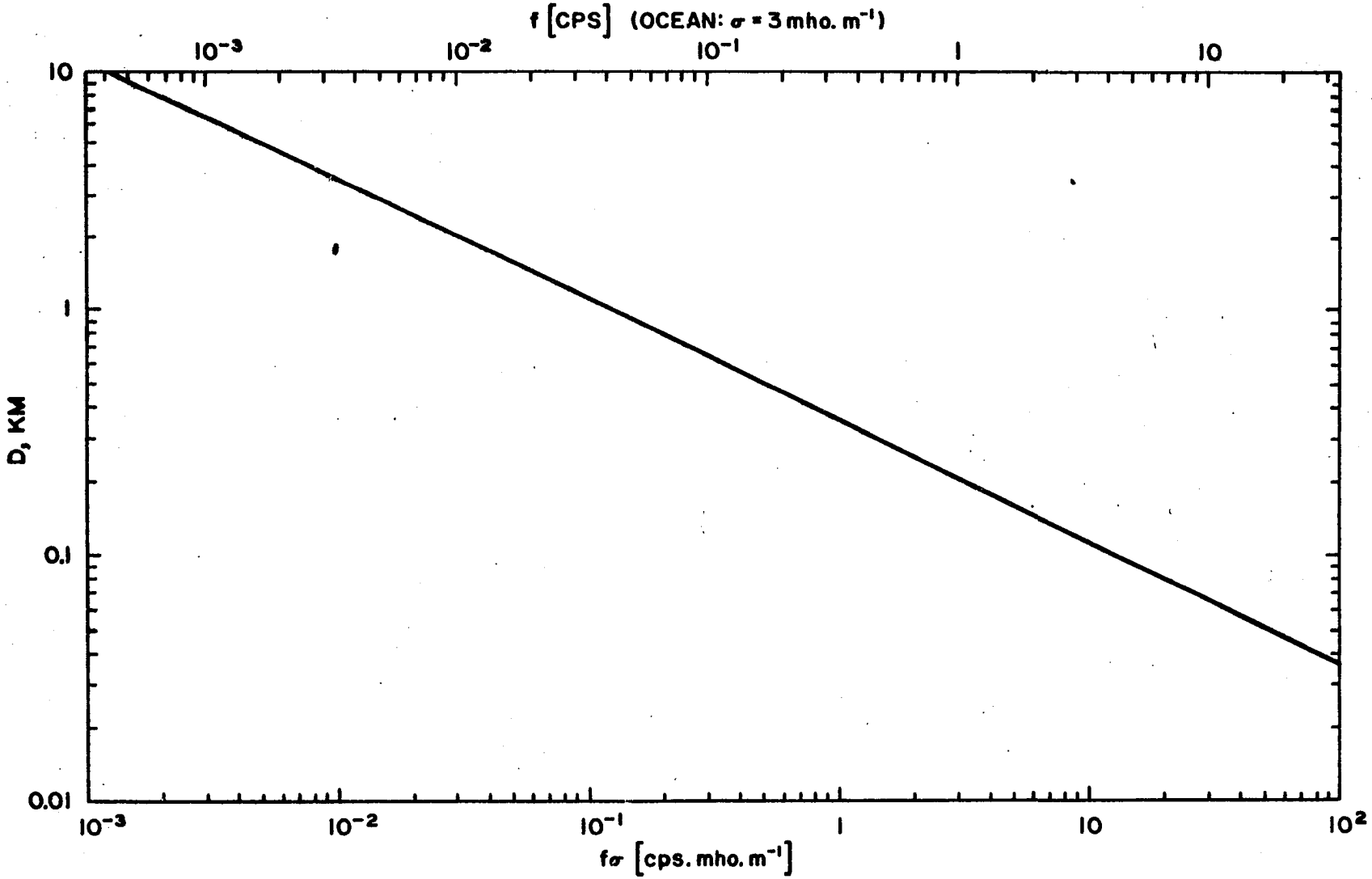

Fig. 3.1 Penetration depth $D = \eta^{-1} = (\mu_o \omega \sigma)^{-\frac{1}{2}}$ as a function of $(f\sigma)$, with the specific frequency dependence f, for the ocean, assuming $\sigma_{sea} = 3$ mho. $m.^{-1}$.

To see this, consider Snell's law of refraction for electromagnetic waves in conductive media. If θ_o, k_o represent the vertical incident angle and propagation constant in air, and θ_1, k_1 represent the complex refracted angle and complex propagation constant in the ground, then

$$\sin \theta_1 = \frac{k_o}{k_1} \sin \theta_o$$

For a good conductor the true angle of refraction ψ (defined for the normal to the planes of constant phase) is given approximately (Stratton, 1941, §9.8) by

$$\sin \psi \approx \sqrt{\frac{2\omega\varepsilon_o}{\sigma}} \sin \theta_o$$

Since $\varepsilon_o \sim 10^{-11}$ farad m^{-1}, while $\sigma \gtrsim 10^{-8}$ mho m^{-1} (usually several factors of 10 greater), the refracted angle differs insignificantly from the vertical under most conditions, even at grazing incidence.

Thus the refracted wave within the sea or land can be treated as propagating normally downward from the surface even if there are plane waves incident at a variety of angles. In other words, the medium "sees" the incoming waves as essentially normal to the surface. However, the reflected airwave depends on the angle of incidence, and the surface values of the fields are governed by the continuity relations between the internal and external fields. Since the external field (incident, reflected, and return wave refractions into the atmosphere) will be dependent on the incident angle, there may in fact be a dependence of the surface field on this angle.

This point seems to have been overlooked until Dosso and Lokken (1961) and Dosso (1962, 1965) made some calculations for single, double, and triple-layered plane media. They found that only the magnetic field in the plane of incidence and the electric field normal to the plane are independent of the angle. The orthogonal horizontal components both peak at normal incidence, falling to zero at grazing incidence. The vertical H_z component peaks between 45° and 60° incidence. Usually the fields are dependent on frequency and conductivity.

3.2 The Cagniard-Tikhonov Problem: The Plane-Layered Half-Space

3.2.1 Possible Approaches

The most extensively investigated magnetotelluric problem is probably that in which several layers of differently conducting rock formations lie in horizontal strata. This is perhaps the simplest case to handle mathematically, and is also of great importance to the geophysical prospector, since it provides the "first approximation" to his analysis of the underlying strata.

Some assumption must be made concerning the source of the electromagnetic radiation incident on the earth, and the assumption has caused considerable argument in the literature. Three possible cases have been considered:

(i) Plane-waves, resulting from sources of dimensions considerably larger than those with which the observer is concerned;

(ii) Line current sources, such as occur, for instance, near the auroral or equatorial electrojets;

(iii) Dipole sources, of very localized nature.

We will be concerned with the first of these but the other cases are mentioned in §3.2.4. We note three books which are devoted to the study of wave propagation in stratified media, and which include some aspects of the studies described below: Brekhovskikh (1957, 1960), Wait (1962 b) and Banos (1965).

3.2.2 The Plane Wave Treatment

Magnetotelluric theory is basically a study of the relationship between variations in the horizontal components of the electric and magnetic fields at the earth's surface, and its bearing on the surrounding terrain. Tikhonov (1950) realized this connection and showed that at low frequencies ωH_i (i.e. the time derivative of the H_i-component) is proportional to the orthogonal telluric component E_j, a fact already known experimentally. He pointed out that knowledge of the coefficient of proportionality allows determination of the depth of the upper conductive layer of the earth's crust, while further knowledge of the phase relation would determine the conductivity. His work was later extended, and used with field data, by Tikhonov and Lipskaya (1952) and Lipskaya (1953), in connection with two-layered media.

Kato and Kikuchi (1950 a,b; see also Kato and Yokoto, 1953), realized that departures from 45° of the phase relation between the magnetic and electric field could be explained by treating

the medium as double-layered. Like Tikhonov, they examined the conductivity of the earth's crust at considerable depths. Rikitake (1950 a,b,c; 1951 a,b,c) also realized the connection between the fields and the electrical properties of the earth's crust.

All of these writers were concerned with the study of the earth's interior. However,Cagniard (1953 a,b) published the results of his extensive work in applying the theory to geophysical prospecting over plane multi-layered media, and together with the Russian counterpart to his paper by Tikhonov and Shakhsuvarov (1956), triggered off an enormous number of both experimental and theoretical investigations. The technique is now well established in various forms, particularly in Russia and France.

The subject was further extended and generalized by Lipskaya and Troitskaya (1955) and Sheinman (1958), and comprehensive summaries of the theory have been given by Berdichevskii and Bryunelli (1959), Berdichevskii (1960), and Wait (1962a). All of these investigations assumed plane wave incident on a plane stratified earth. Scholte and Veldkamp (1955) studied the influence of the earth's curvature and concluded that it would not affect the E/H ratios greatly, although this was not true for the H_z/H ratio. Wait (1962a) and Srivastava (1965 b, 1966) reached similar conclusions.

Bondarenko (1953 a,b) showed that the induced earth currents could cause phase effects in magnetic micropulsations.

The investigations in applied geophysics have all been concerned with determining the surface impedance of the magnetotelluric fields,

(see §3.1.6). The impedance of a two-layered medium, with an upper layer of conductivity σ_1, and depth h, and a lower infinitely deep layer of conductivity σ_2 is:

$$Z = \frac{E_i}{H_j} = \sqrt{\frac{-i\mu_o\omega}{\sigma_1}} \cdot \frac{1 + \varepsilon \tanh \sqrt{-i}\, \eta_1 h}{\varepsilon + \tanh \sqrt{-i}\, \eta_1 h} \tag{3.10}$$

Here the time dependence is taken as $e^{-i\omega t}$; $\varepsilon = \sqrt{\sigma_2/\sigma_1}$, the skin depth ratio; and $\eta_1 = \sqrt{\mu_o \omega \sigma_1}$, the parameter discussed in §3.1.8. For a homogeneous single-layered earth ($\varepsilon = 1$), relation (3.10) yields the well-known relation:

$$\frac{E_i}{H_j} = \sqrt{\frac{-i\mu_o\omega}{\sigma}} \tag{3.11}$$

There is a 45^o phase difference between the magnetic and telluric vectors, and an inverse dependence of E on $\sqrt{T\sigma}$. (Note that, if low frequencies are considered, we recover Tikhonov's (1950) result for a relatively shallow, highly conducting upper layer, by allowing $\sigma_1 \to o$. Then Z varies as T^{-1}.)

A frequency and layer dependent "apparent resistivity" is then defined (in mks units) by

$$\rho_A = \frac{|Z|^2}{2\pi\mu_o} T = 0.2T\, |Z|^2$$

where the units used in the later relation are E (mV/Km), H(γ), T(sec), ρ_A(ohm.m). Curves depicting the variation of apparent resistivity for various numbers of strata have been drawn up to assist in analysis of observational data (Cagniard, 1953; Berdichevskii, 1960; Wait, 1962 a). Similar curves for the phase behavior of Z are also given.

Many experimental studies of this method have been made (Niblett and Sayn-Wittgenstein, (1960); Vladimirov, (1960); Vladimirov and Kolmakov, (1960); Valdimirov et al, (1961 a,b); Bostick and Smith, (1961); Smith et al, (1961); Berdichevskii et al (1962); Srivastava et al, (1963); Srivastava and Jacobs, (1964)). Cagniard, in his 1953 papers, discussed the law of similitude in the interpretation of his curves and Rankin et al (1965), and Dosso (1966a) applied this to scale models. Model experiments for other geometries have also been made by Wescott and Hessler (1962) and Dosso (1966 d,f), (see §3.4).

Geophysical prospectors confine their studies to the electric fields within the earth. Duffus, Shand and their co-workers in Canada (see §2.6.2) considered the effect of a major conductivity change (notably the Pacific Ocean) on micropulsations in the magnetic field. Their results led Dosso and Lokken (1961) to study the magnetic field over a stratified-layer model similar to that of Cagniard. They assumed a simple conducting half-space and investigated the behavior of the field with angle of incidence and conductivity, as well as with the geological parameters ε and μ, and the polarization of the incoming wave. They particularly investigated the ratio of vertical ($|H_z|$) to total horizontal ($|H_x|^2 + |H_y|^2)^{\frac{1}{2}}$ fields, for frequencies between 10^{-3} and 10^6 cps., concentrating on the range 0.02 to 40 cps. They noted a dependence on the angle of incidence in the H_z and H_y components peaking between 45^o and 60^o for H_z. Here H_y represents the component in the plane of

incidence. The response of the vertical component was also quite sensitive to conductivity and frequency. The H_x component (normal to the plane of incidence), however, was constant with frequency, conductivity, and angle of incidence. Both horizontal components showed frequency and conductivity dependence at frequencies greater than 10^3 cps.

They noted that, at 1 cps, the computed ratio (R) of vertical to horizontal magnetic fields was about 10^{-3} of the ratios observed over land. However, their results showed that source direction, conductivity, and polarization of the incident wave are all highly significant factors at any particular frequency.

Dosso (1962) extended this study to a two-layered, plane earth, and concluded that, in addition to these factors, layer depth and conductivities are also highly significant in determining the behavior of the vertical magnetic field component. Amplitude, phase and frequency response are all affected, but he found no better agreement with observations, perhaps not surprisingly in view of the number of sensitive parameters involved. He pointed out that better agreement might be obtained with measurements over the sea, since it is a far more homogeneous medium.

Dosso (1965) made a further extension to a three-layered medium, including a calculation of the electric fields, and in (1966 b,c) extended the treatment to multi-layered media, again including the electric field.

3.2.3 The Source Controversy

Suppose we have a localized source of electromagnetic radiation, the source scale size being much smaller than the wave length λ of the emission. The positions (r) of an observer may be classified into three zones, depending on his location relative to the source:

(i) Near (static) zone: $r \ll \lambda$; the observer is relatively near the source. In this region the fields are quasi-static, changing harmonically with time, but otherwise essentially satisfying the conditions of static electric and magnetic theory.

(ii) Intermediate (induction) zone: $r \sim \lambda$; the observer is a wave-length or so from the source.

(iii) Far (radiation) zone: $r \gg \lambda$; the observer is remote from the source. The fields are transverse to the direction of propagation and behave as outgoing spherical waves.

For periods greater than about 10^{-3} sec the surface of the earth is certainly in the near field region for a localized ionospheric source and many studies of the geomagnetic field variations use the static field approximations (Price 1950, Ashour 1950, 1965 a,b, Ashour and Chapman, 1965). Likewise a large number of the "library" examples in telluric current prospecting have been computed using the greatly simplified mathematics of the two-dimensional static cases (see, for instance, Kunetz and Chastenet de Géry, 1956, 1961; Berdichevskii, 1960).

However, in general the electromagnetic fields are solutions of the complex Helmholtz equation (3.3); the static assumption reduces this to Laplace's equation, under the condition that

$$L^2 \mu_o \omega \sigma << 1 \qquad (3.12)$$

(here L is a scale distance for the problem involved). This will not be true at, for instance, micropulsation frequencies, with the conductivities of most terrestrial media (Table 3.1).

Cagniard, Tikhonov and their colleagues assumed that plane waves were normally incident on a plane earth, thus requiring the source to be of very great dimensions. Cagniard (1956) pointed out that telluric currents are often uniform over large areas, and that simultaneous recordings show similarity at widely separated observation points - such as France, North Africa, Madagascar, and Venezuela (see also his interchange of letters with Wait referenced below). Cagniard argued that, since the ionosphere is perhaps the most probable source of the magnetotelluric fields, the source is likely to be a current sheet of global dimensions. The radiation from such a source would certainly resemble a normally incident plane wave, uniform over a small region. This global distribution is not necessarily true at micropulsation frequencies, however, which may be due to quite localized sources (see §2.2.5). A discussion of the source origins has been given by Wait (1962a).

Shortly after Cagniard published his 1953 paper, oriented towards geophysical prospecting, Wait (1954a) pointed out some of the limitations imposed by his assumptions. An exchange of views between

Cagniard and Wait followed the paper. Wait pointed out that the plane wave solution (really based on a "separation of variables" solution of the partial differential equation) must include all the spatial harmonics; a plane wave spectrum must be used. He considered a plane uniform medium; the surface magnetic field component is (using mks rationalized units and $e^{-i\omega t}$ time dependence):

$$H_x(x,y,z) = \int_{-\infty}^{\infty}\int_{-\infty}^{\infty} f(k_1, k_2)\, e^{i(k_1 x + k_2 y + k_3 z)}\, \frac{k_1}{k}\, dk_1 dk_2$$

Here $f(k_1, k_2)$ is the "aperture distribution function" (actually the separation constant) for each harmonic component, and

$k^2 = k_1^2 + k_2^2 + k_3^2 = i\mu_o\omega\sigma + \mu_o\varepsilon\omega^2$ is the general propagation constant.*

Using Maxwell's equations at the surface $z = 0$ with $H_z = 0$, and replacing $\partial/\partial z$ by $ik_3 = ik\,(1 - (k_1^2 + k_2^2)/k^2)^{\frac{1}{2}}$, expanded as a series, he then obtained the expressions for E_y and, similarly, for E_x, at the surface $z = 0$, following Monteath (1951):

$$E_y = -\frac{\mu_o\omega}{k}\left\{H_x + \frac{1}{2k^2}\left(\frac{\partial^2 H_x}{\partial x^2} - \frac{\partial^2 H_x}{\partial y^2} + 2\frac{\partial^2 H_y}{\partial x \partial y}\right) + 0\left(\frac{1}{k^4}\right)\right\}$$

$$E_x = \frac{\mu_o\omega}{k}\left\{H_y + \frac{1}{2k^2}\left(\frac{\partial^2 H_y}{\partial x^2} - \frac{\partial^2 H_y}{\partial y^2} + 2\frac{\partial^2 H_x}{\partial x \partial y}\right) + 0\left(\frac{1}{k^4}\right)\right\} \qquad (3.13)$$

(see also Wait and Surtees, 1954).

---

* Note: there is an error in Wait's paper in the specification of k^2

Cagniard's relation

$$Z = \frac{E_y}{H_x} = -\frac{E_x}{H_y} = \frac{i\mu_o\omega}{k}$$

then follows if we assume the surface H-components vary sufficiently slowly in space that the derivatives higher than the first are negligible. Alternatively k may be large (i.e. the conductivity or frequency is high). If L represents a scale length over which the surface H-fields do not greatly vary, then

$$L << |k|^{-1}$$

That is, at frequencies satisfying (3.2) the displacement currents are negligible, and

$$L << (\mu_o\omega\sigma)^{-\frac{1}{2}} = \eta^{-1} \qquad (3.14)$$

Thus Cagniard's treatment is valid only if the magnetic fields are constant over a horizontal distance equivalent to the penetration depth of the underlying medium (see Fig. 3.1). For ground of conductivity 10^{-3} mho m^{-1} at 0.1 cps, the fields should be constant over a distance of 35 km; over the ocean, however, the distance is less than 1 km.

Price (1962, see also 1964, 1965) noticed that the magnetotelluric method apparently made it possible to use data from one station only, at different frequencies, to infer a conductivity-depth relationship. This suggests that the influence of the source field distribution might be significant. Wait had assumed a homogeneous half-plane in his criticism of Cagniard's assumptions, but Price pointed

out that if the conductivity were depth dependent, even an inducing field of global scale cannot be ignored. He assumed a similar geometry to Wait but allowed $\sigma = \sigma(z)$. He took the solution of the $\underset{\sim}{E}$ equation (3.3) in the form

$$\underset{\sim}{E} = e^{-i\omega t}\, Z(z)\, \underset{\sim}{F}(x,y)$$

with $$\underset{\sim}{F}(x,y) = \left(\frac{\partial P}{\partial y};\ -\frac{\partial P}{\partial x};\ 0\right)$$

$$\frac{\partial^2 P}{\partial x^2} + \frac{\partial^2 P}{\partial y^2} + \nu^2 P = 0 \quad ; \quad \frac{\partial^2 Z}{\partial z^2} + (i\eta^2(z) - \nu^2)\, Z = 0$$

Here P represents the magnetic potential dependence on the surface coordinates x and y. He then deduced that for a single value of the separation constant ν, the magnetic field is

$$i\omega\mu_o \underset{\sim}{H} = e^{-i\omega t}\left(\frac{dZ}{dz}\frac{\partial P}{\partial x};\ \frac{dZ}{dz}\frac{\partial P}{\partial y};\ \nu^2 ZP\right)$$

The surface impedance is

$$-\frac{Z(o)}{(\partial Z/\partial z)_o} \tag{3.15}$$

which is dependent on ν, where ν^{-1} is a measure of the horizontal scale of the source field. This treatment was an extension of an earlier paper, Price (1950).

Cagniard's treatment is equivalent to $\nu = 0$, $P = y$, corresponding to a uniform, oscillating, <u>total</u> field (induced plus inducing), parallel to the conductor.

In the solution for a single value of ν, the $\underset{\sim}{E}$ and $\underset{\sim}{H}$ fields are orthogonal, but this is not necessarily true when all ν are

taken into account. The non-orthogonality is governed by the inducing field, and if the band-width of ν is small (as is probably the case in most geomagnetic fluctuations with a globally defined period) approximate orthogonality will hold. The limiting extremes of ν^{-1} are $(10^2, 10^4)$ km, governed by the earth's circumference and the height of the ionosphere.

For a two-layered medium, where the lower one ($z > D$) is non-conducting, Price's solution is:

$$-\frac{E_x}{i\mu_o\omega H_y} = \frac{\theta+\nu+(\theta-\nu)e^{-2\theta D}}{\theta\{\theta+\nu-(\theta-\nu)e^{-2\theta D}\}} \qquad (3.16)$$

where

$$\theta = \{\left[\sqrt{\eta^4+\nu^4} + \nu^2\right]^{\frac{1}{2}} - i\left[\sqrt{\eta^4+\nu^4} - \nu^2\right]^{\frac{1}{2}}\}/\sqrt{2}$$

The two special cases of Cagniard and Wait follow from this:

(i) Cagniard's solution: $\nu = 0$

$$\frac{E_x}{-i\mu_o\omega H_y} = \frac{1 + e^{-2D\theta_o}}{\theta_o\,(1 - e^{-2D\theta_o})}$$

where $\theta_o = \sqrt{-i\mu_o\omega\sigma}$; $\mathrm{Re}\ \sqrt{-i} > 0$

Then $\frac{E_x}{H_y} \approx \frac{1}{D\sigma}$ where $|D\theta_o| \ll 1$

This last condition is equivalent to specifying the thickness of the conducting medium as much less than its own penetration depth $\eta^{-1} = |\theta_o|^{-1}$.

(ii) Wait's solution: $\nu = \infty$, $D = \infty$

$$\frac{E_x}{-i\mu_o \omega H_y} = \frac{1}{\theta}$$

or for small values of the parameter ν

$$\frac{E_x}{H_y} \approx \sqrt{\frac{-i\omega}{\mu_o \sigma}} \left(1 + \frac{\nu^2}{2i\mu_o \omega \sigma}\right)$$

Price's solution (3.16) is shown in Fig. 3.2 for the case $\sigma f = 10^{-5}$ mho m.$^{-1}$ sec^{-1}, for several values of the depth D and the wave number $\lambda = 2\pi/\nu$. Figures 3.2(a) and (b) show the amplitude $|E_x/\mu_o \omega H_y|$ as functions of ν (or λ) and D respectively, while Fig. 3.2 (c) shows the phase difference as a function of D. As Price used emu in his development, the ordinate in the magnitude relations is presented as ($E_x/\omega H_y$ emu) and the values of ν are in cm^{-1}. He also used a harmonic time dependence $e^{+i\omega t}$, so that his phase curves are 180° out of phase with the development above in mks rationalized units and $e^{-i\omega t}$ time dependence. Price's numerical results may be extended by observing that $\sqrt{\sigma f}\, D$ and $\sqrt{\sigma f}\, \lambda$ are invariant.

From Price's curves, it is evident that Wait's correction ($D = \infty$) is unimportant for fairly localized sources ($\lambda < 600$ km), but that for D < about 10 km the source field correction is important for <u>all</u> geomagnetic fluctuations, even those having a source of global distribution. Price concluded that Cagniard's results give the approximate value of E_x/H_y over a limited region of the surface if the source field is of much greater extent and the total vertical

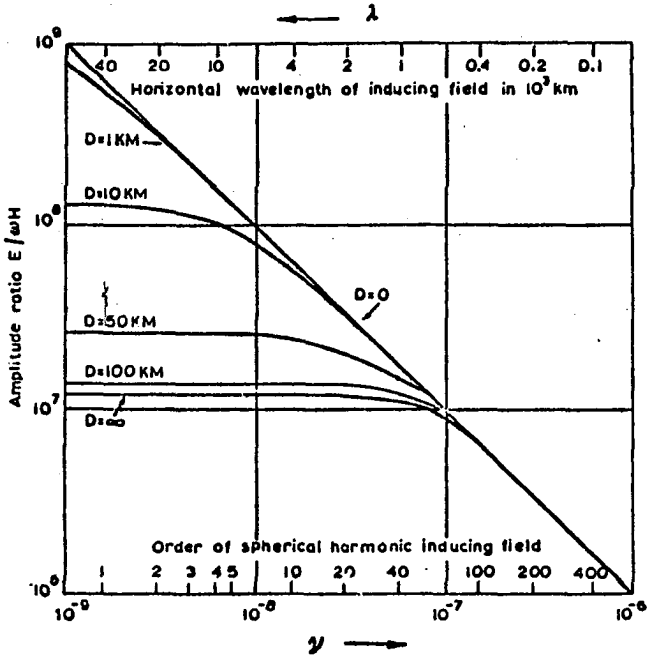

(a)

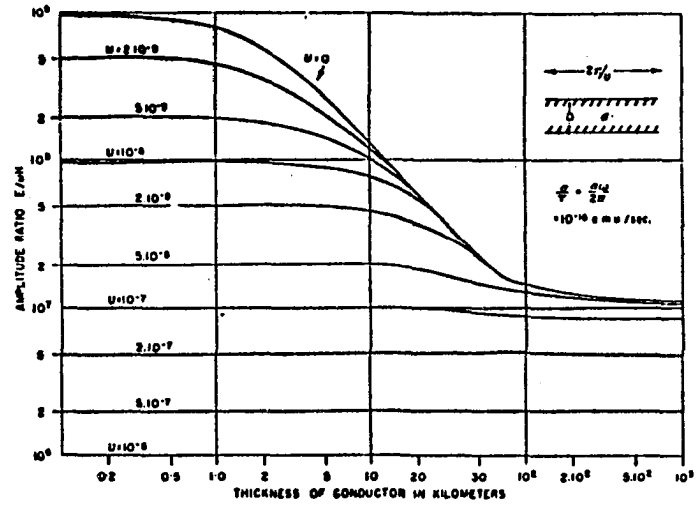

(b)

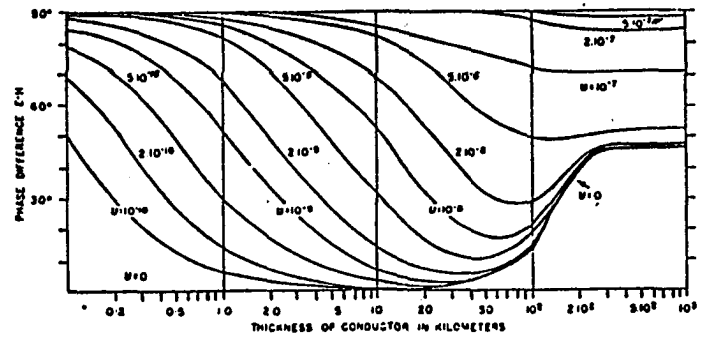

(c)

Fig. 3.2 Behavior of E/H over a conductor, underlain by a non-conductor, after Price (1962). $\sigma f = 10^{-5}$ mho. m.$^{-1}$ sec^{-1} (a) variation of amplitude with source size parameter ν or wave length λ, for various thicknesses D, (b) variation of amplitude with thickness D for various source sizes (ν). (c) variation of phase with thickness D for various source sizes (ν).

Note: Price's curves are given for emu, ν in cm^{-1}, time dependence $e^{+i\omega t}$

magnetic field is very small. However, he warned against attempting to use magnetotelluric methods to determine the conductivity at great depths within the earth's interior, without taking into account the distribution of the horizontal magnetic field over the earth. Wait (1954a, 1962a) pointed out that the influence of the source field is not as serious when the underlying substratum is highly conducting. Rikitake (1966) computed curves similar to Price's (Fig. 3.2a) for this case by idealizing the lower layer to a perfect conductor. His results indicate that only quite localized sources cause any correction.

Quon (1963) has further discussed the importance of the source field in magnetotelluric prospecting. He presented several curves of apparent resistivity, calculated for various cases according to the theories of Cagniard and Price, and for a dipole source.

Ward and Morrison (1966) have criticized the analysis of records from Tikhaya Bay, USSR, by Hoffman and Horton (1966). They point out that Wait (1962a) and Madden and Nelson (1964) have defined a critical distance over which the observed fields should be uniform. In all three of these papers this distance is computed. The criteria used are that the change in apparent resistivity must be less than a certain quantity at a given frequency (within 10% for Wait, and Ward and Morrison, 20% for Madden and Nelson). In general the longer the period the greater the scale distance.

Madden and Nelson (1964) have examined the assumptions underlying Cagniard's theory. They consider the case used by Price

(that of a good conductor overlying a poor conductor) to be physically unrealistic in application to magnetotelluric studies over most land areas, and find that Cagniard's assumptions are usually valid in practice. They consider the changes in conductivity in the horizontal direction to be of more importance and attribute many of the apparent inconsistencies in observed data to such variations.

Srivastava (1965 a,b) studied various conductivity models (two and three-layered) to examine the source effect, and concluded that for periods of less than 10^4 sec. with a moderate conductivity distribution in "shallow" regions (10-20 km), the effect of the source would be negligible.

Weaver (1964a) computed the total magnetic field for a general inducing field, under the low frequency conditions (3.2) and (3.17). He assumed the source to be some system of ionospheric currents anywhere in the region $z \leq -h < 0$, above the earth's surface $z = 0$. The field above the earth's surface is then derivable from a Laplace potential Ω comprising an internal part Ω_i and an external part Ω_e. For a given source distribution, Ω_e is known. For a plane two-layered medium $0 < z < d < \infty$, with conductivities σ_1 and σ_2 respectively, the Cartesian components of the field satisfy the complex scalar Helmholtz equation derivable from (3.3). This may be solved by applying a double Fourier transform in the horizontal variables x, y and applying the boundary conditions of §3.1.1 at each interface. He obtained the three components as double integrals, and showed that they reduce to Price's (1950) expressions under the appropriate conditions. He

treated fields with rotational symmetry, and two-dimensional fields, including dipole and line-current sources, as special cases.

He pointed out that a simple extension to aperiodic fields may be made by using Laplace transforms in place of Fourier transforms.

Nishida (1962, 1964) and Weaver (1963 b) have pointed out an objection to the neglect of displacement currents in the non-conducting atmosphere, an approximation made in deriving the magnetic field from potential solutions. The displacement currents may be neglected if the dimensions of the region are much smaller than the wavelength of the radiation. In our case, if the source is assumed to be the ionosphere at height h, the near and induction fields must dominate the radiation field. Thus, a further condition to (3.2) is imposed on the frequency, viz.

$$\omega << \frac{c}{h} \tag{3.17}$$

For a source height of 100 km, the frequencies must be much less than about 500 cps, certainly valid for most geomagnetic applications.

3.2.4 Other Sources

A large number of papers have been written considering the fields produced by line-current (cylindrical wave) and dipole (spherical wave) sources. We mention a few of them briefly.

Price (1950), in his study of induction in a homogeneous conductor, considered the special case of an oscillating line current as an example. Wait (1954b) briefly reviewed several earlier studies

and further considered the multi-layered case. Law and Fannin (1961) returned to the case of the homogeneous earth, and treated the radiation from a current filament with respect to micropulsations. For a source height of 200 km, angular frequencies of 0.3 rad sec^{-1} and conductivity of 1.25×10^{-4} mho m^{-1}, they found the vertical magnetic field could be up to 50% of the horizontal field, within the observed frequency range. They also found the apparent surface impedance differed by only 10% in amplitude and 8^{o} in phase from the impedance calculated from plane waves. Weaver (1961) extended this treatment by considering a cylindrical earth, and found a favorable comparison with the results of Law and Fannin. These were extended by Dosso (1966e) who found that all the field components were strongly dependent on source distance. The vertical magnetic and horizontal electric fields, and also the impedance, were strongly dependent on frequency, conductivity, and source height, but the horizontal magnetic field was fairly insensitive to these. Evidence of line current sources has been suggested, for instance, by Horton (1965).

The study of dipole sources has a long history, most of it referring to radio frequencies. Quon (1963) gave an extensive historical review. Wait (1951) and Slichter (1950) both considered two-layered plane media, and treated magnetic dipole sources from the geophysical prospecting aspect. Bhattacharyya (1955) extended Price's (1950) work to a two-layered earth for a magnetic dipole at the surface and (1956) considered artificially induced dipole transients (see also Bhattacharyya, 1959, 1963).

Bomke (1962) reported micropulsation observations which he interpreted as originating from dipole sources. Quon (1963) considered the surface fields from both horizontally and vertically oriented electric and magnetic dipole fields, over a two-layered earth, and derived expressions for them. He compared the apparent resistivity curves calculated from his results and from Cagniard's and Price's theories. Wait has published extensively on the subject of dipole fields over a plane earth (Quon noted some 25 of his works between 1951 and 1962)*. His researches are collected in his book (Wait, 1962 b; see also Wait, 1958, 1959). The book by Baños (1965) is also devoted to a study of dipole radiations.

The general studies of Weaver (1964a) and Price (1962) also include these sources as special cases.

3.2.5 Application to Electromagnetic Fields Over an Ocean

One of the applications to which the magnetotelluric theory of a plane multi-layered earth has been put is the estimation of the "ocean-effect" - the effect which the highly conducting ocean has on the magnetic and telluric fields at various frequencies (cf. §2.6.1).

Fonarev (1961a) assumed a two-layered geometry and concluded that the electric fields in the ocean would be increased at decreasing depth. He estimated the fields for a sea of 1 km depth, for magnetic variations with periods from 20 sec to several hours, and showed

* A study of dipole sources over an inclined fault has been published recently by Schlak and Wait (1967).

that the effect of the basement conductivity is important in assessing the behavior of the fields. Figure 2.1 (a) depicts the calculated effect (from Fonarev, 1961c).

Fonarev (1961b) also considered a three-layered case, the lower layer being infinitely deep and perfectly conducting (to simulate the mantle), the other two having conductivities σ_1 and σ_2 and thicknesses h_1 and h_2, respectively. The calculations were carried out for long-period variations (3, 6, 12, 24 hours) for an ocean of depth h_1 = 5 km, and two different crustal conditions. He concluded that the oceanic electric current density would be greatly enhanced in comparison with the land currents and that the phases were very sensitive to the parameters of the upper layers.

Price (1962), corrected by McCann and Price (1965), applied his study of the effect of the source size to magnetotelluric measurements at sea. He concluded that the source field could be ignored for seas deeper than 200 m and periods less than about 100 sec. The Cagniard treatment was then valid. For periods up to one day and oceanic depths of 5 km or more, Cagniard's relations would be valid for source dimensions greater than about 3.10^4 km, i.e. sources of global dimensions. The minimum source dimensions fall almost linearly with decreasing period, and Cagniard's relations are then valid for periods up to a day, for sufficiently large sources. The sphericity of the earth has little influence, but Price pointed out that the finite extent of the oceans is probably important.

Swift and Hessler (1964) applied Price's theory to calculate the ratios H/E for several source sizes (L = 10^2, 10^3, 10^4 km), with depths ranging from 100 m to 6 km, periods between 0.1 sec and 29 hours, and an assumed basement conductivity of 2.10^{-3} mho $m.^{-1}$ (see Figure 3.3). A similar calculation was also made by Rokityanskii (1963), based on the Cagniard-Tikhonov theory. He gave the relationship of impedance (E/H) to period (T) at Mirny and Chernomorsk (N. W. Crimea) based on one, two, and three-layered geometries. Swift and Hessler noted that the high and low-frequency asymptotic solutions represent the homogeneous case of an infinitely deep ocean, and Tikhonov's (1950) result, respectively. The high frequency limit is a $\frac{3\pi}{4}$ phase difference with E/H varying as $\sqrt{\omega/\sigma}$; the low frequency limit is a 90^{o}-phase-difference with E/H proportional to ω and L. They found the observed E/H ratio to be nearly independent of frequency between periods of 1 min and 1 hour (see §2.6.1). With their assumed basement conductivity, this response implies a very large source distribution. Two factors may also contribute to the discrepancy from the true depth in their depth calculations: first, a sloping ocean floor, not allowed for in Cagniard's or Price's theories, and second the unknown conductivity ratio between sea and basement.

Price (1965) pointed out that the penetration of the electric and magnetic fields into a multi-layered medium is reduced from the simple skin-depth estimate for a single-layered medium (§3.1.8). For an ocean of depth D, the depth variation of the electric fields and induced currents is

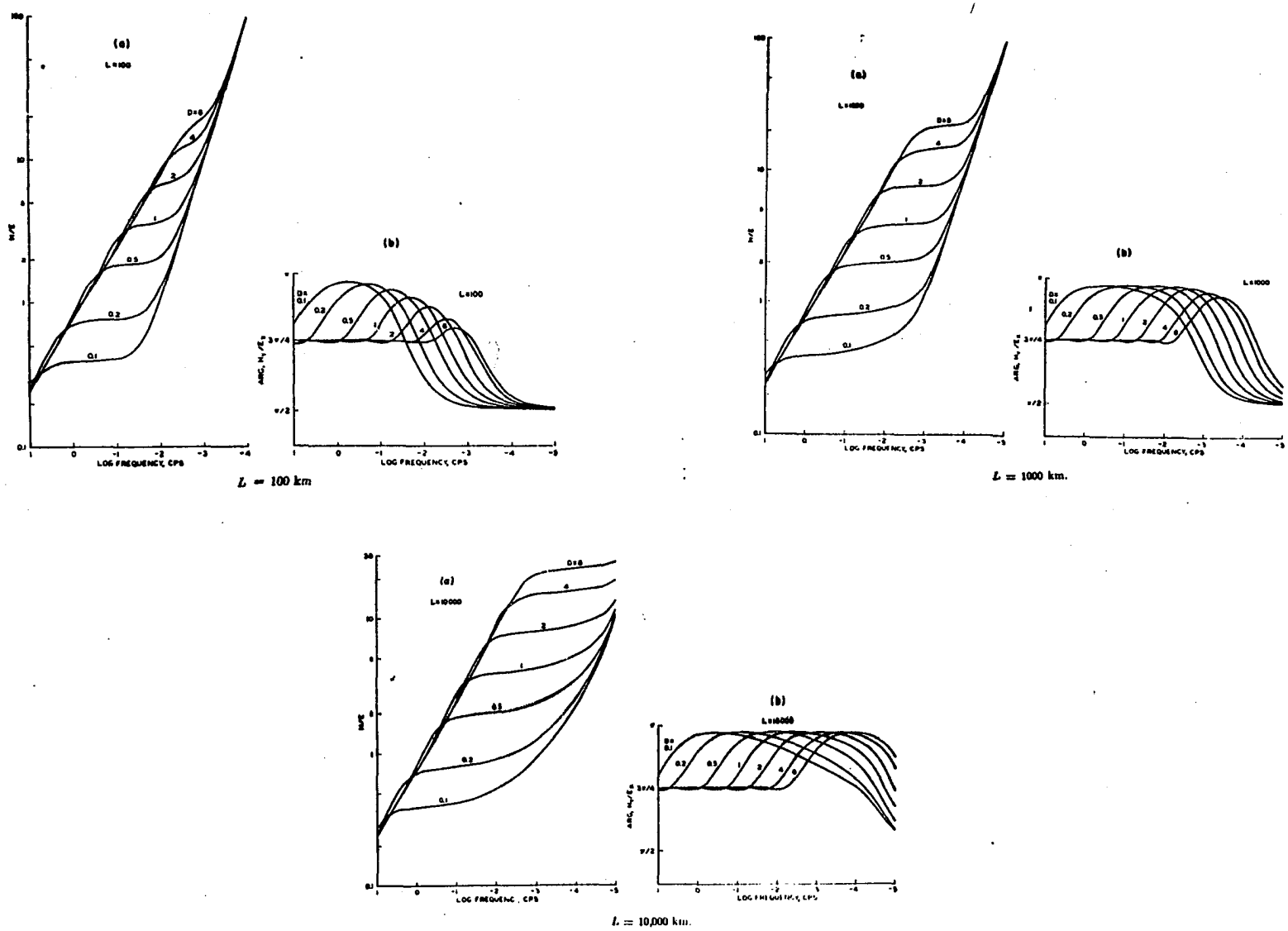

Fig. 3.3 H/E ratio for a two-layered medium, for various source sizes, according to Price's theory (Swift and Hessler, 1964).

$$\frac{I(z)}{I(o)} = \frac{e^{-\theta z}\left[1 + \beta e^{-2\theta(D-z)}\right]}{1 + \beta e^{-2\theta D}} \tag{3.18}$$

where

$$\beta = \frac{\theta - \nu}{\theta + \nu}$$

$$\theta = \nu^2 - i\mu_o \omega\sigma$$

Here mks units and $e^{-i\omega t}$ time dependence are used, and $2\pi/\nu$ again defines a scale size of the source field. The horizontal magnetic fields fall off as:

$$\frac{H(z)}{H(o)} = \frac{e^{-\theta z}\left[1 - \beta e^{-2\theta(D-z)}\right]}{1 - \beta e^{-2\theta D}} \tag{3.19}$$

but the vertical magnetic fields fall off according to (3.18).

The horizontal component thus attenuates more rapidly with depth than the vertical magnetic field or electric fields and currents. The amplitude of the vertical component is only slightly attenuated even at the bottom of an ocean 2000 m deep, although it is already greatly reduced at the surface by the induced electric currents. The horizontal component, however, is increased at the surface by the induced currents.

3.2.6 Determination of the Internal Contribution to the Total Magnetic Field by Induced Currents.

The problem of determining the origin of the fluctuations in the geomagnetic field led several investigators (see Chapman and Bartels, 1940) to the techniques of spherical harmonic analysis, based on the potential representation of the field (see §2.1.1). After the various techniques of magnetic and geomagnetic prospecting

had been developed, this problem was studied to locate bodies of anomalous magnetic and conductive properties. A short review of several approaches has been given by Weaver (1964b).

Price (1965), Novysh and Fonarev (1963) and Fonarev and Ivanov (1966) have determined the contribution by the "ocean effect" to the total magnetic field for oceans of finite depth. Fonarev and his colleagues used the relation (converted to mks) proved in the last-mentioned paper, that:

$$H_T = \tfrac{1}{2}\sigma \int_0^h E(z)dz \qquad (3.20)$$

where H_T represents the internal contribution to the horizontal magnetic field from currents flowing between the surface $z = 0$ and depth $z = h$ of the sea. Their estimates (1963) were based on the assumption that the current density was constant with depth (see also §2.6.1). In their (1965) paper they extended this, and calculated that for a two-layer model:

$$\left|\frac{H_t}{H_o}\right|^2 = \frac{(k_1 + k_2)^2 + k_3^2 \tan^2 kh}{k^2 + k_3^2 + \tan^2 kh} \qquad (3.21)$$

where $k = \delta^{-1} = (\mu_o \omega\sigma/2)^{\frac{1}{2}}$.

$k_1 = \tanh kh + \epsilon$

$k_2 = -\epsilon/\cos kh \cosh kh$

$k_3 = 1 + \epsilon \tanh kh$

$\epsilon = \sqrt{\sigma_1/\sigma_2} < 1$ for a finitely deep ocean.

The induction contribution at the surface will be equal to the primary field (ie. a two-fold enhancement of the horizontal field) at short periods. Some results of the computation are given in Fig. 2.1.

Price (1965) extended his (1950) work and gave the contributions to both the horizontal and vertical components of the surface magnetic field, for a two-layered case. He allowed for the source size, but assumed a non-conducting basement and found that:

$$\frac{H_1}{H_o} = -\frac{Z_1}{Z_o} = \frac{\beta(1-e^{-2\theta D})}{1-\beta^2 e^{-2\theta D}} \qquad (3.22)$$

where (H_o, Z_o) refer to the primary inducing field, (H_1, Z_1) to the induced component, and β, θ, ν are defined as for eq. (3.18). Price calculated these relations for an inducing field of scale length $(2\pi/\nu)$ 1000 km, period 1000 sec and conductivity 4 mho $m.^{-1}$. The results show the vertical component to be nearly extinguished, but the horizontal component nearly doubled; the phases are not greatly different, however. Agreement with Zhigalov's (1960) results is not exact, probably due to a combination of the several unknown factors (source size, sloping floor, base conductivity, finite area of ocean, etc.). However, Price concluded that Zhigalov's results were adequately explained by ocean induction.

Over land areas, Price calculated that induction effects predominate at periods $\sim$ 1 sec, except for very limited sources. At periods $\sim 10^3$ sec, the importance of induction is critically dependent on the source size.

3.3 Non-Horizontal Layers and Non-Uniform Media

Several other types of interface problems have been studied. These fall into three classes: firstly, layers with non-planar interfaces, secondly, homogeneous media with anisotropic conductivities, and finally, particular subterranean features which have electrical properties markedly different from their surroundings.

3.3.1 Sinusoidal Interfaces

Mann (1964) examined the magnetotelluric field in a two-layered earth where the boundary between the layers was sinusoidal in the y-z plane. He assumed plane waves were incident vertically on a plane air-earth interface and considered the two polarizations (see §3.4.2). He used a Fourier transform technique, similar to that developed by Weaver (1964a), to solve the scalar Helmholtz equations for the field components by reducing them to ordinary differential equations in the vertical coordinate z. In contrast to the plane-interface case, he found the impedances E_x/H_y and E_y/H_x unequal, although the difference is usually small. He also found a vertical magnetic field associated with the former impedance, again in contrast to the Cagniard-Tikhonov problem.

Rikitake (1965) considered a semi-infinite perfect conductor with a sinusoidal surface. He treated only the case where the incident magnetic field was polarized across the undulations and concluded that the horizontal field would be enhanced over the peaks and suppressed over the troughs of the surface variations. The vertical field would be anti-symmetrically distributed across the peak.

3.3.2 Continuously Anisotropic Media

According to the model treated by Cagniard and Tikhonov, the impedances obtained from the two sets of orthogonal surface fields should be the same. This conclusion however depends on the isotropy of the electrical conductivity in the various strata, even though the strata are actually in plane layers. In media which are either anisotropic or inhomogeneous (or both), this equality between the two impedances breaks down and the surface impedance must be considered a tensor.

Chetaev (1960) considered a homogeneous, but anisotropically conducting, semi-infinite medium, with orthogonal conductivities σ_t and σ_n along and normal to the bedding planes. He also assumed a tilt in the bedding plane, at angle α relative to the surface, and treated the electric field of the incident plane wave as polarized normal to the strike (y). Maxwell's equations then yield the expression for the horizontal magnetic field under $e^{-i\omega t}$ time dependence as

$$\lambda^2 \frac{\partial^2 H}{\partial y^2} + \frac{\partial^2 H}{\partial z^2} + i\mu_o \omega \sigma_t H = 0$$

$\lambda^2 = \sigma_t/\sigma_n$ is called the coefficient of anisotropy. The solution for H and therefore E, gives the surface impedance as

$$Z(y) = \frac{E_y}{H_x} = \sqrt{\frac{-i\mu_o \omega}{\sigma_t} [1 + (\lambda^2 - 1) \sin^2 \alpha]}$$

which reduces to the well-known result for an isotropic conductivity σ_t, when $\alpha = 0$.

Chetaev (1966) extended this result to the case of an anisotropic layer between depth h_1 and h_2, with a tilted bedding plane. The analysis naturally becomes very much more involved and he solved Maxwell's equations by introducing a generalized Lorentz condition such that the vector potential $\underset{\sim}{A}$ has only two components in a coordinate system oriented with the bedding planes:

$$\phi = - \frac{1}{\mu\sigma_t} \text{div } \underset{\sim}{A}$$

The solution was then obtained through a difference equation.

Barsukov and Zybin (1960) attempted to determine the anisotropic properties of a body by using the non-orthogonality of the E and H components. However Rokityanskii (1961) criticized their technique and examined the problem to determine the coefficient of anisotropy and the azimuth of the axis of anisotropy. He applied his analysis to the data obtained at Alushta in the Crimea, 1.5 km from the Black Sea (see §2.6.2).

Cantwell (1960) outlined procedures for determining the effects of anisotropy in either anisotropic or inhomogeneous structures. Bostick and Smith (1962) extended his work in an application to their observations in Texas, USA. Fournier (1963), Madden and Nelson (1964), and Mann (1965), also stress the importance of representing conductivity by a tensor relation when interpreting magnetotelluric field data.

Inhomogeneous media have also been treated by assuming an anisotropic conductivity, due to the inhomogeneity. Several of the above papers on magnetotelluric prospecting include this approach, and

Kovtun (1961) also used it in examining a basement fault overlain by a higher conducting layer of varying depth. The data from the Crimean coastal station Alushta at a period of 120 sec was used as an example. However, Wait (1962a) has criticized Kovtun's analysis.

3.3.3 Miscellaneous Discontinuities

Exploration geophysicists are interested in interpreting the magnetotelluric fields which arise when they are over some form of localized subterranean structure with a different conductivity. Such structures, occurring on ocean beds as well as underground, may cause noticeable effects on the surface fields. This problem becomes exceedingly difficult to treat mathematically in even the simplest cases; most of these have been considered only in the limit of steady current flow. In particular, induction in the presence of cylindrical bodies has been applied to conductivity anomalies in Central Europe and Northern Canada. Weaver (1964b) and Rikitake (1966) summarized the work of Hartmann, Kertz, Siebert and Scheube in Germany: see also Schmucker (1959) and Kertz (1960). Rikitake and Whitham (1964), Whitham and Anderson (1966) have discussed the Canadian anomaly in terms of circular and cylindrical cross-sections. Wait (1960) and Parasnis (1964a) have also discussed potential solutions over cylindrical bodies.

In cases where the geometry may be reduced to two dimensions, current flow around an "obstruction" can be treated with the powerful analytical tool of conformal mapping. Kunetz and Chastenet de Géry (1956, 1961) list a large number of solutions obtained in this way

and others are given by Berdichevskii (1960). These cases include a vertical fault overlain by a continuous uniform medium, a valley and anticlines of various shapes, undulations and buried anomalies, a water filled channel, and synclines and folds of various forms. Extensions to three dimensions have been made in a few cases. Utzmann and Favre (1957) studied the effect of a buried rectangular block, using model experiments and steady state currents. Wait (1960) considered buried spherical and spheroidal bodies.

Studies of frequency dependent cases have been made for several vertical discontinuities, but we defer the review of these to the next section. We mention here only the model experiments of Nagata et al (1955), Wescott and Hessler (1962), and Dosso (1966 a,d,f) for a number of geometries, and the study of Latka (1966) who treated a rectangular, buried anomaly using a numerical relaxation technique. Nabighian (1965) considered a semi-elliptical infinite channel.

3.4 Vertical Discontinuities and the Coast Effect

The effect of the ocean on the magnetic and telluric fields has been described from the observational viewpoint in §2.6. Several attempts have been made theoretically to understand the effect of an ocean on the magnetic and telluric fields; the models necessarily involve simplified geometries. The vertical discontinuity is one such model. The geophysical prospector is also interested in vertical interfaces, such as occur in faults and dykes, and much of the theoretical investigation has been made in this connection.

In this section, we also introduce certain basic concepts and nomenclature used in the succeeding chapters.

3.4.1 The Coast Effect Around an Ocean Basin

Early attempts were made by mathematicians, especially Lamb, to solve problems of current induction in electrically conducting discs. Bruckshaw (1936) and others experimentally investigated the induced fields in discs, in connection with telluric prospecting. Ashour (1950) again took up the study and mathematically treated induction in a uniformly conducting disc. He determined the distribution and also the free decay time of the electric currents. Application to an ocean of 1000 km radius and 5 km depth, for periods of 1 day in the inducing field, showed a magnitude increase in the currents near the edge. The decay time increased with both depth and radius, varying from 1/4 hour for a circular ocean of 1 km depth and 1000 km radius, to 6½ hours for a 5 km deep ocean of 5000 km radius.

DeWet (1949) calculated the induced currents at long periods in the great ocean basins, by conveniently approximating the continents, and allowing for the ocean depth distribution. Rikitake (1950a) also studied an ocean spanning 90° in meridian for currents induced by Sq variations.

All of these writers were concerned with variations of long periods. However, shorter period variations are also affected near a coastline and Rikitake and Yokoyama (1955) studied them for the magnetic anomaly in Japan. They treated a hemispherical shell of uniform conductivity, to represent a global ocean, and assumed an impulsive change in the external uniform magnetic field (simulating, for instance, a sudden commencement). They found that the induced

vertical magnetic field practically cancels the inducing one over the ocean, but enhances the vertical component over the land near the coast, to as much as 60% of the total field. They termed this the "coast effect".

In the same paper these authors also study a more local problem, represented by periodically repeating step-function changes in conductivity, the land and sea being of equal width. Price (1949) had developed the theory of induction in sheets and Rikitake and Yokoyama followed his treatment. They assumed time varying potentials for both inducing and induced fields and deduced current functions for the induced currents. The conductivity ratio between land and sea was approximated as both zero and infinite. They again found a coast effect on the vertical magnetic field, but the results of both analyses differ so significantly from the Japanese data that the anomaly in the magnetic records cannot be due only to the effect of the sea. See also Nagata et al (1955).

Rikitake (1960, 1961a, 1962) studied the global ocean effect on Sq and on impulsive magnetic changes (1961b). In this last paper, he concluded that Rikitake and Yokoyama overestimated the ocean's influence, because they neglected currents deep in the earth's conducting interior. Roden (1964) carried out a further study, at periods of 6, 8, 12 and 24 hours, for an ocean of 4000 km width, 5 km depth, represented by an infinitely long, plane sheet. He considered the mantle to be at a depth of 600 km. Roden's investigation was prompted by the observations of Hill and Mason (1962), who observed an

enhancement in the magnitude of diurnal magnetic variations over the edge of the continental shelf, at the southern end of the English Channel.

Roden also made a model experiment, using a copper sheet to simulate the ocean in the Japanese region. He pointed out the difficulty of determining the effective coastline for his model study, since the real ocean shelved gradually. He was unable to allow for this. Nabighian (1965) attempted to do so, by assuming an infinitely long, semi-elliptical cylinder. He treated micropulsation frequencies and assumed a plane wave of normal incidence.

Shuleykin (1958, 1960) studied the distribution of induced electric currents in a shallow, circular sea. He assumed a sufficiently low frequency that the displacement currents were negligible (see §3.1.2). He concluded that oscillations in the vertical component of the earth's magnetic field result in electric eddy currents directed along the shoreline, and markedly enhanced near the coast.

Ashour (1965 b,c) also considered the edge effect around a hemispherical ocean shell, when a uniform inducing field is applied in any direction. Rikitake and Yokoyama had considered this problem only when the inducing field is parallel to the ocean boundary; their solution is an approximation while Ashour's is exact. The electric current flow near the coast is greatly enhanced and reverses the direction of the vertical magnetic component on land and the horizontal component at sea.

All of these studies of the coast effect were made for a global or near-global ocean. A number of other studies of the coast effect have been made on a much smaller scale. Before mentioning these we digress to describe the mathematical approaches and boundary conditions which apply to the simplified mathematical models.

3.4.2 The Two "Polarization" Conditions of a Wave at an Interface

Some of the most useful models for theoretically treating vertical interfaces, consist of infinitely long, plane boundaries. An example of such a model is given in Fig. 3.4a, representing an infinitely long coastline. We specify a right-handed Cartesian coordinate system as in Fig. 3.4b. The z-axis is vertically downwards, and the x and y axes are located in the surface plane such that the y-axis is normal and the x-axis parallel to the coast. For convenience we sometimes refer to this model as the 'fault' geometry. The fault plane is then the plane $y = 0$, while the surface is the plane $z = 0$.

In dealing with the zero frequency limit of steady current flow, two independent situations are evident: the current flow may be either normal or parallel to the coastline. An arbitrary current flow will then resolve into some combination of these two cases.

In the wave case, where frequency is no longer ignored, two similarly independent situations may be considered. If we assume an arbitrarily oriented plane wave, incident normally on the surface, it may be resolved as shown in Fig. 3.5.

(a) $\underset{\sim}{E}$ parallel to the coast or strike, $\underset{\sim}{H}$ in the plane of incidence, and normal to the fault plane at incidence. We designate this case as $\underset{\sim}{E}$-polarization.

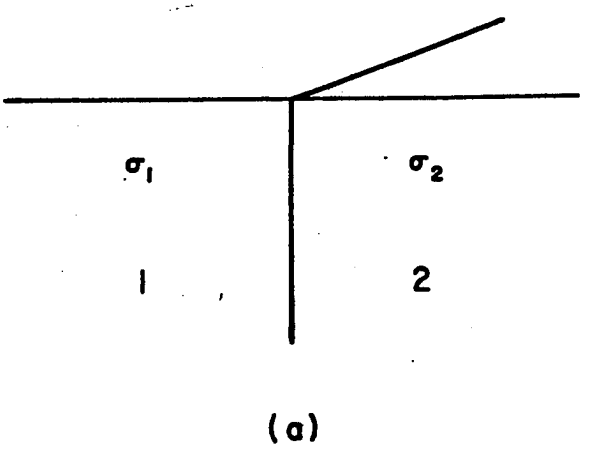

(a)

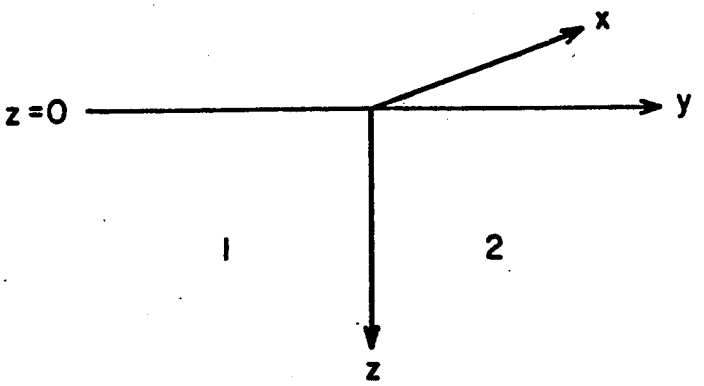

(b)

Fig. 3.4 (a) Model of a vertical fault
(b) Coordinate system

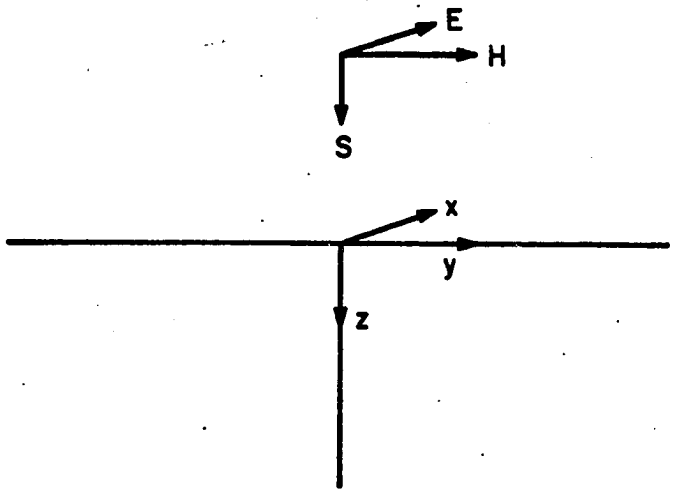

(a)

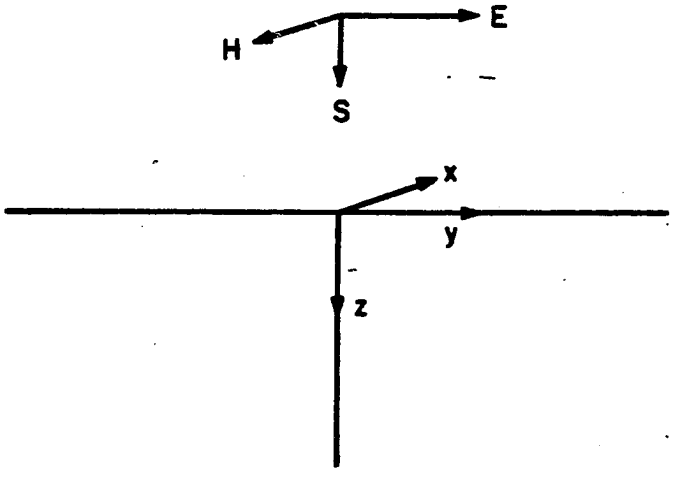

(b)

Fig. 3.5 (a) E-polarization
(b) H-polarization

(b) $\underset{\sim}{H}$ parallel to the coastline, $\underset{\sim}{E}$ in the plane of incidence, and normal to the fault at incidence. This case we term $\underset{\sim}{H}$-polarization.

We use these terms in preference to the designations "parallel" and "normal", to avoid the ambiguity. Some writers treat the discontinuity plane as the reference, others the "plane of incidence" of the wave -- the yz-plane (eg. Stratton, 1941; Berdichevskii, 1961).

Treating each case separately greatly simplifies Maxwell's equations. Since the geometry is "cylindrical", and there are no x gradients involved, the problem is now two dimensional.

(i) E-Polarization:

By definition the components of the $\underset{\sim}{E}$-field are

$$\underset{\sim}{E} = [E_x(y,z) \; ; \; 0 \; ; \; 0]$$

From Maxwell's relation for plane waves:

$$\text{curl } \underset{\sim}{E} = i\omega\mu_o \underset{\sim}{H}$$

we are also able to determine the components of the $\underset{\sim}{H}$-wave:

$$\left.\begin{aligned} H_x &= 0 \\ H_y &= H_y(y,z) = \frac{1}{i\omega\mu_o}\frac{\partial E_x}{\partial z} \\ H_z &= H_z(y,z) = -\frac{1}{i\omega\mu_o}\frac{\partial E_x}{\partial y} \end{aligned}\right\} \qquad (3.23)$$

The diffusion Helmholtz equation (3.3) in $\underset{\sim}{E}$ then reduces to a scalar equation in E_x.

$$\frac{\partial^2 E_x}{\partial y^2} + \frac{\partial^2 E_x}{\partial z^2} + i\eta^2 E_x = 0 \quad : \quad \eta^2 = \mu_o \omega \sigma \tag{3.24}$$

(ii) H-polarization:

Again by definition the $\underset{\sim}{H}$-field is given by

$$\underset{\sim}{H} = [+H_x(y,z);\ 0\ ;\ 0]$$

A negative sign must be introduced in the value of H_x to allow for the opposite orientations of H_x and the x-coordinate. From Maxwell's relation

$$\text{curl } \underset{\sim}{H} = \sigma \underset{\sim}{E} ,$$

the $\underset{\sim}{E}$-wave, has components:

$$\left.\begin{aligned} E_x &= 0 \\ E_y &= \frac{1}{\sigma}\frac{\partial H_x}{\partial z} \\ E_z &= -\frac{1}{\sigma}\frac{\partial H_x}{\partial y} \end{aligned}\right\} \tag{3.25}$$

and the vector Helmholtz equation (3.3) in $\underset{\sim}{H}$ becomes the scalar equation:

$$\frac{\partial^2 H_x}{\partial y^2} + \frac{\partial^2 H_x}{\partial z^2} + i\eta^2 H_x \quad ; \quad \eta^2 = \mu_o \omega \sigma \tag{3.26}$$

3.4.3 The Boundary Conditions at Vertical and Horizontal Interfaces

For steady current flow, the boundary conditions described in §3.1.1 reduce to

(a) $\sigma_1 E_{1n} = \sigma_2 E_{2n}$

(b) $E_{1t} = E_{2t}$

at any interface. When the current flow is normal to the interface (Fig. 3.4), there is a discontinuity in the electric field:

$$E_{1y} = \frac{\sigma_2}{\sigma_1} E_{2y}$$

Equivalently, the current is the same in each medium

$$J_{1y} = J_{2y}$$

If the current flow is parallel to the strike, the electric field is continuous across the boundary, while the current shows a change:

$$E_{1x} = E_{2x}$$

or

$$J_{1x} = \frac{\sigma_1}{\sigma_2} J_{2x}$$

This situation is illustrated in Figs. 4.1 and 5.2. All components of the magnetic fields always remain continuous.

For the wave case, we will apply the boundary conditions described in §3.1.1, to the vertical faults and horizontal planes used in the later chapters.

Weaver (1964a) reduced the general three-dimensional fields in each medium of a horizontally-layered earth by applying a

double Fourier transform (§3.2.3). He then used the exact boundary conditions of §3.1.1 to obtain the relationships between the fields in each medium. The field above the earth was specified by a magnetic potential. This exact approach yields mathematical difficulties when vertical discontinuities are involved, and to overcome them we use the result of §3.1.7. Following Weaver (1963a), we showed here that, for a plane wave incident on a layered earth, the total magnetic field at the surface is essentially independent of the underground conductivity structure, at least to a first order of approximation.

Let us assume a situation involving both a vertical interface (say the plane $y = 0$) and a horizontal interface ($z = h$), with the earth's surface at $z = 0$ (Fig. 4.2). For each of the two polarizations of the surface wave, there will be three sets of boundary conditions at (a) the vertical face, (b) the two horizontal planes, and (c) an infinite distance from any of the interfaces.

We term the region $y < 0$, medium 1, with conductivity σ_1; the region $y > 0$, we term medium 2, with conductivity σ_2. The underlying basement $z > h$, we designate medium 3, and assume it to be composed of some highly resistant material such as certain of the igneous and metamorphic rocks (see Table 3.1). Its conductivity is taken as $\sigma_3 = 0$. An electromagnetic wave will thus have an infinite penetration depth and, since we may assume the magnetic field variation to be zero at infinite depth, we may also take the horizontal magnetic field as zero at $z = h$. The continuity of the tangential

electric and magnetic fields provides a pair of independent boundary conditions at each interface. The resulting conditions are given in Table 3.2.

3.4.4 Dimensionless Parameters and their Physical Significance.

In problems which involve several physical dimensions, it is usually possible to reduce the number of independent variables by using a set of dimensionless parameters. A dimensionless quantity expresses a particular dimension in terms of a special system of units. In the cases considered here, we have as physical variables, conductivities σ_1, σ_2, frequency ω, basement depth h, dyke width ℓ, and the two-dimensional coordinates of the observation point (y,z). These may be combined in a variety of ways; we choose the following definitions as a basic set:

$$\varepsilon = \sqrt{\sigma_1/\sigma_2} = \eta_1/\eta_2$$

$$Q = \tfrac{1}{2}\ell \sqrt{\mu_o \omega \sigma_2} = \tfrac{1}{2}\ell\eta_2$$

$$H = h \sqrt{\mu_o \omega \sigma_2} = h\eta_2$$

$$Y = (|y|/\tfrac{1}{2}\ell) - 1$$

$$Y_i = y \sqrt{\mu_o \omega \sigma_1} = y\eta_i$$

In addition we define

$$\gamma = h/\tfrac{1}{2}\ell = H/Q$$

$$H_o = H/\pi$$

Various combinations of these are useful in expressing the behavior of the electromagnetic fields; their physical significance is given in Table 3.3.

Table 3.2

Summary of Boundary Conditions

	E-polarization	H-polarization
Components	E_x, H_y, H_z	H_x, E_y, E_z
Defining Equation	$(\nabla^2 + i\eta^2)\, E_x = 0$	$(\nabla^2 + i\eta^2)\, H_x = 0$
Connecting Relations	$\underset{\sim}{H} = \frac{1}{i\omega\mu_o}\left\{\hat{\xi}_y \frac{\partial E_x}{\partial z} - \hat{\xi}_z \frac{\partial E_z}{\partial y}\right\}$	$\underset{\sim}{E} = \frac{1}{\sigma}\left\{\hat{\xi}_y \frac{\partial H_x}{\partial z} - \hat{\xi}_z \frac{\partial H_x}{\partial y}\right\}$

(a) Vertical Interface y = 0

Continuity of	Tangential Electric Field	Tangential Magnetic Field
(i)	$E_{1x} = E_{2x}$	$H_{1x} = H_{2x}$
	Tangential Magnetic Field	**Tangential Electric Field**
(ii)	$H_{1z} = H_{2z}$	$E_{1z} = E_{2z}$
	or	
	$\frac{\partial E_{1x}}{\partial y} = \frac{\partial E_{2x}}{\partial y}$	$\frac{1}{\sigma_1}\frac{\partial H_{1x}}{\partial y} = \frac{1}{\sigma_2}\frac{\partial H_{2x}}{\partial y}$

(b) Horizontal Earth's Surface z = 0

Continuity of	Tangential Magnetic Field	
(iii)	$H_{1y} = H_{2y} = A$ = constant	$H_{1x} = H_{2x} = -B$ = constant
	or	
	$\frac{\partial E_{1x}}{\partial z} = \frac{\partial E_{2x}}{\partial z} = i\omega\mu_o A$	

Horizontal Basement Surface z = h

Continuity of	Tangential Magnetic Field	
(iv)	$H_{1y} = H_{2y} = 0$	$H_{1y} = H_{2y} = 0$
	or	
	$\frac{\partial E_{1x}}{\partial z} = \frac{\partial E_{2x}}{\partial z} = 0$	

(c) Conditions at Infinity

$\lvert y\rvert \to \infty$		
(v)	$\frac{\partial E_{ix}}{\partial y} \to 0$	$\frac{\partial E_{ix}}{\partial y} \to 0$
		$i = 1,2$

If h = ∞

$\lvert z\rvert \to \infty$		
(vi)	$E_{ix}, \frac{\partial E_{ix}}{\partial z} \to 0$	$H_{ix}, \frac{\partial H_{ix}}{\partial z} \to 0$

In the geometry discussed in Chapter V, where a pair of vertical interfaces is involved, an additional symmetry condition will apply to the fields in both media.

(vii) $E_{ix}\Big|_{y>0} = E_{ix}\Big|_{y<0}$ $\qquad H_{ix}\Big|_{y>0} = H_{ix}\Big|_{y<0}$ $\qquad i = 1,2$

Table 3.3

Physical Significance of Dimensionless Parameters

Parameter	Definition	Physical Meaning*
ε	$\sqrt{\sigma_1/\sigma_2}$	Skin depth ratio; ocean (2): land (1)
Q	$\frac{1}{2}\,\ell\sqrt{\mu_o\omega\sigma_2}$	Half-width in units of oceanic penetration depth
$Q\varepsilon$	$\frac{1}{2}\,\ell\sqrt{\mu_o\omega\sigma_1}$	Half-width in units of land penetration depth
H	$h\sqrt{\mu_o\omega\sigma_2}$	Depth of basement in units of oceanic penetration distance
$H\varepsilon$	$h\sqrt{\mu_o\omega\sigma_1}$	Basement depth in units of land penetration distance
γ	$h/\frac{1}{2}\ell$	Basement depth in units of half-width
Y	$(\lvert y\rvert/\frac{1}{2}\ell) - 1$	Distance from nearest shore line measured in half-width units. Range is from -1 at center of dyke, to 0 at shoreline, to $+\infty$ remote from dyke
Y_i	$\lvert y\rvert\sqrt{\mu_o\omega\sigma_i}$	Distance from shoreline in units of penetration distance of respective medium
QY	$(\lvert y\rvert - \frac{1}{2}\ell)\sqrt{\mu_o\omega\sigma_2}$	Distance from nearest coast in units of oceanic penetration distance.
$Q\varepsilon Y$	$(\lvert y\rvert - \frac{1}{2}\ell)\sqrt{\mu_o\omega\sigma_1}$	Distance from nearest coast in units of land penetration distance.

* The skin depth $\delta = \sqrt{2}\,\eta^{-1}$ and penetration depth η^{-1} are defined in §3.1.8

Table 3.4

Values of a Linear Dimension R, Expressed in Units of the Oceanic Penetration Distance

r(m) \ f(cps	10^{-3}	10^{-2}	10^{-1}	1	10	10^{2}	10^{3}
1	$1.54.10^{-4}$	$4.87.10^{-4}$	$1.54.10^{-3}$	$4.87.10^{-3}$	$1.54.10^{-2}$	$4.87.10^{-2}$	0.154
10	$1.54.10^{-3}$	$4.87.10^{-3}$	$1.54.10^{-2}$	$4.87.10^{-2}$	0.154	0.487	1.54
10^{2}	$1.54.10^{-2}$	$4.87.10^{-2}$	0.154	0.487	1.54	4.87	1.54.10
10^{3}	0.154	0.487	1.54	4.87	1.54.10	4.87.10	$1.54.10^{2}$
10^{4}	1.54	4.87	1.54.10	4.87.10	$1.54.10^{2}$	$4.87.10^{2}$	$1.54.10^{3}$

To give some physical character to the dimensionless quantities of Table 3.3, we give in Table 3.4 the numerical values R of a linear dimension r defined by

$$R = r\sqrt{\mu_o \omega \sigma_2}$$

Here r may be taken as any of the quantities h, $\frac{1}{2}\ell$, $|y|$ or $(|y| - \frac{1}{2}\ell)$ within the relevant ranges, so that R specifies respectively H, Q, Y_2, QY. Taking $\sigma_2 = 3$ mho m^{-1} with r measured in m, f in cps and $\mu_o = 4\pi\ 10^{-7}$ henry m^{-1}, we may write

$$R = 4.87 \times 10^{-3}\ r\sqrt{f}$$

The diagonal dashed line indicates the values where $R << 1$, a condition imposed on H and Q in later chapters.

3.4.5 The Vertical Fault or Coastline

Neves (1957) investigated the effect of inclined faults on the apparent resistivity, determined from the surface impedance of the magnetotelluric fields (see §3.2.2). Since the ratio of the electric fields at great distances from the fault is $\sqrt{\sigma_1/\sigma_2}$, the apparent resistivity ratio is asymptotic to the true resistivity ratio. However, at points closer to the fault line, the impedance behaves differently for each of the two types of polarization, owing to the different effect the conductivity change has on each field. Neves applied a finite difference technique to the complex Helmholtz equations, and used a relaxation method to find solutions for various cases, including that of the infinitely deep, vertical fault. He found both magnitude and phase of the apparent resistivity, for

each type of polarization. However, in treating the case of electric polarization he assumed that the surface E-field is constant and this provides one of the boundary conditions for the solution. This assumption is evidently erroneous, since the tangential E-field is continuous across the fault, but behaves as $\sigma^{-\frac{1}{2}}$ in the asymptotic limit. It must therefore vary. This behavior is indicated in the calculation of §3.1.7; the coefficient ν_E remains conductivity dependent even at low frequencies. Neves' solutions for the E-polarization case must therefore be treated with caution and are, at best, only very approximate.

D'Erceville and Kunetz (1962) treated H-polarization at a vertical fault in a uniformly deep upper stratum, underlain by a homogeneous medium. They assumed the basement to be either infinitely resistive or infinitely conducting. The latter situation is unrealistic, but provides an upper bound on the case where the basement has a finite, but non-zero, conductivity. Like Neves, they consider an infinitely long, plane fault, so that the problem reduces to the two-dimensional one already described. The parallel magnetic field may be treated as a scalar. They assumed the H-field comprises the asymptotic field H_o at a great distance from the fault, together with a superposed "perturbation" field P, due to the fault. They expanded the perturbation P-field as a Fourier series with respect to the vertical coordinate z and applied the boundary conditions to determine P. The E-fields were then derived from Maxwell's equations.

Weaver (1963a) studied an infinitely deep fault with reference to the behavior of micropulsations near a coastline. He used a transform technique and treated the magnetic field as constant across the coast, under either polarization, to obtain solutions for the electric and magnetic fields (see Chapter IV). Some additional study of the surface conditions was also made by Coode (1963).

A step-function change in the depth of a lower layer apparently has not been treated theoretically for transient waves. Telluric prospectors have obtained the steady-state solution by conformal mapping – see Logn (1954), Kunetz and Chastenet de Géry (1956, 1961), Berdichevskii (1960), and Li (1963).

Dosso (1966d) studied various submerged faults and conducting dykes using scale model measurements and the similarity principle. He also simulated an ocean of finite depth adjoining infinitely deep land, a problem mathematically difficult to solve analytically. The various parameters used by Dosso in his models are given in §3.4.7. He found that the enhancement of the H_z/H_{normal} ratio is reduced for shallower "faults", or seas. The normal electric field is very sensitive to depth, while the parallel electric field is fairly insensitive. The vertical magnetic field is very sensitive to the presence of the discontinuity, although the parallel field is not. The normal magnetic field does not remain constant across the interface, as assumed by Weaver, but his computed H_z/H_{normal} ratio is in good agreement with the model results, though of greater maximum at the interface. All of Dosso's measurements were carried

out at a fixed frequency (0.3 cps); it is possible that Weaver's condition may be more valid at other frequencies.

3.4.6 The Shelving Coastline or Inclined Fault

Although the vertical discontinuity may be reasonably realistic as a representation of many geological structures, it is usually not a good model for most coastlines. The sea floor slopes gradually away from the shore, and a better model would be an ocean with a wedge-shaped vertical profile. The exact treatment of such a model causes mathematical difficulties, however, even in the zero frequency limit.

The horizontal magnetic field at the surface is unlikely to remain nearly constant across the discontinuity, since there may be a vertical component of the electric field near the "apex" of the wedge. We expect a mathematical singularity at this point.

If we attempt to solve the problem with some kind of elementary transform technique, such as that applied by Weaver, we find that either the transform is inapplicable due to the azimuthal asymmetry, or else the transform may be applicable but the boundary conditions cannot be matched at the boundary.

Neves (1957) obtained an integral solution of the Helmholtz equation (3.3) in cylindrical coordinates, based on a Green's function, initially developed by Dougall (1899), for a wedge-space. The solution involved integration over the order of the Bessel functions, and the boundary matching required the integrals, rather than the integrands. He obtained a set of four singular integral

equations for the coefficients, and these were solved by the Kantorovich-Lebedev transform to yield an analytical solution. However, this solution is complicated to the point of impracticality (see §6.1.2). Neves developed a finite difference technique for the practical solution of the differential equation. His work always assumed as boundary conditions that both $H_{//}$ and $E_{//}$ are constant at the surface, and consequently his solution for the case of E-polarization is suspect. Coode (1963) has further discussed the boundary conditions for the inclined interface.

Ponomarev (1960) tried to explain theoretically the coast effect observed at Mirny (see §2.6.2). He considered a spectrum of plane waves incident at grazing angle on the surface, and originating from a line source extended parallel to the shore-line. The sea bed was assumed to slope at an angle ϕ for a specific distance and then remain uniformly deep. He obtained an approximate analytical solution, but only performed calculations for the simplified case when the bed slopes to infinity at a small inclination. He took the H-vector to be initially vertical and assumed the land to be non-conducting. The solution indicates that at the shore itself $H_n/H_t = \tan \phi$, but the asymptotic conditions are not realistic; the normal field approaches zero while the vertical field does not. Although the solution does show qualitatively the general behavior of the field components, the agreement with the Mirny data is poor. However, Ponomarev points out that it is possible to obtain good quantitative agreement by relaxing the condition that the waves

be monochromatic. By assuming three waves of different amplitudes and frequencies, he found excellent agreement with the observations.

Berdichevskii (1961) also considered the "sloping basement" problem. His technique is applicable at some distance seawards from the actual coastline, and is described in more detail in §6.1.3. He assumed a non-conducting basement, with plane waves incident normally on the surface of the sea. He ignored the effects generated at the junction of sea and land, treating rather a submerged sea-floor. He allowed for both kinds of wave polarization and also considered the zero frequency limit with a steady electric current flowing in the sea. His method, which he termed the "method of images"*; is based on the reflection of the electromagnetic waves at the interfaces. The expressions deduced for the electric and magnetic field components show good agreement with several sets of magnetotelluric data obtained in various parts of the USSR, over inclined basements of very low conductivity. Anishenko (1965) discussed the interpretation of magnetotelluric prospecting curves when the basement surface is inclined.

Naidu (1962, 1965) studied the problem of an inclined "step" in a basement surface. He assumed a line source parallel to the strike of the fault. For a non-conducting basement he obtained a solution for steady current flow, by conformal mapping of the potential distribution, using a Schwarz-Christoffel transformation. He also allowed for anisotropy in the vertical and horizontal conductivities.

* sposob izobrazhenii

Dosso (1966f) applied his analogue model techniques to various situations involving sloping shorelines, and measured the magnitudes and phases of the electric and magnetic field resulting from a simulated planewave source. He treated channels with sloping sides, sloping coastlines and, at lower frequencies, sloping coastlines over an upwelling mantle block underlying the sea, with a vertical edge either to the seawards or inland from the shoreline. The equivalent frequencies he treated were from 0.3 to 10^{-2} cps for the first categories and 1.2×10^{-2} to 4×10^{-4} cps for the cases involving the mantle. He assumed a land-sea conductivity ratio of 1.75×10^{-4}, and took the angle of slope of the sea bed as $\alpha = 5.7^{o}$ ($\tan \alpha = 0.1$). Both polarizations were considered. Dosso concluded that the sloping interface would have a significant effect on the H_z/H_y ratio (y normal to strike) at frequencies near 0.01 cps. However, the mantle upwelling contributes to the enhancement near the coast, especially at lower frequencies, and the observations of Schmucker (1964) and Lambert and Caner (1965) may be explained in this way.

3.4.7 The Dyke, Including a Long Promontory, and a Sea Channel

Several geophysical prospectors have studied the magnetotelluric effect of a dyke, or vertical intrusion of different material into an otherwise homogeneous medium (for instance Logn, 1954; Berdichevskii, 1960; Parasnis, 1964b). However, all of these investigations assumed steady current flow, with potential solutions derivable from Laplace's equation. In particular, the limiting case of an infinitely deep dyke and an infinitely deep, uniform current distribution is a

nearly trivial application of the boundary conditions, (see §3.4.3). The normal electric vector is enhanced by σ_2/σ_1 over the low conducting dyke, while the other fields are continuous.

Rankin (1962) applied the technique of d'Erceville and Kunetz (1962) to a finitely deep dyke for a magnetically polarized wave (ie. where the magnetic vector is polarized along the strike of the dyke). He also assumed the basement to be either perfectly resistive or perfectly conducting. He considered both resistive and conductive dykes, with penetration depth ratios $\varepsilon = 0.025$ and 40 respectively. In terms of the parameters of Table 3.3, §3.4.4, the cases considered were $H = 2Q$, $Q = 0.32 \times 1, 10^{-1}, 10^{-2}$, corresponding for instance to $\ell = h = 1$ km, and periods of 0.78 sec, 1 min 18 sec, and 2 hr. 10 min. respectively.

Dosso (1966d) made analogue model measurements for a variety of conducting dykes or sea channels, of various finite depth: width ratios. His parameters were equivalent to a frequency of 0.3 cps, and a conductivity ratio $\varepsilon^2 = 1.75 \times 10^{-4}$. Using the nomenclature of Table 3.3, the conditions he treated correspond to $\gamma = h/\frac{1}{2}\ell = 0.0173, 0.103, 0.190, 0.276$ at a constant width ($Q = 24.4$) for both polarizations: 2.0, 1.0, 0.667, 0.5, 0.4, 0.333, 0.1 at a constant depth ($H = 8.41$) for H-polarization; 290, 580, 1160 at depth $H = 48.8$ for E-polarization; and also a case of greater depth: $H = 103$ for $Q = 19.5$ ($\gamma = 1.33$), for both polarizations. Some of these values (those with very large Q or γ) are equivalent to faults rather than dykes.

3.4.8 The Island and Lake Effects

All of the above geometries involve infinite extensions along the strike or coastline, and reduce the problem to a two-dimensional one. But in practice, this idealization will not hold; the problem retains its full three-dimensional aspect and the mathematics is greatly complicated.

The simplest extension, for which many observations have been made (see §2.6.3), is to an island in a large ocean. If the island is treated as non-conducting, the zero frequency limit of steady telluric current flow in the surrounding ocean becomes analogous to streamline flow around an obstacle.

Similarly, the magnetic field lines represent the streamline conjugate to the magnetic potential and Rikitake (1964b) computed the resulting magnetic field around an infinite, thin, perfectly conducting plate with a circular hole in it. He found that the field lines could be reversed near the edge, even when a conducting layer underlies the island. By reversal, he means that the field line direction can be such as to penetrate some distance into the hole before reemerging. However he concluded that the model is rather too simplified to be realistic.

If the conductivity of the island is not entirely neglected, the potential in the zero frequency limit still remains a solution of Laplace's equation and may be solved by standard techniques (Smythe, 1950). Swift and Wescott (1964) used such a solution for a laminar elliptic island to approximate Macquarie I. They were then able

to explain the almost complete linear polarization of the telluric currents in a direction normal to the extent of the island.

Ashour and Chapman (1965) determined the magnetic field about a laminar, conducting, circular island when the magnetic field was distorted by the telluric current flow. They derived the current functions for flow about conducting elliptic and circular islands, and in the latter case, were able to determine analytically the magnetic potential over the island, by using a Hankel transfrom. The vertical magnetic component is much enhanced near the boundary, the effect diminishing with height above the surface.

All of these treatments involve the zero-frequency limit and are idealized to laminar sheets for mathematical handling. The general wave case is much more difficult mathematically, since it involves the vector Helmholtz equation (3.3) in all components, and to this writer's knowledge no solution has yet been obtained, even approximately. However Dosso (1966d), in his extensive model experiments, studied conducting circular cylinders, thus simulating the reverse case of a cylindrical "lake" of great depth in a land medium. The effect of bay-like curvature may be to reduce the enhancement of H_z/H_{normal} below that for a straight shore, while the phase of the $E_{parallel}/H_{normal}$ ratio close to the edge would probably vary greatly from 45^o.

CHAPTER IV

THE COAST OR FAULT EFFECT ON THE MAGNETOTELLURIC FIELD

In reality the actual geometry of an interface between two media will be very complicated; in fact the concept of the interface itself is an idealization. Nevertheless the effect of these "microgeometries" will be of much lower order than that of the major structure involved. It is therefore useful to study greatly simplified models which represent the essentials of reality, without the less significant features. This may be done in two ways, either experimentally by the use of model structures in the manner of Dosso (see §3.4) or mathematically.

The simplest way to represent a coast is by an infinitely deep fault-like change in the conductivity. This is a severe idealization, since it ignores the presence of the ocean floor; however, it does represent the first order problem. More important, such a model will provide a limit to the field behavior near coastlines which fall off steeply into very deep water.

In this chapter we consider the effect of such a vertical fault, and also allow for effects of the sea-floor.

4.1 The Infinitely Deep Fault

4.1.1 The Static Case

The boundary conditions which apply to steady current flow across an interface were described in §3.4.3. The tangential electric field is continuous and hence is unchanged in going from one medium

to the other. The normal electric field, on the other hand, changes in the inverse ratio of the conductivity, thus maintaining continuous normal current flow. The tangential and normal magnetic fields both remain continuous. This behavior is depicted in Fig. 4.1; it represents the limit to the behavior exhibited by the more general wave case as the frequency becomes progressively lower.

4.1.2 The Wave Case

When the frequency is not zero, the trivial behavior of the static limit no longer applies and the fields must be determined from Maxwell's equations. Weaver (1963a) applied a trigonometric Fourier transform technique to the scalar Helmholtz equation (3.3) under the boundary conditions listed in Table 3.2. He obtained solutions for the electric and magnetic fields under each of the polarization conditions of §3.4.2. Since his analysis is similar to that used in the next chapter, we will only quote the results here. The geometry he assumed is shown in Fig. 3.4, where σ_1 is the conductivity of the land and σ_2 is the ocean conductivity. The two polarization conditions are shown in Fig. 3.5.

Weaver used emu and a harmonic time dependence $e^{+i\omega t}$, and his nomenclature differs slightly from ours. In terms of our nomenclature and mks units, the expressions for the various field components are collected in Table 4.1.*

* There is a typographical error in the expression for E_2 eq. (19) of Weaver's paper. The coefficient of the integral term should be preceded by -, not +.

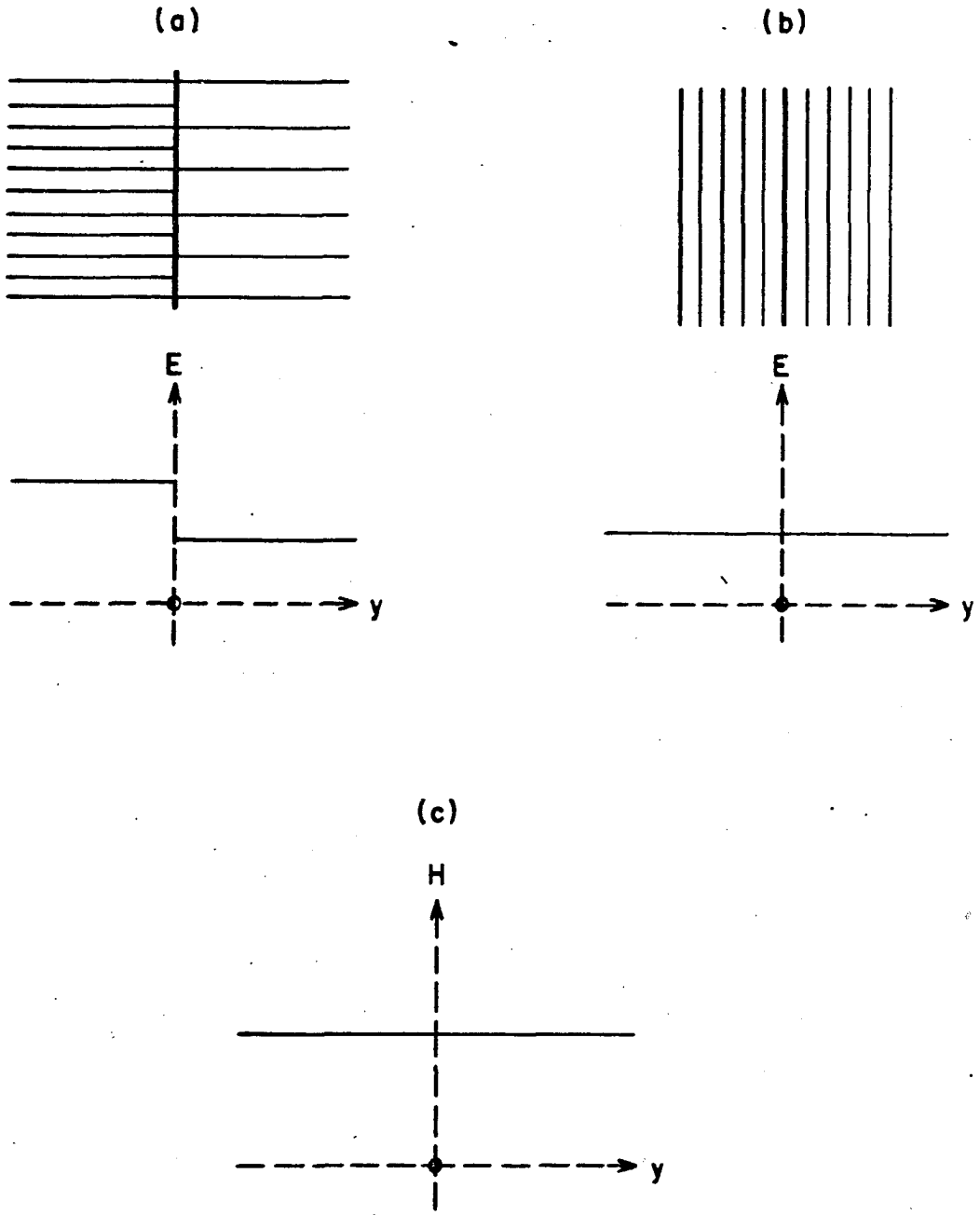

Fig. 4.1 The limiting behavior of fields near an infinitely deep fault, at zero frequency, (a) normal electric field $E_{\perp}$ (b) tangential electric field $E_{//}$ (c) magnetic fields $H_{\perp}$ and $H_{//}$.

Table 4.1

Field Components Near a Coastline or Fault

$$E_{x1} = \mu_o \omega A \left\{ \frac{\sqrt{-i}}{\eta_1} e^{-\sqrt{-i}\eta_1 z} + \frac{2}{\pi}(\eta_2^2-\eta_1^2) \int_0^\infty \frac{e^{\zeta_1 y}}{\zeta_1^2\zeta_2(\zeta_1+\zeta_2)} \cos \xi z \, d\xi \right\}$$

$$E_{x2} = \mu_o \omega A \left\{ \frac{\sqrt{-i}}{\eta_2} e^{-\sqrt{-i}\eta_2 z} - \frac{2}{\pi}(\eta_2^2-\eta_1^2) \int_0^\infty \frac{e^{-\zeta_2 y}}{\zeta_1\zeta_2^2(\zeta_1+\zeta_2)} \cos \xi z \, d\xi \right\} \quad (4.1)$$

$$E_{y1} = \mu_o \omega B \left\{ \frac{\sqrt{-i}}{\eta_1} e^{-\sqrt{-i}\eta_1 z} - \frac{2i}{\pi}(1-\epsilon^2) \int_0^\infty \frac{\xi^2 e^{\zeta_1 y}}{\zeta_1^2\zeta_2(\zeta_1+\epsilon^2\zeta_2)} \cos \xi z \, d\xi \right\}$$

$$E_{y2} = \mu_o \omega B \left\{ \frac{\sqrt{-i}}{\eta_2} e^{-\sqrt{-i}\eta_2 z} + \frac{2i}{\pi}(1-\epsilon^2) \int_0^\infty \frac{\xi^2 e^{-\zeta_2 y}}{\zeta_1\zeta_2^2(\zeta_1+\epsilon^2\zeta_2)} \cos \xi z \, d\xi \right\} \quad (4.2)$$

$$E_{z1} = -\mu_o \omega B \frac{2i}{\pi}(1-\epsilon^2) \int_0^\infty \frac{\xi e^{\zeta_1 y}}{\zeta_1\zeta_2(\zeta_1+\epsilon^2\zeta_2)} \sin \xi z \, d\xi$$

$$E_{z2} = -\mu_o \omega B \frac{2i}{\pi}(1-\epsilon^2) \int_0^\infty \frac{\xi e^{-\zeta_2 y}}{\zeta_1\zeta_2(\zeta_1+\epsilon^2\zeta_2)} \sin \xi z \, d\xi \quad (4.3)$$

$$H_{x1} = -B \left\{ e^{-\sqrt{-i}\eta_1 z} + \frac{2i}{\pi}\epsilon^2(\eta_2^2-\eta_1^2) \int_0^\infty \frac{\xi e^{\zeta_1 y}}{\zeta_1^2\zeta_2(\zeta_1+\epsilon^2\zeta_2)} \sin \xi z \, d\xi \right\}$$

$$H_{x2} = -B \left\{ e^{-\sqrt{-i}\eta_2 z} - \frac{2i}{\pi}(\eta_2^2-\eta_1^2) \int_0^\infty \frac{\xi e^{-\zeta_2 y}}{\zeta_1\zeta_2^2(\zeta_1+\epsilon^2\zeta_2)} \sin \xi z \, d\xi \right\} \quad (4.4)$$

Table 4.1 (cont'd)

$$\left.\begin{aligned} H_{y1} &= A\left\{e^{-\sqrt{-i}\eta_1 z} + \frac{2i}{\pi}(\eta_2^2-\eta_1^2)\int_0^\infty \frac{\xi\, e^{\zeta_1 y}}{\zeta_1^2\zeta_2(\zeta_1+\zeta_2)}\sin \xi z\, d\xi\right\} \\ H_{y2} &= A\left\{e^{-\sqrt{-i}\eta_2 z} - \frac{2i}{\pi}(\eta_2^2-\eta_1^2)\int_0^\infty \frac{\xi\, e^{-\zeta_2 y}}{\zeta_1\zeta_2^2(\zeta_1+\zeta_2)}\sin \xi z\, d\xi\right\} \end{aligned}\right\} \quad (4.5)$$

$$\left.\begin{aligned} H_{z1} &= \frac{2i}{\pi} A (\eta_2^2-\eta_1^2)\int_0^\infty \frac{e^{\zeta_1 y}}{\zeta_1\zeta_2(\zeta_1+\zeta_2)}\cos \xi z\, d\xi \\ H_{z2} &= \frac{2i}{\pi} A (\eta_2^2-\eta_1^2)\int_0^\infty \frac{e^{-\zeta_2 y}}{\zeta_1\zeta_2(\zeta_1+\zeta_2)}\cos \xi z\, d\xi \end{aligned}\right\} \quad (4.6)$$

$$\left.\begin{aligned} \zeta_i^2 &= \xi^2 - i\eta_i^2 \\ \eta_i^2 &= \mu_o \omega \sigma_i \\ \varepsilon &= \eta_1/\eta_2 \end{aligned}\right\} \quad (4.7)$$

Table 4.2

Surface Field Components Near a Coastline, Expressed in Dimensionless Parameters

$$\sqrt{\frac{\sigma_1}{\mu_o \omega}}\,\frac{E_{x1}}{A} = \sqrt{-i} + \frac{2}{\pi}\,\varepsilon(1-\varepsilon^2)\int_0^\infty \frac{e^{-Y_1\sqrt{u^2-i\varepsilon^2}/\varepsilon}}{(u^2-i\varepsilon^2)\sqrt{u^2-i}\;D_1}\,du$$

$$\sqrt{\frac{\sigma_2}{\mu_o \omega}}\,\frac{E_{x2}}{A} = \sqrt{-i} - \frac{2}{\pi}\,(1-\varepsilon^2)\int_0^\infty \frac{e^{-Y_2\sqrt{u^2-i}}}{\sqrt{u^2-i\varepsilon^2}\;(u^2-i)\;D_1}\,du \qquad \Big\} (4.8)$$

$$\sqrt{\frac{\sigma_1}{\mu_o \omega}}\,\frac{E_{y1}}{B} = \sqrt{-i} - \frac{2i}{\pi}\,\varepsilon(1-\varepsilon^2)\int_0^\infty \frac{u^2\, e^{-Y_1\sqrt{u^2-i\varepsilon^2}/\varepsilon}}{(u^2-i\varepsilon^2)\sqrt{u^2-i}\;D_2}\,du$$

$$\sqrt{\frac{\sigma_2}{\mu_o \omega}}\,\frac{E_{y2}}{B} = \sqrt{-i} + \frac{2i}{\pi}\,(1-\varepsilon^2)\int_0^\infty \frac{u^2\, e^{-Y_2\sqrt{u^2-i}}}{\sqrt{u^2-i\varepsilon^2}\;(u^2-i)\;D_2}\,du \qquad \Big\} (4.9)$$

$$\frac{H_{z1}}{A} = \frac{2i}{\pi}\,(1-\varepsilon^2)\int_0^\infty \frac{e^{-Y_1\sqrt{u^2-i\varepsilon^2}/\varepsilon}}{\sqrt{(u^2-i\varepsilon^2)(u^2-i)}\;D_1}\,du$$

$$\frac{H_{z2}}{A} = \frac{2i}{\pi}\,(1-\varepsilon^2)\int_0^\infty \frac{e^{-Y_2\sqrt{u^2-i\varepsilon^2}}}{\sqrt{(u^2-i\varepsilon^2)(u^2-i)}\;D_1}\,du \qquad \Big\} (4.10)$$

$$D_1 = \sqrt{u^2-i\varepsilon^2} + \sqrt{u^2-i}$$

$$D_2 = \sqrt{u^2-i\varepsilon^2} + \varepsilon^2\sqrt{u^2-i} \qquad \Big\} (4.11)$$

At the surface, $z = 0$, the only non-trivial components are those for E_x, E_y and H_z. They may be expressed in terms of the dimensionless constants ε, Y_1, Y_2 of Table 3.3; the relations are given in Table 4.2. The integration variable ξ has been changed to u by the substitution:

$$\xi = \eta_2 u$$

4.1.3 Special Cases

(a) Transition to a Uniform Medium

At great distances from the discontinuity, the field components approach asymptotically the conditions for homogeneous media. From Table 4.1, we see that as $|y| \to \infty$

$$\begin{aligned}
E_{xj} &\to \mu_o \omega A \frac{\sqrt{-i}}{\eta_j} e^{-\sqrt{-i}\eta_j z} \\
E_{yj} &\to \mu_o \omega B \frac{\sqrt{-i}}{\eta_j} e^{-\sqrt{-i}\eta_j z} \\
E_{zj} &\to 0 \\
H_{xj} &\to -B\, e^{-\sqrt{-i}\eta_j z} \\
H_{yj} &\to A\, e^{-\sqrt{-i}\eta_j z} \\
H_{jz} &\to 0
\end{aligned} \tag{4.12}$$

These expressions apply to the uniform media 1 or 2. The more useful criterion is evident from Table 4.2. If $Y_j >> 1$ (i.e. $|y| >> \eta_j^{-1}$)

the integral terms become very small and the expressions reduce to those of (4.12).

It is also evident that as $\eta_1 \to \eta_2$ ($\varepsilon \to 1$), the conductivities of the two media become more nearly equal, and the relations of Table 4.1 again reduce to those for a homogeneous medium. We conclude that the coast effect will certainly diminish with distance from the shore, and will be small when the conductivity ratio across the "fault" is close to unity.

(b) Values for the Field Components at the Plane of Discontinuity

(i) The Vertical Magnetic Field H_z:

Weaver examined the vertical magnetic field component H_z at the plane of the shoreline $y = 0$. H_z is continuous there, and Weaver found that it could be evaluated analytically. He obtained:

$$\left.\frac{H_z}{A}\right|_{y=0} = \frac{2}{\pi}\left\{\left[\ker(\eta_2 z) - \ker(\eta_1 z)\right] - i\left[\mathrm{kei}(\eta_2 z) - \mathrm{kei}(\eta_1 z)\right]\right\}$$

Since we are only interested in the fields at the surface, $z = 0$, this expression may be simplified, either by direct evaluation of the original integral (4.10), or by using the series expansions for the Bessel functions of the second kind ker x and kei x (eg. Dwight, 1961, 824.3 and 824.4; Abramowitz and Stegun, 1964, 9.9.12). The simplified relation is:

$$\frac{H_z\ (0,0)}{A} = \frac{2}{\pi} \ln \varepsilon \qquad (4.13)$$

The value of ε is always less than unity, so that at the interface the vertical surface magnetic field H_z is always completely out

of phase (180^{o}) with the normal magnetic field H_y (=A). The magnitude of the field increases with the difference in conductivity, and will be highly sensitive to the ratio for a great conductivity disparity between the media. Since the vertical field peaks at the interface, the enhancement can be obtained easily from (4.13).

Values of $(2/\pi)|\ln\varepsilon|$ are given in Table 4.3 for various values of ε.

(ii) Tangential Electric Field E_x:

Similarly, at the interface y = 0, we may evaluate analytically the expression for the continuous tangential electric field E_x, at the surface z = 0. This is done in Appendix 2, the result being:

$$\sqrt{\frac{\sigma_2}{\mu_o \omega}} \frac{E_x\,(0,0)}{A} = \sqrt{-1}\,\frac{2}{\pi}\,K\left(\sqrt{1-\varepsilon^2}\right) \qquad (4.14)$$

where K (k) is the Complete Elliptic Integral of the first kind with modulus $k = \sqrt{1-\varepsilon^2}$. Useful tables of this function are given by Fettis and Caslin (1964) who use the modulus k and parameter k^2 as arguments; Byrd and Friedmann (1954, p. 322), who use the modular angle α = arsin k as argument; and for small values of ε, Airey (1935), who uses the complementary parameter $h = 1-k^2 = \varepsilon^2$ as argument. For small values of ε, the asymptotic relation

$$K\left(\sqrt{1-\varepsilon^2}\right) \sim \ln\,(4/\varepsilon) \qquad (4.15)$$

is very useful in determining the magnitude of E_x (0,0).

Evidently as the conductivity decreases, the value of E_x (0,0) increases. The increase is much "slower" than the ratio of the

asymptotic values $E_{x1}(\infty,0)/E_{x2}(\infty,0)$; ie. much slower than ε^{-1}. This means that the transition in E_x ($z = 0$) from the land medium to the oceanic one becomes very steep on the landward side and approaches a step function type of change. The change on the oceanic side is much more gradual.

The phase difference between E_x (0,0) and H_y (0,0), nevertheless remains constant at 45^o, the same value as the asymptotic phase. This phase angle differs from 45^o at intermediate distances.

Values of $(2/\pi)$ K $(\sqrt{1-\varepsilon^2})$ are given in Table 4.3 for several values of ε.

(iii) Normal Electric Field E_y:

Unlike the two field components discussed above, the normal electric field at the interface $y = 0$ is not continuous, and hence there are two relations for the value of E_y there. It does not seem possible to evaluate exactly either of these expressions in terms of known functions, but if we restrict the conductivity ratio so that $\varepsilon^2 << 1$, we may obtain closely approximate expressions for both values of the E_y field. These approximate values provide upper limits on the departure of the E_y field from its asymptotic (uniform medium) limit.

The derivations are given in App. 2, the final expressions being:

$$\left.\begin{aligned}
\sqrt{\frac{\sigma_1}{\mu_o \omega}}\,\frac{E_{1y}\,(0,0)}{B} &\approx \frac{\sqrt{-i}}{\sqrt{1+\varepsilon^2}}\left\{1+\frac{2}{\pi}\,\frac{\delta}{1-\varepsilon^4}\left[(1+\varepsilon^2-\varepsilon^4)\,K(k)-E(k)\right]\right\}\\
\sqrt{\frac{\sigma_2}{\mu_o \omega}}\,\frac{E_{2y}\,(0,0)}{B} &\approx \sqrt{-i}\,\delta\left\{1+\frac{2}{\pi}\,\frac{\delta}{1-\varepsilon^4}\left[(1+\varepsilon^2-\varepsilon^4)\,K(k)-E(k)\right]\right\}
\end{aligned}\right\} \quad (4.16)$$

where $k^2 = 1-\varepsilon^2$; $\delta^2 = \varepsilon^2/(1+\varepsilon^2)$; and $\varepsilon^2 << 1$

For very small values of ε, the asymptotic relation (4.15) is valid, together with the approximation $E(k) \approx 1$. Then (4.16) may be written:

$$\left.\begin{aligned}
\sqrt{\frac{\sigma_1}{\mu_o \omega}}\,\frac{E_{1y}\,(0,0)}{B} &\approx \frac{\sqrt{-i}}{\sqrt{1+\varepsilon^2}}\left\{1+\frac{2}{\pi}\,\delta\left[(1+\varepsilon^2)\,\ln\left|4/\varepsilon\right|-1\right]\right\}\\
\sqrt{\frac{\sigma_2}{\mu_o \omega}}\,\frac{E_{2y}\,(0,0)}{B} &\approx \sqrt{-i}\,\delta\left\{1+\frac{2}{\pi}\,\delta\left[(1+\varepsilon^2)\,\ln\left|4/\varepsilon\right|-1\right]\right\}
\end{aligned}\right\} \quad (4.17)$$

The ratio $E_{2y}\,(0,0)/E_{1y}\,(0,0) = \varepsilon^2 = \sigma_1/\sigma_2$ is still preserved in this approximate relation. We notice again that the phase of E_y relative to $H_x = -B$ is always $+45^\circ$ over the fault line, independent of the value of ε, although the phase away from the fault must evidently differ from this value.

As an example of the small error involved in using relations (4.17), consider the evaluations of (E_1, E_2) from each pair of equations, when $\varepsilon = 0.1$. Equation (4.16) gives (1.14, 0.114), while (4.17) gives (1.17, 0.117). The values computed from the exact expression (4.9) are (1.131, 0.1131). The relation (4.16) is thus accurate to about 1%, and (4.17) to a few percent. The accuracy

Table 4.3

Values of E_x (0,0), E_y (0,0) and H_z (0,0) Over a Fault

ε	ε^2	k^2	$\frac{H_z(0,0)}{H_y}$	$\frac{E_x(0,0)}{E_{x2}(\infty,0)}$	$\frac{E_{2y}(0,0)}{E_{2y}(\infty,0)}$
	$= \sigma_1/\sigma_2$	$= 1-\varepsilon^2$	$= \frac{2}{\pi}\lvert\ln\varepsilon\rvert$	$= \frac{2}{\pi}K(\sqrt{1-\varepsilon^2})$	(4.16 & 4.17)*
1.0	1.0	0	0	1.0000	(1.0)
0.5	0.25	0.75	0.4413	1.3729	
0.3162	0.10	0.90	0.7330	1.6413	
0.1	10^{-2}	0.99	1.4659	2.3527	0.114(0.1131)
0.0316	10^{-3}	0.999	2.1989	3.0820	0.0340
0.0173	3.10^{-4}	0.9997	2.5821	3.4647	0.0181
10^{-2}	10^{-4}	0.9999	2.9317	3.8144	0.01032
0.316×10^{-2}	10^{-5}	$1-10^{-5}$	3.6647	4.5473	0.320×10^{-2}
10^{-3}	10^{-6}	$1-10^{-6}$	4.3976	5.2802	1.005×10^{-3}

*The values in this column are approximate (see text). The figures in parentheses are more precise.

both sets of relations improves at smaller values of ϵ, but then there is very little distortion of the fields from the limit (1.0, ϵ) over the fault line. The land value will not change appreciably with distance from the shore, but in the highly conducting ocean (medium 2) the coastal suppression of the E_{2y} field will decay rapidly, and the magnitude will rise with increasing distance towards the asymptotic value of 1.0.

Some values of E_{2y} $(0,0)/E_{2y}(\infty,0)$ calculated from equations (4.16) and (4.17) are given in Table 4.3.

4.1.4 Numerical Evaluation of the Fields Near a Coastline

The equations of Tables 4.1 or 4.2 express the fields at any distance from the fault line. Since they cannot, in general, be evaluated analytically, numerical procedures are necessary to obtain the more detailed behavior away from the coastline. Weaver (1963a) has given the results of such computations for the vertical magnetic field at the surface, in both media, for a conductivity ratio of 2.5×10^{-4} ($\epsilon = 0.0158$).

The computation of the surface electric fields from Weaver's relations was programmed for an IBM 7094 computer by D. Smith and B. Morton of this Institute's computing group, for D. Swift of this Institute. The calculation was performed by Western Data Processing Center at the University of California, and the results have been made available to me by courtesy of Mr. Swift.

A five-point Gaussian integration technique was applied to each of the real and imaginary parts of the integrals in equations (4.1) and (4.2). The results are discussed in §4.3.

4.2 The Fault of Finite Depth

The geometry assumed by Weaver in his treatment cannot allow for the effect of the sea bed in perturbing the fields. In a medium comprising two homogeneous layers with a horizontal plane interface this effect is well-known. The presence of the base layer of lower conductivity modifies the results obtained from a model such as Weaver's.

It seems more realistic to consider a semi-infinite ocean of rectangular vertical cross-section, abutting a homogeneous, infinitely deep land medium. The material of the sea-base might be considered uniformly conducting with a conductivity either different or equal to that of the land. Such a model proves difficult to treat mathematically, however, and one which is more amenable to mathematical analysis must be chosen.

A model which can be treated in an approximate manner is shown in Fig. (4.2a). It consists of land and ocean media of equal depth, both underlain by a non-conducting, homogeneous medium of infinite depth. The land medium is designated by the subscript 1 and the ocean medium by the subscript 2 in the analysis. D'Erceville and Kunetz (1962) used this model in their discussion of the H-polarization case (see §3.4.5).

4.2.1 The Static Case

In the zero frequency limit there will be direct electric current flow in the conducting media. The behavior of the fields involved will be very similar to that already discussed in dealing with the

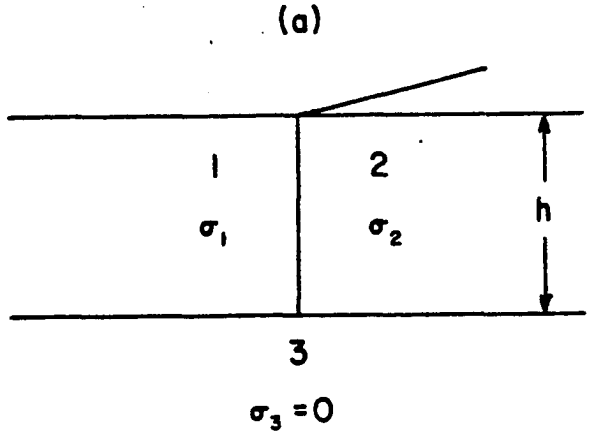

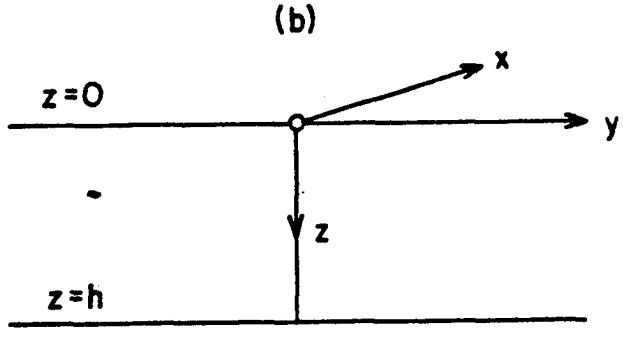

Fig. 4.2 Fault of finite depth (a) model geometry (b) coordinate system.

infinitely deep fault (§4.1.1). The current flow normal to the fault will be continuous, ie. the normal electric field will be discontinuous. The other fields will be continuous.

4.2.2 The Wave Case

When frequency dependence of the fields is admitted, it is necessary to solve Maxwell's equations under the conditions imposed by the geometry of Fig. 4.2a and Table 3.2. We use the coordinate system shown in Fig. 4.2b and the two polarization conditions of Fig. 3.5 are treated separately.

(a) E-Polarization: The surface E-vector is parallel to the strike of the fault or coast. The equation to be solved is eq. (3.24), viz.

$$\frac{\partial^2 E_x}{\partial y^2} + \frac{\partial^2 E_x}{\partial z^2} + i\eta^2 E_x = 0 \qquad (4.18)$$

where

$$\eta^2 = \mu_o \omega \sigma$$

Since we have a geometry involving a constant finite depth in the z coordinate, with known boundary conditions at z = 0, h (Table 3.2, conditions (iii) and (iv)), a finite Fourier cosine transformation is used. This transform and its inverse are defined by (Tranter, 1956):

$$\tilde{E}_x(y,\xi) = \int_0^{\pi} E_x(y,\chi) \cos \xi\chi \, d\chi \qquad (4.19)$$

$$E_x(y,z) = \frac{1}{\pi}\bar{E}_x(y,0) + \frac{2}{\pi}\sum_{\xi=1}^{\infty}\bar{E}_x(y,\chi)\cos\xi\chi \tag{4.20}$$

where $\chi = \frac{\pi}{h}z$ (4.21)

If we apply (4.19) to (4.18) and use conditions (iii) and (iv) of Table 3.2 in the form

$$\left[\frac{\partial E_x}{\partial \chi}\right]_{x=0} = i\omega\mu_o A\frac{h}{\pi}$$

$$\left[\frac{\partial E_x}{\partial \chi}\right]_{x=\pi} = 0$$

then eq. (4.18) reduces to

$$\frac{d^2\bar{E}_x}{dy^2} - \zeta^2\bar{E}_x = i\omega\mu_o A\frac{\pi}{h} \tag{4.22}$$

where $\zeta^2 = (\frac{\pi}{h})^2\xi^2 - i\eta^2$ (4.23)

The general solution of (4.22) is

$$\bar{E}_x(y,\xi) = \alpha(\xi)e^{\zeta y} + \beta(\xi)e^{-\zeta y} - \frac{i\omega\mu_o A}{\zeta^2}\frac{\pi}{h}$$

If we always take Re $(\zeta) > 0$, and apply the conditions at infinity (v), we obtain

$$\begin{aligned} y<0:\ \bar{E}_{1x}(y,\xi) &= \alpha_1(\xi)e^{\zeta_1 y} - \frac{i\omega\mu_o A}{\zeta_1^2}\frac{\pi}{h} \\ y>0:\ \bar{E}_{2x}(y,\xi) &= \beta_2(\xi)e^{-\zeta_2 y} - \frac{i\omega\mu_o A}{\zeta_2^2}\frac{\pi}{h} \end{aligned} \tag{4.24}$$

The conditions (i) and (ii) at the interface y = 0 provide simultaneous equations for the solution of the coefficients:

$$\alpha_1(\xi) = \mu_o \omega A \frac{\pi}{h} \frac{\eta_2^2-\eta_1^2}{\zeta_1^2\zeta_2(\zeta_1+\zeta_2)}$$

$$\beta_2(\xi) = -\mu_o \omega A \frac{\pi}{h} \frac{\eta_2^2-\eta_1^2}{\zeta_1\zeta_2^2(\zeta_1+\zeta_2)} \tag{4.25}$$

We now take the inverse transform (4.20) of (4.24). We note first that to maintain the condition Re $(\zeta_i) > 0$ always, it is necessary to take

$$\sqrt{-i} = -i\sqrt{i} = (1-i)/\sqrt{2}$$

Then:

$$\bar{E}_{1x}(y,0) = \frac{\mu_o \omega A}{\eta_1^2} \frac{\pi}{h} \left\{ 1 - \left(1 - \frac{\eta_1}{\eta_2} \right) e^{\sqrt{-i}\eta_1 y} \right\}$$

$$\bar{E}_{2x}(y,0) = \frac{\mu_o \omega A}{\eta_2^2} \frac{\pi}{h} \left\{ 1 + \left(\frac{\eta_2}{\eta_1} - 1 \right) e^{-\sqrt{-i}\eta_2 y} \right\} \tag{4.26}$$

The inverse transform is

$$E_{1x}(y,z) = \frac{1}{\pi} E_{1x}(y,0) + \frac{2\mu_o \omega A}{h} \sum_{\xi=1}^{\infty} \frac{1}{\zeta_1^2} \left\{ \frac{\eta_2^2-\eta_1^2}{\zeta_2(\zeta_1+\zeta_2)} e^{\zeta_1 y} - i \right\} \cos \frac{\pi}{h} \xi z$$

$$E_{2x}(y,z) = \frac{1}{\pi} \bar{E}_{2x}(y,0) - \frac{2\mu_o \omega A}{h} \sum_{\xi=1}^{\infty} \frac{1}{\zeta_2^2} \left\{ \frac{\eta_2^2-\eta_1^2}{\zeta_1(\zeta_1+\zeta_2)} e^{-\zeta_2 y} + i \right\} \cos \frac{\pi}{h} \xi z \tag{4.27}$$

The second term in the summations may be evaluated explicitly (see App. 3):

$$\sum_{\xi=1}^{\infty} \frac{\cos \alpha\xi}{(\frac{\pi}{h})^2 \xi^2 - i\eta^2} = \frac{1}{2i\eta^2} - \frac{h}{2} \frac{\cos\left[\sqrt{i}\,\eta h\,(1 - \alpha/\pi)\right]}{\sqrt{i}\,\eta \sin \sqrt{i}\,\eta h} \tag{4.28}$$

where $\alpha = \frac{\pi}{h} z$

Equations (4.27) may then be reduced to the relations:

$$E_{1x}(y,z) = \mu_o \omega A \left\{ \frac{\sqrt{i}}{\eta_1} \frac{\cos\sqrt{i}\eta_1(h-z)}{\sin\sqrt{i}\eta_1 h} - \frac{\eta_2-\eta_1}{h\eta_1^2\eta_2} e^{\sqrt{-i}\eta_1 y} + \right.$$

$$\left. + \frac{2(\eta_2^2-\eta_1^2)}{h} \sum_{\xi=1}^{\infty} \frac{e^{\zeta_1 y} \cos\pi \frac{z}{h} \xi}{\zeta_1^2 \zeta_2 (\zeta_1+\zeta_2)} \right\}$$

$$E_{2x}(y,z) = \mu_o \omega A \left\{ \frac{\sqrt{i}}{\eta_2} \frac{\cos\sqrt{i}\eta_2(h-z)}{\sin\sqrt{i}\eta_2 h} + \frac{\eta_2-\eta_1}{h\eta_1\eta_2^2} e^{\sqrt{-i}\eta_2 y} - \right. \tag{4.29}$$

$$\left. - \frac{2(\eta_2^2-\eta_1^2)}{h} \sum_{\xi=1}^{\infty} \frac{e^{-\zeta_2 y} \cos\pi \frac{z}{h} \xi}{\zeta_1 \zeta_2^2 (\zeta_1+\zeta_2)} \right\}$$

always with $\mathrm{Re}\,(\zeta_1) > 0$

This pair of relations is the solution of (4.18) and satisfies the boundary conditions (i) - (v) of Table 3.2 The expressions for the H_y and H_z field components may be derived from them, using Maxwell's equations in the form shown in Table 3.2. All the relations are collected together in Table 4.4.

(b) H-Polarization: The surface H-vector is parallel to the strike. The H_x component satisifes eq. (3.26), viz.

$$\frac{\partial^2 H_x}{\partial y^2} + \frac{\partial^2 H_x}{\partial z^2} + i\eta^2 H_x = 0 \tag{4.30}$$

$$\eta^2 = \mu_o \omega \sigma$$

The boundary conditions (Table 3.2, (iii) and (iv)) indicate that the finite Fourier sine transform is appropriate in this case. The transform and its inverse are defined by (Tranter, 1956):

$$\bar{H}_x(y,\xi) = \int_0^\infty H_x(y,\chi) \sin \xi\chi \, d\chi \tag{4.31}$$

$$H_x(y,\xi) = \frac{2}{\pi} \sum_{\xi=1}^{\infty} \bar{H}_x(y,\xi) \sin \xi\chi \tag{4.32}$$

where $$\chi = \frac{\pi}{h} z \tag{4.33}$$

The application of (4.31) to (4.30) together with boundary conditions (iii) and (iv) of Table 3.2 reduce the partial differential equation to

$$\frac{d^2\bar{H}_x}{dy^2} - \zeta^2 \bar{H}_x = \left(\frac{\pi}{h}\right)^2 B \, \xi \tag{4.34}$$

with again $$\zeta^2 = \left(\frac{\pi}{h}\right)^2 \xi^2 - i\eta^2 \tag{4.35}$$

The general solution of the ordinary differential equation (4.34) is

$$\bar{H}_x(y,\xi) = \alpha(\xi) \, e^{\zeta y} + \beta(\xi) \, e^{-\zeta y} - \left(\frac{\pi}{h}\right)^2 B \frac{\xi}{\zeta^2}$$

With Re (ζ) > 0 always, the infinity conditions (v) reduce the relation in each region to:

$$y<0: \quad \bar{H}_{1x}(y,\xi) = \alpha_1(\xi)\, e^{\zeta_1 y} - \left(\frac{\pi}{h}\right)^2 B \frac{\xi}{\zeta_1^2}$$

$$y>0: \quad \bar{H}_{2x}(y,\xi) = \beta_2(\xi)\, e^{-\zeta_2 y} - \left(\frac{\pi}{h}\right)^2 B \frac{\xi}{\zeta_2^2} \tag{4.36}$$

The interface conditions (i) and (ii) at y = 0 determine the coefficients as

$$\alpha_1(\xi) = -\, i\, B \left(\frac{\pi}{h}\right)^2 \xi \frac{\varepsilon^2(\eta_2^2-\eta_1^2)}{\zeta_1^2\zeta_2(\zeta_1+\varepsilon^2\zeta_2)}$$

$$\beta_2(\xi) = i\, B \left(\frac{\pi}{h}\right)^2 \xi \frac{\eta_2^2-\eta_1^2}{\zeta_1\zeta_2^2(\zeta_1+\varepsilon^2\zeta_2)} \tag{4.37}$$

The inverse transforms of (4.36) yield:

$$H_{1x}(y,z) = -\frac{2\pi B}{h^2} \sum_{\xi=1}^{\infty} \left[1 + i\varepsilon^2(\eta_2^2-\eta_1^2) \frac{e^{\zeta_1 y}}{\zeta_2(\zeta_1+\varepsilon^2\zeta_2)}\right] \frac{\xi \sin \frac{\pi}{h}\xi z}{\zeta_1^2}$$

$$H_{2x}(y,z) = -\frac{2\pi B}{h^2} \sum_{\xi=1}^{\infty} \left[1 - i\,(\eta_2^2-\eta_1^2) \frac{e^{-\zeta_2 y}}{\zeta_1(\zeta_1+\varepsilon^2\zeta_2)}\right] \frac{\xi \sin \frac{\pi}{h}\xi z}{\zeta_2^2} \tag{4.38}$$

The first terms of these summations may be explicitly evaluated (App. 3);

$$\sum_{\xi=1}^{\infty} \frac{\xi \sin \alpha\xi}{\left(\frac{\pi}{h}\right)^2 \xi^2 - i\eta^2} = \frac{h^2}{2\pi} \frac{\sin \sqrt{i}\,\eta(h-z)}{\sin \sqrt{i}\,\eta h} \tag{4.39}$$

where $\alpha = \frac{\pi}{h} z$

We obtain

$$H_{1x}(y,z) = -B\left\{\frac{\sin\sqrt{i}\eta_1(h-z)}{\sin\sqrt{i}\eta_1 h} + 2\pi i \frac{\varepsilon^2(\eta_2^2-\eta_1^2)}{h^2} \sum_{\xi=1}^{\infty} \frac{\xi\, e^{-\zeta_2 y} \sin\frac{\pi}{h} z\xi}{\zeta_1^2\zeta_2(\zeta_1+\varepsilon^2\zeta_2)}\right\}$$

$$H_{2x}(y,z) = -B\left\{\frac{\sin\sqrt{i}\eta_2(h-z)}{\sin\sqrt{i}\eta_2 h} - 2\pi i \frac{(\eta_2^2-\eta_1^2)}{h^2} \sum_{\xi=1}^{\infty} \frac{\xi\, e^{-\zeta_2 y} \sin\frac{\pi}{h} z\xi}{\zeta_1\zeta_2^2(\zeta_1+\varepsilon^2\zeta_2)}\right\} \quad (4.40)$$

These relations satisfy eq. (4.30) and the boundary conditions (i) - (v) of Table 3.2. The expression for E_y and E_z may be obtained from (4.40) from the relations listed in this Table.

In addition to the boundary conditions of Table 3.2, a short calculation shows that, at the interface $y = 0$, the relations for E_y also satisfy the condition

$$\sigma_1 E_{1y}(0,z) = \sigma_2 E_{2y}(0,z)$$

All of the relations expressing the various field components are collected in Table 4.4. We are only interested in the fields at the surface, $z = 0$. Here the E_z, H_x and H_y fields are trivial, and the remaining components are given in Table 4.5, expressed in terms of the dimensionless constants of Table 3.3.

4.2.3 Special Cases

(a) Transition to Double-Layered Medium

As with the infinitely deep fault, at great distances from the discontinuity plane, the asymptotic behavior of the fields is the same as for the fields in a double-layered medium, where the lower

Table 4.4

Field Components Near a Finitely Deep Fault

$$\left.\begin{aligned}
E_{x1} &= \mu_o \omega A \left\{ \frac{\sqrt{i}}{\eta_1} \cdot \frac{\cos\sqrt{i}\,\eta_1(h-z)}{\sin\sqrt{i}\,\eta_1 h} - \frac{1-\varepsilon}{h\eta_1^2} e^{\sqrt{-i}\,\eta_1 y} + 2\,\frac{\eta_2^2-\eta_1^2}{h} \sum_{\xi=1}^{\infty} \frac{e^{\zeta_1 y}\cos\frac{\pi}{h}z\xi}{\zeta_1^2\zeta_2\,(\zeta_1+\zeta_2)} \right\} \\
E_{x2} &= \mu_o \omega A \left\{ \frac{\sqrt{i}}{\eta_2} \cdot \frac{\cos\sqrt{i}\,\eta_2(h-z)}{\sin\sqrt{i}\,\eta_2 h} + \frac{1-\varepsilon}{h\eta_1\eta_2} e^{-\sqrt{-i}\,\eta_2 y} - 2\,\frac{\eta_2^2-\eta_1^2}{h} \sum_{\xi=1}^{\infty} \frac{e^{-\zeta_2 y}\cos\frac{\pi}{h}z\xi}{\zeta_1\zeta_2^2(\zeta_1+\zeta_2)} \right\}
\end{aligned}\right\} \qquad (4.41)$$

$$\left.\begin{aligned}
E_{y1} &= \mu_o \omega B \left\{ \frac{\sqrt{i}}{\eta_1} \cdot \frac{\cos\sqrt{i}\,\eta_1(h-z)}{\sin\sqrt{i}\,\eta_1 h} - 2\pi^2 i\,\frac{1-\varepsilon^2}{h^3} \sum_{\xi=1}^{\infty} \frac{\xi^2 e^{\zeta_1 y}\cos\frac{\pi}{h}z\xi}{\zeta_1^2\zeta_2\,(\zeta_1+\varepsilon^2\zeta_2)} \right\} \\
E_{y2} &= \mu_o \omega B \left\{ \frac{\sqrt{i}}{\eta_2} \cdot \frac{\cos\sqrt{i}\,\eta_2(h-z)}{\sin\sqrt{i}\,\eta_2 h} + 2\pi^2 i\,\frac{1-\varepsilon^2}{h^3} \sum_{\xi=1}^{\infty} \frac{\xi^2 e^{-\zeta_2 y}\cos\frac{\pi}{h}z\xi}{\zeta_1\zeta_2^2\,(\zeta_1+\varepsilon^2\zeta_2)} \right\}
\end{aligned}\right\} \qquad (4.42)$$

$$\left.\begin{aligned}
E_{z1} &= \mu_o \omega B\,\frac{2\pi i}{h^2}\,(1-\varepsilon^2) \sum_{\xi=1}^{\infty} \frac{\xi\, e^{\zeta_1 y}\sin\frac{\pi}{h}z\xi}{\zeta_1\zeta_2(\zeta_1+\varepsilon^2\zeta_2)} \\
E_{z2} &= \mu_o \omega B\,\frac{2\pi i}{h^2}\,(1-\varepsilon^2) \sum_{\xi=1}^{\infty} \frac{\xi\, e^{-\zeta_2 y}\sin\frac{\pi}{h}z\xi}{\zeta_1\zeta_2(\zeta_1+\varepsilon^2\zeta_2)}
\end{aligned}\right\} \qquad (4.43)$$

Table 4.4 (cont'd)

Field Components Near a Finitely Deep Fault

$$H_{x1} = -B\left\{\frac{\sin\sqrt{i}\,\eta_1(h-z)}{\sin\sqrt{i}\,\eta_1 h} + 2\pi i\,\frac{\eta_1^2(1-\epsilon^2)}{h^2}\sum_{\xi=1}^{\infty}\frac{\xi\, e^{\zeta_1 y}\sin\frac{\pi}{h}z\xi}{\zeta_1^2\zeta_2\,(\zeta_1+\epsilon^2\zeta_2)}\right\}$$

$$H_{x2} = -B\left\{\frac{\sin\sqrt{i}\,\eta_2(h-z)}{\sin\sqrt{i}\,\eta_2 h} - 2\pi i\,\frac{\eta_2^2(1-\epsilon^2)}{h^2}\sum_{\xi=1}^{\infty}\frac{\xi\, e^{-\zeta_2 y}\sin\frac{\pi}{h}z\xi}{\zeta_1\zeta_2^2\,(\zeta_1+\epsilon^2\zeta_2)}\right\} \qquad (4.44)$$

$$H_{y1} = A\left\{\frac{\sin\sqrt{i}\,\eta_1(h-z)}{\sin\sqrt{i}\,\eta_1 h} + 2\pi i\,\frac{\left(\eta_2^2-\eta_1^2\right)}{h^2}\sum_{\xi=1}^{\infty}\frac{e^{\zeta_1 y}\sin\frac{\pi}{h}z\xi}{\zeta_1^2\zeta_2\,(\zeta_1+\zeta_2)}\right\}$$

$$H_{y2} = A\left\{\frac{\sin\sqrt{i}\,\eta_2(h-z)}{\sin\sqrt{i}\,\eta_2 h} - 2\pi i\,\frac{\left(\eta_2^2-\eta_1^2\right)}{h^2}\sum_{\xi=1}^{\infty}\frac{e^{-\zeta_2 y}\sin\frac{\pi}{h}z\xi}{\zeta_1\zeta_2^2(\zeta_1+\zeta_2)}\right\} \qquad (4.45)$$

$$H_{z1} = A\left\{-\sqrt{i}\,\frac{1-\epsilon}{\eta_1 h}\, e^{\sqrt{-i}\,\eta_1 y} + 2i\,\frac{\left(\eta_2^2-\eta_1^2\right)}{h}\sum_{\xi=1}^{\infty}\frac{e^{\zeta_1 y}\cos\frac{\pi}{h}z\xi}{\zeta_1\zeta_2\,(\zeta_1+\zeta_2)}\right\}$$

$$H_{z2} = A\left\{\sqrt{i}\,\frac{1-\epsilon}{\eta_1\eta_2 h}\, e^{-\sqrt{-i}\,\eta_2 y} + 2i\,\frac{\left(\eta_2^2-\eta_1^2\right)}{h}\sum_{\xi=1}^{\infty}\frac{e^{-\zeta_2 y}\cos\frac{\pi}{h}z\xi}{\zeta_1\zeta_2(\zeta_1+\zeta_2)}\right\} \qquad (4.46)$$

$$\zeta_i^2 = \left(\frac{\pi}{h}\right)^2\xi^2 - i\eta_i^2 \quad ; \quad \eta_i^2 = \mu_o\omega\sigma_i \quad ; \quad \mathrm{Re}\sqrt{-i} > 0 \qquad (4.47)$$

Table 4.5

Surface Field Components Near a Fault of Finite Depth in Dimensionless Parameters

$$\sqrt{\frac{\sigma_1}{\mu_o\omega}}\frac{E_{x1}}{A} = \sqrt{i}\cot\sqrt{i}\,H_\varepsilon - \frac{1-\varepsilon}{H_\varepsilon}e^{-\sqrt{-i}\,Y_1} + \frac{2}{\pi}\varepsilon(1-\varepsilon^2)H_o^3\sum_{\xi=1}^{\infty}\frac{e^{-\frac{Y_1}{H_o\varepsilon}\sqrt{\xi^2-i(H_o\varepsilon)^2}}}{\left[\xi^2-i(H_o\varepsilon)^2\right]\sqrt{\xi^2-iH_o^2}\,D_1}$$

$$\sqrt{\frac{\sigma_2}{\mu_o\omega}}\frac{E_{x2}}{A} = \sqrt{i}\cot\sqrt{i}\,H + \frac{1-\varepsilon}{H_\varepsilon}e^{-\sqrt{-i}\,Y_2} - \frac{2}{\pi}(1-\varepsilon^2)H_o^3\sum_{\xi=1}^{\infty}\frac{e^{-\frac{Y_2}{H_o}\sqrt{\xi^2-iH_o^2}}}{\sqrt{\xi^2-i(H_o\varepsilon)^2}\left[\xi^2-iH_o^2\right]D_1} \qquad (4.48)$$

$$\sqrt{\frac{\sigma_1}{\mu_o\omega}}\frac{E_{y1}}{B} = \sqrt{i}\cot\sqrt{i}\,H\varepsilon - \frac{2}{\pi}i(1-\varepsilon^2)H_o\varepsilon\sum_{\xi=1}^{\infty}\frac{\xi^2 e^{-\frac{Y_1}{H_o\varepsilon}\sqrt{\xi^2-i(H_o\varepsilon)^2}}}{\left[\xi^2-i(H_o\varepsilon)^2\right]\sqrt{\xi^2-iH_o^2}\,D_2}$$

$$\sqrt{\frac{\sigma_2}{\mu_o\omega}}\frac{E_{y2}}{B} = \sqrt{i}\cot\sqrt{i}\,H + \frac{2}{\pi}i(1-\varepsilon^2)H_o\sum_{\xi=1}^{\infty}\frac{\xi^2 e^{-\frac{Y_2}{H_o}\sqrt{\xi^2-iH_o^2}}}{\sqrt{\xi^2-i(H_o\varepsilon)^2}\left[\xi^2-iH_o^2\right]D_2} \qquad (4.49)$$

Table 4.5 (cont'd)

Surface Field Components Near a Fault of Finite Depth, in Dimensionless Parameters

$$\frac{H_{z1}}{A} = -\sqrt{i}\,\frac{1-\varepsilon}{H\varepsilon}\,e^{-\sqrt{-i}\,Y_1} + i\,\frac{2}{\pi}\,(1-\varepsilon^2)H_o^2 \sum_{\xi=1}^{\infty} \frac{e^{-\frac{Y_1}{H_o\varepsilon}\sqrt{\xi^2-i(H_o\varepsilon)^2}}}{\sqrt{\xi^2-i(H_o\varepsilon)^2}\,\sqrt{\xi^2-iH_o^2}\,D_1}$$

$$\frac{H_{z2}}{A} = -\sqrt{i}\,\frac{1-\varepsilon}{H_\varepsilon}\,e^{-\sqrt{-i}\,Y_2} + i\,\frac{2}{\pi}(1-\varepsilon^2)H_o^2 \sum_{\xi=1}^{\infty} \frac{e^{-\frac{Y_2}{H_o}\sqrt{\xi^2-iH_o^2}}}{\sqrt{\xi^2-i(H_o\varepsilon)^2}\,\sqrt{\xi^2-iH_o^2}\,D_1} \qquad (4.50)$$

$$D_1 = \sqrt{\xi^2-i(H_o\varepsilon)^2} + \sqrt{\xi^2-iH_o^2}$$

$$D_2 = \sqrt{\xi^2-i(H_o\varepsilon)^2} + \varepsilon^2\sqrt{\xi^2-iH_o^2} \qquad (4.51)$$

layer is non-conducting and infinitely deep. From Table 4.4 the transition can be seen by allowing $|y| \to \infty$.

More usefully, we may impose limiting values on y, beyond which the coast effect is negligible. In all three fields of Table 4.5, the term before the summation requires $Y_j >> 1$ or $|y| >> \eta_j^{-1}$. For the E_y-fields, this condition may be relaxed when H_o (or $H_o\varepsilon$) $<< 1$; ie. when $h << 3\ \eta_j^{-1}$. Then it is only necessary that $Y_2 >> H_o$ (or $Y_1 >> H_o\varepsilon$), which is equivalent to $y >> h/3$. Under these conditions:

$$\left.\begin{matrix} E_{xj}/A \\ E_{yj}/B \end{matrix}\right\} \to \sqrt{i}\,\frac{\mu_o\omega}{\eta_j}\,\frac{\cos\sqrt{i}\,\eta_j(h-z)}{\sin\sqrt{i}\,\eta_j h}$$

$$E_{zj} \to 0$$

$$\left.\begin{matrix} H_{xj}/-B \\ H_{yj}/A \end{matrix}\right\} \to \frac{\sin\sqrt{i}\,\eta_j(h-z)}{\sin\sqrt{i}\,\eta_j h}$$

$$H_{zj} \to 0$$

These expressions are the well-known solutions for such a double-layered half-space; the derivation is outlined in App. 4.

Thus the effect of the fault is negligible at distances much greater than the penetration depth within the medium. If the basement depth is small compared to the penetration depth in either medium, the effect of the fault on the E_y-field is negligible at distances much greater than h/3.

If the conductivities σ_1 and σ_2 are nearly equal ($\eta_1 \to \eta_2$ or $\varepsilon \to 1$), the relations of Table 4.4 also show the above limiting behavior.

(b) Transition to an Infinitely Deep Fault

As the depth of the basement layer increases, the solutions of Table 4.4 approach those of Weaver (Table 4.1). We need only consider the E_x and H_x relations, since the other components are derived from them. By expanding the numerator of the first terms and considering the exponential representation, the limits as $h \to \infty$, may be easily found. The central term of the E_x expressions approaches zero in the limit. In treating the limit of the summation terms we note that although $h \to \infty$, the summation over ξ is also taken to infinity. Therefore we must replace $\sum_{\xi=1}^{\infty} f(\pi\xi/h)$ by $\int_0^{\infty} f(\xi')\, d\xi'$ and remember that the ζ_j's are defined differently in each case. Then for the E_x expressions (4.41):

$$\lim_{h \to \infty} \frac{\sqrt{i}}{\eta_j} \frac{\cos \sqrt{i}\, \eta_j (h-z)}{\sin \sqrt{i}\, \eta_j h} = \frac{\sqrt{-i}}{\eta_j} e^{-\sqrt{-i}\eta_j z}$$

$$\lim_{h \to \infty} \frac{2}{h} (\eta_2^2 - \eta_1^2) \sum_{\xi=1}^{\infty} \frac{e^{-\zeta_j |y|} \cos \frac{\pi}{h} z\xi}{\zeta_j \zeta_1 \zeta_2 (\zeta_1 + \zeta_2)} =$$

$$= \frac{2}{\pi} (\eta_2^2 - \eta_1^2) \int_0^{\infty} \frac{e^{-\zeta_j' |y|} \cos \xi' z \, d\xi'}{\zeta_j' \zeta_1' \zeta_2' (\zeta_1' + \zeta_2')}$$

where $\zeta_j' = \xi'^2 - i\eta_j^2$

With these limits the relations (4.41) become those of (4.1). Similarly in the H_x expressions (4.44):

$$\lim_{h \to \infty} \frac{\sin \sqrt{i}\, \eta_j (h-z)}{\sin \sqrt{i}\, \eta_j h} = e^{-\sqrt{-i}\, \eta_j z}$$

$$\lim_{h \to \infty} \frac{2\pi i\, \eta_j^2 (1-\varepsilon^2)}{h^2} \sum_{\xi=1}^{\infty} \frac{e^{-\zeta_j |y|} \sin \frac{\pi}{h} \xi z}{\zeta_j \zeta_1 \zeta_2 \, (\zeta_1 + \varepsilon^2 \zeta_2)} =$$

$$= i \frac{2}{\pi} \eta_j^2 (1-\varepsilon^2) \int_0^{\infty} \frac{\xi' e^{-\zeta_j' |y|} \sin \xi' z}{\zeta_j' \zeta_1' \zeta_2' \, (\zeta_1' + \varepsilon^2 \zeta_2')} \, d\xi'$$

Relations (4.44) then become (4.4).

The conditions for this transition to occur can be determined from the equations of Table 4.5. All of the fields behave as though the medium is infinitely deep if

$$H \varepsilon \gg 1$$

ie. if $$h \gg \eta_1^{-1} = (\mu_o \omega \sigma_1)^{-\frac{1}{2}}$$

Thus if the basement depth is much greater than the penetration depth in the land medium, the model may be treated as an infinitely deep fault. At shallower depths some of the fields will start to show differences in behavior. The oceanic electric field normal to the shoreline (E_{y2}) becomes insensitive to the basement depth if

$$H \gg 1$$

or $$h \gg \eta_2^{-1} = (\mu_o \omega \sigma_2)^{-\frac{1}{2}}$$

and since $\sigma_1 << \sigma_2$, this is usually an appreciably shallower depth than is required by the other components. Thus the E_y field is much less sensitive to the presence of the ocean bottom than the other field components.

(c) The Field Components at the Fault Plane

(i) Vertical Magnetic Field H_z

If we try to obtain an analytic expression for the H_z field component (4.50) in the plane of the fault, we obtain the relation:

$$\frac{H_z\Big|_{y=0}}{A} = -\sqrt{i}\,\frac{1-\epsilon}{H\epsilon} + \frac{2}{\pi} \sum_{\xi=1}^{\infty} \left\{ \frac{1}{\sqrt{\xi^2 - iH_o^2}} - \frac{1}{\sqrt{\xi^2 - i(H_o\epsilon)^2}} \right\} \cos \frac{\pi}{h} z\xi$$

The series obtained by separating this expression are divergent at the surface z = 0, although the complete series is not. An analogous relation to the expression (4.13) for an infinitely deep fault cannot be derived explicitly.

(ii) Tangential Electric Field E_x

Here, too, the series expressions in the relations (4.48) cannot be summed explicitly; the expressions reduce to:

$$\sqrt{\frac{\sigma_1}{\mu_o \omega}}\,\frac{E_x}{A} = \frac{1}{H} - \frac{2}{\pi} iH_o\epsilon \sum_{\xi=1}^{\infty} \frac{1}{\sqrt{\xi^2 - i(H_o\epsilon)^2}\sqrt{\xi^2 - iH_o^2}}$$

The summation term is not known in closed form, although the series is certainly convergent.

(iii) Normal Electric Field E_y

Since the analogous case for the fault of infinite depth did not yield on exact analytical expression for the value of the normal electric field immediately over the fault, a similar behavior might be expected for the present model:

The relations (4.49) cannot be explicitly summed; they reduce to:

$$\sqrt{\frac{\sigma_2}{\mu_o \omega}}\frac{E_{y2}}{B} = \varepsilon\sqrt{\frac{\sigma_1}{\mu_o \omega}}\frac{E_{y1}}{B} = \sqrt{i}\,\delta \cot \sqrt{i}\,H\delta -$$

$$- i\,\frac{2}{\pi} H_o \delta^2 \sum_{\xi=1}^{\infty} \frac{\xi^2}{\left[\xi^2 - i(H_o\delta)^2\right]\sqrt{\left[\xi^2 - i(H_o\varepsilon)^2\right]\left[\xi^2 - iH_o^2\right]}}$$

where $\delta^2 = \varepsilon^2/(1+\varepsilon^2)$.

Thus the analytical expressions obtained in §4.1.3(b), for the fields above a vertical fault of infinite depth, do not have simple analogues when the effect of an underlying basement is introduced. Therefore, we cannot obtain easily the values of the field components, either to estimate the changes while traversing the fault, or to use as a check on computer calculations. It is possible to approximate these relations for shallow basements, however.

4.2.4 Approximations for Shallow Basement Depths

We have already studied the limiting behavior of the field expressions when the basement layer is taken to be infinitely deep. It is of interest also to examine the opposite limit, where the depth of the basement is shallow in comparison with the penetration

depth in the ocean. In terms of the parameters described in Table 3.3, this means that we take

$$H = h\sqrt{\mu_o \omega \sigma_2} << 1 \tag{4.52}$$

If this condition is applied to Table 4.5, we see that the summation terms reduce to the form

$$\sum_{\xi=1}^{\infty} \frac{e^{-\xi Y_2/H_o}}{\xi^n}$$

where n = 2, 3, 4 for E_y, H_z, E_x respectively. This sum is a form of the polylogarithm of order n (see van Wijngaarden, 1954, Lewin, 1958, Fletcher et al., 1962), defined by

$$L_n(x) = \sum_{\xi=1}^{\infty} \frac{x^\xi}{\xi^n} \tag{4.53}$$

We also note the approximation:

$$\sqrt{i}\cot\sqrt{i}\,x \approx \frac{1}{x} - \frac{ix}{3} + \frac{x^3}{45} + \ldots \text{ as } x \to 0 \tag{4.54}$$

The expressions of Table 4.5 can be simplified considerably, under the approximation (4.52), and they are presented in Table (4.6).

The polylogarithm $L_n(x) \to \zeta(n)$, the Riemann Zeta Function, as the argument $x \to 1$. The expressions for the fields directly over the fault ($Y_j = 0$) are therefore greatly simplified, and they still satisfy the boundary conditions that E_x, σE_y, and H_z be continuous across the interface.

We note that $\zeta(n)$ has the values $\pi^2/6$; $\pi^3/25.8$; $\pi^4/90$ for n = 2, 3, 4 respectively.

4.2.5 Computation of the Fields Near a Fault of Finite Depth

The equations of Table 4.6 were used to provide a "shallow-depth" limit on the field behavior, and so avoid the time-consuming and expensive computer calculations necessary to evaluate the more precise expressions of Table 4.5. We mention here that d'Erceville and Kunetz (1962) have carried out such computations for the normal E_y field. We evaluated equations (4.54) - (4.56) using a desk-calculator, and, where necessary, the polylogarithm tables of van Wijngaarden (1954). The contributions to the fields from the last terms however are usually very small, especially for larger values of Y_1 or Y_2.

4.3 Discussion of Results

The equations in Tables 4.2 and 4.6 describe respectively the two limiting situations of an infinitely deep fault and a very shallow fault. While perhaps neither case is applicable to a given situation, we can expect the fields to provide limitations on the behavior of the true field.

Figures 4.3 (a, b, c) show the behavior of the three field components E_x, E_y, and H_z respectively, for a penetration depth ratio $\epsilon = 0.1$. The E_x and E_y magnitudes have been normalized to unity at the oceanic asymptote, so as to compare the relative changes across the coastline. The phases have not been normalized, and represent the phase difference between E_i and H_j.

The results of d'Erceville and Kunetz (1962) for the E_y component are included in Fig. 4.3 b, and the asymptotic limits of the magnitude

Table 4.6

The Field Components Near a Shallow Fault

$$\sqrt{\frac{\sigma_1}{\mu_o \omega}}\,\frac{E_{x1}}{A} \doteq \frac{1-(1-\varepsilon)\,e^{-\sqrt{-i}Y_1}}{H\varepsilon} - i\frac{H\varepsilon}{3} + \frac{H_o^3\varepsilon}{\pi}(1-\varepsilon^2)\,L_4\left[e^{-Y_1/H_o\varepsilon}\right]$$

$$\sqrt{\frac{\sigma_2}{\mu_o \omega}}\,\frac{E_{x2}}{A} \doteq \frac{\varepsilon+(1-\varepsilon)\,e^{-\sqrt{-i}Y_2}}{H\varepsilon} - i\,\frac{H}{3} + \frac{H_o^3}{\pi}(1-\varepsilon^2)\,L_4\left[e^{-Y_2/H_o}\right] \qquad (4.55)$$

$$\sqrt{\frac{\sigma_1}{\mu_o \omega}}\,\frac{E_{y1}}{B} \doteq \frac{1}{H\varepsilon} - i\,\frac{H\varepsilon}{3} - \frac{2}{\pi} iH_o\varepsilon\,\frac{1-\varepsilon^2}{1+\varepsilon^2}\,L_2\left[e^{-Y_1/H_o\varepsilon}\right]$$

$$\sqrt{\frac{\sigma_2}{\mu_o \omega}}\,\frac{E_{y2}}{B} \doteq \frac{1}{H} - i\,\frac{H}{3} + \frac{2}{\pi} iH_o\,\frac{1-\varepsilon^2}{1+\varepsilon^2}\,L_2\left[e^{-Y_2/H_o}\right] \qquad (4.56)$$

$$\frac{H_{z1}}{A} \doteq -\sqrt{1}\,\frac{1-\varepsilon}{H\varepsilon}\,e^{-\sqrt{-i}Y_1} + \frac{i\,(1-\varepsilon^2)}{\pi}\,H_o^2\,L_3\left[e^{-Y_1/H_o\varepsilon}\right]$$

$$\frac{H_{z2}}{A} \doteq -\sqrt{1}\,\frac{1-\varepsilon}{H\varepsilon}\,e^{-\sqrt{-i}Y_2} + \frac{i\,(1-\varepsilon^2)}{\pi}\,H_o^2\,L_3\left[e^{-Y_2/H_o}\right] \qquad (4.57)$$

and phase of both the E_x and E_y components are also shown in Figs. 4.3 (a, b), to indicate the trend of the fields at intermediate depths. Weaver's (1963a) result for the vertical magnetic field H_z (with $\varepsilon = 0.0159$; $H = \infty$) is likewise included in Fig. 4.3 c.

In Fig. 4.4 the electric field components have been combined by the method described in App. 1, to give the characteristics of the polarization ellipses. Some of the ellipses are also shown.

Before discussing the field behavior shown in Figs. 4.3 and 4.4, a few remarks should be made concerning the normalization of the electric fields. The electric fields at the surface depend on the depth of the basement (specified here by the parameter H) through the relationship given in App. 4, so that the normalization factor $E_{2\infty}$ applied to the E field is different for each depth. It is evident from Table 4.6 that when $H \ll 1$, this factor is very nearly 1/H. The normalization of the fields eliminates this variation due to the asymptotic geometry and allows the effect of the fault to be seen more clearly.

If the exact behavior of the E_i/H_j ratio is required, each of the magnitude curves in Figs. 4.3 a,b must be multiplied by the relevant normalization factor τ, given in Fig. 4.5, where

$$\tau = \sqrt{\frac{\sigma_2}{\mu_o \omega}} \quad \frac{E_{2\infty}}{H_{2\infty}} \tag{4.58}$$

4.3.1 The Vertical Magnetic Field H_z

The enhancement of the vertical magnetic field magnitude $|H_z/H_y|$ over the discontinuity is seen in Fig. 4.3 c. Weaver (1963a)

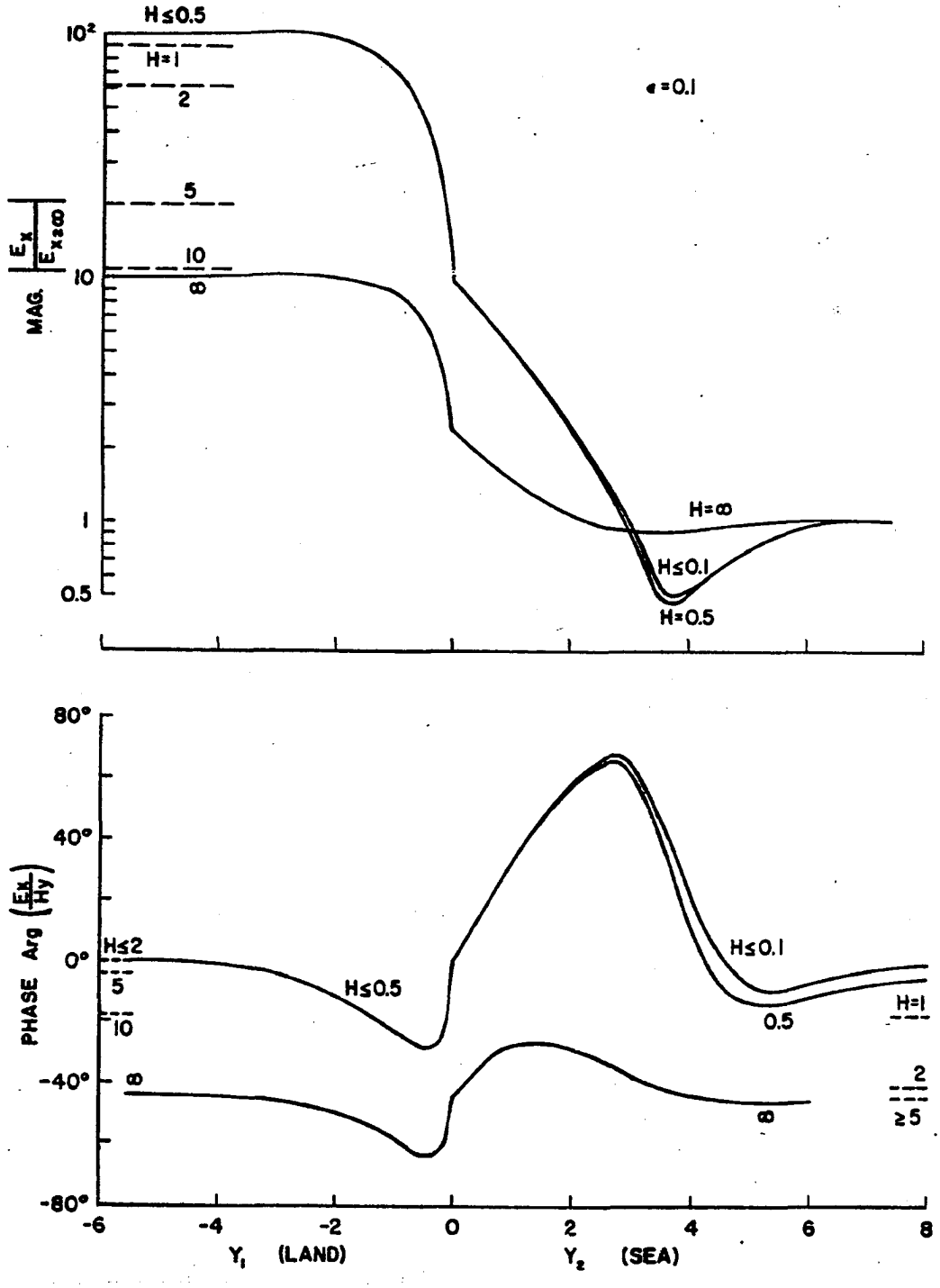

Fig. 4.3 (a) Parallel electric field near a fault, $\varepsilon = 0.1$

$\left|\frac{E_x}{E_{x2\infty}}\right|$; Arg $\frac{E_x}{H_y}$; parameters defined in Table 3.3

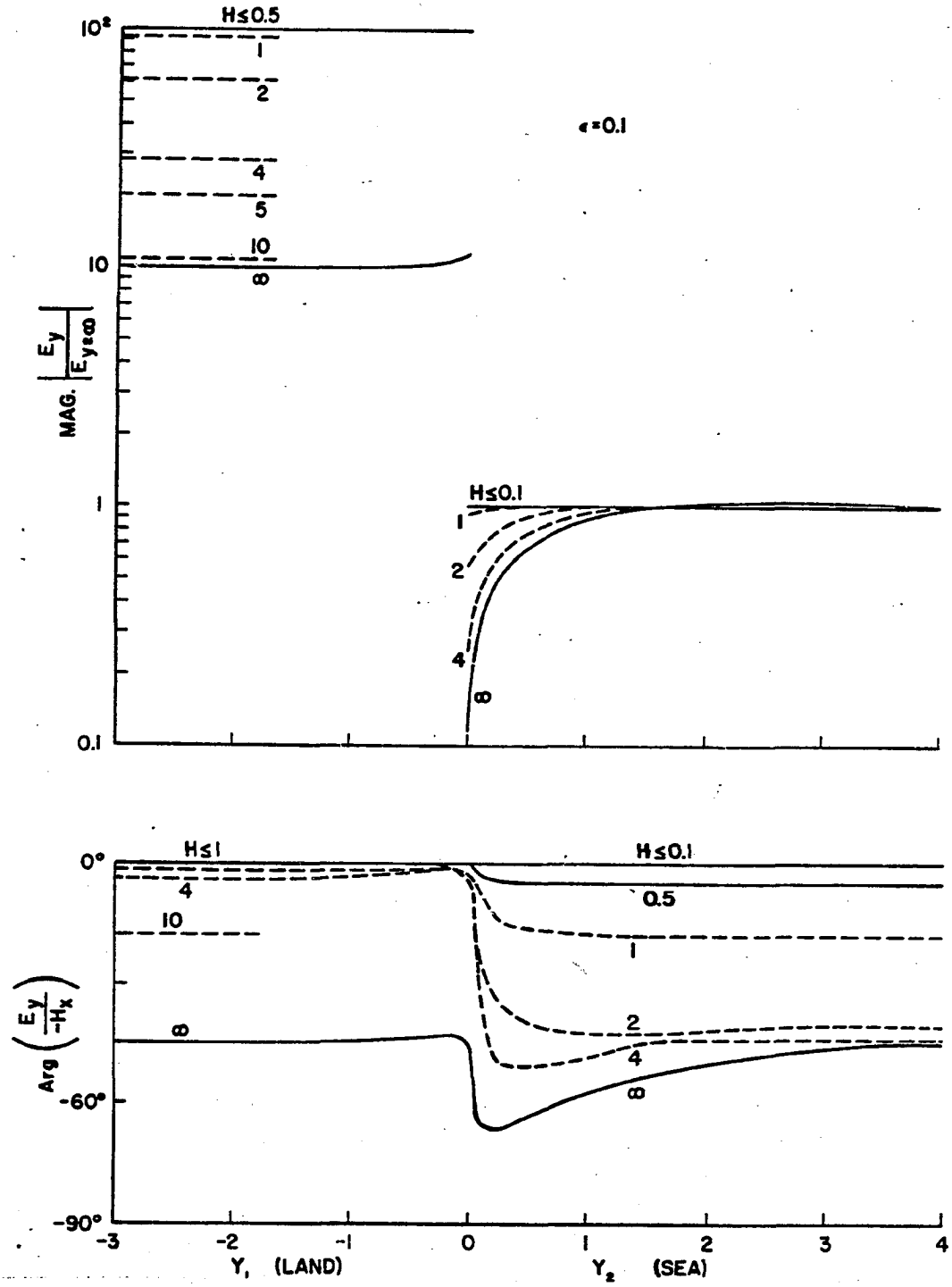

Fig. 4.3 (b) Normal electric field near a fault, e= 0.1

$\left|\frac{E_x}{E_{x2\infty}}\right|$ Arg $\frac{E_y}{-H_x}$

——Curves from d'Erceville and Kunetz (1962)

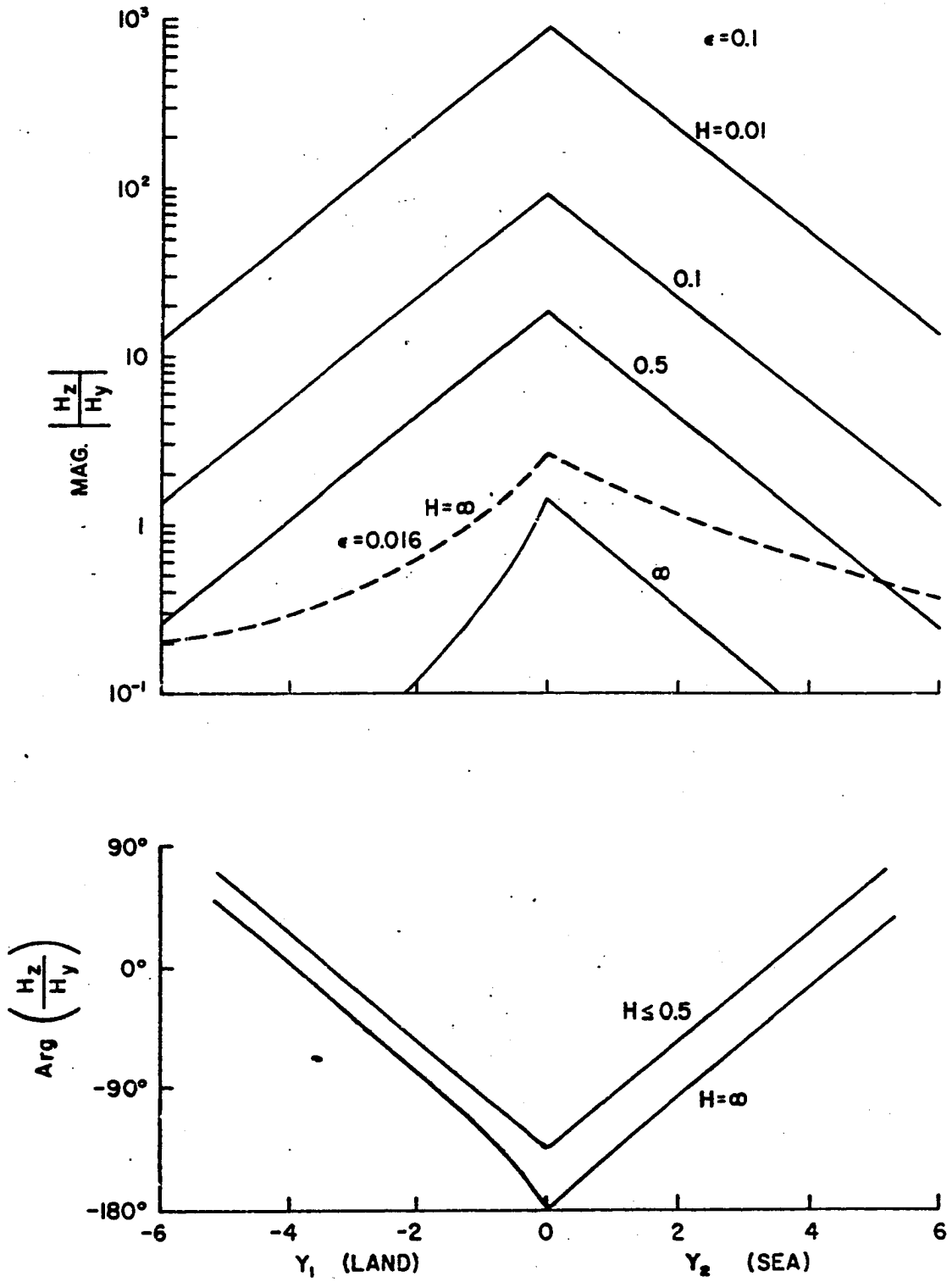

Fig. 4.3 (c) Vertical magnetic field near a fault, $\varepsilon = 0.1$

$\left|\frac{H_z}{H_y}\right|$; Arg $\frac{H_z}{H_y}$

---Curves from Weaver (1963a)

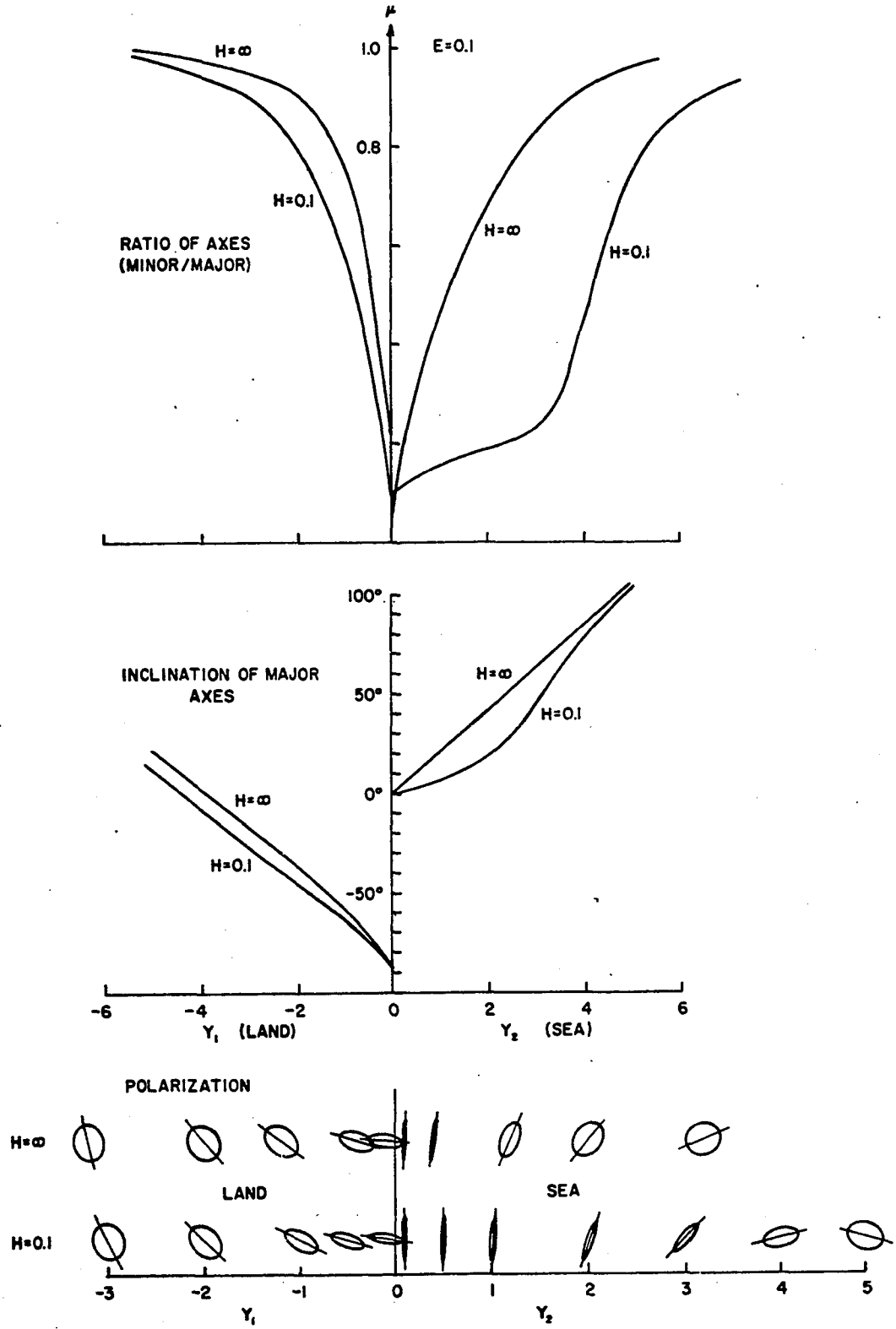

Fig. 4.4 The polarization of the electric field near a fault, $\varepsilon = 0.1$, assuming a left circularly polarized surface magnetic field. The parameters are defined in Table 3.3.

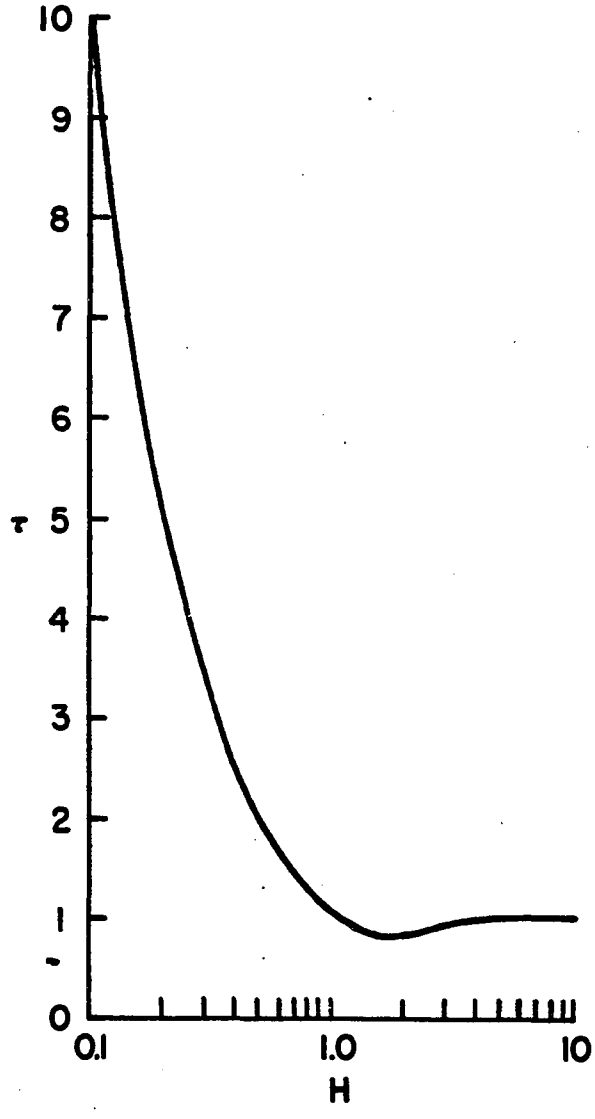

Fig. 4.5 The variation of the surface electric field over a plane double-layered half space with a non-conducting base layer, for varying basement depths H, as defined in Table 3.3. Also the normalization factor τ used in specifying the electric fields.

calculated this effect for infinitely deep media, but it is evident that the presence of a basement layer of low conductivity at a finite depth can greatly increase the degree of the enhancement. Over the fault itself the ratio becomes approximately $(1-\varepsilon)/H\varepsilon$ at small values of H, with an almost exponential decay on each side of the interface. Thus the enhancement is very dependent on the depth (measured in land penetration depths) provided it is relatively shallow, but is much less sensitive at greater depths.

Thus Weaver's estimate is probably a minimum-curve, although the values at the cusp are overestimates for any particular curve, a result of the idealization of the mathematical model. Such gradient discontinuities will not occur naturally, and the cusp would smooth over.

Different horizontal scales are used in Fig. 4.3. The near symmetry of the magnetic field curves in Fig. 4.3 c indicates that, at the same number of skin depths within each medium, measured from the fault, the vertical component of the magnetic field is nearly the same, at least for shallow basement depths. Since the land conductivity is usually much less than the oceanic conductivity, this means that the field falls off very much more slowly inland than to seawards when distance is measured in, say, meters, instead of penetration depths.

The influence of the conductivity ratio (land:ocean) on the vertical magnetic field is, probably seen most easily by examining the peak values directly over the fault (see Fig. 4.6 a). At

shallow depths ($H << 1$), the field component is nearly inversely proportional to ϵ at $Y = 0$, while for an infinitely deep fault, Weaver has shown the proportionality to $|\ln \epsilon|$ (see eq. 4.13). The vertical magnetic field increases as the disparity in the conductivity from land to ocean becomes greater. It can also be seen from Fig. 4.6 a that the field is much more sensitive to the conductivity ratio when a resistive basement is present at a shallow depth, than it is where an infinitely deep geometry is involved.

The effect of a change in the depth H on the phase difference between H_z and H_y is, however, not as marked as the effect on the magnitude. Over basements at a very shallow depth, the phase difference is evidently quite insensitive to H, although there is some change in phase, as the sub-stratum progresses to greater depth.

We note that, for a given physical situation where h and ϵ are fixed, the parameter H can be considered a measure of the frequency, since it is indeed proportional to $\sqrt{f}$. Figure 4.6 a then indicates the behavior of $|H_z/H_y|$ with ϵ over a fault of fixed depth, for various frequencies.

The frequency response for the vertical magnetic field where $\epsilon = 0.1$ is replotted in Fig. 4.7 a. For the values of H used here the curves of Fig. 4.3 c are very closely symmetrical, so that Fig. 4.7 a may be used to represent the field over both the land and the sea. It is direct reading over the sea, but to convert to readings over the land, the curves designated by $\lambda = n$ ($n = 0, 1, 2, 5, 10, 20, 30$) represent instead the curves $\lambda\epsilon = n$. The values of y, the

distance from the shore measured in meters, are given in the table on the figure. They also must be increased by the factor ε^{-1}. Thus, for example, the curves specify land distances, y, of 0, 50, 100, 250, 500, 1000, 1500, meters respectively, when h = 5m.

This simple transformation from the results at sea to those on land is only possible at low values of H (for $\varepsilon = 0.1$); at greater values of H, the curves of Fig. 4.3 c lose their symmetry as they approach the limit $H = \infty$ more closely. We have not carried out the calculations for these values, for the reasons stated in §4.2.5, but it can be seen from the examples given on Fig. 4.7 a and Table 4.7 that the curves given here cover a number of practical ranges of frequency and depth.

The frequency response of the vertical magnetic field H_z/H_y for the case $H = \infty$ is presented in Fig. 4.8 a for both the ocean and land media, assuming an ocean conductivity of 3 mho m^{-1}, and $\varepsilon = 0.1$. We notice that, while the ratio H_z/H_y directly over the fault is frequency dependent when there is a resistive basement at a finite depth, it becomes completely insensitive to frequency when the two media are considered to be uniform to great depth.

If the basement depth h were much greater than the land penetration depth η_1^{-1}, or $H \gg \varepsilon^{-1}$, the geometry could be treated as having conducting media of infinite depth, (see §4.2.3b). This conclusion means that Fig. 4.8 a may be used in place of Fig. 4.7 a when both the depth and frequency are sufficiently high. The examples incorporated in Fig. 4.7 a indicate, for instance, that Fig. 4.8 a would apply for $h \gtrsim 1$ km and $f > 10$ cps, or $H > 15$.

When the infinite fault geometry is applicable, the enhancement of $|H_z/H_y|$ immediately over the fault is quite independent of frequency. If the depth of the basement is finite, however, this is no longer true. At points away from the discontinuity, the H_z/H_y ratio is dependent on the frequency in all cases, but at great depths (see Fig. 4.8 a), points very close to the fault may be very frequency insensitive.

We conclude that, within a short distance on either side of a very deep vertical fault, the magnitude of the vertical magnetic field component will be enhanced, but the enhancement will be fairly insensitive to the frequency of the field. However, if the fault is terminated by a non-conducting basement at a finite depth below the surface, the field is enhanced more greatly and the increase is dependent on both the depth of the basement and the frequency. The $|H_z/H_y|$ ratio also increases in all cases, as the ratio between the conductivites on either side of the fault differs further from unity (i.e. as $\varepsilon \to 0$).

At low values of H, the phase of H_z relative to H_y remains constant (-135°) with frequency immediately over the fault, but changes toward -180° at greater H values. For the infinitely deep fault, this value is maintained independent of frequency. At points close to the discontinuity the phase is relatively insensitive to frequency at both very large and very small values of H; at intermediate values, however, it may be quite sensitive.

Table 4.7

Parameter Conversion Table for Use with Fig. 4.7

(i) Frequency f (cps)

h H=	10^{-4}	10^{-3}	10^{-2}	10^{-1}	1.0	10	10^{2}
5 m	0.169	1.69	16.9	169	1.69×10^{3}		
100 m	0.42×10^{-3}	0.42×10^{-2}	0.042	0.42	4.22	42.2	422
1 km			0.42×10^{-3}	0.42×10^{-2}	0.042	0.42	4.22

(ii) Distance from Fault (y over ocean y/ε over land)

h λ=	0	1	2	5	10	20	30	
5 m	0	5	10	25	50	100	150	(m)
100 m	0	0.1	0.2	0.5	1.0	2.0	3.0	(km)
1 km	0	1	2	5	10	20	30	(km)

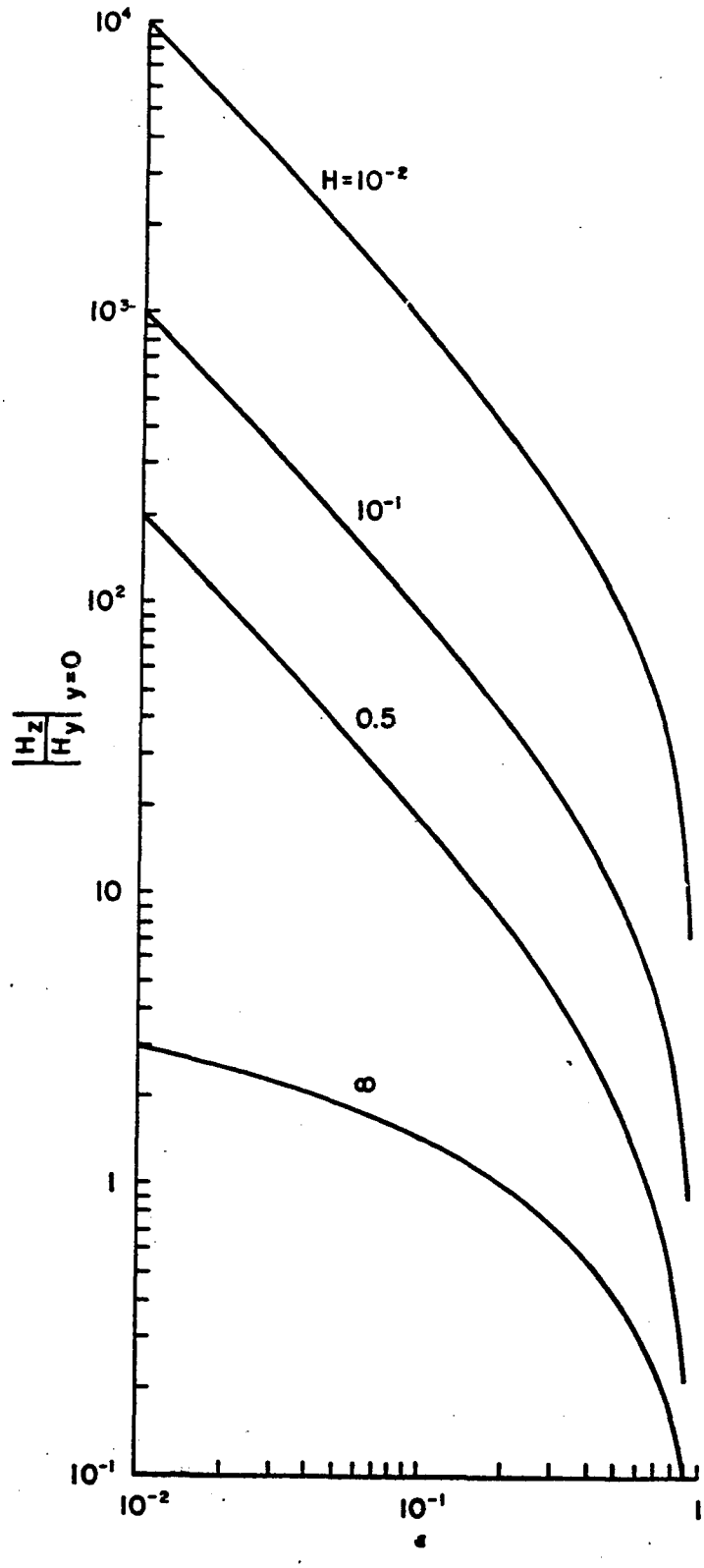

Fig. 4.6 (a) Enchancement of $|H_z/H_y|$ over a fault with various basement depths as a function of ε. The parameters are defined in Table 3.3.

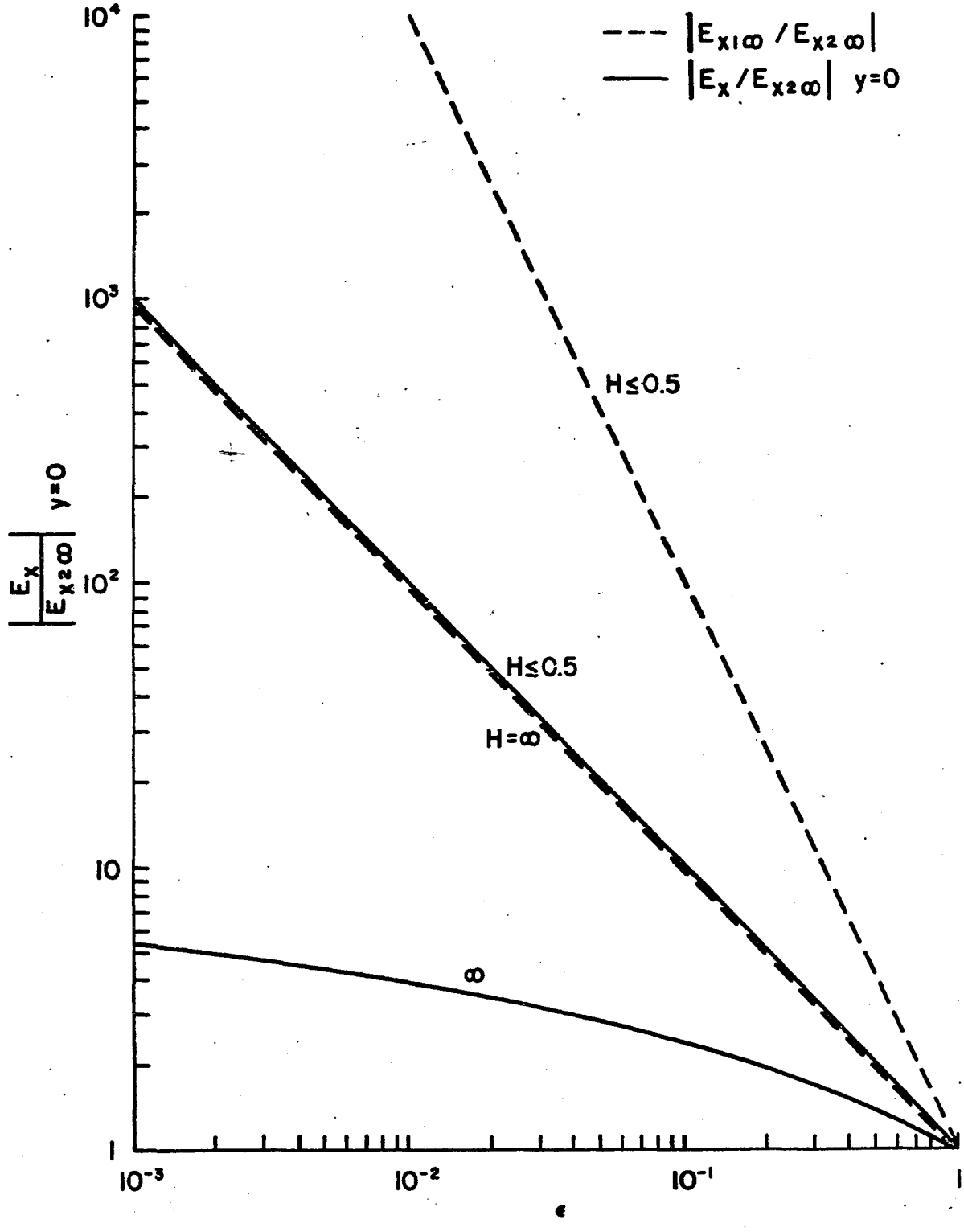

Fig. 4.6 (b) The variation of $|E_x/E_{x2\infty}|$ with ϵ.

—— The field directly over the fault
--- The asymptotic field on land $|E_{x1\infty}/E_{x2\infty}|$

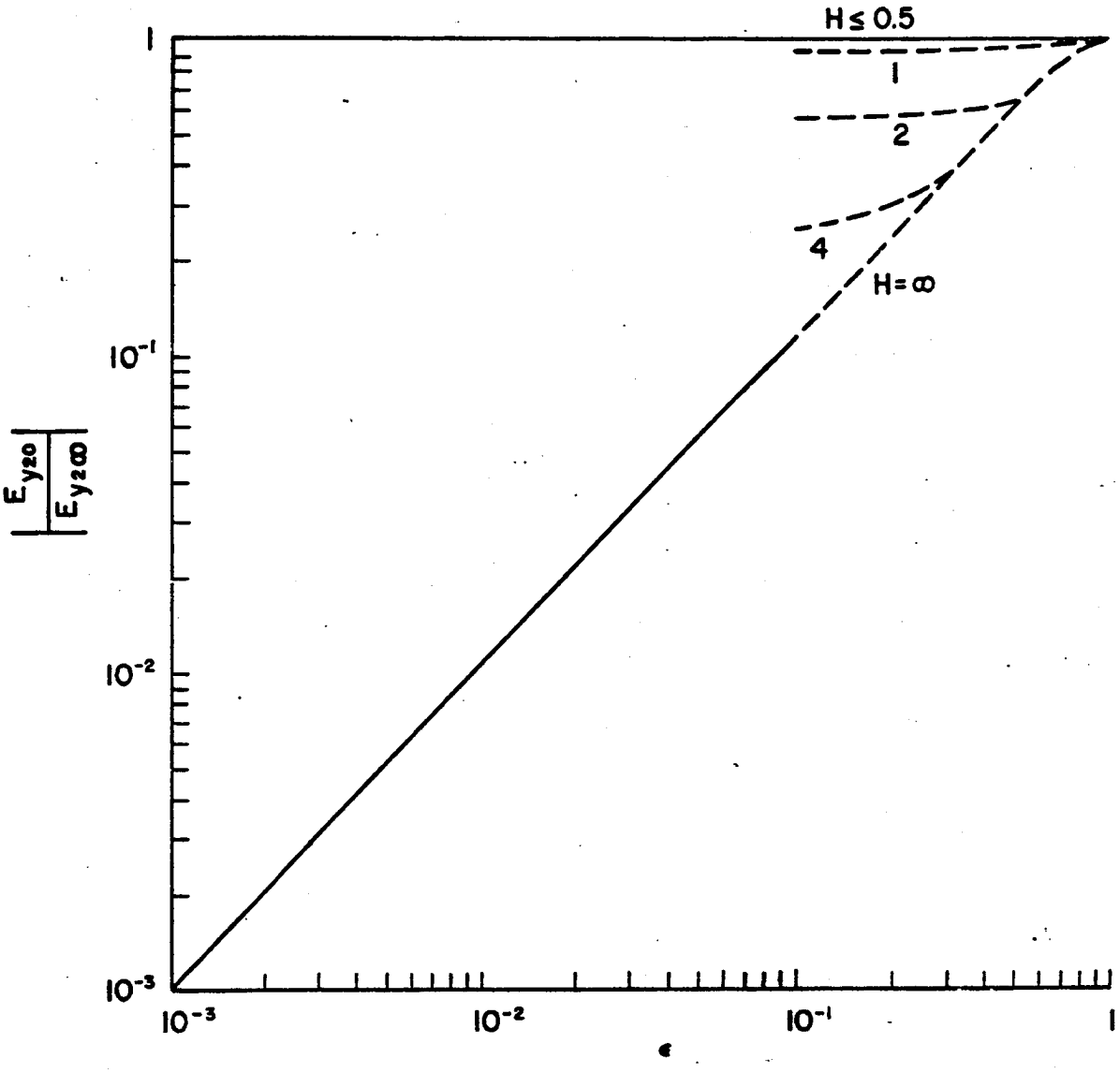

Fig. 4.6 (c) The variation of $|E_{y2}/E_{y2\infty}|$ over a fault, against ε.

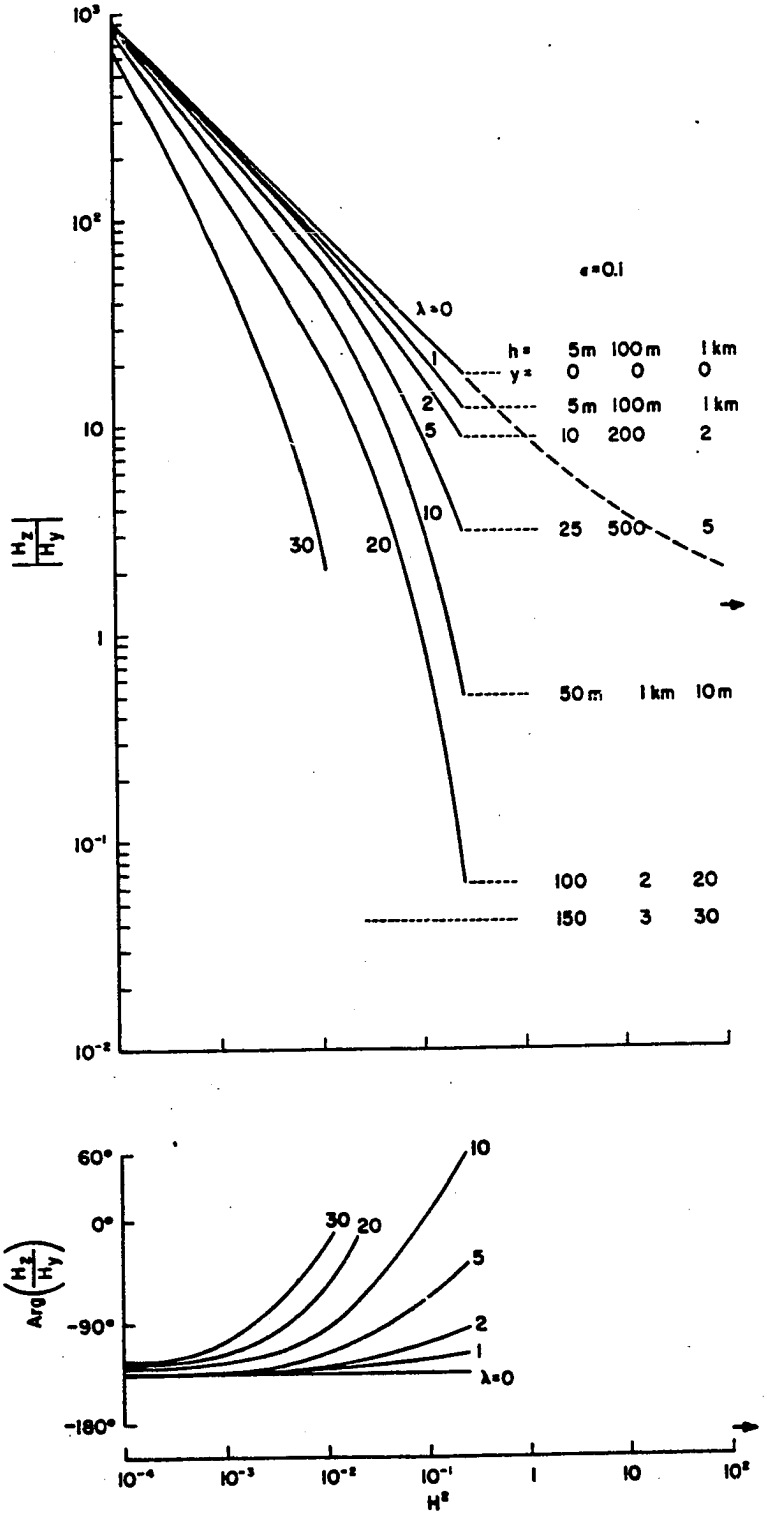

Fig. 4.7 (a) The frequency response of the vertical magnetic field H_z at sea near a vertical fault of various depths. Parameter $\lambda=y/h=Y_2/H$. To obtain the response over land, replace λ by $\lambda\varepsilon$. The abscissa $H^2 = 2\pi\mu_o\sigma_2 h^2 f = 0.2369 \times 10^{-4}\, h^2 f$ may be converted directly to frequency f in cps by multiplying by factors 1.69×10^3, 4.22, 0.0422 respectively when h = 5, 100 or 1000 meters. The arrow on the right hand side indicates the limit of the curve for $\lambda = 0$ as $H \to \infty$.

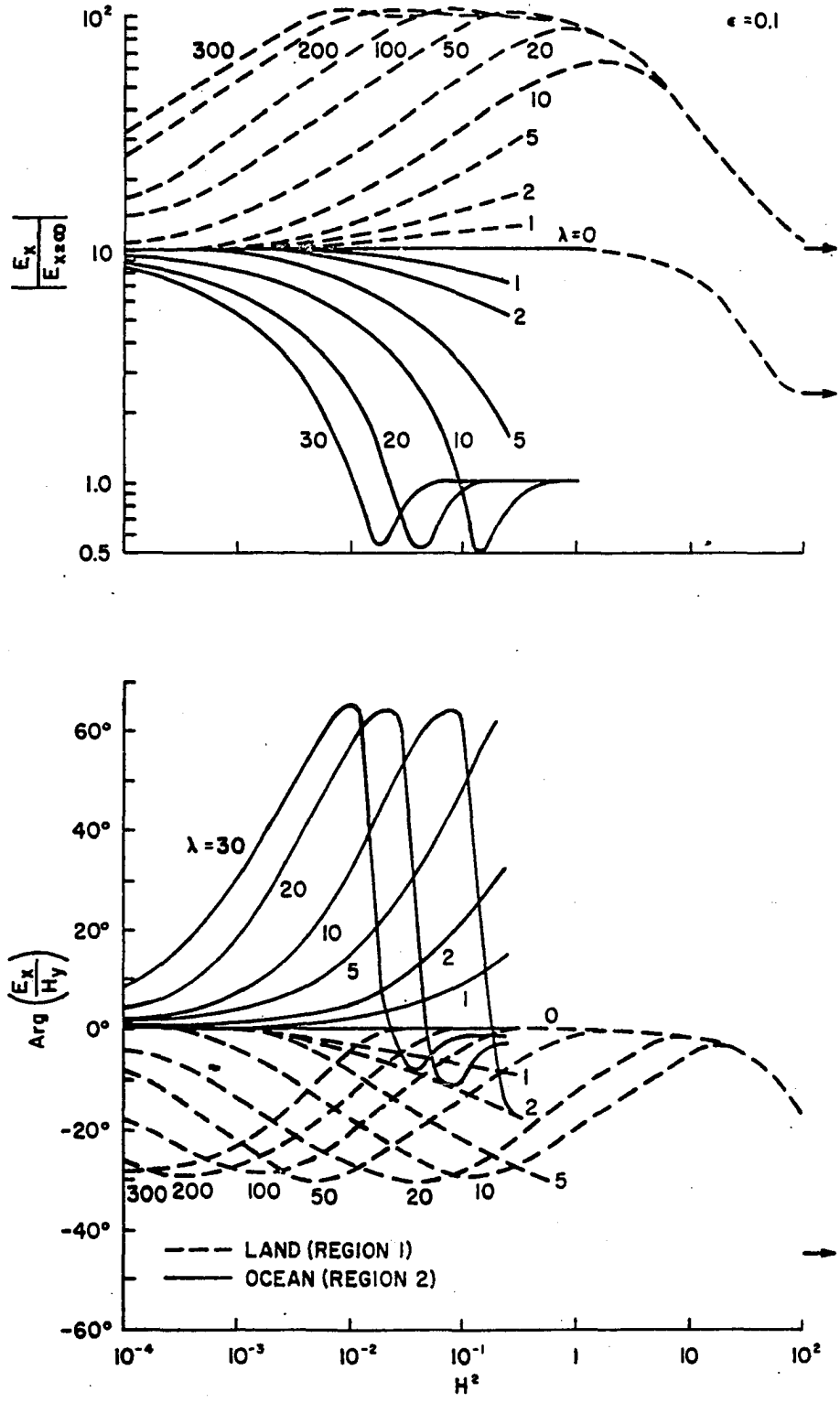

Fig. 4.7 (b) The frequency response of the tangential electric field E_x near a vertical fault of various depths. Parameter $\lambda=y/h=Y_2/H=Y_1/H\varepsilon$. For numerical value see Fig. 4.7(a). Abscissa $H^2 = 2\pi\mu_o\sigma_2 h^2 f = 0.2369 \times 10^{-4} h^2 f$ (h meter, f cps).

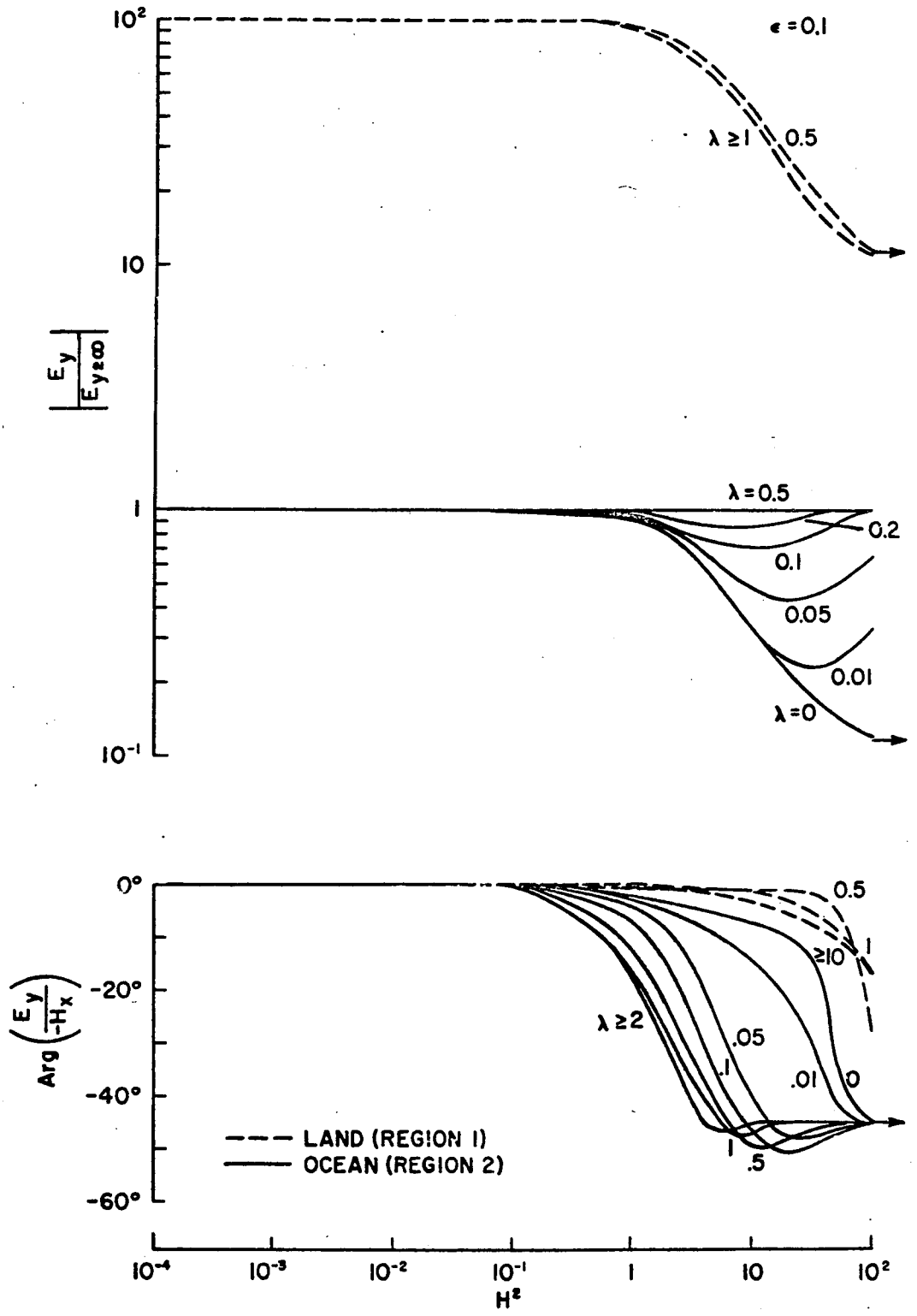

Fig. 4.7 (c) The frequency response of the normal electric field E_y near a vertical fault of various depths. Parameter $\lambda=y/h=Y_2/H=Y_1/H\varepsilon$. For numerical values see Fig. 4.7(a). Abscissa $H^2 = 2\pi\mu_o\sigma_2 h^2 f = 0.2369 \times 10^{-4} h^2 f$ (h meter, f cps).

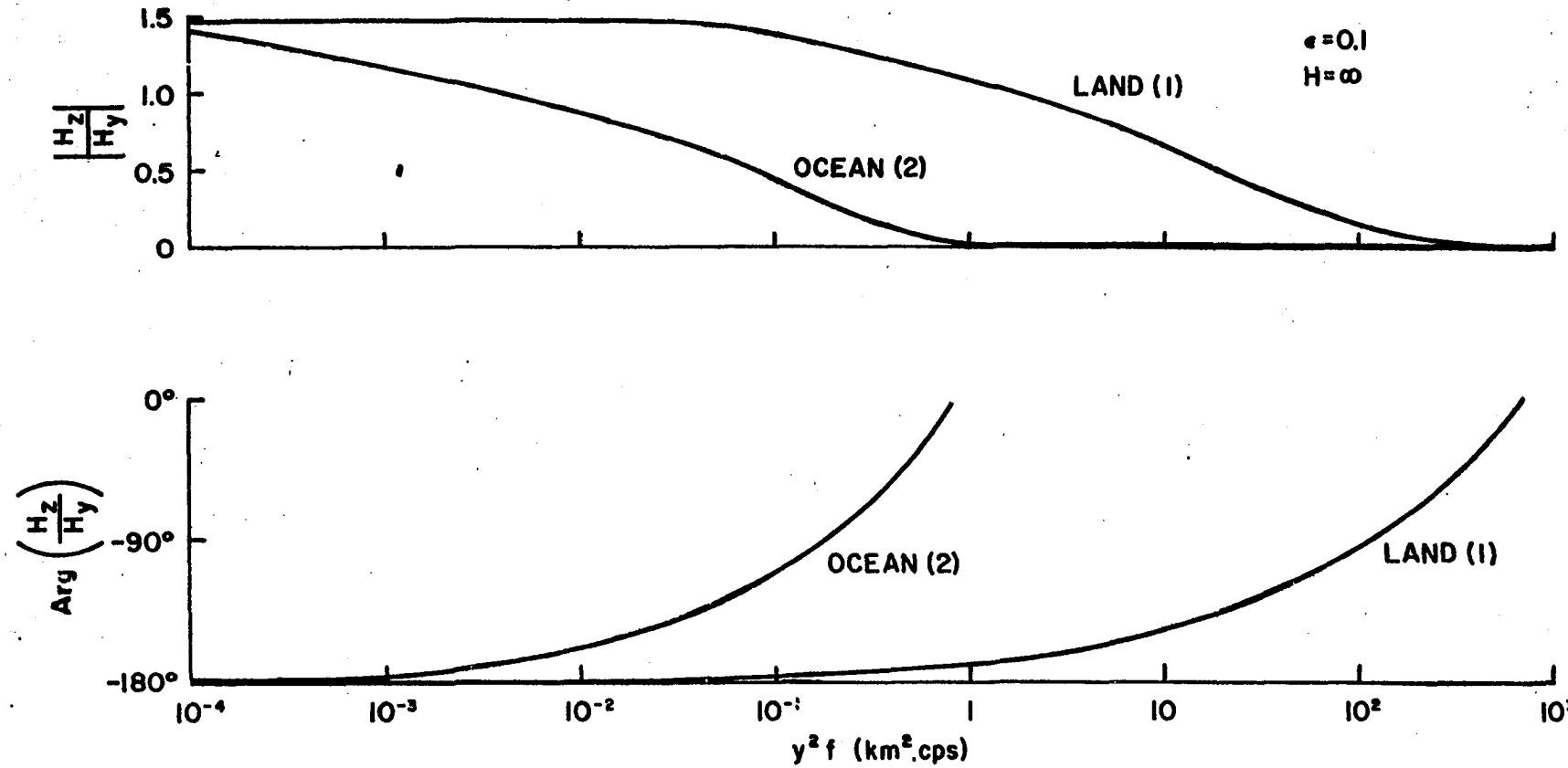

Fig. 4.8 (a) The frequency response of the vertical magnetic field H_z/H_y near an infinitely deep fault, for both land and sea. Distance y is measured in km, f in cps, for the abscissa $y^2 f$.

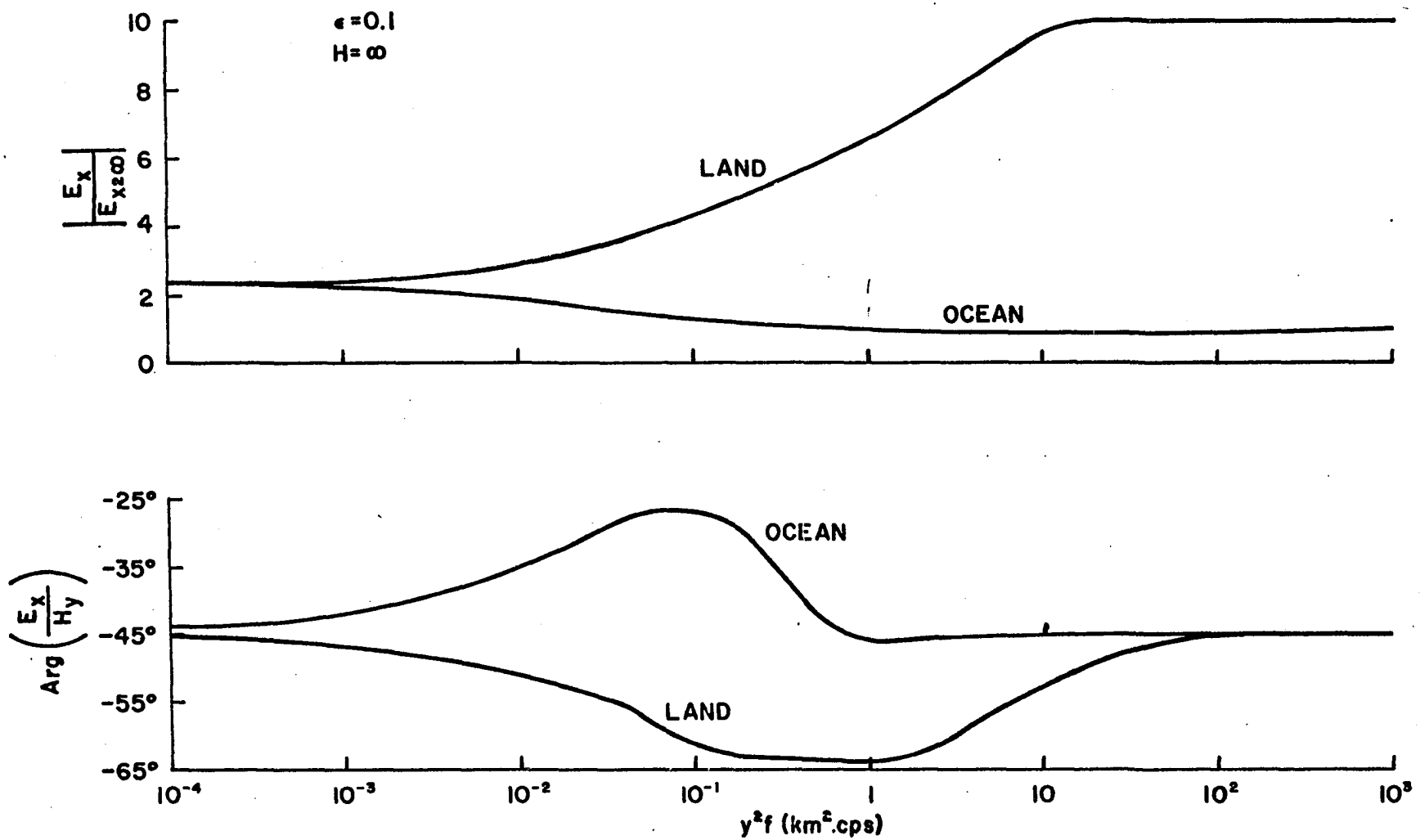

Fig. 4.8 (b) The frequency response of the tangential electric field, $|E_x/E_{x2\infty}|$ and Arg (E_x/H_y), near an infinitely deep fault, for land and sea. Distance y is measured in km, f in cps, for the abscissa y^2f.

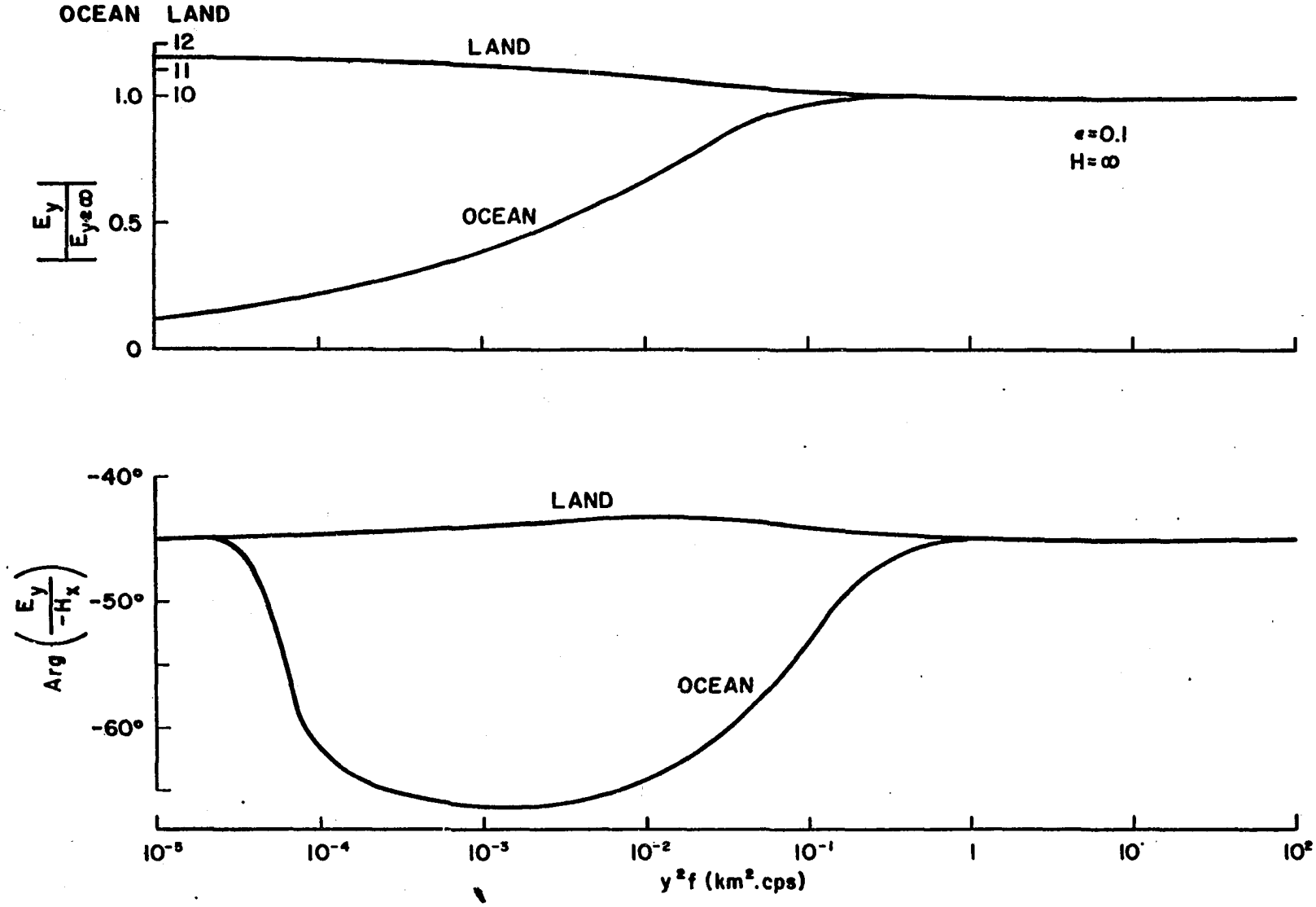

Fig. 4.8 (c) The frequency response of the normal electric field $|E_y/E_{y2\infty}|$ and Arg $(E_y/-H_x)$, near an infinitely deep fault, for land and sea. Note the change in ordinate scale over each medium. Distance y is measured in km, f in cps, for the abscissa y^2f.

4.3.2 The Horizontal Electric Fields E_x, E_y

The behavior of the electric fields near the fault is shown in Figs. 4.3 a,b. The fields are normalized in the manner described above; the normalization factors are given in Fig. 4.5. Evidently the presence of a basement increases the magnitudes of both $|E/E_{2\infty}|$ ratios and changes the phase of E_i/H_j in the asymptotic limit from -45^o towards 0^o. The presence of the fault further increases the tangential E_x field on the ocean side, and correspondingly reduces it on the land side. There is very little effect on the normal E_y field on the land side of the fault; the field on the ocean side however, is quite markedly reduced from its asymptotic value, the reduction increasing with the basement depth but becoming insensitive to depth for $H > 5$. It is the ocean E_y-field which is forced to change in order to satisfy the boundary conditions across the fault.

Similarly there is very little modification to the phase of the E_y/H_x field on the land side, but a sharp change occurs on the ocean side. The effect on the phase of E_x/H_y is appreciable in both media, but tends to be more pronounced at shallow depths, on the ocean side.

The combined effect of the fault on both electric fields is best studied through the polarization of the fields. Figure 4.4 shows the characteristics of the polarization ellipses computed by the method described in App. 1. It is evident that, immediately to the seaward of the fault, the fields are strongly polarized

along the coast. The inclination of the major axis gradually becomes more normal to the strike, and the ellipticity becomes less marked, with increase in either the frequency (at a fixed position) or the distance from the shore (at a fixed frequency). The presence of the non-conducting basement increases the linearity of the polarization ellipse at any given Y_2, and also retards the rotation of the major axis. This behavior may be interpreted as due to an electric current flow which is intensified by being confined to the shallow ocean.

On the land side the electric field is predominantly normal to the coastline. The inclination of the major axis decreases from normal with increasing distance from the coast or with increasing frequency, while the ellipticity is simultaneously reduced. The presence of the non-conducting basement reduces this effect.

Figure 4.6 b shows the variation of the E_x field with the conductivity ratio ε. The solid curves show the value of the field $|E_x/E_{x2\infty}|$ immediately over the fault for the two limiting cases when H is very small or very large. These values are always intermediate between the two asymptotic results, one of which is always unity here because of our normalization. The other asymptotic curves are also shown in Fig. 4.6 b for the two extreme cases - additional curves may be obtained from the relation

$$\left| \frac{E_{1\infty}}{E_{2\infty}} \right| = \frac{1}{\varepsilon} \left| \frac{\cot \sqrt{i}\, H_\varepsilon}{\cot \sqrt{i}\, H} \right|$$

Figure 4.6 c shows a similar plot for the E_y field. The ratio $|E_{y20}/E_{y2\infty}|$ is used, as the effect of the fault on the E_{y1} field is quite small. D'Erceville and Kunetz (1962) have made calculations for $\varepsilon = 0.33$, as well as the curves shown in Fig. 4.3 b, and these enable us to indicate the trend of the conductivity dependence of the E_y field, at intermediate values of H (Fig. 4.6 c).

The effect of the coast or fault on both the tangential (E_x) and normal (E_y) electric fields becomes more pronounced as the conductivity ratio changes further from unity. The effect on the tangential field is further increased by the presence of a non-conducting basement at some finite depth, but the effect on the normal field is reduced by the presence of a basement. The polarization ellipses at a particular Y-value thus become more linear as the value of ε decreases, especially at points relatively close to the fault plane. This will be true at any fixed value of the depth H (expressed in units of penetration depth).

The frequency response curves of the electric field components E_x and E_y are shown in Figs. 4.7 b and c respectively, with $\varepsilon = 0.1$. As the curves representing the fields over the land and sea in Fig. 4.3 a,b are quite distinct, there is a different set in Fig. 4.7 b,c for each region, unlike Fig. 4.7a. The curves of Fig. 4.7 b,c may be interpreted in practical cases through the examples of Fig. 4.7 a, or Table 4.7. They apply when the basement is at some finite depth; as $H \to \infty$, the frequency response is presented in Figs. 4.8 b,c. These last curves have been calculated for an ocean conductivity of 3 mho. m^{-1}.

The electric fields E_x and E_y immediately over the fault ($\lambda = 0$) are quite insensitive to frequency over either very shallow or very deep basements. However, they show a frequency dependence at some intermediate range of depths. The normal field (E_y) is quite insensitive to frequency over a wide range of both frequency and distance, as can be seen from Fig. 4.7 c. For instance, with a basement depth $h = 100$ m and $\varepsilon = 0.1$, the magnitude of the E_y field on the ocean side of the fault plane shows a dependence on frequency only for $f > 5$ cps, and then only within 50 m of the shore. The phase angle, however, is sensitive for $f > 0.5$ cps and exhibits a coast-effect behavior within about 100m; the response beyond this becomes that for a two-layered medium. On the land side of the fault plane, there is very little effect on either the magnitude or the phase of the E_y field, which can be attributed to the presence of the fault. A small phase effect occurs within 100 m of the shore, at frequencies exceeding about 1 cps. Although the normal E_y field is not greatly influenced, the tangential E_x-field shows a strong frequency dependence, as can be seen in Fig. 4.7 b. The characteristics of the polarization ellipses at a particular location will thus vary with frequency, the linearity increasing and the angle of inclination of the major axis changing towards normal (on land) or tangential (over the sea), as the frequency decreases.

4.3.3 Comparison with Observations

Most of the observations of the coast effect (see §2.6.2) either involve coastal geometries which are unlike ours, or are concerned

with determining the approximate enhancement of the vertical magnetic field. However Mansurov's observations at Mirny may be compared with the theory developed here. At Mirny the land falls sharply into the sea, and then flattens out at a depth of about 100 m. The observations have already been described and we use the analysis of Rokityanskii (1963), summarized in Fig. 2.1.

Rokityanskii gives a frequency response curve for the tangential telluric field E_t in the ocean; this has been replotted in Fig. 4.9 in terms of the parameters used in this discussion. The ocean floor near Mirny, actually slopes from 100 m depth at offshore distance 100 m, to 400 m depth at 10 km distance, but the factor of 4 in depth h makes no difference to the emu normalization parameter $\tau\sqrt{f/2\sigma}$ (see Fig. 4.5), needed to modify Rokityanskii's values. The value of the ocean conductivity was taken as σ_2 = 3 mho m^{-1} = 3.10^{-11} emu, so that τ = 2.65 mV km^{-1} γ^{-1}.

In our analysis, we have assumed that the underlying substratum is completely non-conducting. This is unlikely to hold true in reality, and Rokityanskii has shown the response when this condition is relaxed. He gave the frequency response of the E-field over a plane double-layered medium, for several conductivity ratios (Fig. 2.1 c). The field at 10^{-4} cps would be reduced to 18%, 36%, and 64% of the field at 0.1 cps, when $\varepsilon = 2\text{x}10^{-3}$, $6.3\text{x}10^{-3}$, $2\text{x}10^{-2}$ respectively. The non-zero conductivity of the basement is undoubtedly the cause of the decrease in the E_t field at 10^{-4} cps to 14% of its value at 0.1 cps (Fig. 4.9 a). Such a decrease indicates that the value of ε is 10^{-3} or less.

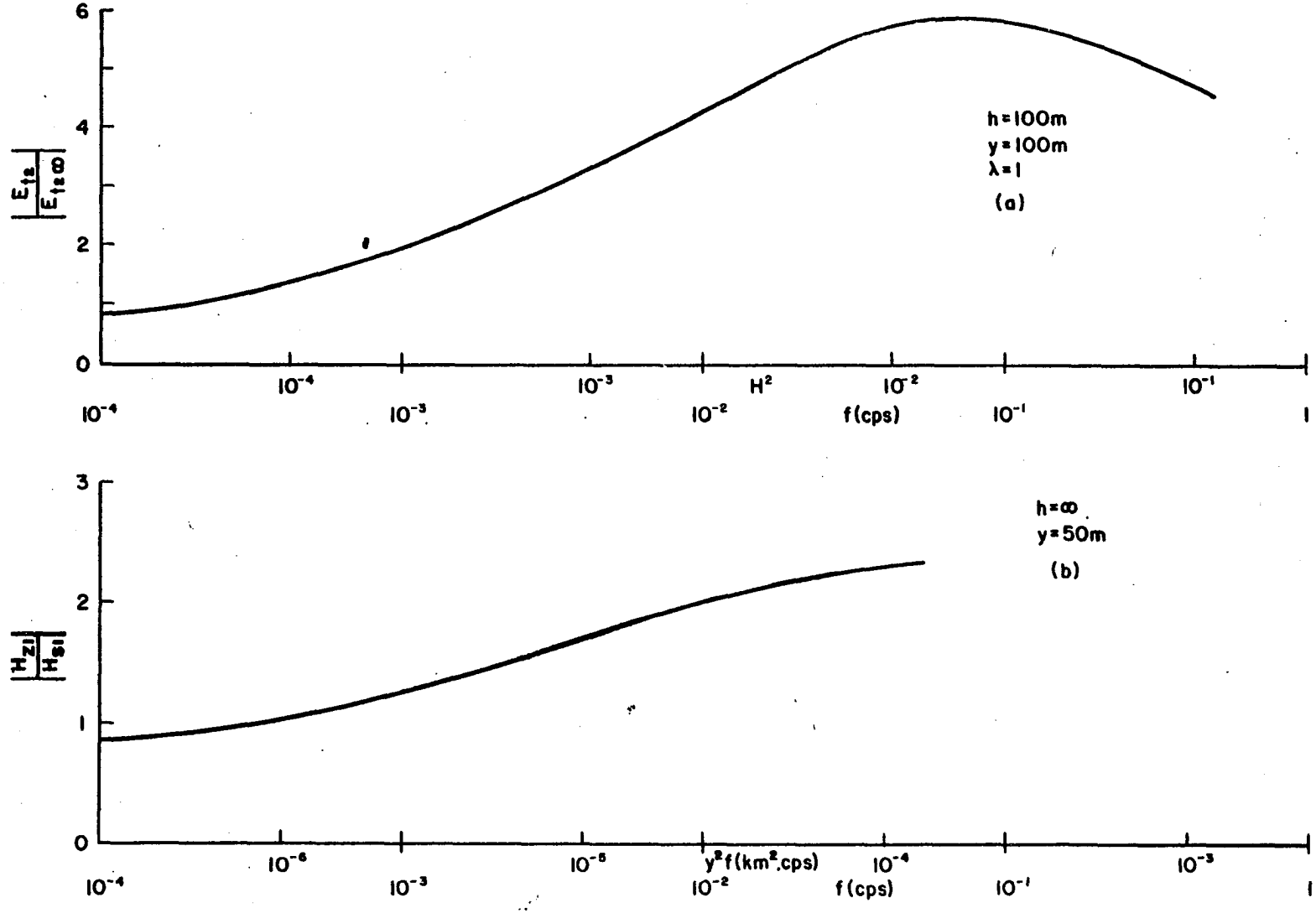

Fig. 4.9 The frequency response of the fields at Mirny, replotted from Rokityanskii (1963) in terms of the parameters of this discussion. (a) $|E_{t2}/E_{t2\infty}|$, 100 m to seawards of the shoreline (b) $|H_{z1}/H_{s1}|$, 50 m inland from the shore. The scale for (a) assumes h = 100 m, σ_2 = 3 mho. m.$^{-1}$.

The observation point was situated 100 m offshore so that $\lambda = y/h = 1$. Our frequency response curves for E_t (Fig. 4.7 b) were calculated for $\varepsilon = 10^{-1}$ and therefore are not directly applicable. However, the $\lambda = 1$ curve shows a decrease of the E_t-field to 85% at $H^2 = 0.1$ from the field at $H^2 = 10^{-2}$. Examination of Figs. 4.3 c and 4.6 b indicates that a more rapid fall off in the $|E_t/E_{t\infty}|$ frequency response would be expected at a value of $\varepsilon = 10^{-3}$. The observation point is close to the shore, and the $\lambda = 1$ curve is sufficiently close to the $\lambda = 0$ curve of Fig. 4.7 b, that, at $H^2 = 0.1$, the fall off for $\varepsilon = 10^{-3}$ would not be much sharper than for $\varepsilon = 10^{-1}$. In Fig. 4.9 a we see that there is a decrease to 80% observed between $H^2 = 10^{-2}$ and 10^{-1}, in good agreement with the theory.

We thus verify quantitatively Rokityanskii's suggestion that the decline in the frequency response of the tangential field E_t at periods below 10 sec is due to the presence of the coast.

The behavior of the vertical magnetic field is not so well verified, but as the model is less realistic over the land, perhaps this is to be expected. There is no evidence for a non-conducting basement 100 m underground at Mirny and, as the rock is metamorphic, we are probably justified in assuming it to be very deep and not underlain by a non-conducting medium. If we used the curves for $H = \infty$ (Fig. 4.8 a) to compare with Fig. 4.9 b, taking $y = 0.05$ km, we see that the frequency response for $f < 0.1$ cps is flat. This behavior would occur for $\varepsilon = 10^{-3}$ as well as $\varepsilon = 10^{-1}$. The downward trend of the $|H_z/H_s|$ response curve below 10^{-1} cps is therefore

unlikely to be due to the presence of the coast. (H_s is the total horizontal surface vector.) It is more likely that, at these frequencies, a variation in the deep stratification of the earth is responsible.

The selection of $h = \infty$ for the land medium is also supported by the small enhancement of H_z - unless the medium were exceedingly deep, the enhancement of $|H_z/H_y|$ would be very much greater than the factor of two observed (see Fig. 4.6 a). Much larger enhancements of the vertical field were found by the Canadian investigators, in the several studies reviewed in §2.6.2. However they do not approach the values obtained in this calculation for the field immediately over the fault, probably because the idealized geometry results in an overestimation of the H_z-field.

The studies of Lambert and Caner (1965) in the Vancouver Island area also yielded frequency response data. At the coastal station Tofino, the frequency response curve shows a decrease of the H_z ratio between Tofino and the observatory at Abbotsford (30 km inland). The decrease at 50 sec period is about 87% of the ratio at 200 sec period. Figure 4.8 a shows a decrease in the $|H_z/H_y|$ ratio of about 90-95% in this period range if we assume Tofino to be 2-3 km from the coast. The Abbotsford response may be assumed flat at these frequencies. The experimental results (accurate to within about 10%) thus agree with the theory when the basement is assumed infinitely deep, and the conductivity ratio is taken as 1:100. The effect of the ocean bed would be to reduce the higher frequency response

further, but the unknown parameters (h, y, ε) make the application of Fig. 4.7 a too unreliable.

The computations of this chapter are further applied to a specific case in §5.4.

CHAPTER V

THE EFFECT OF A DYKE OR LONG PROMONTORY ON THE MAGNETOTELLURIC FIELD

In this chapter we consider the influence of a dyke or long promontory on the magnetotelluric field. In regarding a dyke as a model of a long promontory, we assume both ends of the promontory are sufficiently remote that the effects due to them may be neglected.

The treatment follows that of the previous chapter. First, we study the infinitely deep dyke and then extend the work of Rankin (1962) (see §3.4.7) to allow for the effects of the basement. The shorter term "dyke" is usually used, even in situations where a coast is being discussed.

5.1 The Infinitely Deep Dyke

For the geometry of our model we refer to Fig. 5.1a. The dyke is of width ℓ and the dyke material has an electrical conductivity σ_1; the external medium has a conductivity σ_2. The coordinate system used is shown in Fig. 5.1b, having z vertically downwards, x parallel and y normal to the strike of the dyke and the discontinuity planes at $y = \pm\frac{1}{2}\ell$. The surface of the earth is the plane $z = 0$.

5.1.1 The Static Case

The behavior of the fields in the limit as the frequency becomes zero is discussed in §3.4.3 with reference to a single vertical discontinuity--$E_{//}$, $\sigma E_{\perp}$, $H_{//}$, $H_{\perp}$ are all continuous across the interface.

For a parallel-sided vertical fault, the form of the fields is shown in Fig. 5.2. Again these represent the limiting behavior of the fields in the general wave case, as the frequency decreases.

5.1.2 The Wave Case

When the frequency is non-zero, the trivial solutions above are no longer valid, and the fields must be determined from Maxwell's equations. We use the boundary conditions described in §3.4.3) to solve Maxwell's equations under the dyke geometry. The two polarization conditions (§3.4.2) are treated separately.

(a) E-Polarization. The surface E-vector is parallel to the dyke. The equation to be solved is (3.24), viz.

$$\frac{\partial^2 E_x}{\partial y^2} + \frac{\partial^2 E_x}{\partial z^2} + i\eta^2 E_x = 0 \tag{5.1}$$

where

$$\eta^2 = \mu_o \omega \sigma$$

Since we know $\partial E_x/\partial z$ at the surface $z = 0$ and at infinity (conditions (iii) and (vi) of Table 3.2) we may use the Fourier cosine transformation and its inverse, defined by:

$$\bar{E}_x(y,\xi) = \sqrt{\frac{2}{\pi}} \int_0^\infty E(y,z) \cos \xi z \, dz \tag{5.2}$$

$$E_x(y,z) = \sqrt{\frac{2}{\pi}} \int_0^\infty \bar{E}(y,\xi) \cos \xi z \, d\xi \tag{5.3}$$

If we apply the transform (5.2) to (5.1) and use the boundary conditions (iii) and (vi) of Table 3.2, eq. (5.1) reduces to

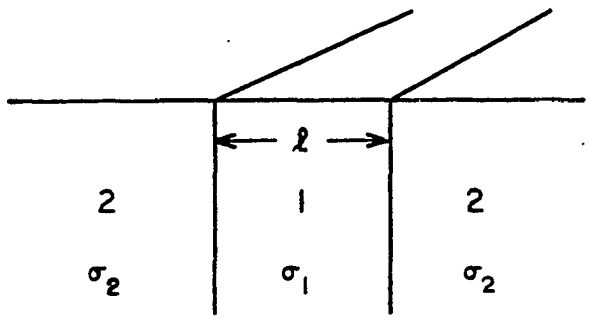

(a)

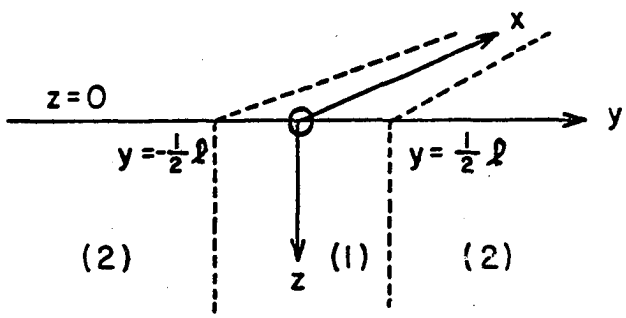

(b)

Fig. 5.1 (a) Model of an infinitely deep dyke.
(b) The coordinate system.

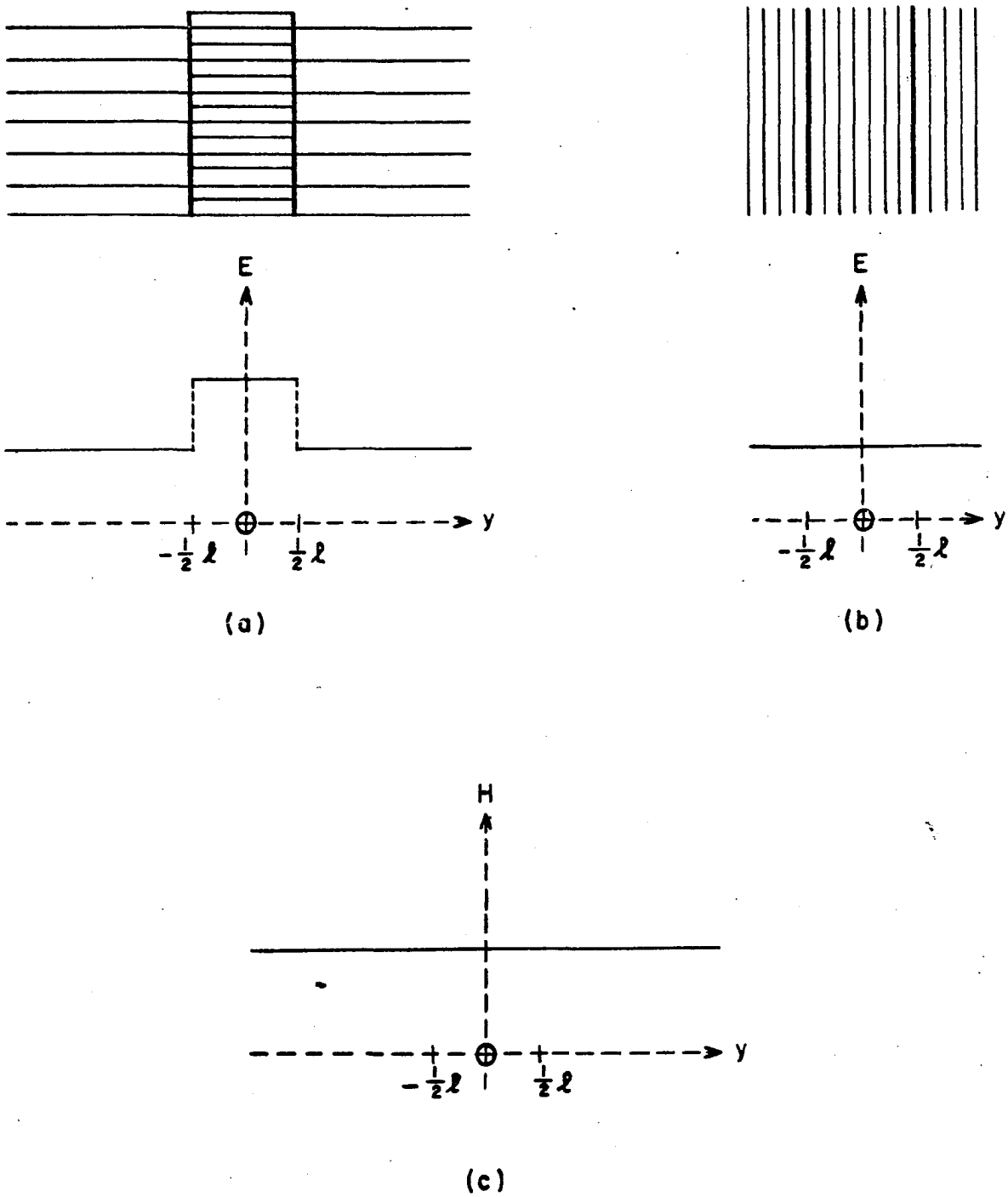

Fig. 5.2 Static fields near a dyke (a) normal electric field (b) tangential electric field (c) magnetic field.

$$\frac{d^2\bar{E}_x}{dy^2} - \zeta^2 \bar{E}_x = \sqrt{\frac{2}{\pi}}\, i\omega\mu_o A \tag{5.4}$$

where

$$\zeta^2 = \xi^2 - i\eta^2 \tag{5.5}$$

This second order differential equation has the general solution

$$\bar{E}_x(y,\xi) = \alpha(\xi)\, e^{\zeta y} + \beta(\xi)\, e^{-\zeta y} - \frac{i\mu_o \omega A}{\zeta^2}\sqrt{\frac{2}{\pi}}$$

where the coefficients $\alpha(\xi)$, $\beta(\xi)$ are determined by the boundary conditions.

Since $\mathrm{Re}(\zeta) > 0$ always, the symmetry condition (vii) and the condition at infinity (v) of Table 3.2 give:

Region 1: $|y| < \frac{1}{2}\ell$ $\qquad \alpha(\xi) = \beta(\xi) = \frac{1}{2}\gamma_1(\xi)$, say

Region 2: $|y| > \frac{1}{2}\ell$ $\qquad \alpha(\xi) = 0 \;;\quad \beta(\xi) = \gamma_2(\xi)$, say

The solution in each region is then:

$$\begin{aligned} |y| < \tfrac{1}{2}\ell \;:\; \bar{E}_{1x}(y,\xi) &= \gamma_1(\xi)\cosh \zeta_1 y - \frac{i\mu_o \omega A}{\zeta_1^2}\sqrt{\frac{2}{\pi}} \\ |y| > \tfrac{1}{2}\ell \;:\; \bar{E}_{2x}(y,\xi) &= \gamma_2(\xi)\, e^{-\zeta_2 |y|} - \frac{i\mu_o \omega A}{\zeta_2^2}\sqrt{\frac{2}{\pi}} \end{aligned} \tag{5.6}$$

Conditions (i) and (ii) of Table 3.2, when applied to the interfaces $y = \pm\frac{1}{2}\ell$, provide a pair of simultaneous equations from which the coefficients $\gamma_j(\xi)$ may be determined:

$$\gamma_1(\xi) = \mu_o \omega A \sqrt{\frac{2}{\pi}} \frac{(\eta_2^2 - \eta_1^2)}{\zeta_1^2 \zeta_2} \frac{1}{\Delta_1}$$

$$\gamma_2(\xi) = -\mu_o \omega A \sqrt{\frac{2}{\pi}} \frac{(\eta_2^2 - \eta_1^2)}{\zeta_1 \zeta_2^2} \frac{e^{\frac{1}{2}\ell\zeta_2} \sinh \frac{1}{2}\ell\zeta_1}{\Delta_1} \tag{5.7}$$

$$\Delta_1 = \zeta_1 \sinh \tfrac{1}{2}\ell\zeta_1 + \zeta_2 \cosh \tfrac{1}{2}\ell\zeta_1$$

The solution for E_x is now obtained by taking the inverse transform (5.3) of (5.6). The inverses of the last terms of relations (5.6) may be explicitly expressed (see App. 5), since:

$$\int_0^\infty \frac{\cos \xi z}{\xi^2 - i\eta^2} d\xi = \frac{\sqrt{i}\pi}{2\eta} e^{-\sqrt{-i}\eta z} \quad ; \quad \text{Re } \sqrt{-i} > 0 \tag{5.8}$$

The inverse trnasforms in the two regions are then:

$$|y| < \tfrac{1}{2}\ell : E_{1x}(y,z) = \frac{\mu_o \omega A}{\sqrt{i}} \left\{ \frac{e^{-\sqrt{-i}\eta_1 z}}{\eta_1} + \sqrt{i} \frac{2}{\pi} (\eta_2^2 - \eta_1^2) \int_0^\infty \frac{\cosh \zeta_1 y}{\zeta_1^2 \zeta_2 \Delta_1} \cos \xi z \, d\xi \right\}$$

$$|y| > \tfrac{1}{2}\ell : E_{2x}(y,z) = \frac{\mu_o \omega A}{\sqrt{i}} \left\{ \frac{e^{-\sqrt{-i}\eta_2 z}}{\eta_2} - \sqrt{i} \frac{2}{\pi} (\eta_2^2 - \eta_1^2) \int_0^\infty \frac{e^{-(|y| - \frac{1}{2}\ell)\zeta_2} \sinh \frac{1}{2}\ell\zeta_1}{\zeta_1 \zeta_2^2 \Delta_1} \cos \xi z \, d\xi \right\} \tag{5.9}$$

with $\mathrm{Re}(\zeta_j) > 0$, always.

These relations for E_x constitute the solution of eq. (5.1), which satisfies the boundary conditions (i) - (vii) of Table 3.2. The H_y and H_z field components may be obtained from them, using Maxwell's equations in the form given in this table. The expressions for all the field components are collected in Table 5.1.

(b) H-Polarization. The H-vector at the surface is parallel to the strike. The relevant equation is (3.26):

$$\frac{\partial^2 H_x}{\partial y^2} + \frac{\partial^2 H_x}{\partial z^2} + i\eta^2 H_x = 0 \tag{5.10}$$

where again

$$\eta^2 = \mu_o \omega \sigma$$

Since H_x is known at the surface $z = 0$ and at $z = \infty$ (Table 3.2, conditions (iii) and (vi)), the Fourier sine transformation and its inverse may be used. These are defined by:

$$\bar{H}_x(y,\xi) = \sqrt{\frac{2}{\pi}} \int_0^\infty H(y,z) \sin \xi z \, dz \tag{5.11}$$

$$H_x(y,z) = \sqrt{\frac{2}{\pi}} \int_0^\infty \bar{H}(y,\xi) \sin \xi z \, d\xi \tag{5.12}$$

Application of the transform (5.11) and the boundary conditions (iii) and (vi) of Table 3.2, reduce eq. (5.10) to

$$\frac{d^2 \bar{H}_x}{dy^2} - \zeta^2 \bar{H}_x = \sqrt{\frac{2}{\pi}} \, B\xi \tag{5.13}$$

where

$$\zeta^2 = \xi^2 - i\eta^2$$

This equation has the general solution

$$\bar{H}_x(y,\xi) = \lambda(\xi)\, e^{-\zeta y} + \nu(\xi)\, e^{-\zeta y} - \frac{2}{\pi} B \frac{\xi}{\zeta^2}$$

where again the coefficients $\lambda(\xi)$ and $\nu(\xi)$ are determined by the boundary conditions. The symmetry condition (vii) and condition at infinity (v) of Table 3.2 require

$$|y|<\tfrac{1}{2}\ell : \lambda_1(\xi) = \nu_1(\xi) = \tfrac{1}{2}\delta_1(\xi), \text{ say.}$$

$$|y|>\tfrac{1}{2}\ell : \lambda_2(\xi) = 0 \;;\; \nu_2(\xi) = \delta_2(\xi), \text{ say.}$$

The solution in each region is therefore:

$$|y|<\tfrac{1}{2}\ell : \bar{H}_{1x}(y,\xi) = \delta_1(\xi) \cosh \zeta_1 y - \sqrt{\frac{2}{\pi}} B \frac{\xi}{\zeta_1^2}$$

$$|y|>\tfrac{1}{2}\ell : \bar{H}_{2x}(y,\xi) = \delta_2(\xi)\, e^{-\zeta_2|y|} - \sqrt{\frac{2}{\pi}} B \frac{\xi}{\zeta_2^2} \qquad (5.14)$$

The coefficients $\delta_j(\xi)$ are determined from the pair of simultaneous equations which result when conditions (i) and (ii) of Table 3.2 are applied to the interfaces $y = \pm\tfrac{1}{2}\ell$:

$$\delta_1(\xi) = -iB\sqrt{\frac{2}{\pi}} \frac{\eta_1^2}{\eta_2^2} (\eta_2^2 - \eta_1^2) \frac{\xi}{\zeta_1^2 \zeta_2 \Delta_2}$$

$$\delta_2(\xi) = iB\sqrt{\frac{2}{\pi}} (\eta_2^2 - \eta_1^2) \frac{e^{\frac{1}{2}\ell\zeta_2} \sinh \tfrac{1}{2}\ell\zeta_1}{\zeta_1 \zeta_2^2 \Delta_2} \qquad (5.15)$$

$$\Delta_2 = \zeta_1 \sinh \tfrac{1}{2}\ell\zeta_1 + \frac{\eta_1^2}{\eta_2^2} \zeta_2 \cosh \tfrac{1}{2}\ell\zeta_1$$

The inverse transform (5.12) of relations (5.14) may now be taken. The inverses of the last terms of these relations may be evaluated explicitly since (App. 5):

$$\int_0^\infty \frac{\xi \sin \xi z}{\xi^2 - i\eta^2} \, d\xi = \frac{\pi}{2} \, e^{-\sqrt{-i}\eta z} \tag{5.16}$$

The inverse transforms of (5.14) are then:

$|y| < \frac{1}{2}\ell$:

$$H_{1x}(y,z) = -B \left\{ e^{-\sqrt{-i}\eta_1 z} + i \frac{2}{\pi} \frac{\eta_1^2}{\eta_2^2} (\eta_2^2 - \eta_1^2) \int_0^\infty \frac{\xi \cosh \zeta_1 y}{\zeta_1^2 \zeta_2 \Delta_2} \sin \xi z \, d\xi \right\}$$

$|y| > \frac{1}{2}\ell$:

$$H_{2x}(y,z) = -B \left\{ e^{-\sqrt{-i}\eta_2 z} - i \frac{2}{\pi} (\eta_2^2 - \eta_1^2) \int_0^\infty \frac{\xi \sin \frac{1}{2}\ell\zeta_1 \, e^{-(|y| - \frac{1}{2}\ell)\zeta_2}}{\zeta_1 \zeta_2^2 \Delta_2} \sin \xi z \, d\xi \right\} \tag{5.17}$$

with $\mathrm{Re}(\zeta_j) > 0$ always.

These relations for H_x constitute the solution of eq. (5.10) under the boundary conditions (i) - (vii) of Table 3.2. The expressions for E_y and E_z may be obtained from them, using the Maxwell relations listed in this table.

In addition to the boundary conditions of Table 3.2, a short calculation shows that, at the interfaces $y = \pm\frac{1}{2}\ell$, the E_y relations also satisfy the condition

$$\sigma_1 E_{1y}(0,z) = \sigma_2 E_{2y}(0,z)$$

All of the relations for the various field components are collected together in Table 5.1. The only fields in which we are interested are those at the surface z = 0. The E_z, H_x and H_y fields here are trivial but the other components are listed in Table 5.2, in terms of the dimensionless variables defined in Table 3.3. We have changed the integration variable from ξ to u by

$$u = \xi/\eta_2 \tag{5.18}$$

The uniform convergence of all of the infinite integrals involved in Tables 5.1 and 5.2 may be established using Dirichlet's test for integrals (see for instance Carslaw, 1930). The differentiations under the integrals, and their continuity with respect to the y and z coordinates, are thus ensured.

5.1.3 Special Cases

(a) The Transition to a Fault at Large Dyke Widths

When the frequency is sufficiently high, or the dyke sufficiently wide, the effect of the dyke on the fields at a given point, approaches that of a plane fault; i.e. the influence of the more distant interface becomes negligible.

The definition of Y (Table 3.3) changes the origin of the coordinate system from the dyke center (Fig. 5.1) to one of the discontinuity planes. Since Q is a measure of the dyke thickness, the transition from dyke to fault occurs when Q becomes large.

It is evident from the expressions in Table 5.2 that all of the hyperbolic functions reduce to exponentials when their arguments become large in magnitude. This only happens to all of the hyperbolic

Table 5.1

Summary of the Field Components Near a Dyke

$$E_{x1} = \mu_o \omega A \left\{ \frac{e^{-\sqrt{-i}\,\eta_1 z}}{\sqrt{i}\,\eta_1} + \frac{2}{\pi}\left(\eta_2^2 - \eta_1^2\right)\int_0^\infty \frac{\cosh \zeta_1 y}{\zeta_1^2 \zeta_2 \Delta_1} \cos \xi z \, d\xi \right\}$$

$$E_{x2} = \mu_o \omega A \left\{ \frac{e^{-\sqrt{-i}\,\eta_2 z}}{\sqrt{i}\,\eta_2} - \frac{2}{\pi}\left(\eta_2^2 - \eta_1^2\right)\int_0^\infty \frac{e^{-(|y|-\frac{1}{2}\ell)\zeta_2} \sinh \frac{1}{2}\ell\zeta_1}{\zeta_1 \zeta_2^2 \Delta_1} \cos \xi z \, d\xi \right\} \qquad \Big\} (5.19)$$

$$E_{y1} = \mu_o \omega B \left\{ \frac{e^{-\sqrt{-i}\,\eta_1 z}}{\sqrt{i}\,\eta_1} - i\,\frac{2}{\pi}\left(1 - \frac{\eta_1^2}{\eta_2^2}\right)\int_0^\infty \frac{\xi^2 \cosh \zeta_1 y}{\zeta_1^2 \zeta_2 \Delta_2} \cos \xi z \, d\xi \right\}$$

$$E_{y2} = \mu_o \omega B \left\{ \frac{e^{-\sqrt{-i}\,\eta_2 z}}{\sqrt{i}\,\eta_2} + i\,\frac{2}{\pi}\left(1 - \frac{\eta_1^2}{\eta_2^2}\right)\int_0^\infty \frac{\xi^2 e^{-(|y|-\frac{1}{2}\ell)\zeta_2} \sinh \frac{1}{2}\ell\zeta_1}{\zeta_1 \zeta_2^2 \Delta_2} \cos \xi z \, d\xi \right\} \qquad \Big\} (5.20)$$

$$E_{z1} = i\mu_o \omega B\,\frac{2}{\pi}\left(1 - \frac{\eta_1^2}{\eta_2^2}\right)\int_0^\infty \frac{\xi \sinh \zeta_1 y}{\zeta_1 \zeta_2 \Delta_2} \sin \xi z \, d\xi$$

$$E_{z2} = \pm i\mu_o \omega B\,\frac{2}{\pi}\left(1 - \frac{\eta_1^2}{\eta_2^2}\right)\int_0^\infty \frac{\xi e^{-(|y|-\frac{1}{2}\ell)\zeta_2} \sinh \frac{1}{2}\ell\zeta_1}{\zeta_1 \zeta_2 \Delta_2} \sin \xi z \, d\xi \qquad \Big\} (5.21)$$

Table 5.1 (con't)

Summary of Field Components Near a Dyke

$$H_{x1} = -B\left\{e^{-\sqrt{-i}\,\eta_1 z} + i\,\frac{2}{\pi}\left(1 - \frac{\eta_1^2}{\eta_2^2}\right)\eta_1^2 \int_0^\infty \frac{\xi \cosh \zeta_1 y}{\zeta_1^2 \zeta_2 \Delta_1} \sin \xi z \, d\xi\right\}$$

$$H_{x2} = -B\left\{e^{-\sqrt{-i}\,\eta_2 z} + i\,\frac{2}{\pi}\left(\eta_2^2 - \eta_1^2\right)\int_0^\infty \frac{\xi\, e^{-(|y|-\frac{1}{2}\ell)\zeta_2} \sinh \frac{1}{2}\ell\zeta_1}{\zeta_1 \zeta_2^2 \Delta_2} \sin \xi z \, d\xi\right\} \quad (5.22)$$

$$H_{y1} = A\left\{e^{-\sqrt{-i}\,\eta_1 z} + i\,\frac{2}{\pi}\left(\eta_2^2 - \eta_1^2\right)\int_0^\infty \frac{\xi \cosh \zeta_1 y}{\zeta_1^2 \zeta_2 \Delta_1} \sin \xi z \, d\xi\right\}$$

$$H_{y2} = A\left\{e^{-\sqrt{-i}\,\eta_2 z} - i\,\frac{2}{\pi}\left(\eta_2^2 - \eta_1^2\right)\int_0^\infty \frac{\xi e^{-(|y|-\frac{1}{2}\ell)\zeta_2} \sinh \frac{1}{2}\ell\zeta_1}{\zeta_1 \zeta_2^2 \Delta_1} \sin \xi z \, d\xi\right\} \quad (5.23)$$

$$H_{z1} = iA\,\frac{2}{\pi}\left(\eta_2^2 - \eta_1^2\right)\int_0^\infty \frac{\sinh \zeta_1 y}{\zeta_1 \zeta_2 \Delta_1} \cos \xi z \, d\xi$$

$$H_{z2} = \pm iA\,\frac{2}{\pi}\left(\eta_2^2 - \eta_1^2\right)\int_0^\infty \frac{e^{-(|y|-\frac{1}{2}\ell)\zeta_2} \sinh \frac{1}{2}\ell\zeta_1}{\zeta_1 \zeta_2 \Delta_1} \cos \xi z \, d\xi \quad (5.24)$$

Table 5.1 (con't)

Summary of Field Components Near a Dyke

$$\Delta_1 = \zeta_1 \cosh \tfrac{1}{2}\ell\zeta_1 + \zeta_2 \sinh \tfrac{1}{2}\ell\zeta_1$$

$$\Delta_2 = \zeta_1 \cosh \tfrac{1}{2}\ell\zeta_1 + \epsilon^2\zeta_2 \sinh \tfrac{1}{2}\ell\zeta_1$$

$$\zeta_j^2 = \xi^2 - i\eta_j^2 \quad ; \quad \eta_j^2 = \mu_o\omega\sigma_j$$

Table 5.2

The Surface Field Components Near a Dyke, in Terms of Dimensionless Parameters

$$\sqrt{\frac{\sigma_1}{\mu_o\omega}}\frac{E_{x1}}{A} = \sqrt{-i} + \frac{2}{\pi}\varepsilon(1-\varepsilon^2)\int_0^\infty \frac{\cosh[Q(Y+1)\sqrt{u^2-i\varepsilon^2}]}{\sqrt{u^2-i}\,(u^2-i\varepsilon^2)\,D_1}\,du$$

$$\sqrt{\frac{\sigma_2}{\mu_o\omega}}\frac{E_{x2}}{A} = \sqrt{-i} - \frac{2}{\pi}(1-\varepsilon^2)\int_0^\infty \frac{e^{-QY\sqrt{u^2-i}}\sinh Q\sqrt{u^2-i\varepsilon^2}}{(u^2-i)\sqrt{u^2-i\varepsilon^2}\,D_1}\,du \qquad (5.25)$$

$$\sqrt{\frac{\sigma_1}{\mu_o\omega}}\frac{E_{y1}}{B} = \sqrt{-i} - i\frac{2}{\pi}\varepsilon(1-\varepsilon^2)\int_0^\infty \frac{u^2\cosh[Q(Y+1)\sqrt{u^2-i\varepsilon^2}]}{\sqrt{u^2-i}\,(u^2-i\varepsilon^2)\,D_2}\,du$$

$$\sqrt{\frac{\sigma_2}{\mu_o\omega}}\frac{E_{y2}}{B} = \sqrt{-i} + i\frac{2}{\pi}(1-\varepsilon^2)\int_0^\infty \frac{u^2 e^{-QY\sqrt{u^2-i}}\sinh[Q\sqrt{u^2-i\varepsilon^2}]}{(u^2-i)\sqrt{u^2-i\varepsilon^2}\,D_2}\,du \qquad (5.26)$$

$$\frac{H_{z1}}{A} = i\frac{2}{\pi}(1-\varepsilon^2)\int_0^\infty \frac{\sinh[Q(Y+1)\sqrt{u^2-i\varepsilon^2}]}{\sqrt{u^2-i}\,\sqrt{u^2-i\varepsilon^2}\,D_1}\,du$$

$$\frac{H_{z2}}{A} = i\frac{2}{\pi}(1-\varepsilon^2)\int_0^\infty \frac{e^{-QY\sqrt{u^2-i}}\sinh[Q\sqrt{u^2-i\varepsilon^2}]}{\sqrt{u^2-i}\,\sqrt{u^2-i\varepsilon^2}\,D_1}\,du \qquad (5.27)$$

$$D_1 = \sqrt{u^2-i\varepsilon^2}\,\sinh[Q\sqrt{u^2-i\varepsilon^2}] + \sqrt{u^2-i}\,\cosh[Q\sqrt{u^2-i\varepsilon^2}]$$

$$D_2 = \sqrt{u^2-i\varepsilon^2}\,\sinh[Q\sqrt{u^2-i\varepsilon^2}] + \varepsilon^2\sqrt{u^2-i}\,\cosh[Q\sqrt{u^2-i\varepsilon^2}] \qquad (5.28)$$

functions simultaneously when $Q\varepsilon >> 1$ (ie. $\frac{1}{2}\ell >> \eta_1^{-1}$). The expressions in Table 5.2 then reduce to those in Table 4.2, independently of Y.

Thus an observer anywhere on either the land or the ocean will see a "coast effect" influence on the fields, when the half-width of the dyke much exceeds the penetration depth of the electromagnetic wave in the dyke medium. The effect of the double shore-line only becomes evident when the half-thickness is less than or comparable to, the penetration depth in the land medium.

That is, an observer in either medium "sees" (electromagnetically speaking) the land as a continent when $Q\varepsilon >> 1$, but as a dyke or promontory, when $Q\varepsilon \lesssim 1$.

It is also evident from the relations in these two tables that no value of Y governs the transition from promontory to continent. In other words, the behavior of the fields is everywhere according to the "dyke effect" or everywhere according to the "coast effect". Similarly, it is not possible to observe a "coast effect" in, say, the oceanic medium and a "dyke effect" in the land medium, for the same physical parameters.

These conclusions are evident from a consideration of the denominator expressions D_1 and D_2 in the integrands: the only condition under which they simplify usefully is that $Q\varepsilon >> 1$, and they are also independent of Y.

(b) The Transition to a Homogeneous Medium (Asymptotic Condition)

At a great distance from the interface in the oceanic medium (2), the effect of the discontinuity in conductivity becomes

negligible and the expressions for the field components reduce to those for a homogeneous medium.

Consider either Table 5.1 or 5.2. As $v \to +\infty$ (or $Y \to +\infty$) the integral terms of all the field components approach zero, leaving only the first terms. More usefully, this behavior will occur when $O(Y-1) \gg 1$; the integral terms then become very small in comparison with the initial terms, and:

$$E_{x2} \to \frac{\mu_o \omega A}{\sqrt{i}\,\eta_2} e^{-\sqrt{-i}\,\eta_2 z} \to \frac{\mu_o \omega}{\sqrt{i}\,\eta_2} A \text{ at } z = 0$$

$$E_{y2} \to \frac{\mu_o \omega B}{\sqrt{i}\,\eta_2} e^{-\sqrt{-i}\,\eta_2 z} \to \frac{\mu_o \omega}{\sqrt{i}\,\eta_2} B \text{ at } z = 0$$

$$H_{x2} \to -B\, e^{-\sqrt{-i}\,\eta_2 z} \to -B \text{ at } z = 0$$

$$H_{y2} \to A\, e^{-\sqrt{-i}\,\eta_2 z} \to A \text{ at } z = 0$$

E_{z2} and H_{z2} both $\to 0$

The condition that $O(Y-1) \gg 1$ outside the dyke means that the observer must be considerably further seawards from the shore line than the sum of the dyke half-width and the oceanic penetration distance. There the fields are not significantly affected by the presence of the dyke, and are governed by the homogeneous ocean only.

A similar behavior occurs within the dyke, provided it is sufficiently wide for the coastlines to have no influence on the fields. The integral terms in the field component expressions for

Region 1 all become small as $Y \to -1$ (the center of the dyke) since the numerator terms always exceed the D terms of the denominator.

If at the same time $Q\varepsilon >> 1$, the denominator dominates and the integral terms become negligible. These two conditions mean that the dyke half-width must be much greater than the land penetration distance, with the observation point a small fraction of that width from the center. The expressions for the field components near the center of the dyke are then analogous to those listed above; they correspond to the fields in uniform media (cf. 4.1.3a).

Thus, at a point distant from the shore line by considerably more than the penetration distance in the particular medium, the effect of the dyke is negligible. Within the dyke this implies that its half-width is much greater than the land penetration distance.

(c) The Field Components Directly Over the Discontinuity Planes

The relations of Table 5.2 do not simplify appreciably when the observation point is directly over the discontinuity planes ($Y = 0$), and analytical analogues of the expressions in §4.1.3b cannot be obtained.

5.1.4 The Numerical Computation of the Fields Near a Dyke

The relations of Table 5.2 cannot be simplified in terms of analytical functions, and to obtain the behavior of the fields at any point, they must be numerically evaluated. Since the expressions are complex and we are interested in the phase-amplitude relation, the computations are required in the form

$$\mathrm{Re}^{\,i\phi}$$

where R, ϕ specify the magnitude and phase-angle respectively.

For numerical integration, however, the integrands had to be separated into real and imaginary parts. This is done in App. 6. Each part was integrated using Simpson's rule, the real and imaginary parts of each field component computed, and finally converted to polar form.

The integrands themselves are quite complicated in behavior. To express the twelve relations necessary for the real and imaginary parts of the three field components in both regions 1 and 2, some 30 parametric relations must be defined. Each integrand requires 13 relations to specify it. To see how the integrands varied with the changing value of the integration variable u, the integrands were evaluated for several values of u and for various values of the other parameters ϵ, Q, and Y, using the IBM 1620 computer at the University of Alaska. A computational check was provided by the asymptotic expressions for the integrands at large values of the integration variable u (see App. 7).

The behavior of the integrands is critically dependent on the value of ϵ; the dependence on Q and Y is much weaker. In many cases the gradients with respect to u change very rapidly within the range $0 \leq u \leq \epsilon$, the contribution from $\epsilon \leq u \leq 1$ also being of importance. Beyond $u = 1$ the integrands fall off, although in some cases the contributions to the integral are still significant at or beyond $u = 10$.

The programming of the calculations and the actual program are discussed further in App. 9. Because of computer storage and speed limitations, the IBM 1620 could not be used for the complete calculation, and the computations were carried out on an IBM 7094, under the auspices of the Western Data Processing Center, at the University of California.

5.1.5 Discussion of Results

A variety of coordinates may be used to represent the relations of Table 5.2. Figures 5.3 - 5.4 show curves of $\sqrt{\sigma_2/\mu_o\omega}\ |E_j/H_k| = |E_j/E_{j2\infty}|$, Arg E_j/H_k, and H_z/H_y as functions of Y for various Q, ϵ. Here H_k represents the surface value of the horizontal magnetic field component which is normal to E_j. Thus the electric field magnitude curves are normalized to unity at a great distance from the dyke in the oceanic medium, but the phase difference of 45^o between the E_j and H_k components at great distances is retained.

The use of Y for the abscissa is equivalent to a representation in terms of the distance from the shore-line in units of the half-width of the ridge, for various thicknesses of the ridge. The more common method of plotting the field components as functions of distance measured in terms of the penetration depth factor, may be obtained by mentally converting the scale of the abscissa to OY in region 2 (or $Q\epsilon Y$ in region 1) instead of Y. For a general idea of the behavior over several penetration depths, the curves for $Q = 1$ (in region 2) or $Q = \epsilon^{-1}$ (in region 1) may be regarded as representing the variation over integral numbers of depth-parameters. The

adjacent curves for smaller and greater Q then represent expanded or compressed analogues for different ranges of ΩY (or $\Omega\varepsilon Y$), for the respective values of Q.

We are here dealing with the effect on the fields of a known geological structure. This is just the reverse of the situation encountered by a magnetotelluric prospector; he measures the fields and attempts to deduce the structure from their behavior. From his point of view the plot in terms of skin-depth is by far the most convenient. He may not know the value of our "ℓ" or even know that there is one. In our case, however, we may assume the half-width "$\frac{1}{2}\ell$" is known and measure distances in terms of it, in either medium. This enables us to fix the distance from a shoreline and easily determine the effect at that point, at different frequencies, by examining the different Q-curves.

The results of the computations are given in Figs. 5.3 and 5.4 for ε-values of 0.5 and 0.1, representing conductivity ratios of 1:4 and 1:100 respectively. The curves for $\Omega = 1$ are shown more heavily for easy reference.

(a) Electric Field (Figs. 5.3a,b, 5.4a,b, 5.5)

Within approximately twice the penetration depth on the oceanic side of the discontinuity the effect of the coast on the magnitude of the field components E_x and E_y becomes very small. The magnitude of the electric field then behaves as though the medium were an infinitely deep, uniform ocean. On land for a dyke which is very narrow compared with the land penetration depth, ($\Omega\varepsilon \ll 1$), the

electric field normal to the shoreline is increased towards its steady-state value (see §5.1.1), while the parallel component is less affected; it also approaches its steady state limit for very narrow dykes. As the frequency increase (ie. the electromagnetic wave "sees" the dyke to be of smaller dimensions), the normal component is depressed and the parallel component enhanced towards the asymptotic limits for a uniform land medium of infinite depth. At thicknesses great compared with the penetration depth in the land ($Q\varepsilon >> 1$) the influence of each coast becomes separate and the observer inland sees a "coast effect" rather than a "dyke effect" in the fields as he approaches either shoreline. The fields in the interior then behave as though no coastlines were present; this was anticipated in §5.1.3a.

At frequencies intermediate between these two situations there is a behavior peculiar to the dyke or promontory. Suppose the frequency rises above that at which a steady state behavior obtains. The normal electric field component has its magnitude affected at much lower frequencies ($Q\varepsilon < 10^{-3}$) than the parallel component ($Q\varepsilon \sim 10^{-1}$). The normal field also approaches the asymptotic behavior at lower frequencies ($Q\varepsilon \sim 10^{-1}$) than the parallel component ($Q\varepsilon \sim 1$). In other words, the normal component is more frequency sensitive to a departure from the steady state conditions (often used in geomagnetic prospecting, for instance) than is the parallel component; it also remains sensitive over a wider frequency range. However, the parallel component is more frequency sensitive to a departure from the asymptotic situation. We will return to this again later.

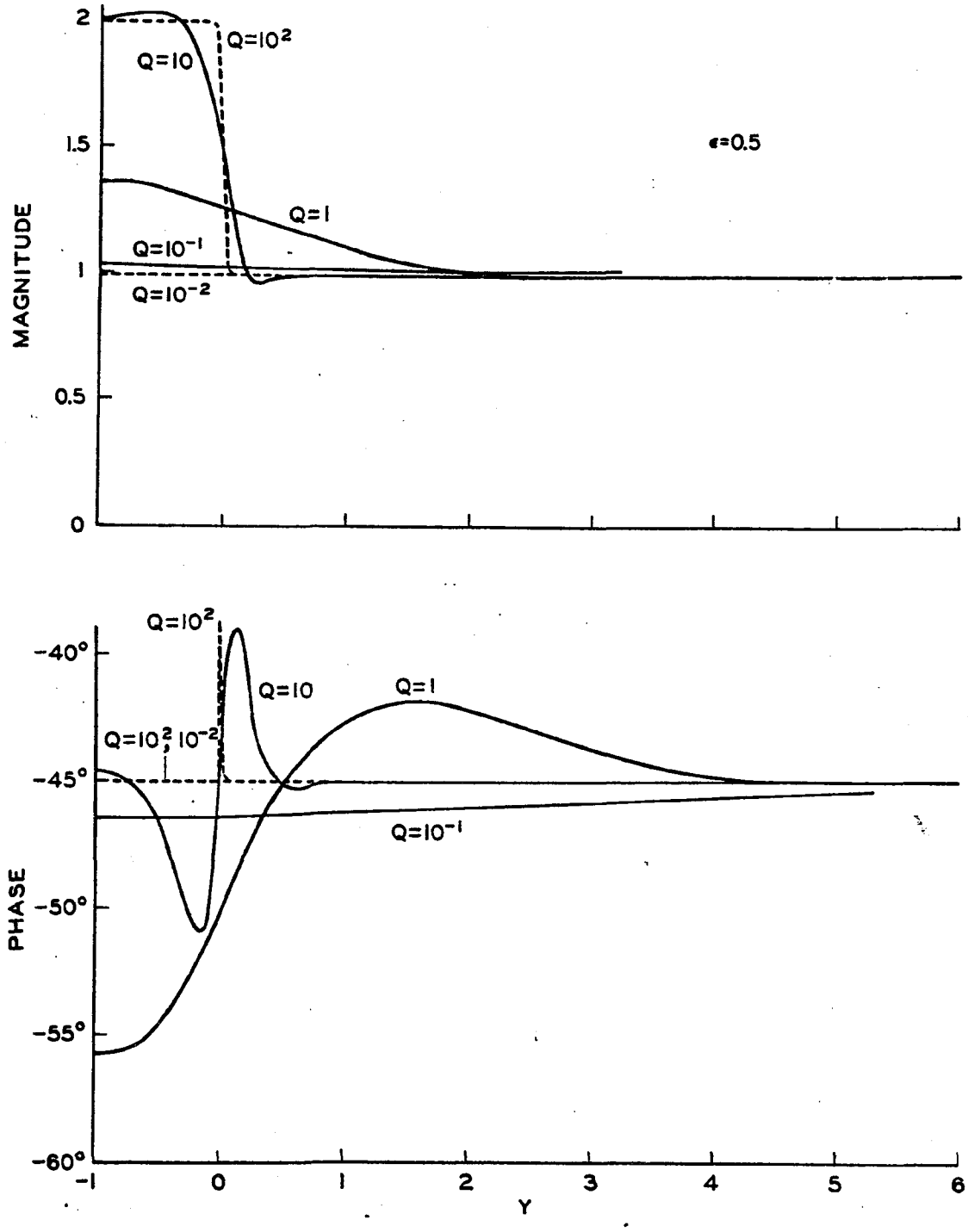

Fig. 5.3 (a) The parallel electric field near an infinitely deep dyke; $\varepsilon = 0.5$

$$\frac{E_x}{|E_{x2\infty}|} = \sqrt{\frac{\sigma_2}{\mu_o \omega}} \quad \frac{E_x}{H_y}$$

The parameters ε, Q, Y are defined in Table 3.3

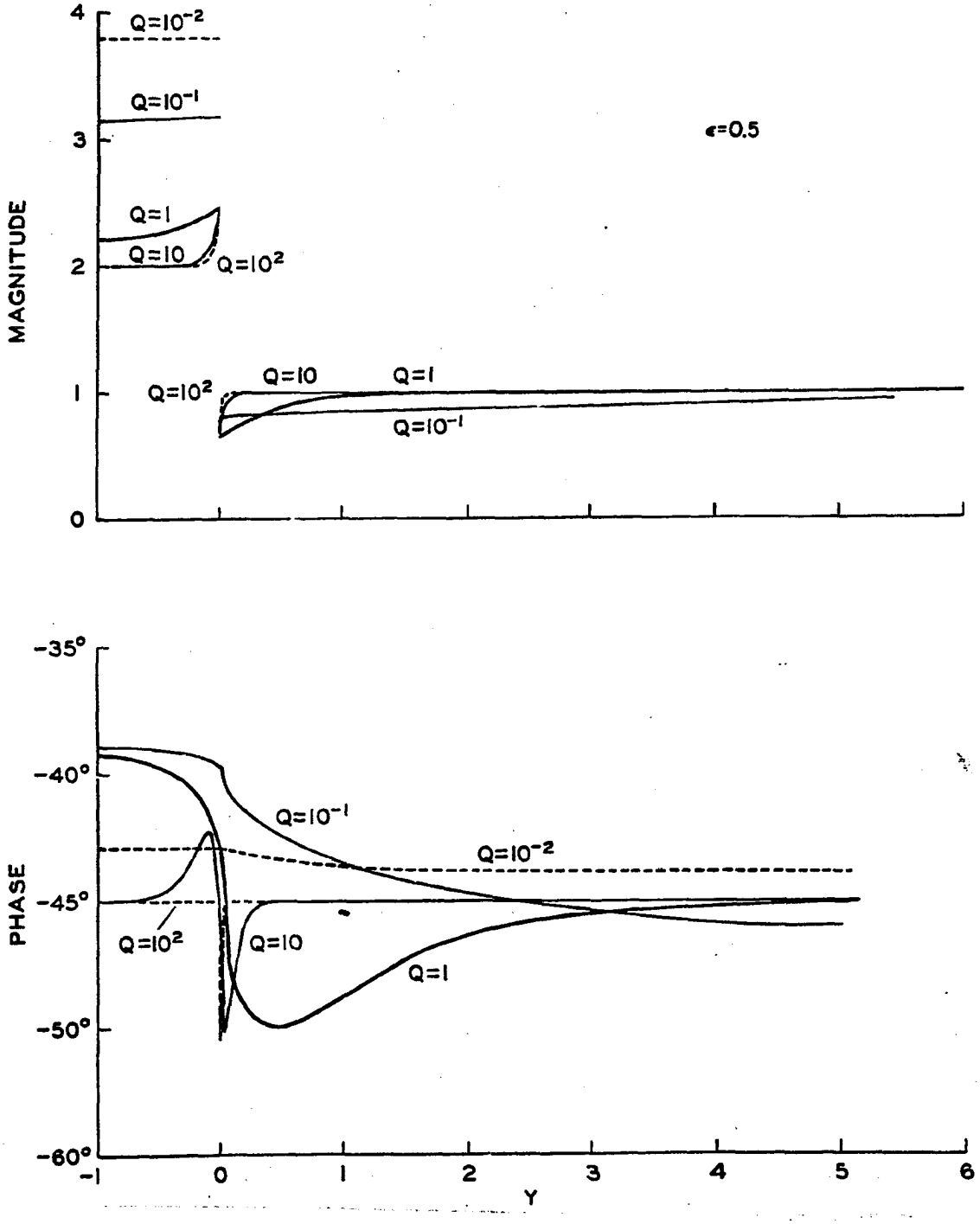

Fig. 5.3 (b) The normal electric field near an infinitely deep dyke; $\varepsilon = 0.5$

$$\frac{E_y}{|E_{y2\infty}|} = \sqrt{\frac{\sigma_2}{\mu_o \omega}} \frac{E_y}{H_x}$$

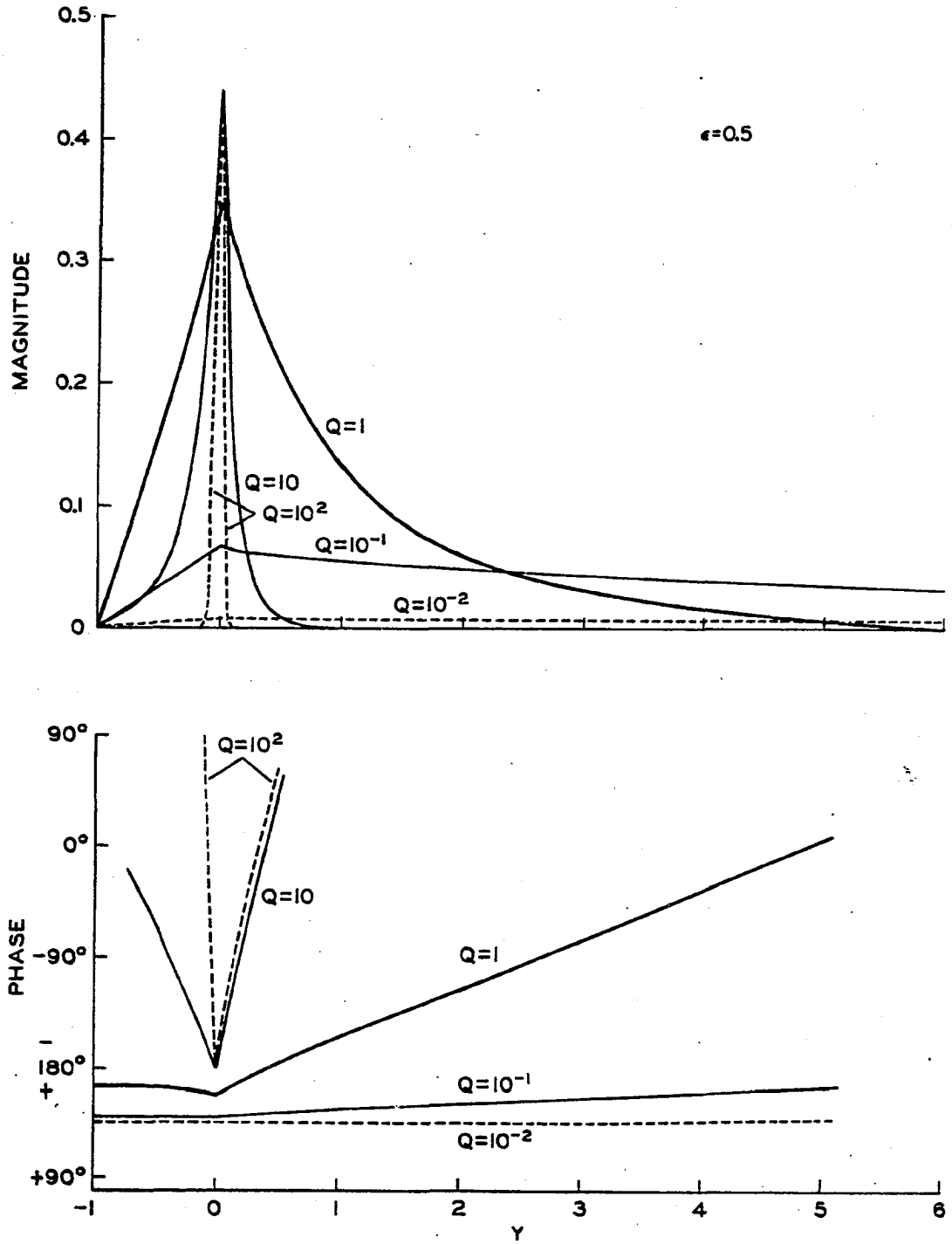

Fig. 5.3 (c) The vertical magnetic field near an infinitely deep dyke, $\varepsilon = 0.5$

H_z/H_y

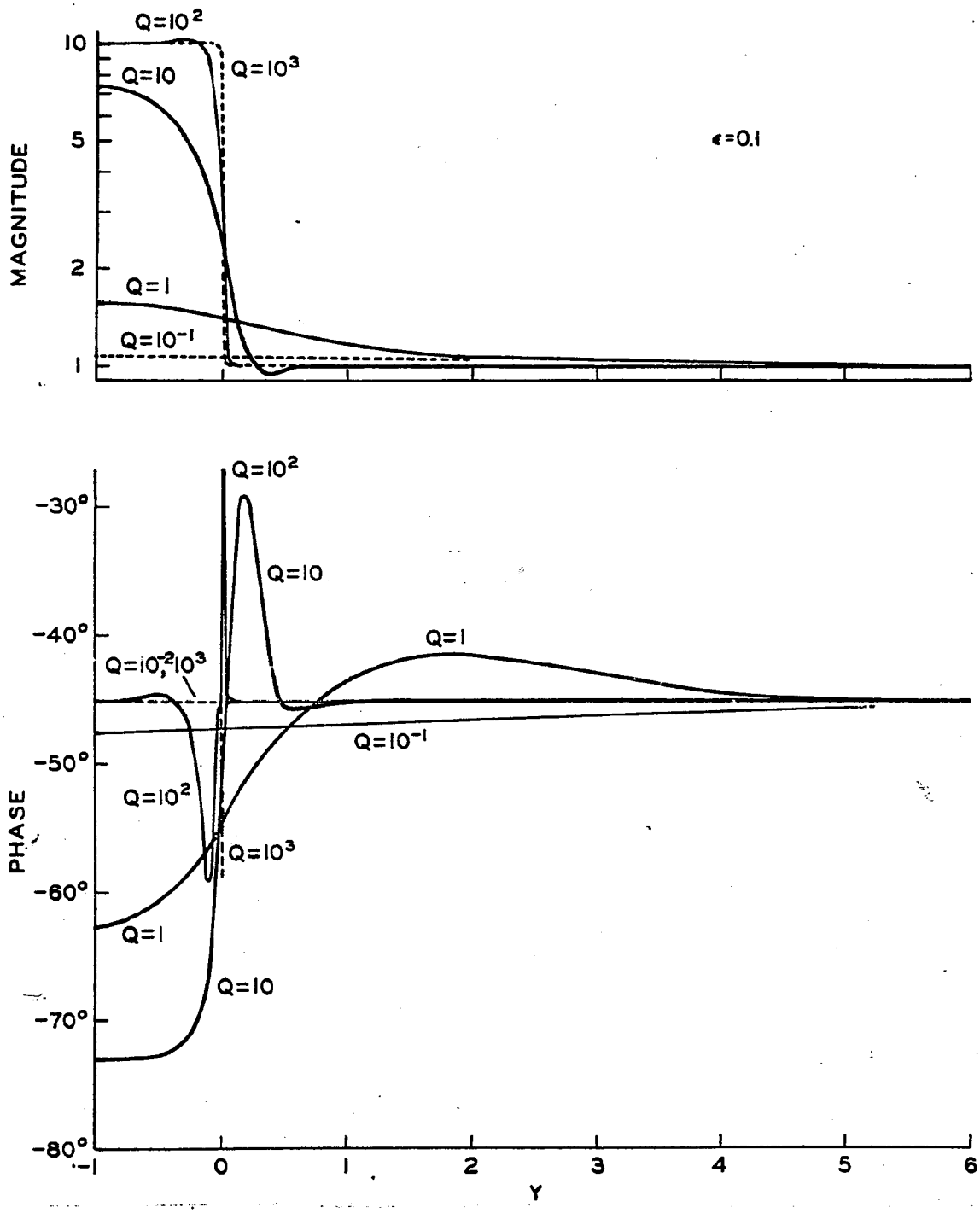

Fig. 5.4 (a) The parallel electric field near an infinitely deep dyke; $\varepsilon = 0.1$

$$\frac{E_x}{|E_{x2\infty}|} = -\sqrt{\frac{\sigma_2}{\mu_o \omega}}\ \frac{E_x}{H_y}$$

The parameters ε, Q, Y are defined in Table 3.3

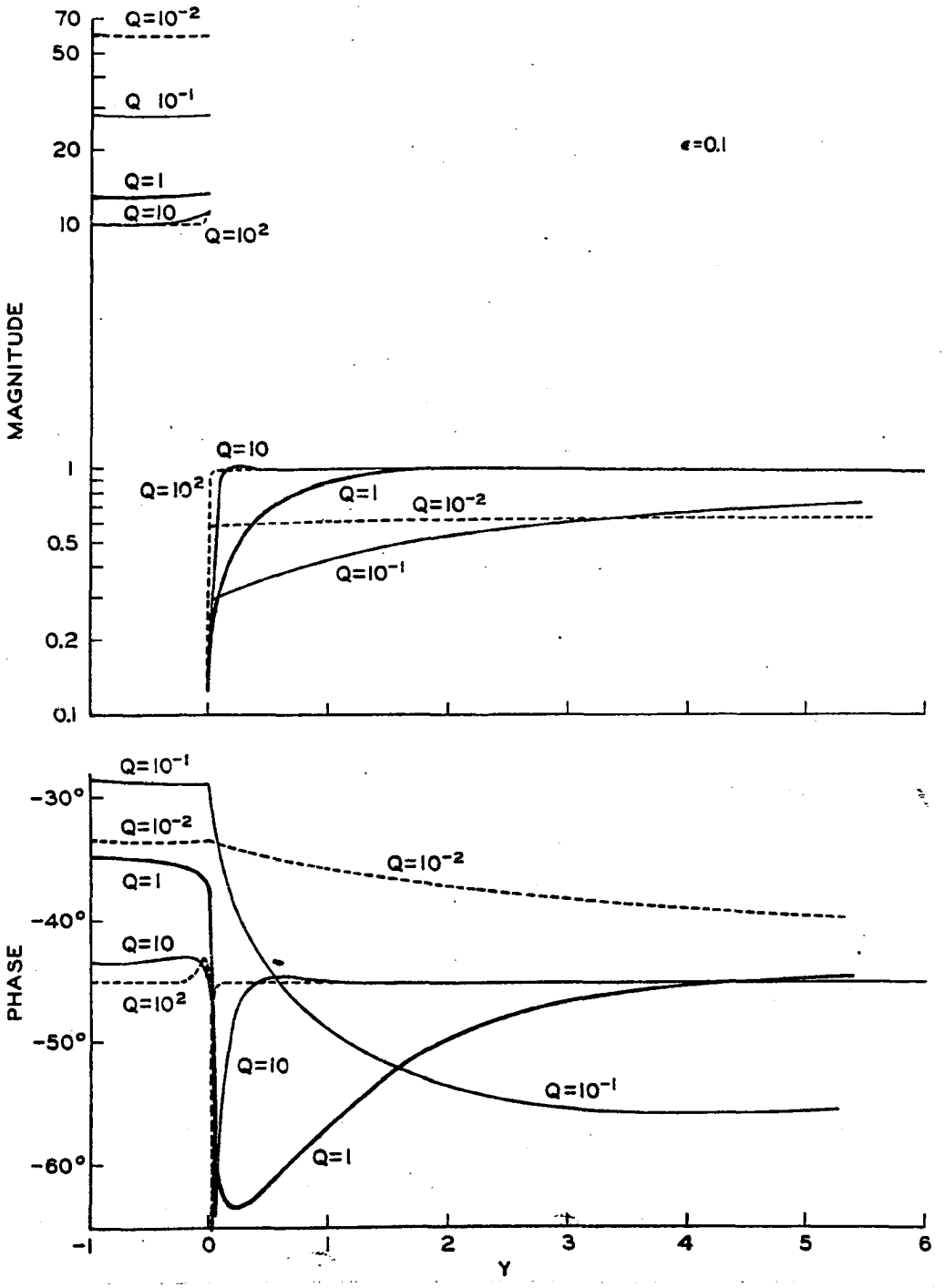

Fig. 5.4 (b) The normal electric field near an infintely deep dyke, $\varepsilon = 0.1$

$$\frac{E_y}{|E_{y2\infty}|} = \sqrt{\frac{\sigma_2}{\mu_o \omega}} \; \frac{E_y}{-H_x}$$

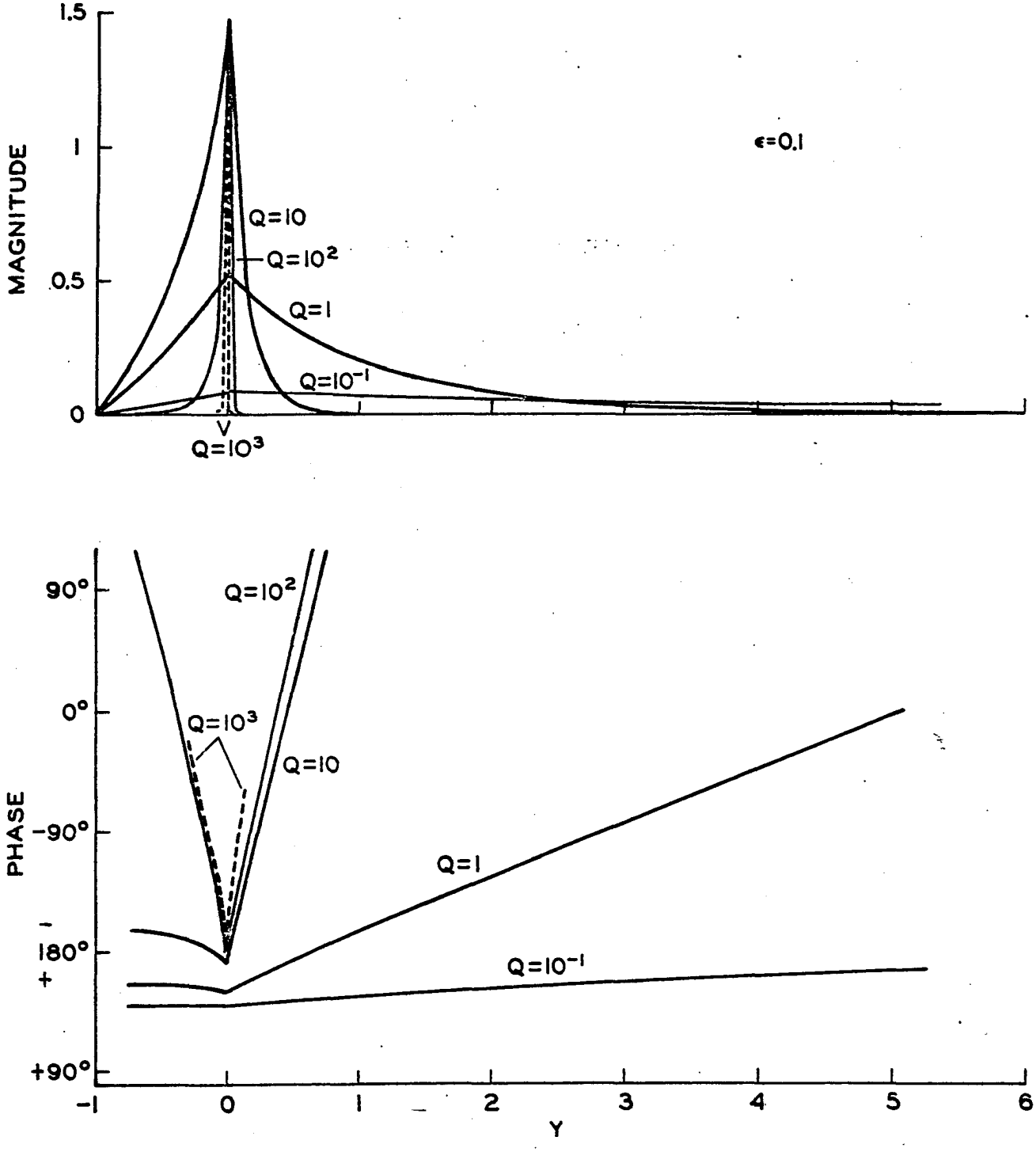

Fig. 5.4 (c) The vertical magnetic field near an infintely deep dyke, ε = 0.1
H_z/H_y

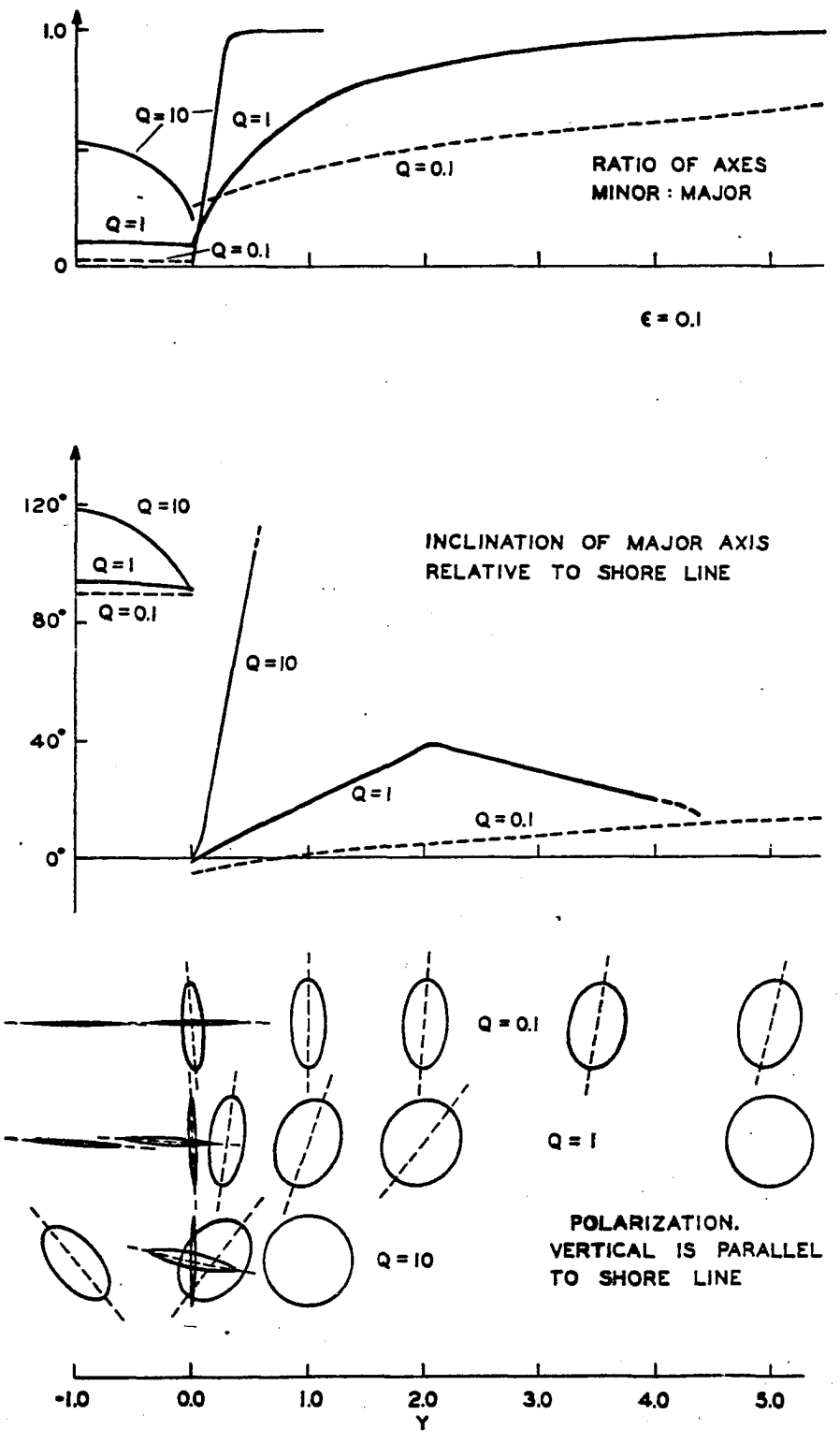

Fig. 5.5 The polarization behavior of the surface electric fields near a infinitely deep dyke, $\varepsilon = 0.1$. A left circularly polarized, surface magnetic field is assumed.

Evidently the effects on the phase difference between the orthogonal and electric magnetic fields penetrate further into both oceanic and land media than do the effects on the field magnitudes. Again the normal electric field is more sensitive than the parallel component, in its phase response to departures from the low frequency limit. The parallel component, however, remains more sensitive to departures from the asymptotic limit.

The combined effect of the electric field components is best represented by considering the polarization of the surface E-waves. The E-wave at the surface may be expressed in the form

$$\underset{\sim}{E} = (E_x \hat{\underset{\sim}{\varepsilon}}_x + E_y \hat{\underset{\sim}{\varepsilon}}_y)\, e^{-i\omega t}$$

and will in general be elliptically polarized. Since we have computed the E-components in terms of the horizontal H-components, the polarization ellipses may be determined if we assume some condition on the surface H-wave. The most convenient is to take the total surface H-wave as circularly polarized; this case is easily identified in practice. We assume left-handed polarization; the relevant details of the computation are given in App. 1. The results for the case $\varepsilon = 0.1$ are presented in Fig. 5.5, in terms of the ratio of the minor axis to the major axis of the ellipse, and the inclination of its major axis to the strike or line of the coast. The ellipses themselves are also shown.

From Fig. 5.5, we see that for ar observer on land the E-vector is very strongly polarized in a direction normal to the shoreline, at low frequencies. As the frequency rises (ie. the width

of the promontory "increases", as far as the electromagnetic wave is concerned) the polarization becomes less linear and more elliptical: the orientation also becomes more inclined to the normal. But as an observer approaches the coast, he sees a more pronounced trend towards linear polarization perpendicular to the shoreline. At higher frequencies the effect of the coast becomes confined to its immediate neighborhood--a "coast effect" behavior is apparent. The polarization towards the center of the ridge takes on the typical circular pattern of the uniform medium.

On the ocean side of the discontinuity, there is a preferential polarization parallel to the coastline. In the region close to the discontinuity, this becomes more marked with increasing frequency, but its angle of inclination rapidly diverges from parallel. The eccentricity of the ellipses also approaches zero rapidly at a given distance from the shore. At a distance of a few times the penetration depth in the oceanic medium, the polarization is very nearly circular. This is tantamount to saying that the phase differences between E and H, for both components, have essentially reached their asymptotic (45^{o}) values for a uniform medium.

This behavior can be understood from the conditions at the zero frequency limit and the asymptotic or uniform medium limit (cf. §5.1.1). The zero frequency condition is

$$E_{1x} = E_{2x} \quad : \text{ parallel component}$$

$$E_{1y} = \frac{\sigma_2}{\sigma_1} E_{2y} \quad : \text{ normal component}$$

The asymptotic limit is

$$E_1 = \frac{\sigma_2}{\sigma_1} E_2 \quad \text{for a non-zero frequency,}$$

and is independent of the distance coordinate. At low frequencies, at a given point on the land medium, the normal component will tend to be greater than its corresponding parallel component. At the high frequency end, however, the two components become approximately the same, since the influence of the coast does not penetrate sufficiently. Thus, at low frequencies, at a given position, we have nearly linear, normal polarization, becoming more circular as the frequency increases. On the ocean, at some point close to the shore, for high frequencies, we have the parallel component greater than the normal component. We therefore have strong polarization parallel to the coastline, in very close proximity to the shoreline, becoming more circular away from it.

We mentioned above the sensitivity of the E-components to change in frequency. We now return to this question and consider it in more detail. In Figs. 5.6a,b the magnitudes and phases of the E_x and E_y components have been rearranged to show the dependence of each function on frequency, for any given observation point on either the land or ocean. These figures were constructued by replotting the data used to compile Figs. 5.3. Smooth curves were drawn through the points at each decade value of Q.

It is evident that, at a given point either over or outside the promontory, the normal component E_y (Fig. 5.6b) is fairly sensitive

in both phase and magnitude to departures from the zero frequency limit. This sensitivity is also quite position dependent in the oceanic medium, but is relatively independent of position within the land medium. The behavior of the E_y component at land sites close to the coast will be highly erratic at higher frequencies, being exceedingly sensitive to both frequency and position. However, even at high frequencies, at a fixed observation point, there is a "cutoff" frequency beyond which the normal electric component reaches its "asymptotic" form.

The parallel component E_x (Fig. 5.6a) on the other hand is quite insensitive, especially in magnitude, to this low frequency end of the spectrum. However, at a given site, the departure from the high frequency, "asymptotic", condition occurs at much higher frequencies in this component than in the normal (E_y) component. The phase and magnitude each exhibit this behavior, over both land and ocean sites. The trend breaks down for oceanic sites which are very close to the shore, when both components become quite frequency sensitive.

An alternative method of depicting this change is again through the behavior of the polarization patterns of the electric vector. If the surface magnetic vector is assumed to have circularly polarized, horizontal components (say, left handedly) the polarization parameters are shown in Fig. 5.7 for the case $\varepsilon = 0.1$. The ratio of the minor to the major axis, and the inclination of the major axis to the line of the coast or strike (ie. the x-axis), are shown.

At low frequencies within the land medium, there will be nearly linear polarization normal to the shoreline, independent of position. As the frequency at some observation station increases, the angle of inclination increases from 90^{o} and at the same time the linear character of the polarization changes to elliptical and eventually circular.

In the oceanic medium, however, there is, in general, elliptic polarization at low frequencies. This at first becomes increasingly linear, but then rapidly becomes more circular. At positions very close to the shoreline the linearity will tend to be parallel to the coast, and at low frequencies the ellipticity will tend to be oriented this way everywhere.

(b) Magnetic Field:

Consider Figs 5.3c and 5.4c, which show the variation of the vertical magnetic field component H_z at the surface as a function of the normal component H_y. It is evident that a marked enhancement of the vertical magnetic field occurs at the shoreline, within certain frequency ranges.

Since a plane wave field incident normally on a uniform medium does not produce any vertical magnetic component, the asymptotic value of H_z is zero. At the center of the dyke, H_z is likewise zero, a consequence of the asymmetry of eq. (5.24a) about $y = 0$ or, in other words, the symmetry of the parallel component of the electric field E_x.

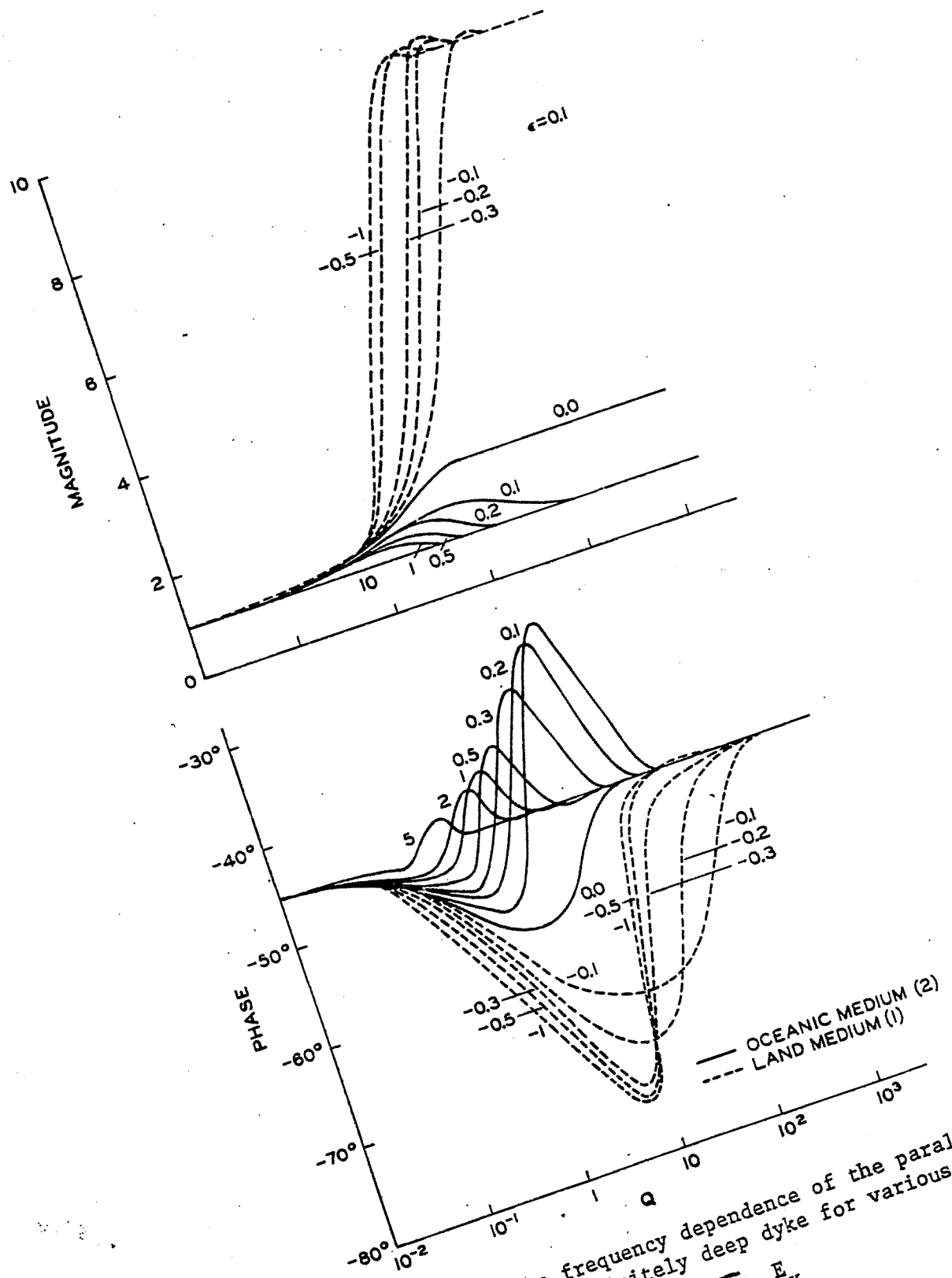

Fig. 5.6 (a) The frequency dependence of the parallel electric field near an infinitely deep dyke for various values of Y; ε = 0.1

$$\frac{E_x}{E_{x2\infty}} = \sqrt{\frac{\sigma_2}{\mu_o \omega}}\,\frac{E_x}{H_y}$$

The parameters ε, Q, Y are defined in Table 3.3.

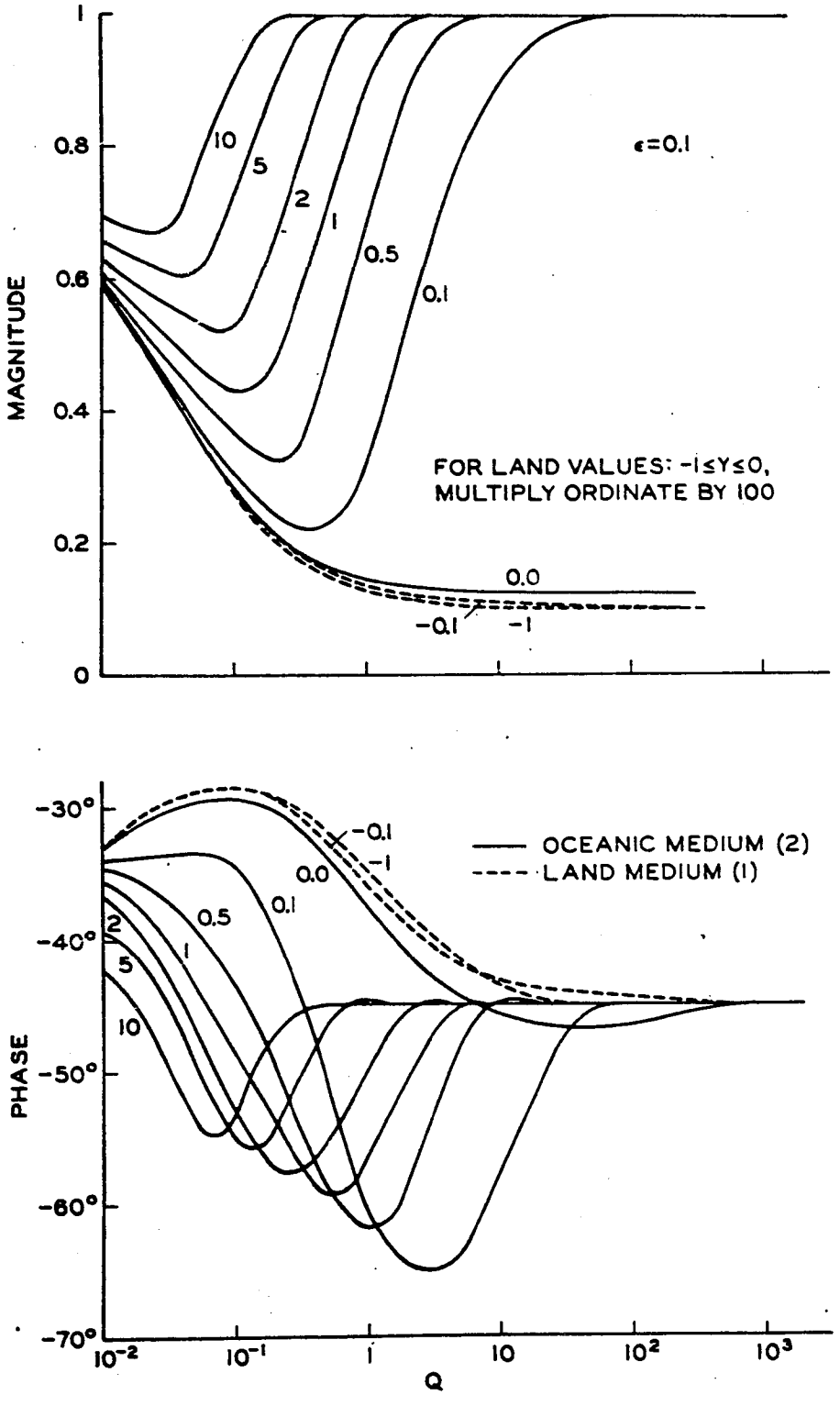

Fig. 5.6 (b) The frequency dependence of the normal electric field near an infinitely deep dyke for various values of Y; $\epsilon = 0.1$

$$\frac{E_y}{|E_{y2\infty}|} = \sqrt{\frac{\sigma_2}{\mu_o \omega}} \frac{E_y}{-H_x}$$

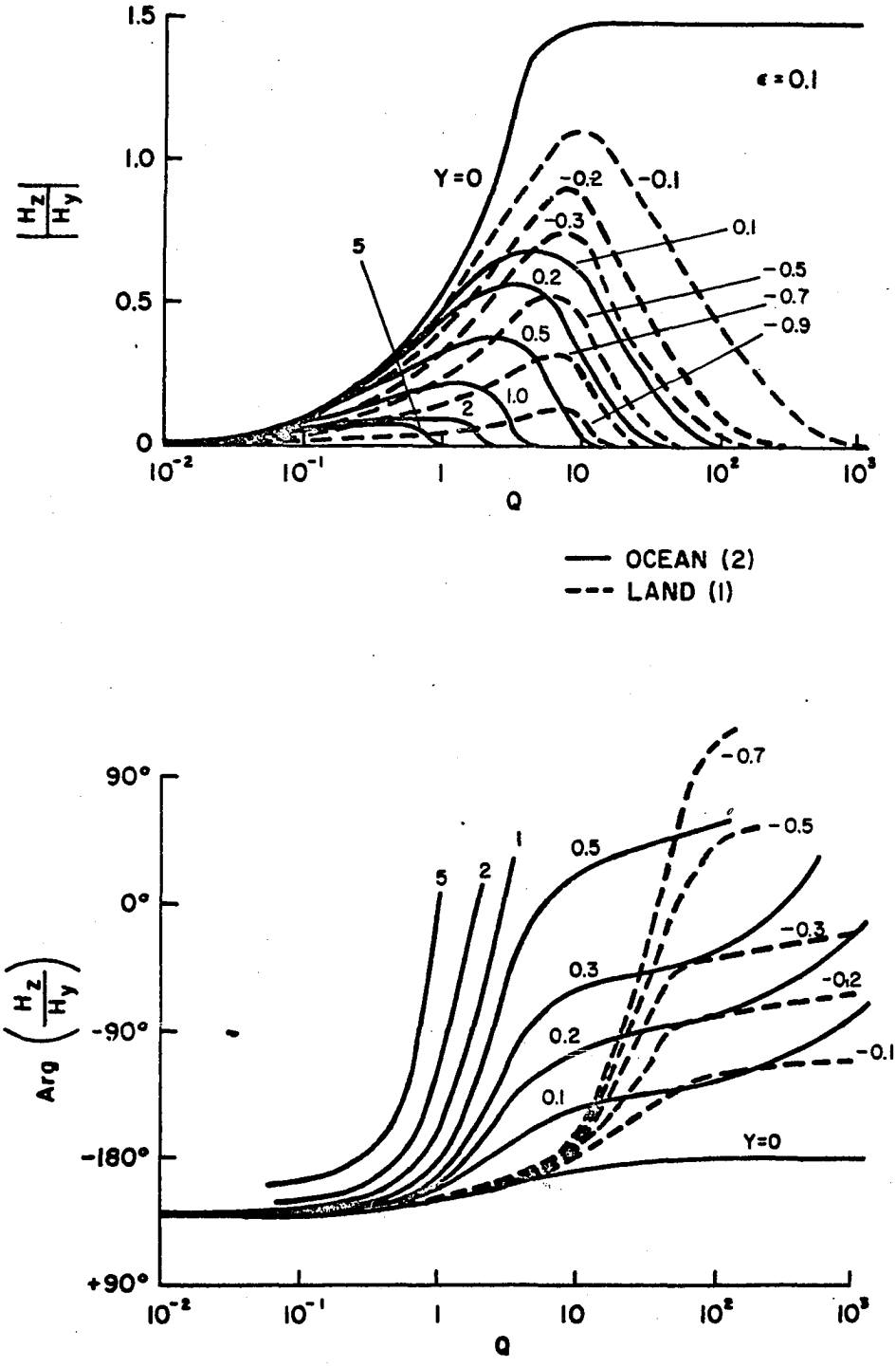

Fig. 5.6 (c) The frequency dependence of the vertical magnetic field near an infinitely deep dyke, for various values of Y; ε = 0.1.

H_z/H_y

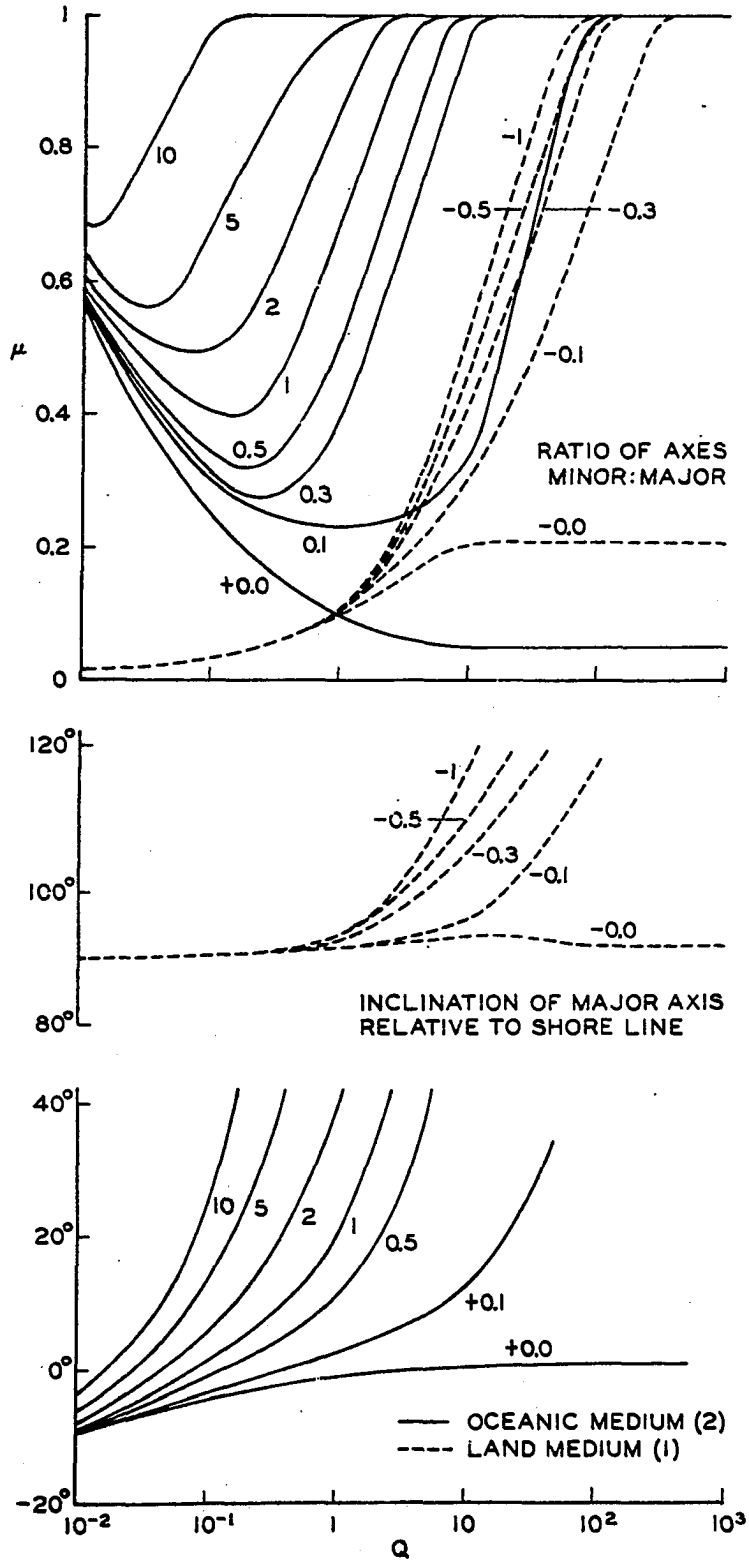

Fig. 5.7 The frequency dependence of the polarization parameters of the electric field, near an infinitely deep dyke, for various values of Y, ($\varepsilon = 0.1$).

Again at high frequencies, where $Q\epsilon >> 1$ inside the dyke or $Q >> 1$ in the oceanic medium 2, the field exhibits a skin-effect decay away from the discontinuity. However, as the dyke becomes progressively thinner to the electromagnetic wave (i.e. the frequency decreases), the exponential decay within the land medium becomes more linear, ie. the effect of the remoter coastline becomes more significant. At the same time the magnitude of the maximum enhancement (directly over the coast) decreases, until it becomes negligible and the "dyke effect" no longer exists. This situation corresponds to the zero-frequency or static limit (§5.1.1). The enhancement at the shore-line increases as the disparity in conductivity between land and sea becomes greater.

As one leaves the coastline, the phase of H_z changes very rapidly over a large range at the high frequency end of the spectrum. This is true in either medium over a distance where the magnitude of H_z remains significant. At low frequencies the phase change with distance is not so rapid, although still covering a large range eventually.

The frequency response curves of the vertical magnetic field are presented in Fig. 5.6c, for various values of Y when $\epsilon = 0.1$. The presence of the dyke evidently affects the low frequency end of the response quite appreciably. Comparison with the general shape of the curve for a fault of infinite depth (Fig. 4.8a) shows that for $Q < 10$ the rising magnitude response suddenly starts to fall again towards zero. The wider the dyke (large Q) and the

nearer the observation point to the boundary, the more likely the response curve to approach the asymptotic value of a fault.

The phase curves show an even greater sensitivity to the presence of the dyke at low frequencies, although the influence of the dyke is less easily described in general.

Some specific examples are given in §5.4, following the study of the influence of a basement.

(c) Comparison with the Fields Near a Vertical Coastline

In §5.1.3a the transition of the "dyke" formulae to the "fault" formulae was discussed. Whenever the dyke becomes sufficiently large or the frequency sufficiently high ($Q\varepsilon \gg 1$) the observer "sees" the dyke or promontory as a "continent" - in other words the fields are essentially unaffected by the remoter discontinuity and exhibit a simple coast-effect behavior.

Precise comparison of Figs. 5.4a,b with Figs. 4.3a,b (which represent the equivalent curves for the fault geometry) indicates the following behavior. The magnitude curves of the normal E_y component are in close agreement even for $Q = 1$, in the oceanic medium, and $Q\varepsilon = 1$ in the land medium. For smaller dykes, however, the magnitude is enhanced over the land and reduced over the sea. The phase difference between the electric and magnetic field components in the oceanic medium is generally rather smaller for a dyke with $Q \leq 1$ than it is for the simple coastline. The phases on the land side of the shoreline differ very little from the asymptotic values for a simple coastline, in marked contrast to

the considerably larger phase differences inside a narrow dyke ($Q\varepsilon \leq 1$). At greater dyke widths (ie. at higher frequencies) the phases again closely approach the asymptotic values.

By comparing the curves for the parallel components E_x, we see that there are appreciable differences in the magnitudes for $Q \leq 1$. The similarity which occurs for $Q = 1$ (ocean) and $Q\varepsilon = 1$ (land) in the normal components is no longer evident. The land magnitudes are lowered while the oceanic ones do not greatly differ from the asymptotic limits for lower frequencies.

The phases are markedly different on land when $Q\varepsilon \gtrsim 1$, and are smaller on the ocean side at low frequencies in the dyke case than for a simple fault. For $Q \geq 10$ the oceanic phases are similar to those for a simple fault.

Thus to summarize the differences between the effects of a fault and a dyke geometry on the field components, we may say the following:

(a) Land:

(i) Normal component E_y: For half-widths of the order of one penetration distance or more ($Q\varepsilon \geq 1$), the fault geometry prevails, and there is no great effect on either the magnitude or phase of this field component. At lower frequencies the magnitude of the field component is enhanced towards the zero frequency limit. The phase difference between the normal electric and tangential magnetic fields remains close to the 45° asymptote for a homogeneous-medium at higher frequencies ($Q\varepsilon \geq 1$). It becomes appreciably smaller at lower frequencies, but returns towards 45° as the

static limit is approached. The degree of reduction in phase difference increases as the conductivity ratio decreases from unity.

(ii) Parallel component E_x: For half-widths considerably greater than one penetration distance ($Q\varepsilon >> 1$), the fault geometry prevails - the field magnitude is greatly reduced as the discontinuity is approached, while the phase difference becomes markedly greater than 45°. At lower frequencies ($Q\varepsilon \geq 1$) the reduction of the field magnitude becomes even greater, approaching the steady state limit. The phase difference at first differs more than the fault-geometry predicts, but as the static limit is approached at still lower frequencies, the phase decreases towards 45°. Towards the center of the dyke both phase and magnitude become more constant as a function of position, even though modified, and this trend becomes more pronounced with falling frequency. The effects become more marked as the conductivity ratio is decreased below unity.

(b) Ocean:

(i) Normal Component E_y: For frequencies at which the half-width is of the order of the penetration depth or greater ($Q \geq 1$), the field behavior follows the coast effect, with some small discrepancies starting to become apparent in the phase. The magnitude is depressed below the asymptotic level in the open ocean, gradually approaching it as the land is left, while the phase is increased appreciably from the asymptotic 45°, gradually returning to 45° at great distances from the shore. As the frequency falls ($Q > 1$)

the magnitude is less supressed, approaching the steady state limit. On the other hand the phase difference is always reduced below the fault-geometry condition, and close to the shore-line it is markedly less than the asymptotic 45^{o}. As one recedes from the shore-line, the phase becomes at first greater than 45^{o}, and then decreases towards 45^{o} again with distance. The dyke-effect becomes smaller in both magnitude and phase as the frequency falls towards the static limit. The effects become more marked with greater conductivity contrasts.

(ii) Parallel Cpmponent E_x: At frequencies for which the half-width is much greater than the penetration depth ($Q >> 1$), the fault-geometry prevails. There is a small enhancement of the magnitude close to the coast, falling off with distance. The phase at first falls below 45^{o}, but increases towards 45^{o} again with distance. At low frequencies ($Q \leq 1$) the effect on both magnitude and phase is similar, but less than the fault-geometry predicts. The phase again tends to 45^{o} everywhere as the static limit is approached. The effect is more marked with a greater conductivity disparity.

5.2 The Dyke at Finite Depth

The assumption of infinite depth made in the calculation in §5.1 is not valid where the ocean is relatively shallow. The sea floor will modify the effect of an infinitely deep dyke, on the electric and magnetic fields, much as it does for the fields near a fault.

Again it is mathematically difficult to treat a model which is physically realistic, such as, for instance, an infinitely deep dyke in a finitely deep ocean. However, it is possible to treat a model analogous to that discussed in §4.2 for a fault of finite depth. We assume that both the "dyke" and the adjoining ocean are underlain by an infinitely deep, non-conducting medium (Fig. 5.8a). This model was used by Rankin (1962) in his study of the H-polarization case (see §3.4.7).

5.2.1 The Static Case

The behavior of the electric currents flowing in the conducting media is similar to that discussed in §5.1.1. Again the magnetic fields, the tangential electric field and the normal electric current are all continuous across the planes of discontinuity, the normal electric field being stronger by a factor σ_1/σ_2 within the dyke.

5.2.2 The Wave Case

To study the transient behavior of the fields, Maxwell's equations must again be solved under the conditions imposed at the various interfaces (see Table 3.2). The coordinate system used is shown in Fig. 5.8b, and each polarization (Fig. 3.5) is treated separately. As the analysis is quite similar to that descrbied in §4.2.2 for the finite fault, only a brief outline will be given.

(a) E-Polarization. The surface $\underset{\sim}{E}$-vector is parallel to the strike.

The relevant equation is again (3.24), viz:

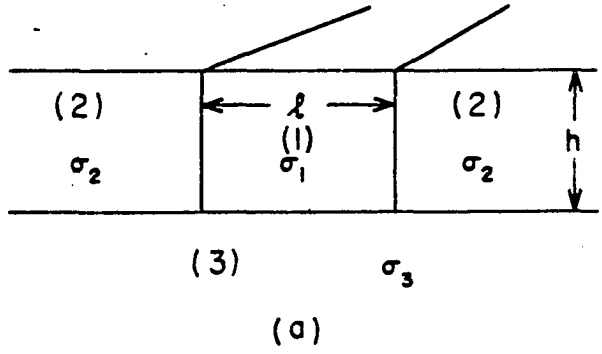

(a)

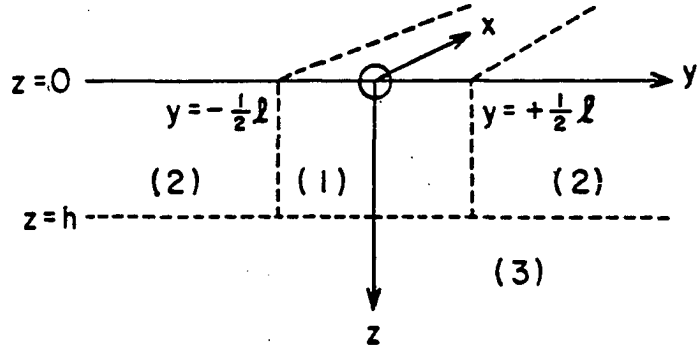

(b)

Fig. 5.8 (a) Model of a dyke of finite depth
(b) The coordinate system

$$\frac{\partial^2 E_x}{\partial y^2} + \frac{\partial^2 E_x}{\partial z^2} + i\eta^2 E_x = 0 \tag{5.29}$$

with

$$\eta^2 = \mu_o \omega \sigma$$

The solution is found by the application of the finite Fourier cosine transformation (4.19), to the z coordinate, using conditions (iii) and (iv) of Table 3.2. We obtain equation (4.22), with the general solution as before.

The symmetry condition (vii) and condition at infinity (v) restrict the coefficients so that:

$$\begin{aligned} |y| < \tfrac{1}{2}\ell: \quad & E_{x1}(y,\xi) = \gamma_1(\xi) \cosh \zeta_1 y - i \frac{\mu_o \omega A}{\zeta_1^2} \frac{\pi}{h} \\ |y| > \tfrac{1}{2}\ell: \quad & E_{x2}(y,\xi) = \gamma_2(\xi)\, e^{-\zeta_2 |y|} - i \frac{\mu_o \omega A}{\zeta_2^2} \frac{\pi}{h} \end{aligned} \tag{5.30}$$

where

$$\zeta^2 = \left(\frac{\pi}{h}\right)^2 \xi^2 - i\eta^2$$

The coefficients $\gamma_j(\xi)$ may be determined by solving the simultaneous equations that result from the application of conditions (i) and (ii) at the interface $y = \pm\frac{1}{2}\ell$

$$\begin{aligned} \gamma_1(\xi) &= \mu_o \omega A \frac{\pi}{h} \frac{\eta_2^2 - \eta_1^2}{\zeta_1^2 \zeta_2 \Delta_1} \\ \gamma_2(\xi) &= -\mu_o \omega A \frac{\pi}{h} \frac{\eta_2^2 - \eta_1^2}{\zeta_1 \zeta_2^2} \frac{e^{\frac{1}{2}\ell\zeta_2} \sinh \frac{1}{2}\ell\zeta_1}{\Delta_1} \end{aligned} \tag{5.31}$$

$$\Delta_1 = \zeta_1 \sinh \tfrac{1}{2}\ell\zeta_1 + \zeta_2 \cosh \tfrac{1}{2}\ell\zeta_1$$

We now apply the inverse finite Fourier cosine transform (4.20) to (5.30) and obtain the E_x fields. With Re $(\zeta) > 0$ always, we have

$$\bar{E}_{x1}(y,0) = \frac{\mu_o \omega A}{\eta_1^2} \frac{\pi}{h} \left\{ 1 - \frac{\eta_2^2 - \eta_1^2}{\eta_1 \eta_2} \frac{\cosh \sqrt{-i}\, \eta_1 y}{\Delta_o} \right\}$$

$$\bar{E}_{x2}(y,0) = \frac{\mu_o \omega A}{\eta_2^2} \frac{\pi}{h} \left\{ 1 + \frac{\eta_2^2 - \eta_1^2}{\eta_1^2} \frac{e^{-\sqrt{-i}\, \eta_2 (|y| - \frac{1}{2}\ell)} \sinh \sqrt{-i}\, \frac{1}{2}\ell \eta_1}{\Delta_o} \right\} \quad (5.32)$$

$$\Delta_o = \cosh \sqrt{-i}\, \tfrac{1}{2}\ell \eta_1 + \frac{\eta_1}{\eta_2} \sinh \sqrt{-i}\, \tfrac{1}{2}\ell \eta_1$$

The inverse transforms are then

$$E_{x1}(y,z) = \frac{1}{\pi} \bar{E}_{x1}(y,0) + \frac{2\mu_o \omega A}{h} \sum_{\xi=1}^{\infty} \frac{1}{\zeta_1^2} \left\{ (\eta_2^2 - \eta_1^2) \frac{\cosh \zeta_1 y}{\zeta_2 \Delta_1} - i \right\} \cos \frac{\pi}{h} \xi z \quad (5.33)$$

$$E_{x2}(y,z) = \frac{1}{\pi} \bar{E}_{x2}(y,0) - \frac{2\mu_o \omega A}{h} \sum_{\xi=1}^{\infty} \frac{1}{\zeta_2^2} \left\{ (\eta_2^2 - \eta_1^2) \frac{e^{-(|y| - \frac{1}{2}\ell)\zeta_2} \sinh \frac{1}{2}\ell \zeta_1}{\zeta_1 \Delta_1} + i \right\} \cos \frac{\pi}{h} \xi z$$

The transforms of the last terms in the summations are known explicitly (see eq. (4.28) and App. 3), so these results may be further reduced:

$$E_{x1}(y,z) = \mu_o \omega A \left\{ \frac{\sqrt{i}}{\eta_1} \frac{\cos \sqrt{i}\, \eta_1 (h-z)}{\sin \sqrt{i}\, \eta_1 h} - \frac{1 - \varepsilon^2}{\eta_1^2 h} \frac{\cosh \sqrt{-i}\, \eta_1 y}{\Delta_o} + \right.$$

$$\left. + \frac{2(\eta_2^2 - \eta_1^2)}{h} \sum_{\xi=1}^{\infty} \frac{\cosh \zeta_1 y}{\zeta_1^2 \zeta_2 \Delta_1} \cos \frac{\pi}{h} \xi z \right\} \quad (5.34)$$

$$E_{x2}(y,z) = \mu_o \omega A \left\{ \frac{\sqrt{i}}{\eta_2} \frac{\cos \sqrt{i}\, \eta_2 (h-z)}{\sin \sqrt{i}\, \eta_2 h} + \frac{1-\varepsilon^2}{\eta_1 \eta_2^2} \frac{e^{-\sqrt{-i}\, \eta_2 (|y| - \frac{1}{2}\ell)} \sinh \sqrt{-i}\, \frac{1}{2}\ell \zeta_1}{\Delta_o} \right.$$

$$\left. - \frac{2(\eta_2^2 - \eta_1^2)}{h} \sum_{\xi=1}^{\infty} \frac{e^{-(|y| - \frac{1}{2}\ell)\zeta_2} \sinh \frac{1}{2}\ell \zeta_1}{\zeta_1 \zeta_2^2 \Delta_1} \cos \frac{\pi}{h} \xi z \right\}$$

This pair of relations is the solution of (5.29) satisfying the conditions (i) - (vii) of Table 3.2. The H_y and H_z relations are obtained from the E_x relations above through Maxwell's equations, as given in this table. The relations are collected together in Table 5.3.

(b) H-Polarization: The H-vector is parallel to the strike. The equation to be solved is (3.26):

$$\frac{\partial^2 H_x}{\partial y^2} + \frac{\partial^2 H_x}{\partial z^2} + i\eta^2 H_x = 0 \tag{5.35}$$

where $\eta^2 = \mu_o \omega \sigma$

We apply the finite Fourier sine transformation (4.31) to the z-coordinate, and (iii), (iv), (v) and (vii) of Table 3.2. Then

$$\begin{aligned} |y|<\tfrac{1}{2}\ell: \quad & \bar{H}_{x1}(y,\xi) = \delta_1(\xi) \cosh \zeta_1 y - B \left(\frac{\pi}{h}\right)^2 \frac{\xi}{\zeta_1^2} \\ |y|>\tfrac{1}{2}\ell: \quad & \bar{H}_{x2}(y,\xi) = \delta_2(\xi)\, e^{-\zeta_2 |y|} - B \left(\frac{\pi}{h}\right)^2 \frac{\xi}{\zeta_2^2} \end{aligned} \tag{5.36}$$

Conditions (i) and (ii), applied at the interfaces $y = \pm\frac{1}{2}\ell$, determine the coefficients $\delta(\xi)$:

$$\begin{aligned} \delta_1(\xi) &= -iB \left(\frac{\pi}{h}\right)^2 \frac{\varepsilon^2 (\eta_2^2 - \eta_1^2)}{\zeta_1^2 \zeta_2 \Delta_2} \\ \delta_2(\xi) &= iB \left(\frac{\pi}{h}\right)^2 (\eta_2^2 - \eta_1^2) \frac{\xi\, e^{\frac{1}{2}\ell\zeta_2} \sinh \frac{1}{2}\ell\zeta_1}{\zeta_1 \zeta_2^2 \Delta_2} \end{aligned} \tag{5.37}$$

$$\Delta_2 = \zeta_1 \sinh \tfrac{1}{2}\ell\zeta_1 + \varepsilon^2 \zeta_2 \cosh \tfrac{1}{2}\ell\zeta_1$$

Application of the inverse transform (4.32) to (5.36) yields:

$$H_{x1}(y,z) = -\frac{2\pi B}{h^2}\sum_{\xi=1}^{\infty}\frac{\xi}{\zeta_1^2}\left\{i\varepsilon^2(\eta_2^2-\eta_1^2)\frac{\cosh\zeta_1 y}{\zeta_2\Delta_2}+1\right\}\sin\frac{\pi}{h}\xi z$$

$$H_{x2}(y,z) = \frac{2\pi B}{h^2}\sum_{\xi=1}^{\infty}\frac{\xi}{\zeta_2^2}\left\{i(\eta_2^2-\eta_1^2)\frac{\sinh\tfrac{1}{2}\ell\zeta_1\, e^{-\zeta_2(|y|-\frac{1}{2}\ell)}}{\zeta_1\Delta_2} - 1\right\}\sin\frac{\pi}{h}\xi z \qquad (5.38)$$

The last summation in each of these is known (eq. 6.39 and App. 3), so that the fields may be written:

$$H_{x1}(y,z) = -B\left\{\frac{\sin\sqrt{i}\,\eta_1(h-z)}{\sin\sqrt{i}\,\eta_1 h} + 2\pi i\frac{\eta_1^2(1-\varepsilon^2)}{h^2}\sum_{\xi=1}^{\infty}\frac{\xi\cosh\zeta_1 y}{\zeta_1^2\zeta_2\Delta_2}\sin\frac{\pi}{h}\xi z\right\}$$

$$H_{x2}(y,z) = -B\left\{\frac{\sin\sqrt{i}\,\eta_2(h-z)}{\sin\sqrt{i}\,\eta_2 h} - 2\pi i\frac{\eta_2^2(1-\varepsilon^2)}{h^2}\sum_{\xi=1}^{\infty}\frac{\xi\sinh\tfrac{1}{2}\ell\zeta_1\, e^{-\zeta_2(|y|-\frac{1}{2}\ell)}}{\zeta_1\zeta_2^2\Delta_2}\sin\frac{\pi}{h}\xi z\right\} \qquad (5.39)$$

These relations constitute the solution to (5.35) under conditions (i) - (vii) of Table 3.2. The E_y and E_z fields are then obtained from Maxwell's equations. The E_y relations also satisfy the condition

$$\sigma_1 E_{y1} = \sigma_2 E_{y2}$$

at the interfaces $y = \pm\frac{1}{2}\ell$.

Table 5.3

A Summary of the Field Components Near a Dyke of Finite Depth

$$E_{x1} = \mu_o \omega A \left\{ \frac{\sqrt{i}}{\eta_1} \frac{\cos\sqrt{i}\,\eta_1(h-z)}{\sin\sqrt{i}\,\eta_1 h} - \frac{1-\epsilon^2}{\eta_1^2 h} \frac{\cosh\sqrt{-i}\,\eta_1 y}{\Delta_o} + 2\frac{\eta_2^2-\eta_1^2}{h} \sum_{\xi=1}^{\infty} \frac{\cosh\zeta_1 y}{\zeta_1^2\zeta_2\Delta_1} \cos\frac{\pi}{h}\xi z \right\}$$

$$E_{x2} = \mu_o \omega A \left\{ \frac{\sqrt{i}}{\eta_2} \frac{\cos\sqrt{i}\,\eta_2(h-z)}{\sin\sqrt{i}\,\eta_2 h} + \frac{1-\epsilon^2}{\eta_1\eta_2 h} \frac{\sinh\sqrt{-i}\,\tfrac{1}{2}\ell\eta_1\, e^{-\sqrt{-i}\,\eta_2(|y|-\frac{1}{2}\ell)}}{\Delta_o} - \right.$$

$$\left. -2\frac{\eta_2^2-\eta_1^2}{h} \sum_{\xi=1}^{\infty} \frac{\sinh\tfrac{1}{2}\ell\zeta_1\, e^{-\zeta_2(|y|-\frac{1}{2}\ell)}}{\zeta_1\zeta_2^2\Delta_1} \cos\frac{\pi}{h}\xi z \right\} \qquad (5.40)$$

$$E_{y1} = \mu_o \omega B \left\{ \frac{\sqrt{i}}{\eta_1} \frac{\cos\sqrt{i}\,\eta_1(h-z)}{\sin\sqrt{i}\,\eta_1 h} - \frac{2\pi^2 i(1-\epsilon^2)}{h^3} \sum_{\xi=1}^{\infty} \frac{\xi^2 \cosh\zeta_1 y}{\zeta_1^2\zeta_2\Delta_2} \cos\frac{\pi}{h}\xi z \right\}$$

$$E_{y2} = \mu_o \omega B \left\{ \frac{\sqrt{i}}{\eta_2} \frac{\cos\sqrt{i}\,\eta_2(h-z)}{\sin\sqrt{i}\,\eta_2 h} + \frac{2\pi^2 i(1-\epsilon^2)}{h^3} \sum_{\xi=1}^{\infty} \frac{\xi^2 e^{-\zeta_2(|y|-\frac{1}{2}\ell)} \sinh\tfrac{1}{2}\ell\zeta_1}{\zeta_1\zeta_2^2\Delta_2} \cos\frac{\pi}{h}\xi z \right\} \qquad (5.41)$$

Table 5.3 (cont'd)

A Summary of the Field Components Near a Dyke of Finite Depth

$$\left.\begin{aligned} E_{z1} &= \mu_o \omega B \frac{2\pi i(1-\epsilon^2)}{h^2} \sum_{\xi=1}^{\infty} \frac{\xi \sinh\zeta_1 y}{\zeta_1\zeta_2\Delta_2} \sin\frac{\pi}{h}\xi z \\ E_{z2} &= \mp\mu_o \omega B \frac{2\pi i(1-\epsilon^2)}{h^2} \sum_{\xi=1}^{\infty} \frac{\xi \sinh\tfrac{1}{2}\ell\zeta_1 \, e^{-\zeta_2(|y|-\frac{1}{2}\ell)}}{\zeta_1\zeta_2\Delta_2} \sin\frac{\pi}{h}\xi z \end{aligned}\right\} \quad (5.42)$$

$$H_{x1} = -B\left\{\frac{\sin\sqrt{i}\,\eta_1(h-z)}{\sin\sqrt{i}\,\eta_1 h} + \frac{2\pi i\eta_1^2(1-\epsilon^2)}{h^2} \sum_{\xi=1}^{\infty} \frac{\xi \cosh\zeta_1 y}{\zeta_1^2\zeta_2\Delta_2} \sin\frac{\pi}{h}\xi z\right\}$$

$$H_{x2} = -B\left\{\frac{\sin\sqrt{i}\,\eta_2(h-z)}{\sin\sqrt{i}\,\eta_2 h} - \frac{2\pi i\,\eta_2^2(1-\epsilon^2)}{h^2} \sum_{\xi=1}^{\infty} \frac{\xi \sinh\tfrac{1}{2}\ell\zeta_1 \, e^{-\zeta_2(|y|-\frac{1}{2}\ell)}}{\zeta_1\zeta_2^2\Delta_2} \sin\frac{\pi}{h}\xi z\right\} \quad (5.43)$$

$$H_{y1} = A\left\{\frac{\sin\sqrt{i}\,\eta_1(h-z)}{\sin\sqrt{i}\,\eta_1 h} + \frac{2\pi i\eta_2^2(1-\epsilon^2)}{h^2} \sum_{\xi=1}^{\infty} \frac{\xi \cosh\zeta_1 y}{\zeta_1^2\zeta_2\Delta_1} \sin\frac{\pi}{h}\xi z\right\}$$

$$H_{y2} = A\left\{\frac{\sin\sqrt{i}\,\eta_2(h-z)}{\sin\sqrt{i}\,\eta_2 h} - \frac{2\pi i\eta_2^2(1-\epsilon^2)}{h^2} \sum_{\xi=1}^{\infty} \frac{\xi \sinh\tfrac{1}{2}\ell\zeta_1 \, e^{-\zeta_2(|y|-\frac{1}{2}\ell)}}{\zeta_1\zeta_2^2\Delta_1} \sin\frac{\pi}{h}\xi z\right\} \quad (5.44)$$

Table 5.3 (cont'd)

A Summary of the Field Components Near a Dyke of Finite Depth

$$H_{z1} = A \left\{ -\frac{\sqrt{i}(1-\epsilon^2)}{\eta_1 h} \frac{\sinh\sqrt{-i}\,\eta_1 y}{\Delta_o} + \frac{2i\eta_2^2(1-\epsilon^2)}{h} \sum_{\xi=1}^{\infty} \frac{\sinh\zeta_1 y}{\zeta_1\zeta_2\Delta_1} \cos\frac{\pi}{h}\xi z \right\}$$

$$H_{z2} = \pm A \left\{ -\frac{\sqrt{i}(1-\epsilon^2)}{\eta_1 h} \frac{\sinh\sqrt{-i}\,\tfrac{1}{2}\ell\eta_1\, e^{-\sqrt{-i}\,(|y|-\frac{1}{2}\ell)\eta_2}}{\Delta_o} + \right.$$

$$\left. + \frac{2i\eta_2^2(1-\epsilon^2)}{h} \sum_{\xi=1}^{\infty} \frac{\sinh\tfrac{1}{2}\ell\zeta_1\, e^{-\zeta_2(|y|-\frac{1}{2}\ell)}}{\zeta_1\zeta_2\Delta_1} \cos\frac{\pi}{h}\xi z \right\} \qquad (5.45)$$

$$\Delta_o = \cosh\sqrt{-i}\,\tfrac{1}{2}\ell\eta_1 + \epsilon \sinh\sqrt{-i}\,\tfrac{1}{2}\ell\eta_1$$

$$\Delta_1 = \zeta_1 \sinh\tfrac{1}{2}\ell\zeta_1 + \zeta_2 \cosh\tfrac{1}{2}\ell\zeta_1$$

$$\Delta_2 = \zeta_1 \sinh\tfrac{1}{2}\ell\zeta_1 + \epsilon^2\zeta_2 \cosh\tfrac{1}{2}\ell\zeta_1 \qquad (5.46)$$

$$\zeta_j^2 = \left(\frac{\pi}{h}\right)^2 \xi^2 - i\eta_j^2 \quad ; \quad \eta_j^2 = \mu_o\omega\sigma_j \quad ; \quad \mathrm{Re}\sqrt{-i} > 0$$

Table 5.4

The Surface Field Components Near a Dyke of Finite Depth
in Terms of Dimensionless Parameters

$$\sqrt{\frac{\sigma_1}{\mu_o\omega}}\ \frac{E_{x1}}{A} = \sqrt{i}\cot\sqrt{i}\,H\varepsilon - \frac{1-\varepsilon^2}{H\varepsilon}\ \frac{\cosh\sqrt{-i}\,Q\varepsilon(Y+1)}{D_o} + \frac{2}{\pi}H_o^3\varepsilon(1-\varepsilon^2)\sum_{\xi=1}^{\infty}\frac{\cosh\left[\frac{Q.Y+1}{H_o}\sqrt{\xi^2-i(H_o\varepsilon)^2}\right]}{\left[\xi^2-i(H_o\varepsilon)^2\right]\sqrt{\xi^2-iH_o^2}\ D_1}$$

$$\sqrt{\frac{\sigma_2}{\mu_o\omega}}\ \frac{E_{x2}}{A} = \sqrt{i}\cot\sqrt{i}\,H + \frac{1-\varepsilon^2}{H\varepsilon}\ \frac{\sinh\sqrt{-i}\,Q\varepsilon\ e^{-\sqrt{-i}\,QY}}{D_o} - \tag{5.47}$$

$$- \frac{2}{\pi}H_o^3(1-\varepsilon^2)\sum_{\xi=1}^{\infty}\frac{\sinh\left[\frac{Q}{H_o}\sqrt{\xi^2-i(H_o\varepsilon)^2}\right]e^{-\frac{QY}{H_o}\sqrt{\xi^2-iH_o^2}}}{\sqrt{\xi^2-i(H_o\varepsilon)^2}\ \left[\xi^2-iH_o^2\right]\ D_1}$$

$$\sqrt{\frac{\sigma_1}{\mu_o\omega}}\ \frac{E_{y1}}{B} = \sqrt{i}\cot\sqrt{i}\,H\varepsilon - \frac{2}{\pi}H_o\varepsilon(1-\varepsilon^2)\sum_{\xi=1}^{\infty}\frac{\xi^2\cosh\left[\frac{Q(Y+1)}{H_o}\sqrt{\xi^2-i(H_o\varepsilon)^2}\right]}{\left[\xi^2-i(H_o\varepsilon)^2\right]\sqrt{\xi^2-iH_o^2}\ D_2}$$

$$\sqrt{\frac{\sigma_2}{\mu_o\omega}}\ \frac{E_{y2}}{B} = \sqrt{i}\cot\sqrt{i}H + \frac{2}{\pi}H_o(1-\varepsilon^2)\sum_{\xi=1}^{\infty}\frac{\xi^2\sinh\left[\frac{Q}{H_o}\sqrt{\xi^2-i(H_o\varepsilon)^2}\right]\ e^{\frac{QY}{H_o}\sqrt{\xi^2-iH_o^2}}}{\sqrt{\xi^2-i(H_o\varepsilon)^2}\ \left[\xi^2-iH_o^2\right]\ D_2} \tag{5.48}$$

Table 5.4 (cont'd)

The Surface Field Components Near a Dyke of Finite Depth
in Terms of Dimensionless Parameters

$$\frac{H_{z1}}{A} = -\frac{\sqrt{i}}{H\varepsilon} \cdot \frac{\sinh\sqrt{-i}\,Q\varepsilon(Y+1)}{D_o} + i\,\frac{2}{\pi}\,H_o^2\,(1-\varepsilon^2)\sum_{\xi=1}^{\infty} \frac{\sinh\left[\frac{Q(Y+1)}{H_o}\sqrt{\xi^2-i(H_o\varepsilon)^2}\right]}{\sqrt{\xi^2-i(H_o\varepsilon)^2}\sqrt{\xi^2-iH_o^2}\,.\,D_1} \qquad (5.49)$$

$$\frac{H_{z2}}{A} = -\frac{\sqrt{i}}{H\varepsilon} \cdot \frac{\sinh\sqrt{-i}\,Q\varepsilon\,.\,e^{-\sqrt{-i}\,QY}}{D_o} + i\,\frac{2}{\pi}\,H_o^2\,(1-\varepsilon^2)\sum_{\xi=1}^{\infty} \frac{\sinh\left[\frac{Q}{H_o}\sqrt{\xi^2-i(H_o\varepsilon)^2}\right] - \frac{QY}{H_o}\sqrt{\xi^2-iH_o^2}}{\sqrt{\xi^2-i(H_o\varepsilon)^2}\,\sqrt{\xi^2-iH_o^2}\,.\,D_1}$$

$$D_o = \cosh\sqrt{-i}\,Q\varepsilon + \varepsilon\sinh\sqrt{-i}\,Q\varepsilon$$

$$D_1 = \sqrt{\xi^2-i(H_o\varepsilon)^2}\,\sinh\left[\frac{Q}{H_o}\sqrt{\xi^2-i(H_o\varepsilon)^2}\right] + \sqrt{\xi^2-iH_o^2}\,\cosh\left[\frac{Q}{H_o}\sqrt{\xi^2-i(H_o\varepsilon)^2}\right] \qquad (5.50)$$

$$D_2 = \sqrt{\xi^2-i(H_o\varepsilon)^2}\,\sinh\left[\frac{Q}{H_o}\sqrt{\xi^2-i(H_o\varepsilon)^2}\right] + \varepsilon^2\sqrt{\xi^2-iH_o^2}\,\cosh\frac{Q}{H_o}\left[\sqrt{\xi^2-i(H_o\varepsilon)^2}\right]$$

All of the field components are summarized in Table 5.3. At the surface $z = 0$, the only non-trivial components are E_x, E_y and H_z, and the expressions for these are given in Table 5.4 in terms of the dimensionless variables of Table 3.3.

5.2.3 Special Cases

(a) The Transition to a Double-Layered Medium (Asymptotic Condition):

Again the solutions for the various field components at large values of Y tend towards those for a double-layered medium, the lower layer of which is non-conducting. This may be seen from the relations of Tables 5.3 and 5.4, as $Y \to \infty$.

To be more definite we must consider the individual fields. The E_x and H_z relations have two "terms" which become negligible in the transition. The first of these requires always $QY \gg 1$ or $y - \tfrac{1}{2}\ell \gg \eta_2^{-1}$. This is sufficient to make the summation term negligible too, whenever $H_o\varepsilon \gtrsim 1$ (ie. when $h \gtrsim 3\eta_1^{-1}$). However, there are two other cases which give conditions in addition to the requirement that $QY \gg 1$. These are

(i) if $H_o\varepsilon \ll 1$ $(h \ll 3\eta_1^{-1})$

then: $\dfrac{QY}{H_o} - 1 \gg 1$ or $y - \tfrac{1}{2}\ell \gg \dfrac{\tfrac{1}{2}\ell}{\eta_2^{-1}}\ h/3$

(ii) if $H_o \ll 1$ $(h \ll 3\eta_2^{-1})$

then: $\dfrac{Q(Y-1)}{H_o} \gg 1$ or $y - \tfrac{1}{2}\ell \gg \tfrac{1}{2}\ell + h/3$

The E_y relations do not require $QY \gg 1$ under all circumstances, but otherwise the E_y-field is governed by the cases given above.

Under the above conditions on the observer's distance from the shore-line ($y - \frac{1}{2}\ell$), the effect of the dyke becomes negligible, since:

$$E_{x2} \to \sqrt{i}\,\frac{\mu_o \omega A}{\eta_2}\,\frac{\cos\sqrt{i}\,\eta_2(h-z)}{\sin\sqrt{i}\,\eta_2 h} \to \sqrt{i}\,\frac{\mu_o \omega A}{\eta_2}\,\cot\sqrt{i}\,\eta_2 h, \text{ at } z = 0$$

$$E_{y2} \to \sqrt{i}\,\frac{\mu_o \omega B}{\eta_2}\,\frac{\cos\sqrt{i}\,\eta_2(h-z)}{\sin\sqrt{i}\,\eta_2 h} \to \sqrt{i}\,\frac{\mu_o \omega B}{\eta_2}\,\cot\sqrt{i}\,\eta_2 h, \quad \text{at } z = 0$$

$$H_{x2} \to -B\,\frac{\sin\sqrt{i}\,\eta_2(h-z)}{\sin\sqrt{i}\,\eta_2 h} \to -B, \qquad \text{at } z = 0$$

$$H_{y2} \to A\,\frac{\sin\sqrt{i}\,\eta_2(h-z)}{\sin\sqrt{i}\,\eta_2 h} \to A, \qquad \text{at } z = 0$$

E_{z2} and $H_{z2} \to 0$

These are the relations for a two-layered medium when the lower is non-conducting.

Within the dyke, an analogous behavior occurs toward the center, provided the width is sufficiently great that the effect of both the coasts is negligible. For all of the fields we need $O/H_o \gg 1$ and $Y + 1 \ll 1$, or in other words $\frac{1}{2}\ell \gg h/3$ and $y \ll \frac{1}{2}\ell$. The E_x and H_z fields require in addition that $O\varepsilon \gg 1$, or equivalently, that $\frac{1}{2}\ell \gg \eta_1^{-1}$. The E_y field will also show very little coast effect inside the dyke if $H_o\varepsilon \ll 1$ or $h/3 \ll \eta_1^{-1}$. Under these conditions the fields behave as though there were no coast or dyke present, and reduce to the expressions above for a two-layered medium. They are equivalent to the limiting conditions that $y \to 0$ $(Y \to -1)$ and $\ell \to \infty$ $(O \to \infty)$.

(b) The Transition to a Fault of Finite Depth:

At high frequencies, or for a dyke of sufficient width, the influence of the remoter coastline on the fields at any given point is negligible. The "dyke" then appears as a "continent" or a fault-like coastline, and the field solutions approach those of §4.2.2.

Again the transition is effected by the exponential behavior of the hyperbolic functions, the only condition being that $Q\epsilon >> 1$. This holds for all fields, but for small values of $H_o\epsilon$, the E_{y2}-field makes the transition when $Q >> H_o$. Thus when the dyke half-width $\frac{1}{2}\ell$ greatly exceeds the land penetration depth $\eta_1^{-1}/3$, the dyke behaves as a continent to all of the fields. If the basement is sufficiently shallow compared with the land penetration depth ($h << 3\eta_1^{-1}$) the E_{y2}-field behaves as though the dyke were infinitely wide.

The conclusions of §5.1.3a are therefore not changed qualitatively be the presence of the ocean floor, except for the normal E_{y2}-field over a shallow conductor underlain by a non-conductor.

(c) The Transition to an Infinitely Deep Dyke

As the basement depth h increases the field components approximate those given in Tables 5.1 and 5.2 for a dyke of infinite depth. We see this by applying the limiting process as $h \to \infty$, described in §4.2.3b to the equations of Tables 5.3 or 5.4. Again the more useful criterion is that, for $H\epsilon >> 1$ ($h >> \eta_1^{-1}$), the fields behave as though the media are of infinite depth. The oceanic E_y-field, however, only requires $H >> 1$ or $h >> \eta_2^{-1}$ and the conclusions of §4.2.3b are unchanged--the normal electric field is much less sensitive to the presence of an ocean floor than the other fields.

(d) The Field Components Directly Over the Discontinuity Planes

When $y = \pm\frac{1}{2}\ell$, there is no appreciable simplification of the field expressions, even to expressions analogous to those in §4.2.3c, for a fault of finite depth.

5.2.4 Approximations for Shallow Basements

In §4.2.4 we derived approximate expressions for the fields near a fault, when the non-conducting basement was located at a depth shallow compared with the oceanic penetration depth (and therefore the land penetration depth also), ie.

$$H = h\sqrt{\mu_o \omega \sigma_2} \ll 1$$

This approximation may also be applied to the fields around a shallow dyke, listed in Table 5.4. The summation terms take the following forms

$$\text{(i) } E_x, H_z \text{ terms: } \sum_{\xi=1}^{\infty} \left[\frac{e^{-\xi Q|Y|/H_o}}{\xi^n} \pm \frac{e^{-\xi Q(|Y|+1)/H_o}}{\xi^n} \right] \tag{5.52}$$

where n = 3, 4 specify the H_z and E_x terms respectively and the ± refer to regions 1 and 2 (inside and outside the dyke) respectively.

$$\text{(ii) } E_y \text{ term: } \sum_{\xi=1}^{\infty} \left[\frac{e^{-\xi Q|Y|/H_o}}{\xi^2} \pm \frac{e^{-\xi Q(|Y|+1)/H_o}}{\xi^2} \right] \frac{1}{1-\delta^2 e^{-\xi(2Q/H_o)}} \tag{5.53}$$

where $\delta^2 = (1-\epsilon^2)/(1+\epsilon^2)$ and the ± refer to regions 1 and 2 respectively. Relations (5.52) specify forms of the polylogarithm defined by (4.53). The expression (5.53) is not simply reducible; the terms are special cases of the relation

$$\Lambda_2(x) = \sum_{\xi=1}^{\infty} \frac{x^{\xi}}{\xi^2} (1-\delta^2\rho^{\xi})^{-1} \qquad (5.54)$$

where $\rho = e^{-2Q/H_o}$

If $r = 2Q/H_o >> 1,$ (5.55)

then $\Lambda_2(x) \to L_2(x)$, the dilogarithm.

This approximation is true to a high order if $r \geq 7$ and is still close for $r \sim 3$.

We recall relation (4.54) and simplify the relations of Table 5.4, under the approximation $H << 1$. The results are given in Table 5.5, and still satisfy the boundary conditions that E_x, σE_y and H_z be continuous at $y = 0$.

It is usually unnecessary to impose the restriction (5.55) on ℓ/h, since the terms in Λ are mostly small in comparison with H^{-1} or $(H\epsilon)^{-1}$ terms, and may be neglected even for cases where r is not large.

5.2.5 Computation of the Fields Near a Shallow Dyke

As with the fault geometry, the equations of Table 5.5 were used to calculate the limiting fields for a relatively shallow basement, using a desk-calculator. This avoided the use of a large computer, which would be necessary to evaluate the relations of Table 5.4. When necessary the polylogarithm tables of van Wijngaarden (1954) were used. Some computations of the E_y-field for the more complete case have been made by Rankin (1962), but his dimensions differ from those used here and no direct comparison can be made.

Table 5.5

The Field Components Near a Shallow Dyke

$$\sqrt{\frac{\sigma_1}{\mu_o\omega}}\frac{E_{x1}}{A} = \frac{1}{H\varepsilon} - i\frac{H\varepsilon}{3} + \frac{(H\varepsilon)^3}{45} - \frac{1-\varepsilon^2}{H\varepsilon}\frac{\cosh\sqrt{-i}\,Q\varepsilon(Y+1)}{D_o} + \frac{1-\varepsilon^2}{\pi}H_o^3\varepsilon\left\{L_4\left[e^{\frac{-Q|Y|}{H_o}}\right] + L_4\left[e^{\frac{-Q(2-|Y|)}{H_o}}\right]\right\}$$

$$\sqrt{\frac{\sigma_2}{\mu_o\omega}}\frac{E_{x2}}{A} = \frac{1}{H} - \frac{iH}{3} + \frac{H^3}{45} + \frac{1-\varepsilon^2}{H\varepsilon}\frac{\sinh\sqrt{-i}\,Q\varepsilon\, e^{-\sqrt{-i}\,QY}}{D_o} - \frac{1-\varepsilon^2}{\pi}H_o^3\left\{L_4\left[e^{\frac{-QY}{H_o}}\right] - L_4\left[e^{\frac{-Q(2+Y)}{H_o}}\right]\right\} \qquad (5.56)$$

$$\sqrt{\frac{\sigma_1}{\mu_o\omega}}\frac{E_{y1}}{B} = \frac{1}{H\varepsilon} - i\frac{H\varepsilon}{3} - \frac{2i}{\pi}\frac{1-\varepsilon^2}{1+\varepsilon^2}H_o\varepsilon\left\{\Lambda_2\left[e^{-Q|Y|/H_o}\right] + \Lambda_2\left[e^{-Q(2-|Y|)/H_o}\right]\right\}$$

$$\sqrt{\frac{\sigma_2}{\mu_o\omega}}\frac{E_{y2}}{B} = \frac{1}{H} - i\frac{H}{3} + \frac{2i}{\pi}\frac{1-\varepsilon^2}{1+\varepsilon^2}H_o\left\{\Lambda_2\left[e^{-QY/H_o}\right] - \Lambda_2\left[e^{-Q(2+Y)/H_o}\right]\right\} \qquad (5.57)$$

$$\frac{H_{z1}}{A} = -\sqrt{i}\frac{1-\varepsilon^2}{H\varepsilon}\frac{\sinh\sqrt{-i}\,Q\varepsilon\,(Y+1)}{D_o} + i\frac{1-\varepsilon^2}{\pi}H_o^2\left\{L_3\left[e^{-Q|Y|/H_o}\right] - L_3\left[e^{-Q(2-|Y|)/H_o}\right]\right\}$$

$$\frac{H_{z2}}{A} = -\sqrt{i}\frac{1-\varepsilon^2}{H\varepsilon}\frac{\sinh\sqrt{-i}\,Q\varepsilon\, e^{-\sqrt{-i}\,QY}}{D_o} + i\frac{1-\varepsilon^2}{\pi}H_o^2\left\{L_3\left[e^{-QY/H_o}\right] - L_3\left[e^{-Q(2+Y)/H_o}\right]\right\} \qquad (5.58)$$

$$D_o = \cosh\sqrt{-i}\,Q\varepsilon + \varepsilon\sinh\sqrt{-i}\,Q\varepsilon$$

5.3 Discussion of Results

In Figs. 5.9a-c the three field components E_x, E_y, H_z are given as functions of Y, for $\epsilon = 0.1$, $Q = 0.1$, 1, 10 and $H = 0.1$ and ∞. The curves for $H = 0.1$ were calculated from the relations of Table 5.5, while those for $H = \infty$ are reproduced from Figs. 5.3a-c for comparison. Figure 5.10 shows characteristics of the polarization ellipses of the electric field. The calculations were made by the method described in App.1, for a surface magnetic field which is left-circularly-polarized.

The magnitude curves for the electric field components have again been normalized to the values in the ocean at great distances from the coastline. The normalization factor τ was given in §4.3 (eq. 4.58) and Fig. 4.5.

5.3.1 The Vertical Magnetic Field H_z (Fig. 5.9c)

Figure 5.9c shows that the vertical magnetic field is enhanced by the presence of the basement to a greater degree than the increase caused by a dyke of infinite depth. The maximum increase immediately over the discontinuity plane is reduced below that for a simple fault, when the dyke is narrow enough for the wave to "see" a dyke rather than a continent. The conditions under which this occurs were discussed in §5.1.3a and §5.2.3b.

Anywhere within a few penetration depths of the shore-line, at any frequency within 10^{-2} - 10^{2} cps (at least), the influence of a basement layer of low conductivity on a fault or dyke in a highly conducting upper layer will result in a large enhancement of the

vertical magnetic field. If the thickness of the conducting layer is shallow compared with the penetration depth, the enhancement of the field may be enormous, when compared with the field over an infinitely deep discontinuity. The numerical results in Fig. 4.9c are overestimates, especially near the shorelines--the cuspoidal nature of the field will be smoothed out in reality by the gradual change in the conductivity from sea to land.

The modification to the phase of the vertical magnetic field by the basement is, however, relatively small, although it is quite uniform at various distances within each medium.

The frequency response of the magnetic field at different locations near the discontinuity planes cannot be determined from Fig. 5.9c in the same way as were those for the fault (finite and infinite) and infinitely deep dyke. In all of these last cases, only one of the dimensionless parameters λ, Q, H, specifying the curves, involved the frequency. However, in Fig. 5.9 the curves involve both Q and H, each of them frequency dependent. Replotting these with Q as the abscissa would not give curves for a constant depth h, but only for constant H, the frequency dependent depth. A whole series of figures similar to Fig. 5.9 would be necessary to determine the response. As the usefulness of the equations of Table 5.5 lay in avoiding excessive computer work, such a computation has not been performed. However, in §5.4 we give a specific example where the frequency dependence has been calculated.

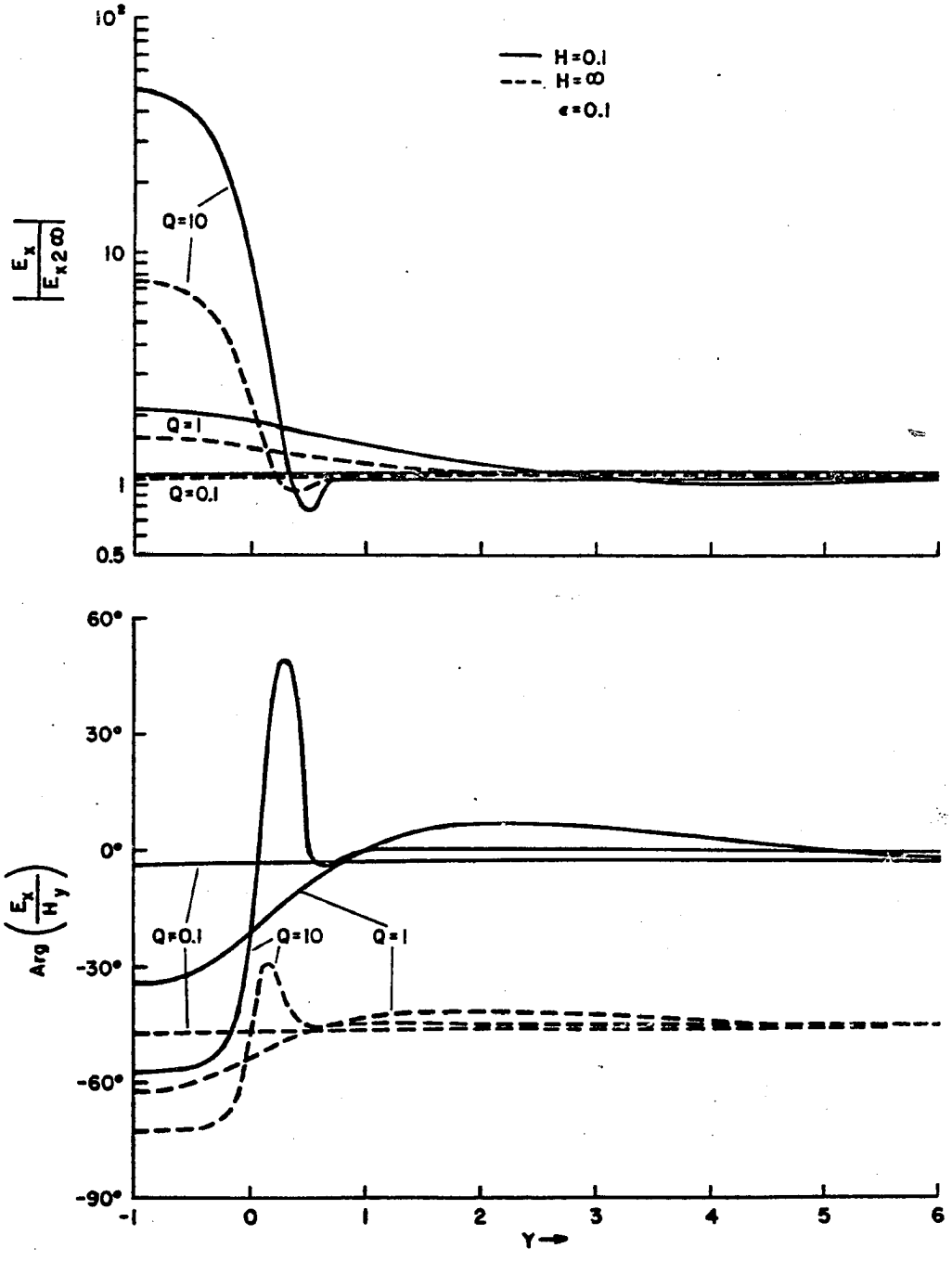

Fig. 5.9 (a) The parallel electric field near a dyke of finite depth (H - 0.1) and of infinite depth (H = ∞) for ε = 0.1 and various widths Q

$$|E_x/E_{x2\infty}| \quad ; \quad \text{Arg } (E_x/H_y)$$

Parameters, ε, Q, H, Y are defined in Table 3.3.

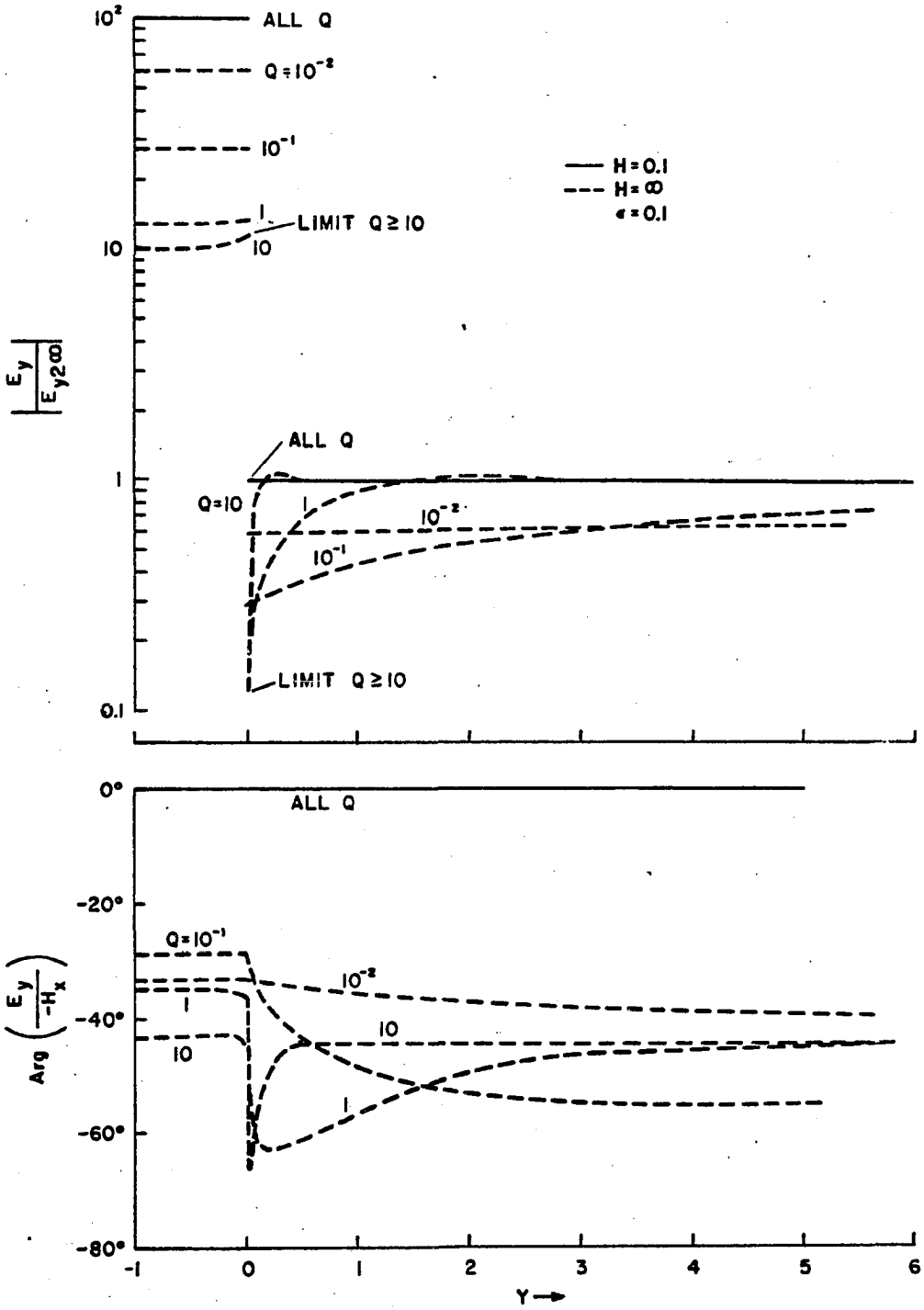

Fig. 5.9 (b) The normal electric field near a dyke of finite depth (H = 0.1) and infinite depth (H = ∞) for ε = 0.1 and various widths Q

$$|E_y/E_{y2\infty}| \quad , \quad \text{Arg } (E_y/-H_x)$$

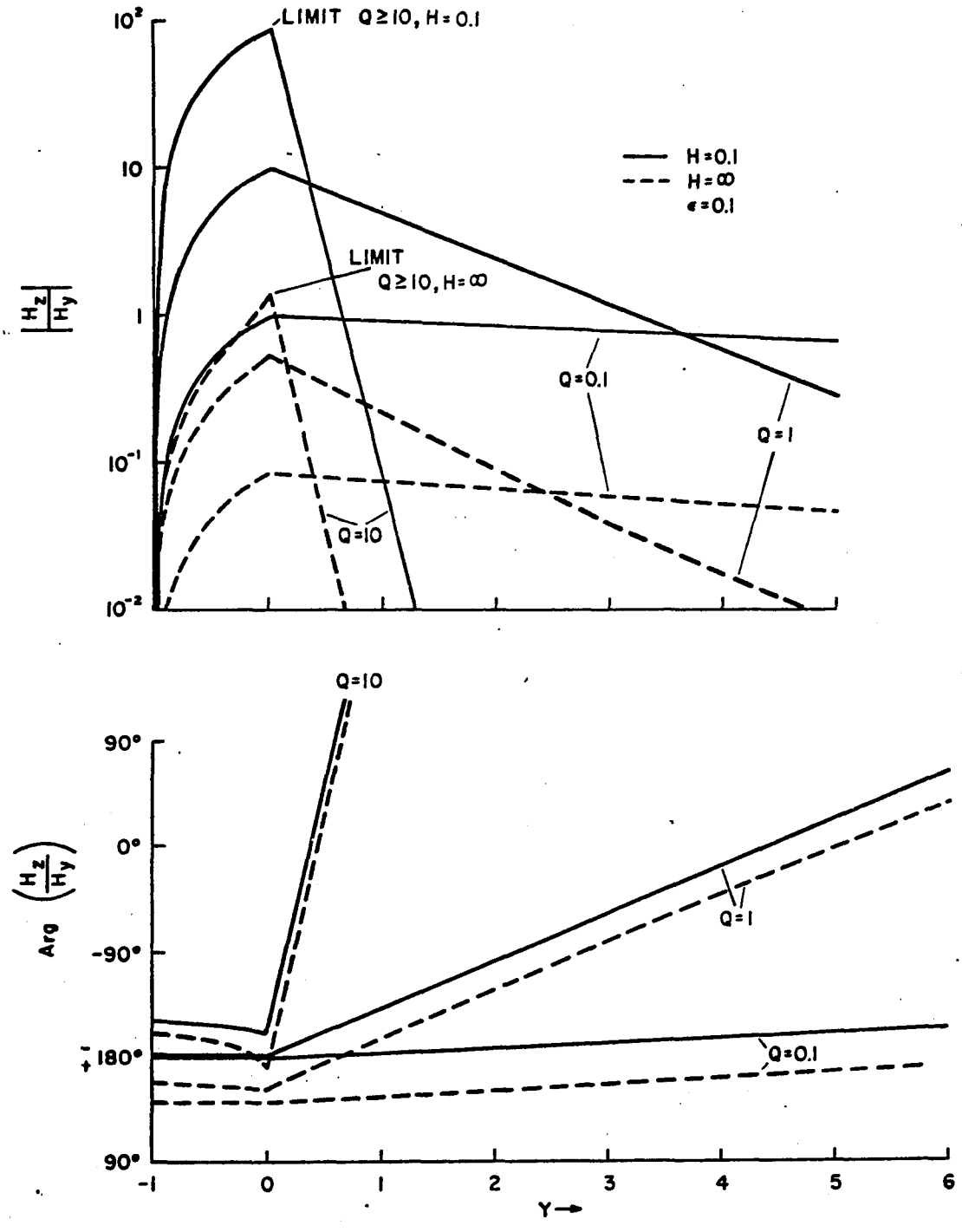

Fig. 5.9 (c) The vertical magnetic field near a dyke of finite depth (H = 0.1) and infinite depth (H = ∞) for ε = 0.1 and various widths Q

H_z/H_y

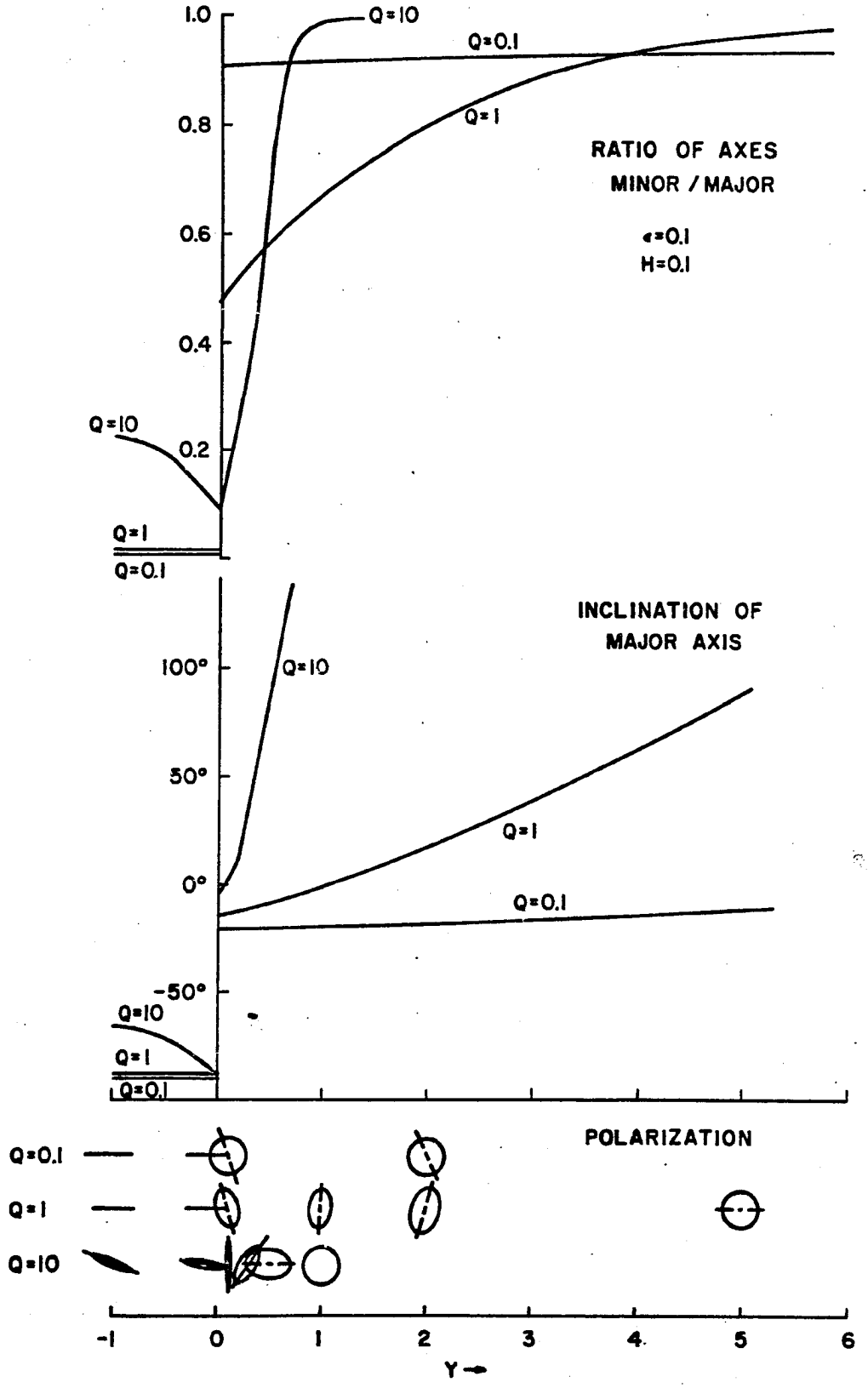

Fig. 5.10 The polarization of the surface electric fields near a dyke of finite depth (H = 0.1) for different widths Q. A left circularly polarized, surface magnetic field is assumed.

5.3.2 The Horizontal Electric Field (Figs. 5.9 a,b, 5.10)

The presence of the basement increases the magnitude of all the electric fields near the shoreline, in both land and sea media, irrespective of the value of Q (ie. independent of the "width" of the dyke, expressed in penetration depths). For the very shallow depths discussed here, the normal E_y field does not vary with distance from the shoreline, just as we found in treating a fault geometry. At great depths, however, there is a variation of the E_y-field with distance, as can been seen from the curves for $H = \infty$.

The phase of the E_y-field is likewise unaffected by the dyke at very shallow depths: there is no change with distance no matter what the dyke thickness. At greater depths however ($H = \infty$ curves) this is no longer the case and the effect of the dyke width is clearly evident. The transition between these cases was mentioned in §5.2.3c.

The influence of the non-conducting basement on the electric field is, therefore, to increase the magnitude, but for the E_y-field, the effect of the discontinuity is suppressed. The influence of the dyke on the phase is also suppressed by the basement; for the E_y-field there may be no phase variation with distance, at very shallow depths.

The polarization characteristics for the electric field are shown in Fig. 5.10 for $\epsilon = 0.1$, $Q = 0.1, 1.0, 10$, for $H = 0.1$. To avoid confusion we have not included the curves for $H = \infty$--see Fig. 5.5. Several of the polarization ellipses in each case are also drawn. It is evident from a comparison of Figs. 5.5 and 5.10

that the non-conducting basement affects the polarization differently at different frequencies. When the electromagnetic wave "sees" a thin dyke (Q = 0.1 curve) the presence of the basement reduces the linearity of the oceanic polarization from that occurring near a very deep dyke, but has little influence on the polarization over the land. On the other hand, when the dyke appears relatively thick, the basement affects the polarization in the same way as for a fault (Fig. 4.4, and §4.3.2) - the linearity over both land and sea is increased, and the land ellipses are polarized more strongly in a direction normal to the coastline.

The frequency response for the electric field under the general conditions of Fig. 5.9, is not given here for the reasons described in the previous subsection. We refer to the next section for a specific example.

5.4 Application to Specific Examples

In §§4.3, 5.1.5, 5.3 the results of the computations for the different geometries of fault and dyke were presented in a general form. We now apply these results to a particular example, by constructing the frequency response curves for each of the field components E_x, E_y, H_z. We take the following values of the parameters:

$\sigma_2 = 3$ mho. m^{-1}

$\mu_o = 4\pi\ 10^{-7}$ henry. m^{-1}

$\frac{1}{2}\ell = 1$ km

$h = 100$ m and ∞

$\epsilon = \sqrt{\sigma_1/\sigma_2} = 0.1$

We assume four observation stations, at distances 100 m and 1 km inland and seawards from the discontinuity plane. Then, for the dyke geometry Y = ±0.1 and ±1 respectively, and if the frequency f is measured in cps:

$$\eta_2^2 = \mu_o \omega \sigma_2 = 2.37 \times 10^{-5} f \qquad (m^{-2})$$

The frequency responses of each component at each of the observation points are shown in Figs. 5.11 a,b,c, for a fault and dyke of either infinite depth or 100 m depth.

The overall effect of the dyke on the frequency response of each component, when compared with the response of the fault-like coastline, may be summarized as follows. The tangential electric field $|E_x|$ and vertical magnetic field $|H_z|$ are both reduced in magnitude, while the normal E_y field is increased. The phases of the E_x and H_z fields are increased negatively, while that of the E_y field is increased positively near a dyke of great depth. However, the E_y phase does not change greatly from its "fault" behavior, when the non-conducting basement is at a shallow depth.

If we consider instead the change in the frequency response caused by the presence of a non-conducting basement, we see that all of the field components are enhanced, at least at low frequencies. There may be some reversal of this behavior at higher frequencies. The phases are all increased positively by the presence of the basement.

The behavior of the fields at higher frequencies is also governed by the limits and their practical approximations, described in §§4.1.3, 4.2.3, 5.1.3, and 5.2.3. Here we found that, if

$$f >> 4.10^6/(\tfrac{1}{2}\ell)^2 = 4 \text{ cps}$$

the dyke geometry becomes indistinguishable from the fault geometry. The effect of the basement on the frequency response becomes negligible when

$$f >> 4.10^6/h^2 = 400 \text{ cps}$$

This trend can be seen in the figure; however at these high frequencies the conditions imposed in (3.2) and (3.17) are likely to break down.

In the presence of a fault of either finite or infinite depth, the frequency responses approach those of the asymptotic, layered or uniform media, the conditions

$$f >> 4.10^7/y_1^2 \quad \text{or} \quad 4.10^5/y_2^2$$

must hold in the relevant media. This behavior can also be seen in Figs. 5.11a-c.

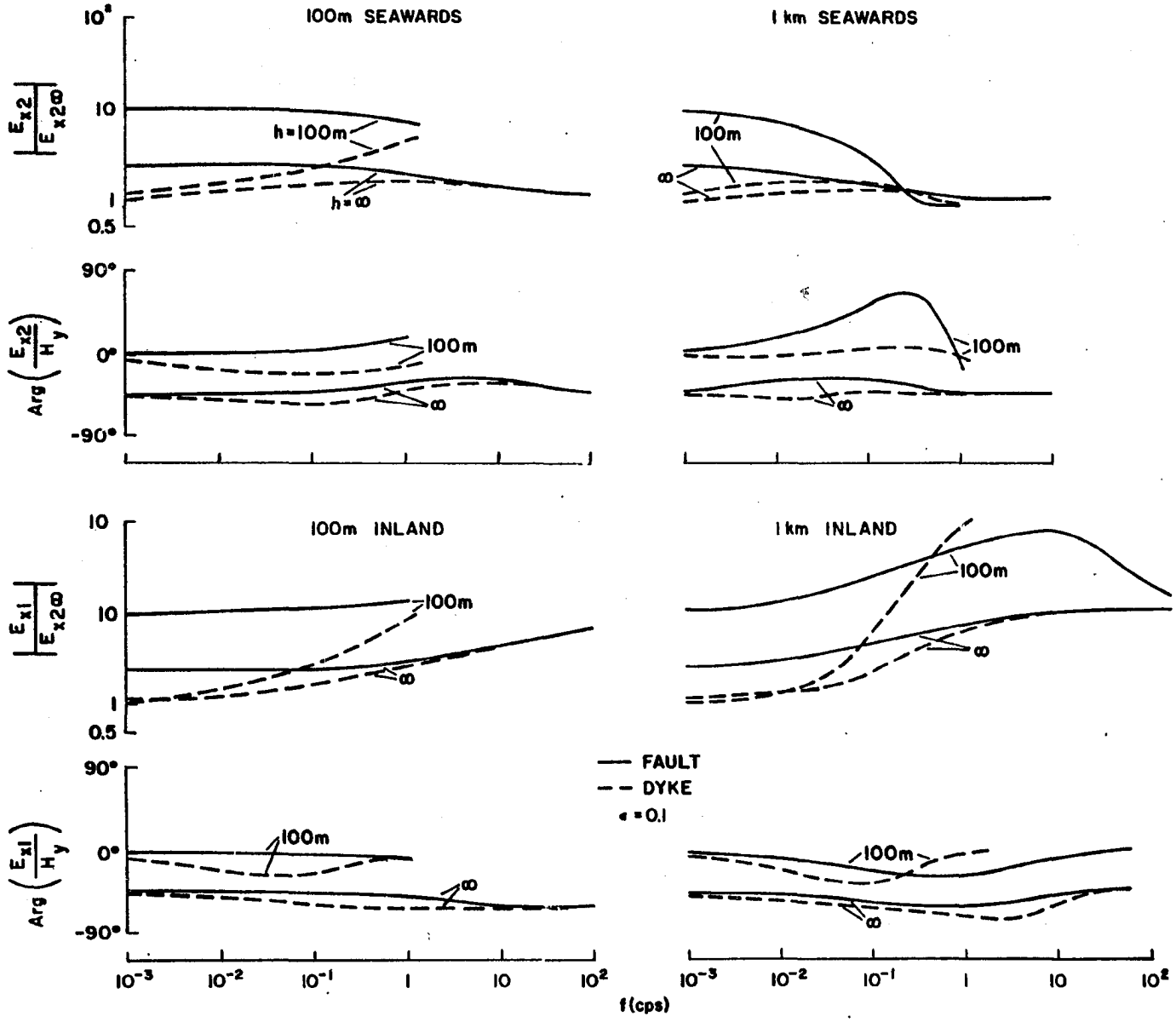

Fig. 5.11 (a) The frequency response of the tangential electric fields E_x for the examples in the text. h = basement depth

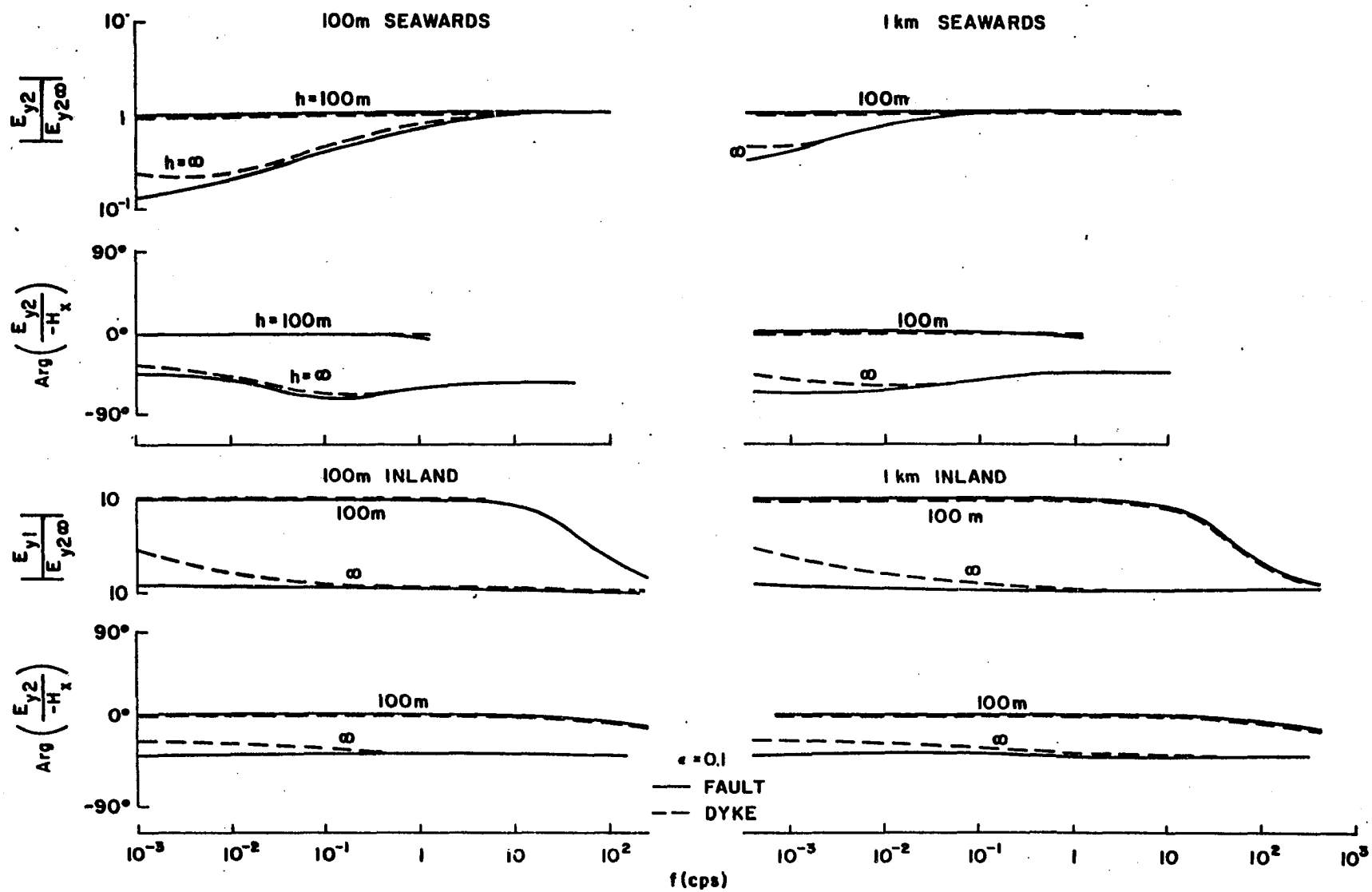

Fig. 5.11 (b) The frequency response of the normal electric fields E_y for the examples in the text.

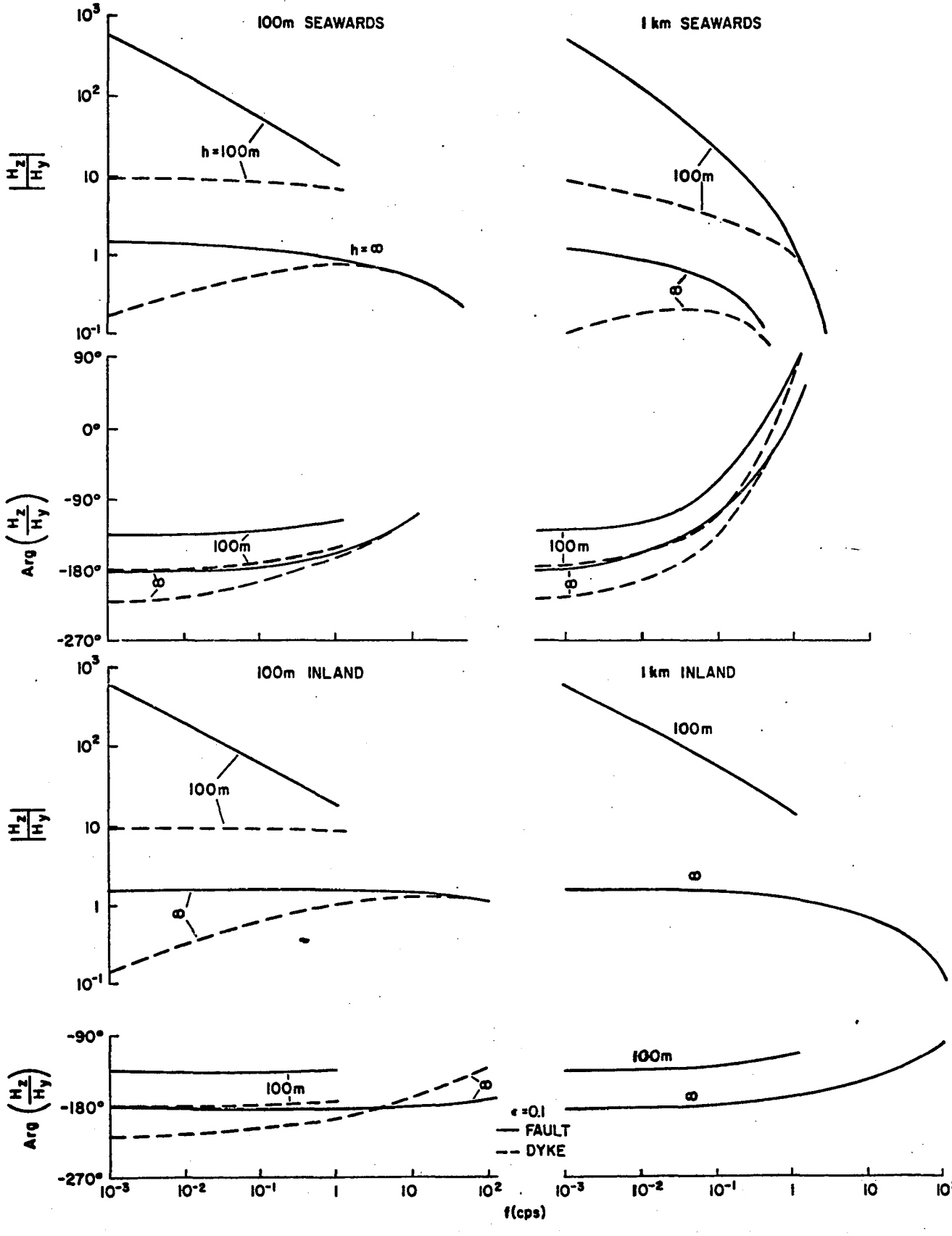

Fig. 5.11 (c) The frequency response of the vertical magnetic fields H_z for the examples in the text.

CHAPTER VI

AN OCEAN WITH A SHELVING FLOOR - AN INCLINED FAULT

In the previous chapters we have dealt with coastlines with such steep profiles that they may be considered vertical. This is an idealization of the conditions prevailing at most coastlines, as is the approximation of the ocean floor to horizontal. A more realistic situation would be the geometry of an inclined fault. Unfortunately, however, such a geometry causes mathematical difficulties, and an exact treatment has not so far been devised. Even if an analytical solution were possible, the treatment of Neves (1957)--see §6.1.2--indicates that its complexity would make such a solution computationally intractable.

6.1 A Review of the Problem

In §3.4.6 a brief description was given of the attempts which have been made to obtain solutions with this geometry. In this section we describe in more detail the solutions of Neves (1957) and Berdichevskii (1961). We first point out the mathematical difficulties.

6.1.1 The Mathematical Difficulties

In §3.1.7 we pointed out that, in the absence of vertical electric fields near the surface, the surface magnetic field over a two-layered structure is independent of the underground conductivity, at least to first order. Following Weaver (1963a), a boundary condition at the earth's surface was then established (Table 3.2). This useful condition may break down for a geometry involving a sloping basement, since a

vertical electric field may occur. Vertical electric currents have certainly been observed under such situations (§2.6.1). A boundary condition such as is used in Table 3.2 could only lead to a solution which is suspect at least near the shoreline.

A second difficulty arises if an attempt is made to solve the Helmholtz equation (3.3) in cylindrical coordinates r, θ, z (z taken to be horizontal parallel to the strike, so that the "wedge" of ocean is bounded by the planes $\theta = 0, \alpha$). A solution obtained by a separation of variables, or by transform technique, will involve combinations of trigonometric functions with Bessel or Hankel functions of argument (ηr), where $\eta^2 = \mu_o \omega \sigma$. Any attempt to match boundary conditions at the inclined interface $\theta = \alpha$ immediately breaks down because of the different arguments $(\eta_j r)$ in each medium. Such a technique therefore cannot be employed.

6.1.2 The Solution by Neves (1957)

Neves has attempted to circumvent the second difficulty described above. He treated the two cases of magnetic and electric polarization (see §3.4.2) and assumed that in the case of magnetic polarization, the surface magnetic field remained constant across the fault, a condition already pointed out as erroneous. In the case of electric polarization, he considered the tangential electric field at the surface to remain constant. While this assumption is true in the zero frequency limit, it cannot hold in the wave case, since at great distances from the shoreline the electric field will behave as in a uniform medium, so that E_t is proportional to $\sigma^{-\frac{1}{2}}$. At the interface,

however, E_t must be continuous, so that E_t certainly cannot remain constant. Neves' solution for the E-polarization is thus incorrect, although his solution for the case of H-polarization is probably valid at some distance from the shore. His solutions are outlined below.

To avoid a confusion of nomenclature we adopt Neves' notation u to represent the magnetic or electric fields in question. Fig. 6.1a shows his coordinate system in which the horizontal magnetic field is H_z (though elsewhere in this work, including later in this chapter, H_z denotes the vertical magnetic field); we have interchanged Neves' media 1 and 2 to be consistent with our specification that medium 2 represents the ocean and medium 1, the land.

Neves overcame the difficulty of boundary matching by using a Green's function representation of the wedge-space solution u, following Dougall (1899). He then matched integrals rather than integrands, the integrals being taken over the order of the Bessel functions to allow for the inclined layer. The solutions then have the form

$$u_j(r,\theta) = \frac{1}{\pi^2} \int_0^\infty K_{is}(\gamma_j r) \; [A_j(s) \cosh s\theta + B_j(s) \sinh s\theta] \, ds \qquad (6.1)$$

where

$$\gamma_j = \sqrt{i}\, \eta_j = \sqrt{i\mu_o \omega \sigma_j} \quad ,$$

subject to the boundary conditions

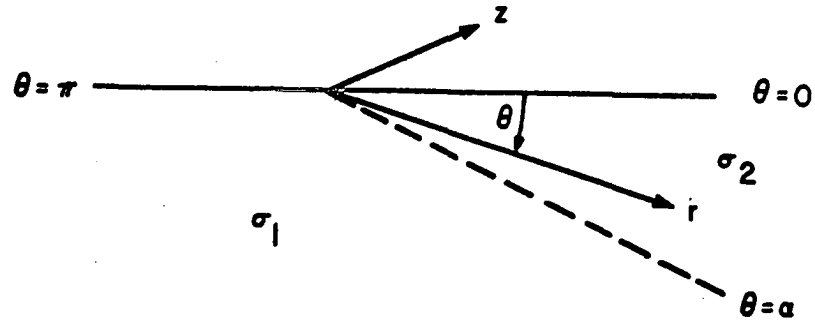

(a)

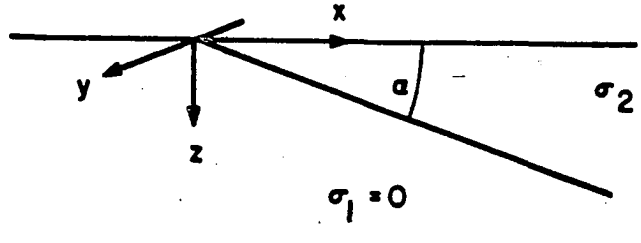

(b)

Fig. 6.1 (a) Neves' (1957) coordinate system and nomenclature.
(b) Berdichevskii's (1961) coordinate system and nomenclature.

$$\left.\begin{aligned} u &= u_o = \text{constant at } \theta = 0, \pi \\ u_1 &= u_2 \\ \frac{1}{\eta_1^2}\frac{\partial u_1}{\partial \theta} &= \frac{1}{\eta_2^2}\frac{\partial u_2}{\partial \theta} \end{aligned}\right\} \text{ at } \theta = \alpha \qquad (6.2)$$

In the expression for u_j, the term $K_{is}(\gamma_j r)$ represents a modified Bessel function of the first kind of imaginary order "is" and complex argument $(\gamma_j r)$.

He treated two cases. First the land was considered to be infinitely resistive, so that $u = o$ at $\theta = \alpha$ and $u = u_o$ at $\theta = o$. Relation (6.1) now gives two simultaneous singular integral equations from which the coefficients A(s) and B(s) must be determined. Neves did this by using the Kantorovich-Lebedev transform pair. (Lebedev, 1946; Erdélyi et al., 1954, T.1.T. 2)

$$F(s) = \int_o^\infty f(x)\, K_{is}(x)\, dx$$

$$x\, f(x) = \frac{2}{\pi^2} \int_o^\infty K_{is}(x)\, s \sinh s\pi\, F(s)\, ds \qquad (6.3)$$

where in this case

$$x = \gamma r; \quad f(x) = u_o/\gamma r \quad ; \quad F(s) = A(s)/2s \sinh s\pi$$

Using Hankel transform integrals and one of the Ramanujan integrals, the solution for the horizontal magnetic field u reduced to

$$u(r,\theta) = u_o\, e^{\gamma r \sin\theta} - \frac{2}{\pi}\int_0^\infty K_{is}(\gamma r)\,\frac{\cosh(\frac{1}{2}\pi-\alpha)s}{\sinh s\alpha}\,\sinh s\theta\, ds \qquad (6.4)$$

Neves also treated the case where the two media are conducting (neither of them infinitely), but applied his analysis to the electric field, with the incorrect boundary condition mentioned above. The analysis for the case of the magnetic field would be quite similar in principle. In the case he treated, the last of the boundary conditions (6.2) becomes

$$\frac{\partial u_1}{\partial \theta} = \frac{\partial u_2}{\partial \theta}$$

where now Neves used u to represent the surface electric field.

The application of the boundary conditions to the two solutions of the form (6.1) yields a system of four simultaneous integral equations for the determination of the four coefficients $A_j(s)$, $B_j(s)$ $(j = 1,2)$. These may be solved by an involved application of the Kantorovich-Lebedev transform pair (6.3). The solutions are:

$$u_1(r,\theta) = \frac{1}{\pi^2}\int_0^\infty K_{is}(\gamma_1 r)\left\{\frac{2}{\pi^2}[\cosh s\theta - \coth s\pi \sinh s\theta]\,\frac{s\sinh s\pi}{h(s)}\int_0^\infty \frac{L(s,\gamma_1,\gamma_2,r)}{r}\,K_{is}(\gamma_1 r)\,dr + u_o\pi\,\frac{\cosh s\pi/2}{\sinh s\pi}\,\sinh s\theta\right\} ds$$

$$u_2(r,\theta) = \frac{1}{\pi^2}\int_0^\infty K_{is}(\gamma_2 r)\left\{u_o\pi\cosh s\pi/2\cosh s\theta + \frac{2}{\pi^2}\,\frac{s\sinh s\theta\sinh s\pi}{h^*(s)}\int_0^\infty \frac{L^*(s,\gamma_1,\gamma_2,r)}{r}\,K_{is}(\gamma_2 r)\,dr\right\} ds \qquad (6.5)$$

where

$$h^*(s) = s \cosh s\alpha \; g(s) - s \; f(s) \sinh s\alpha$$

$$L^*(s,\gamma_1,\gamma_2,r) = s \; f(s) \; W(\gamma_1,\gamma_2,r) - g(s) \; V(\gamma_1,\gamma_2,r)$$

$$h(s) = s \cosh s\alpha \; g(s) \; - s \sinh s\alpha \; f(s)$$

$$L(s) = s \cosh s\alpha \; W(\gamma_1,\gamma_2,r) - \sinh s\alpha \; V(\gamma_1,\gamma_2,r)$$

$$g(s) = \cosh s\alpha - \coth s\pi \sinh s\alpha$$

$$f(s) = \sinh s\alpha - \coth s\pi \cosh s\alpha$$

$$W(\gamma_1,\gamma_2,r) = u_o\pi \int_0^\infty \left\{ K_{is}(\gamma_2 r) \cosh s\alpha - K_{is}(\gamma_1 r) \frac{\sinh s\alpha}{\sinh s\pi} \right\} \cosh s\pi/2 \; ds$$

$$V(\gamma_1,\gamma_2,r) = u_o\pi \int_0^\infty \left\{ K_{is}(\gamma_2 r) \sinh s\alpha - K_{is}(\gamma_1 r) \frac{\cosh s\alpha}{\sinh s\pi} \right\} s \cosh s\pi/2 \; ds$$

The solutions for the surface fields, either electric or magnetic, are thus extremely involved, and even in the case of an infinite conductivity ratio, (eq. 6.4), the numerical evaluation would be very impracticable. Neves himself did not attempt this, but solved the differential equations using a finite difference technique. However, as pointed out in §3.4.6, he again used the suspect boundary conditions on the surface fields.

6.1.3 Berdichevskii's (1961) Solution

Berdichevskii approached the problem of the sloping basement rather differently. He avoided the influence of the actual land-sea boundary and considered the observation point to be well out to sea

over an inclined sea floor*--thus the problem is not the effect of a coastline, but the influence of a sloping sea bottom. His nomenclature is given in Fig. 6.1(b), except that we have interchanged his labels for media 1 and 2 to be consistent with ours. The land conductivity is taken as zero.

Both the static and wave cases were treated. In the former case the electric fields are the same as those of an equivalent line electrode along the y-axis, carrying a total current of I. Then at any point in the conducting medium 2, the electric fields are:

$$\left.\begin{aligned} E_x &= \frac{I}{\alpha\sigma_2}\,\frac{x}{x^2+z^2} \\ E_y &= \text{constant} \end{aligned}\right\} \qquad (6.6)$$

The electric field potential is

$$U = -\frac{I}{\alpha\sigma_2}\cdot\ln\sqrt{x^2+y^2}$$

To determine the fields in the wave case, Berdichevskii assumed a plane wave to be incident normally on the horizontal upper surface. It would undergo successive reflections at each interface bounding the conducting medium 2, and absorption of the wave would occur in the conductor. He treated two cases, where the electric vector of the primary incident wave was polarized either in the plane of incidence ("parallel") or normal to it ("normal"). These two cases are equivalent to our magnetic and electric polarizations respectively.

*A similar analysis for a dipole source has recently been carried out by Schlak and Wait (1967).

The secondary fields, resulting from the reflections, are calculated by a technique which Berdichevskii calls the "method of images,"* for the cases where the angle of dip α is an integral factor of $\pi/4$, i.e. $\alpha = \pi/4N$, where $N = 1,2,3,\ldots$. This condition ensures that the final reflection always occurs from the surface of the basement, in a horizontal direction.

If the incident wave is specified by (E_o, H_o) and the propagation constant in the oceanic medium (2) is

$$k_2 = \sqrt{-i\mu_o\omega\sigma_2} = \sqrt{-i}\,\eta_2 \tag{6.7}$$

the field components at any point in medium 2 are given in Table 6.1. The non-trivial fields at the surface $z = 0$ are given in Table 6.2 (Berdichevskii's analysis employs emu, but the relations in these tables have been changed to mksu).

Evidently the parallel component of the surface magnetic field, H_y, remains constant, independent of both x and σ_2. This appears to confirm the approach of Neves (1957) in his treatment of the magnetic polarization case, but it must be remembered that Berdichevskii's solution is only valid for distances of a wavelength or more from the apex. The wave-length λ_2 in the medium is given by $\lambda_2 = 2\pi\delta_2 = 2\sqrt{2}\pi\eta_2^{-1} = 2\pi\sqrt{2/\mu_o\omega\sigma_2}$. Berdichevskii's solution does not support Neves' treatment of the E-polarization, however.

---

*Sposob izobrazhenii

Table 6.1

The Field Components Over an Inclined Fault with a Non-Conducting Substratum (Berdichevskii, 1961)

$$E_x = E_o \left\{ e^{-k_2 z} + 2 \sum_{m=1}^{N-1} e^{-k_2 x \sin 2m\alpha} \cos 2m\alpha \cosh (k_2 z \cos 2m\alpha) \right\} \quad (6.8)$$

$$E_y = E_o \left\{ e^{-k_2 z} + 2 \sum_{m=1}^{N-1} e^{-k_2 x \sin 2m\alpha} e^{-4m^2 i\alpha} \cosh(2im\alpha + k_2 z \cos 2m\alpha) \right\} \quad (6.9)$$

$$E_z = -2 E_o \sum_{m=1}^{N-1} e^{-k_2 x \sin 2m\alpha} \sin 2m\alpha \sinh(k_2 z \cos 2m\alpha) \quad (6.10)$$

$$H_x = H_o \left\{ e^{-k_2 z} - 2 \sum_{m=1}^{N-1} e^{-k_2 x \sin 2m\alpha} e^{-4im^2 \alpha} \cos 2m\alpha \sinh(2im\alpha + k_2 z \cos 2m\alpha) \right\} \quad (6.11)$$

$$H_y = H_o \left\{ e^{-k_2 z} - 2 \sum_{m=1}^{N-1} e^{-k_2 x \sin 2m\alpha} \sinh(k_2 z \cos 2m\alpha) \right\} \quad (6.12)$$

$$H_z = -2H_o \sum_{m=1}^{N-1} e^{-k_2 x \sin 2m\alpha} e^{-4im^2 \alpha} \sin 2m\alpha \cosh(2im\alpha + k_2 z \cos 2m\alpha) \quad (6.13)$$

$$E_o = \sqrt{\frac{\mu_o \omega}{i\sigma_2}} H_o$$

Table 6.2

The Surface Fields Over an Inclined Fault with a Non-Conducting Substratum (Berdichevskii, 1961)

$$\frac{E_x}{|E_\infty|} = \sqrt{i}\left\{1 + 2\sum_{m=1}^{N-1} e^{-k_2 x \sin 2m\alpha} \cos 2m\alpha\right\} \tag{6.14}$$

$$\frac{E_y}{|E_\infty|} = \sqrt{i}\left\{1+2\sum_{m=1}^{N-1} e^{-k_2 x \sin 2m\alpha}\, e^{-4im^2\alpha} \cos 2m\alpha\right\} \tag{6.15}$$

$$\frac{H_x}{H_o} = 1 + 2\sum_{m=1}^{N-1} e^{-k_2 x \sin 2m\alpha}\, e^{-i(4m^2\alpha + \pi/2)} \sin 4m\alpha \tag{6.16}$$

$$\frac{H_z}{H_o} = \sum_{m=1}^{N-1} e^{-k_2 x \sin 2m\alpha}\, e^{-i(4m^2\alpha + \pi)} \sin 4m\alpha \tag{6.17}$$

It should be noted that at great distances from the shoreline, the fields of Tables 6.1 and 6.2 approach those for a uniform medium. The magnitudes of the electric fields have been normalized to unity at these distances, but the phase is retained at -45°.

6.2 The Inclined Fault Separating Two Conducting Media

In this section we extend Berdichevskii's (1961) solution by taking the substratum to be conducting; we also remove his restriction on the angle α.

6.2.1 Reflection of Electromagnetic Waves at an Interface Between Two Conducting Media

Figure 6.2(a) represents a plane electromagnetic wave in a medium (2) of conductivity σ_2, incident at angle θ_i on an interface with a second medium (1), of conductivity σ_1. The wave will undergo reflection and refraction at the interface. The following discussion is based on Stratton (1941, Ch. 9). The propagation constants k_j in each medium are given by (3.5):

$$k_j^2 = \mu_o \varepsilon_j \omega^2 + i\mu_o \omega \sigma_j$$

Under the low frequency or "good conductor" approximation (3.2)

$$\omega << \sigma_j/\varepsilon ,$$

the propagation constant is

$$k_j^2 = i\mu_o \omega \sigma_j = i\eta_j^2 \qquad (6.18)$$

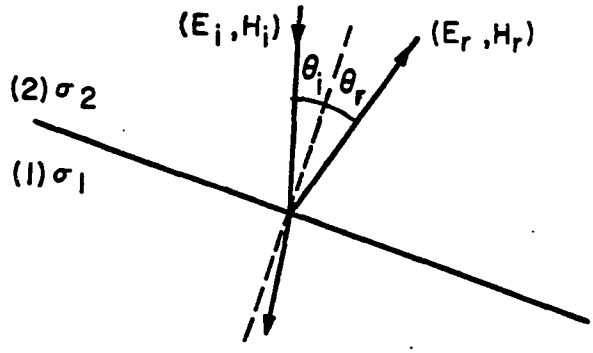

(a)

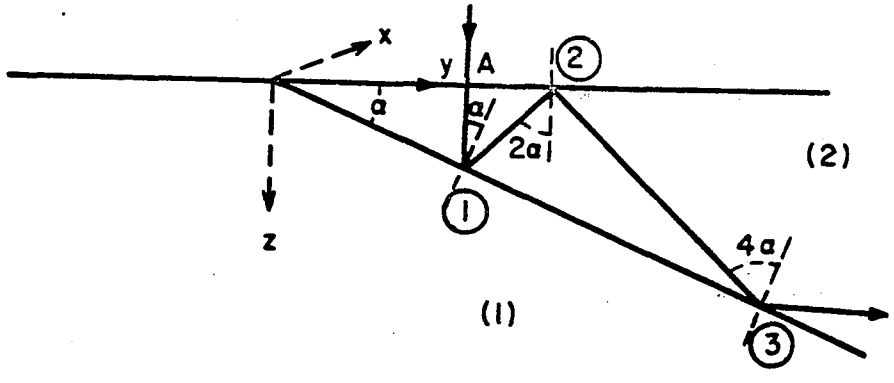

(b)

Fig. 6.2 (a) Reflection at a conductor-conductor interface.
(b) A model of an inclined fault. The circled numbers represent the reflection numbers.

We define the "plane of incidence" as the plane containing the incident and reflected waves. Let the incident wave in medium 2 be designated by the field vectors ($\underset{\sim}{E}_i$, $\underset{\sim}{H}_i$) and the reflected wave by ($\underset{\sim}{E}_r$, $\underset{\sim}{H}_r$). Two cases may then be considered (Stratton, 1941).

(a) $\underset{\sim}{E}_i$ is parallel to the plane of incidence: (H-polarization)

Under this condition it is known that

$$\underset{\sim}{H}_r = D_H \underset{\sim}{H}_i \tag{6.19}$$

where the reflection coefficient D_H is given by

$$D_H = \frac{k_1^2 \cos\theta_i - k_2 \sqrt{k_1^2 - k_2^2 \sin^2\theta_i}}{k_1^2 \cos\theta_i + k_2 \sqrt{k_1^2 - k_2^2 \sin^2\theta_i}} \tag{6.20}$$

Since

$$\varepsilon^2 = \frac{\sigma_1}{\sigma_2} = \frac{k_1}{k_2}$$

we may write the reflection coefficient (6.20) as

$$D_H = -1 + \frac{2}{1+\nu'_H} \tag{6.21}$$

where

$$\nu'_H = \frac{\sqrt{\varepsilon^4 - \sin^2\theta_i}}{\varepsilon^2 \cos\theta_i} \tag{6.22}$$

If medium 1 represents the land and medium 2 the sea, $\varepsilon < 1$ always. We must therefore consider two conditions in (6.22):

(i) $\varepsilon^2 \geq \sin\theta_i$: ν'_H is real.

(ii) $\varepsilon^2 < \sin\theta_i$: ν'_H is purely imaginary.

When ν_H' is purely imaginary we may write

$$\nu_H' = i\nu_H$$

Eq. (6.21) becomes

$$D_H = -1 + \frac{2}{1+\nu_H^2} - i\,\frac{2\nu_H}{1+\nu_H^2} \tag{6.23}$$

In the case shown in Fig. 6.2(b), where the interface is inclined at angle α to the horizontal surface, these conditions mean that if $\alpha \geq \arcsin \varepsilon^2$, case (ii) will apply to all further reflections as well as the first. If however $\alpha < \arcsin \varepsilon^2$, case (i) will apply to at least the first reflection. As the effective "θ_i" increases after each reflection, the criterion for case (i) will eventually break down and case (ii) will apply.

(b) $\underset{\sim}{E}_i$ is normal to the plane of incidence: (E-polarization)

We have

$$\underset{\sim}{E}_r = D_E\ \underset{\sim}{E}_i \tag{6.24}$$

with the reflection coefficient D_E given by

$$D_E = \frac{k_2 \cos\theta_i - \sqrt{k_1^2 - k_2^2 \sin^2\theta_i}}{k_2 \cos\theta_i + \sqrt{k_1^2 - k_2^2 \sin^2\theta_i}} \tag{6.25}$$

Writing

$$\nu_E = \varepsilon^2/\sin\theta_i\ , \tag{6.26}$$

relation (6.25) may be written in two forms:

(i) $\varepsilon^2 \leq \sin\theta_i$, so that $\nu_E \leq 1$.

Then $$D_E = e^{-2i\phi} \tag{6.27}$$

where $$\tan\phi = \sqrt{1 - \nu_E^2}\ \tan\theta_i \tag{6.28}$$

ϕ is in the first quadrant since θ_i is, and $\varepsilon^2 \leq \sin\theta_i$.

(ii) $\varepsilon^2 > \sin\theta_i$, so $\nu_E > 1$

Therefore

$$D_E = -1 + \frac{2}{1+\sqrt{\nu_E^2-1}\ \tan\theta_i} \tag{6.29}$$

The second case will apply to at least the first reflection if $\alpha < \arcsin \varepsilon^2$, but case (i) will eventually become valid as the successive "θ_i" increase. Case (i) is valid for all reflections if $\alpha \geq \arcsin \varepsilon^2$.

Reflections occurring at the surface of medium 2 have much simpler reflection coefficients, since the propagation constant in air is zero for the frequencies satisfying (3.17). The coefficients become

$$\begin{aligned} D_H &= -1 \\ D_E &= e^{-2i\theta_i} \end{aligned} \tag{6.30}$$

In addition to the reflections which occur at the boundaries of medium 2, the wave will also be attenuated as it travels through the

conducting medium. With the propagation constant (6.18), the wave has the form*

$$\underset{\sim}{E} = \underset{\sim}{E}_o \; e^{i\underset{\sim}{k}\cdot\underset{\sim}{r}} \; e^{-i\omega t}$$

$$\underset{\sim}{H} = \underset{\sim}{H}_o \; e^{i\underset{\sim}{k}\cdot\underset{\sim}{r}} \; e^{-i\omega t} \qquad (6.31)$$

The ik term is actually $(-1+i)\eta^{-1}/\sqrt{2}$, the first term representing the absorption modulus. For convenience we will define

$$\kappa = \eta^{-1}/\sqrt{2} = \sqrt{\mu_o \omega\sigma/2} = \delta^{-1} \qquad (6.32)$$

where δ is the skin-depth (3.8)

For convenience, in the following discussion we omit the time-dependent factor $e^{-i\omega t}$.

6.2.2 Application to an Inclined Fault Separating Conducting Media

Consider a plane wave incident normally on the surface, as in Fig. 6.2(b). The odd reflections occur at the conductor-conductor interface, whilst the even reflections are at the surface z=0. Eventually the reflected wave will leave one of the interfaces at such an angle that no further reflections will occur. There are two possible conditions:

(i) The last reflection occurs at the surface.

This situation will occur when the wave is incident at the reflection point with an angle of incidence $\theta_i \geq (\pi/2) - \alpha$. But since $\theta_i = 2n\alpha$ where 2n is the reflection number ($n = 1,2,3,....$), this is equivalent to the smallest n such that

---

*Note the difference in the definition of our propagation constant k, from Berdichevskii's. Berdichevskii (1961) adopts our (-ik) as his wave number k. Our $e^{i\underset{\sim}{k}\cdot\underset{\sim}{r}}$ is his $e^{-\underset{\sim}{k}\cdot\underset{\sim}{r}}$.

$$n \geq \frac{\pi}{4\alpha} - 1/2 \tag{6.33}$$

(ii) The last reflection occurs at the basement.

Then the wave reflected after the (2n-1)-th reflection must leave at an angle $\theta_r \geq (\pi/2) - \alpha$. Since $\theta_r = (2n-1)\alpha$, this means n is the smallest number such that:

$$n \geq \pi/4\alpha \tag{6.34}$$

If we use [a] to mean the nearest integer < a, and let m be the reflection number of the last reflection, then

$$m = \left[\frac{\pi}{2\alpha}\right] \tag{6.35}$$

The last reflection is from the upper surface if m is even, and the lower surface if m is odd. If $\pi/2\alpha$ is an integer the last reflection is the $(\frac{\pi}{2\alpha} - 1)$-th and the reflected wave is parallel to the opposite interface.

Because the electromagnetic wave is attenuated as it traverses the conductor, we must know the total length of the ray path traveled from the point of entry. We adopt the coordinate system of Fig. 6.2(b), and we assume that the plane wave is incident normally on the horizontal surface, at the point A. It passes normally into medium 2, and is attenuated thereafter.

To calculate the ray path we employ Berdichevskii's "method of images" and refer generally to Fig. 6.4. The ray path is ABCD...., and the figure is drawn for an angle $\alpha = 10°$. Figure 6.3 explains the method. Consider first Fig. 6.3(a). For a point between A and B,

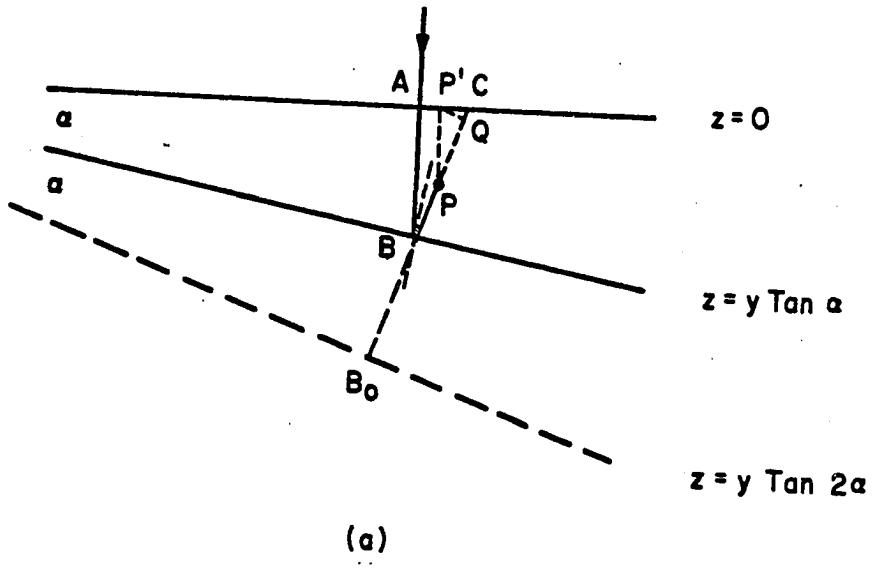

(a)

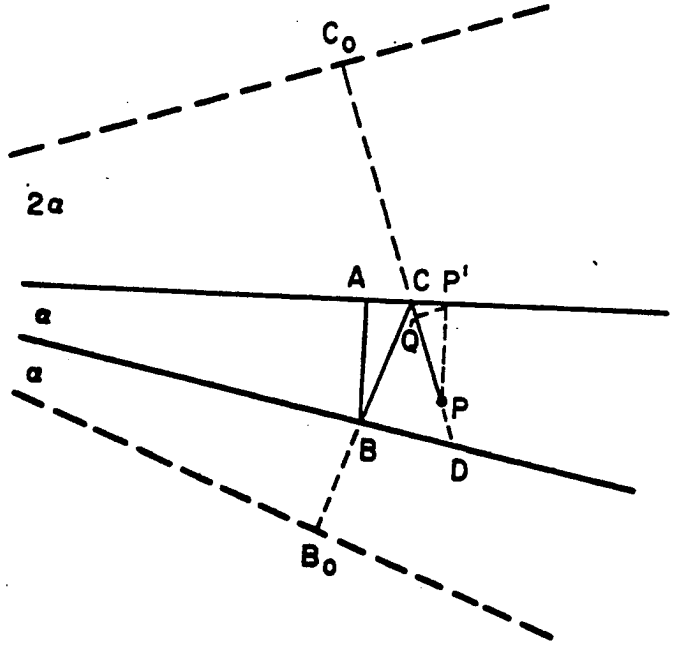

(b)

Fig. 6.3 Calculation of the path length by the "method of images".
(a) after 1st reflection
(b) after 2nd reflection

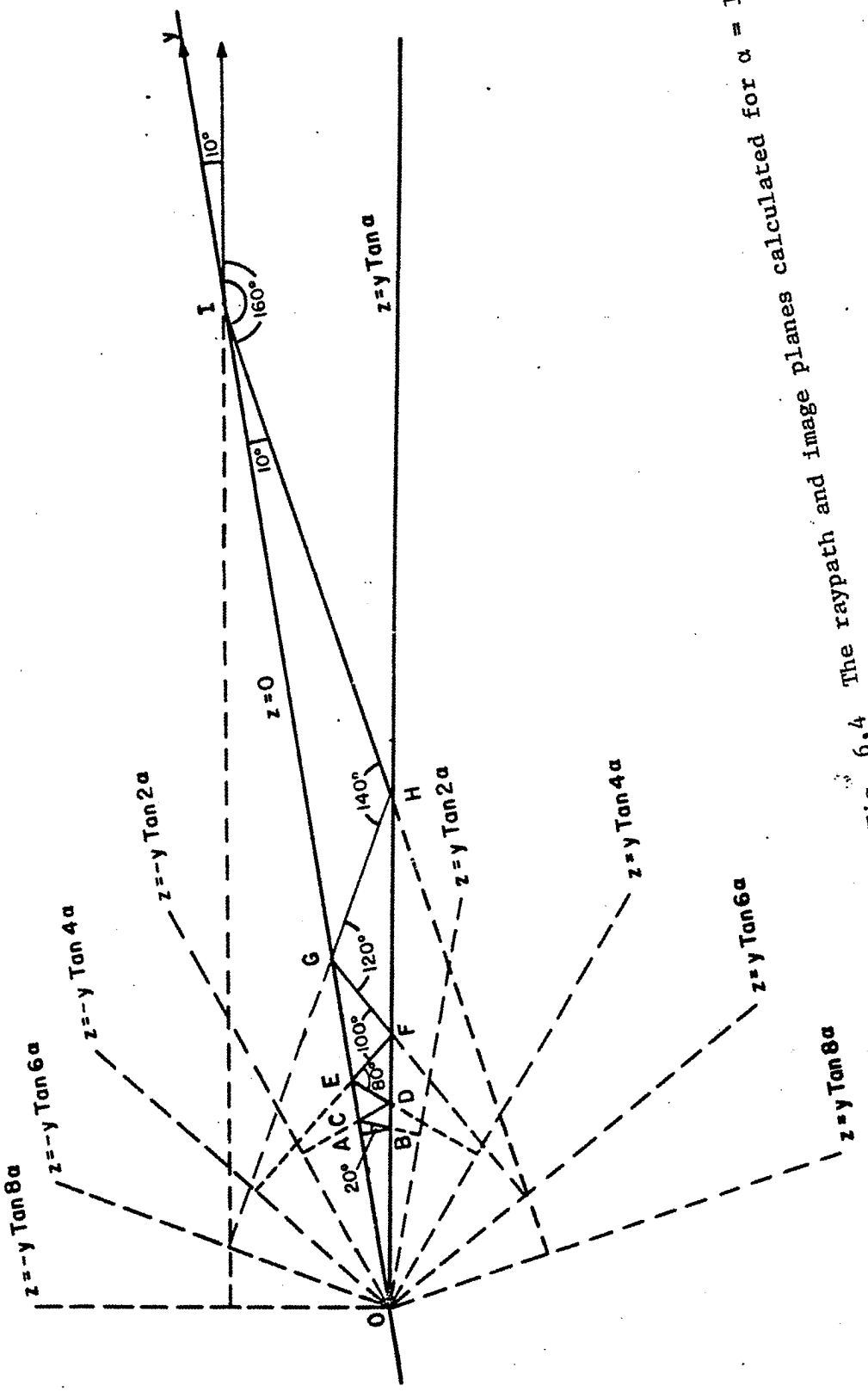

Fig. 6.4 The raypath and image planes calculated for $\alpha = 10^{o}$.

the path length is simply its coordinate z. For a point P(y,z) between B and C, the ray BP is normal to the image plane of the surface in the base interface, so that the ray path is $B_oP = B_oQ - PQ = y \sin 2\alpha - z \cos 2\alpha$.

If we specify the point P to be between C and D (Fig. 6.3b), the ray CP is normal to the image plane of the previous image plane, in the surface z=o. The total ray path is then $C_oP = C_oQ + QP = y \sin 2\alpha + z \cos 2\alpha$

In general, if P is between the (2n-1)th and 2n-th, or 2n-th and (2n+1)th, reflection points, the length of the ray path is obtained by replacing the (2α) in the above expressions by $(2n\alpha)$. The successive image planes would then be those shown in Fig. 6.4.

At any point (y,z) in medium 2, the distances traveled by the ray after m reflections are:

$$\begin{aligned} &\text{(i)} \quad m \text{ even:} \quad s = y \sin m\alpha + z \cos m\alpha \\ &\text{(ii)} \quad m \text{ odd:} \quad s = y \sin (m+1)\alpha - z \cos (m+1)\alpha \end{aligned} \tag{6.36}$$

At a given point on the surface all of the reflection modes must be taken into account in determining the total field at that point. The waves must be considered both before and after reflection. We consider an observation point within medium 2, determine the total field there due to all the reflected waves, and then take the limit to the surface. In the case where the final reflection occurs from the basement, we consider the last reflection from the surface as the last ray to be included in the summation, since the rest of the reflected ray will not reach the surface observation point again.

We take the two cases shown in Fig. 3.5 in turn.

(a) $\underset{\sim}{H}$-polarization: The $\underset{\sim}{E}$-vector is polarized in the plane of incidence

We make the following designations for the magnetic field:

(i) between the entry point (A) and the first reflection:

$$\underset{\sim}{H}_t = \underset{\sim}{H}_o e^{ik_2 z}$$

(ii) immediately prior to the m^{th} reflection: $\underset{\sim}{H}_{im}$

(iii) immediately after the m^{th} reflection: $\underset{\sim}{H}_{rm}$

Here

$$k_2 = \sqrt{i\mu_o \omega \sigma_2} = (1+i)\kappa = \sqrt{i}\,\eta_2$$

when κ is defined by (6.32) and we drop the subscript 2 without ambiguity. When m is odd, the reflection is from the base surface and from (6.19):

$$\underset{\sim}{H}_{rm} = D_{Hm}\ \underset{\sim}{H}_{im} \tag{6.37a}$$

with D_{Hm} denoting the reflection coefficient for an angle of incidence $\theta_m = m\alpha$. If m is odd, the reflection is from the surface and, since the reflection coefficient is then -1 (eq. 6.30), we have:

$$\underset{\sim}{H}_{rm} = -\underset{\sim}{H}_{im} \tag{6.37b}$$

The magnetic vector $\underset{\sim}{H}$ is always in the $-\hat{\underset{\sim}{\varepsilon}}_x$ direction so that we only need to consider the H_x component.

Then using (6.31), (6.36) and (6.37) we may write the expressions for the H-waves in each ray path interval as $H_{j-1,j}$ with

$$H_x = -\sum_{j=1}^{N} H_{j-1,j} \tag{6.38}$$

where N is the nearest integer less or equal to $(\pi/2\alpha)-1$:

$$N = \left[\frac{\pi}{2\alpha} - 1\right] \tag{6.39}$$

Then:

initial transmitted wave $\underset{\sim}{H}_t$: $H_{01} = H_0 \, e^{(-1+i)\kappa z}$

1st reflected wave: $H_{12} = D_{H1} H_0 \, e^{(-1+i)(y \sin 2\alpha - z \cos 2\alpha)\kappa}$

2nd reflected wave: $H_{23} = (-1) D_{H1} H_0 \, e^{(-1+i)(y \sin 2\alpha + z \cos 2\alpha)\kappa}$

3rd reflected wave: $H_{34} = (-1) D_{H1} D_{H3} H_0 \, e^{(-1+i)(y \sin 4\alpha - z \cos 4\alpha)\kappa}$

4th reflected wave: $H_{45} = (-1)^2 D_{H1} D_{H3} H_0 \, e^{(-1+i)(y \sin 4\alpha + z \cos 4\alpha)\kappa}$

Nth reflected wave: $H_{N\infty}$

The form of the last wave depends on whether N is even or odd.

Using (6.38) we may therefore write:

$$H_x = - H_o \, e^{(-1+i)\kappa z} - H_o \sum_{p=1}^{R} (-1)^{p+1} D_{H1} D_{H3} \cdots D_{H(2p-1)} e^{(-1+i)(y \sin 2p\alpha - z \cos 2p\alpha)\kappa} (1 - e^{2(-1+i)\kappa z \cos 2p\alpha})$$

where $R = N/2$ if N is even, $(N-1)/2$ if N is odd (6.40)

The values of the $D_{H(2p-1)}$ are given by (6.21) or (6.23), whichever is appropriate, with $\theta_i = (2p-1)\alpha$. The E_y and E_z components may be determined from (6.40) by Maxwell's equations, in the forms listed in Table (3.2). The relations for all the field components are collected in Table 6.3.

(b) E-polarization: The H vector is polarized in the plane of incidence.

We define the respective rays of the $\underset{\sim}{E}$-wave analogously to those for the $\underset{\sim}{H}$-wave above. Then when m is odd, the reflected wave is

$$\underset{\sim}{E}_{rm} = D_{Em} \underset{\sim}{E}_{im} \tag{6.41}$$

with D_{Em} denoting the reflection coefficient for an angle of incidence $\theta_m = m\alpha$. If m is even, the reflected wave is

$$\underset{\sim}{E}_{rm} = D^{o}_{Em} \underset{\sim}{E}_{im} \tag{6.42}$$

where the electric reflection coefficient is given by (6.30):

$$D^{o}_{Em} = e^{-2i\theta_m} \tag{6.43}$$

Since $\underset{\sim}{E}$ is always in the $+\hat{\underset{\sim}{\varepsilon}}_x$ direction we consider only the E_x component. It may be written

$$E_x = \sum_{j=1}^{N} E_{j-1,j} \tag{6.44}$$

where N is defined by (6.39) and

initial transmitted wave $\underset{\sim}{E}_t$: $E_{01} = E_0 e^{(-1+i)\kappa z}$

1st reflected wave: $E_{12} = D_{E1} E_0 e^{(-1+i)(y \sin 2\alpha - z \cos 2\alpha)\kappa}$

2nd reflected wave: $E_{23} = D^{o}_{E2} D_{E1} E_0 e^{(-1+i)(y \sin 2\alpha + z \cos 2\alpha)\kappa}$

3rd reflected wave: $E_{34} = D^{o}_{E2} D_{E3} \Gamma_{E1} e^{(-1+i)(y \sin 4\alpha - z \cos 4\alpha)\kappa}$

4th reflected wave: $E_{45} = D^{o}_{E4} D^{o}_{E2} D_{E3} D_{E1} e^{(-1+i)(y \sin 4\alpha + z \cos 4\alpha)\kappa}$

N^{th} reflected wave: $E_{N\infty}$

The form of the last term depends on whether N is even or odd. From (6.44):

$$E_x = E_o e^{(-1+i)\kappa z} +$$

$$+E_o \sum_{p=1}^{R} D_{E1}D_{E3}\cdots D_{E(2p-1)} e^{-2ip(p-1)\alpha_e(-1+i)\ (y \sin 2p\alpha - z \cos 2p\alpha)\kappa}$$

$$(1 + e^{-4pi\alpha_e 2(-1+i)\kappa z \cos 2p\alpha})$$

where

$$R = N/2 \text{ if } N \text{ is even}$$
$$(N-1)/2 \text{ if } N \text{ is odd} \qquad (6.45)$$

The values of $D_{E(2p-1)}$ are given by (6.27) or (6.29), whichever applies, where $\theta_i = (2p-1)\alpha$.

In deriving (6.45) we used the result that, since

$$D^o_{E2p} = e^{-4ip\alpha}$$

then

$$\prod_{s=1}^{r} D^o_{E2s} = e^{-2i\alpha r(r+1)}$$

Again the H_y and H_z components may be derived from (6.45) using Maxwell's equations in the forms given in Table 3.2. The relations are collected in Table 6.3.

We make the following substitutions in writing out the fields:

$$a_p = D_{H1} D_{H3} \cdots D_{H(2p-1)}$$

$$b_p = D_{E1} D_{E3} \cdots D_{E(2p-1)} \qquad (6.46)$$

$$(-1+i)\kappa = -\sqrt{-i}\ \eta_2 \quad \text{where} \quad \eta_2 = \sqrt{\mu_o \omega \sigma_2}$$

$$E_{x\infty} = -\sqrt{\frac{\mu_o \omega}{i\sigma_2}}\, H_{y\infty} \ ; \qquad E_{y\infty} = \sqrt{\frac{\mu_o \omega}{i\sigma_2}}\, H_{x\infty}$$

Table 6.3

The Field Components Near an Inclined Fault with a Conducting Substratum

$$E_{x2} = \sqrt{\frac{\mu_o \omega}{i\sigma_2}}\, H_{y\infty} \left\{ e^{-\sqrt{-i}\,\eta_2 z} + \sum_{p=1}^{R} b_p\, e^{-2ip(p-1)\alpha} e^{-\sqrt{-i}\,\eta_2 (y \sin 2p\alpha - z\cos 2p\alpha)} \left(1 + e^{-i4p\alpha} e^{-2\sqrt{-i}\,\eta_2 z \cos 2p\alpha} \right) \right\} \tag{6.47}$$

$$E_{y2} = \sqrt{\frac{\mu_o \omega}{i\sigma_2}}\, H_{x\infty} \left\{ e^{-\sqrt{-i}\,\eta_2 z} - \sum_{p=1}^{R} (-1)^{p+1} a_p \cos 2p\alpha\, e^{-\sqrt{-i}\,\eta_2 (y \sin 2p\alpha - z \cos 2p\alpha)} \left(1 + e^{-2\sqrt{-i}\,\eta_2 z \cos 2p\alpha} \right) \right\} \tag{6.48}$$

$$E_{z2} = -\sqrt{\frac{\mu_o \omega}{i\sigma_2}}\, H_{x\infty} \sum_{p=1}^{R} (-1)^{p+1} a_p \sin 2p\alpha\, e^{-\sqrt{-i}\,\eta_2 (y \sin 2p\alpha - z \cos 2p\alpha)} \left(1 - e^{-2\sqrt{-i}\,\eta_2 z \cos 2p\alpha} \right) \tag{6.49}$$

$$H_{x2} = -H_{x\infty} \left\{ e^{-\sqrt{-i}\,\eta_2 z} + \sum_{p=1}^{R} (-1)^{p+1} a_p e^{-\sqrt{-i}\,\eta_2 (y \sin 2p\alpha - z \cos 2p\alpha)} \left(1 - e^{-2\sqrt{-i}\,\eta_2 z \cos 2p\alpha} \right) \right\} \tag{6.50}$$

$$H_{y2} = H_{y\infty} \left\{ e^{-\sqrt{-i}\,\eta_2 z} - \sum_{p=1}^{R} b_p \cos 2p\alpha\, e^{-2ip(p-1)\alpha} e^{-\sqrt{-i}\,\eta_2 (y \sin 2p\alpha - z \cos 2p\alpha)} \left(1 - e^{-i4p\alpha} e^{-2\sqrt{-i}\,\eta_2 z \cos 2p\alpha} \right) \right\} \tag{6.51}$$

$$H_{z2} = -H_{y\infty} \sum_{p=1}^{R} b_p \sin 2p\alpha\, e^{-2ip(p-1)\alpha} e^{-\sqrt{-i}\,\eta_2 (y \sin 2p\alpha - z \cos 2p\alpha)} \left(1 + e^{-i4p\alpha} e^{-2\sqrt{-i}\,\eta_2 z \cos 2p\alpha} \right) \tag{6.52}$$

Table 6.4

The Surface Field Components Near an Inclined Fault with a Conducting Substratum

$$\sqrt{\frac{\sigma_2}{\mu_o \omega}}\frac{E_{x2}}{H_{y\infty}} = \sqrt{-i}\left\{1+2\sum_{p=1}^{R} b_p e^{-2ip^2\alpha}\cos 2p\alpha\, e^{-\sqrt{-i}\,Y_2 \sin 2p\alpha}\right\} \tag{6.53}$$

$$\sqrt{\frac{\sigma_2}{\mu_o \omega}}\frac{E_{y2}}{H_{x\infty}} = \sqrt{-i}\left\{1+2\sum_{p=1}^{R} (-1)^p a_p \cos 2p\alpha\, e^{-\sqrt{-i}\,Y_2 \sin 2p\alpha}\right\} \tag{6.54}$$

$$H_{y2}/H_{y\infty} = 1-i\sum_{p=1}^{R} b_p e^{-2ip^2\alpha}\sin 4p\alpha\, e^{-\sqrt{-i}\,Y_2 \sin 2p\alpha} \tag{6.55}$$

$$H_{z2}/H_{y\infty} = -\sum_{p=1}^{R} b_p e^{-2ip^2\alpha}\sin 4p\alpha\, e^{-\sqrt{-i}\,Y_2 \sin 2p\alpha} \tag{6.56}$$

$$R = \begin{cases} N/2 \text{ if } N \text{ even} \\ (N-1)/2 \text{ if } N \text{ odd} \end{cases} \qquad N = \left[\frac{\pi}{2\alpha} - 1\right]$$

$$a_p = \prod_{s=1}^{p} D_{H(2s-1)} \qquad b_p = \prod_{s=1}^{p} D_{E(2s-1)} \tag{6.57}$$

(i) $\varepsilon^2 \leq \sin\alpha$

$$D_{H(2s-1)} = \left[-1 + \frac{2}{1+\nu^2_{H(2s-1)}}\right] - i\,\frac{2\nu_{H(2s-1)}}{1+\nu^2_{H(2s-1)}};$$

$$; \quad \nu_{H(2s-1)} = \frac{\sqrt{\sin^2(2s-1)\alpha - \varepsilon^4}}{\varepsilon^2\cos(2s-1)\alpha}$$

$$D_{E(2s-1)} = e^{-2i\phi_{2s-1}} \cdot \tan\phi_{2s-1} = \sqrt{1-\nu^2_{E(2s-1)}}\,\tan(2s-1)\alpha;$$

$$; \quad \nu_{E(2s-1)} = \frac{\varepsilon^2}{\sin(2s-1)\alpha}$$

Table 6.4 (cont'd)

The Surface Field Components Near an Inclined Fault with a Conducting Substratum

(ii) $\varepsilon^2 > \sin\alpha$

$\varepsilon^2 \leq \sin(2s-1)\alpha$: (i) above applies

$\varepsilon^2 > \sin(2s-1)\alpha$:

$$D_{H(2s-1)} = -1 + \frac{2}{1+\nu'_{H(2s-1)}} \quad ; \quad \nu'_{H(2s-1)} = \frac{\sqrt{\varepsilon^4 - \sin^2(2s-1)\alpha}}{\varepsilon^2 \cos(2s-1)\alpha}$$

$$D_{E(2s-1)} = -1 + \frac{2}{1+\sqrt{\nu^2_{E(2s-1)}-1}\ \tan(2s-1)\alpha} \quad ; \quad \nu_{E(2s-1)} = \frac{\varepsilon^2}{\sin(2s-1)\alpha}$$

The expressions for the surface fields at z=o are listed in Table 6.4 in terms of the dimensionless parameter $Y_2 = \eta_2 y = y\sqrt{\mu_o \omega \sigma_2}$. We have also used the simplification:

$$e^{-2ip(p-1)\alpha} \quad (1 \pm e^{-i4p\alpha}) = 2e^{-2ip^2\alpha} \begin{Bmatrix} \cos 2p\alpha \\ i \sin 2p\alpha \end{Bmatrix}$$

6.2.3 Special Cases

(a) Agreement with Berdichevskii's (1961) solution:

Berdichevskii assumed σ_2=o so that ε=o. Then

$$D_{E(2s-1)} = e^{-2i(2s-1)\alpha} \quad ; \quad D_{H(2s-1)} = -1$$

Thus

$$a_p = (-1)^p$$

$$b_p = e^{-2i\alpha \sum_{s=1}^{p}(2s-1)} = e^{-2ip^2\alpha}$$

The relations of Table (6.2) then reduce to those in Table 6.1 with allowance for the different orientation of the x-axis used by Berdichevskii.

The equations of Table 6.4 indicate that the approximation ε=o used by Berdichevskii is valid whenever $\varepsilon^2 << \sin\alpha$, or, for small α, whenever $\varepsilon^2 << \alpha$ (α in radians). Thus we expect the influence of the conductivity to become evident when α is small, i.e. when ε^2 and α are comparable.

(b) Transition to a Uniform Medium

From Table 6.3 we see that as $y \to \infty$, the fields behave as follows

$$E_{x2} \to \sqrt{-i}\sqrt{\frac{\mu_o \omega}{\sigma_2}}\, H_{y\infty}\, e^{-\sqrt{-i}\,\eta_2 z}$$

$$E_{y2} \to \sqrt{-i}\sqrt{\frac{\mu_o \omega}{\sigma_2}}\, H_{x\infty}\, e^{-\sqrt{-i}\,\eta_2 z}$$

$$E_{z2} \to o$$

$$H_{x2} \to -H_{x\infty}\, e^{-\sqrt{-i}\,\eta_2 z}$$

$$H_{y2} \to H_{y\infty}\, e^{-\sqrt{-i}\,\eta_2 z}$$

$$H_{z2} \to o$$

This is the same transition as 4.12 for the vertical fault (§4.1.3a), where we have replaced $H_{x\infty}$ with B and $H_{y\infty}$ with A; the limits represent fields in a uniform medium of conductivity σ_2.

The criterion for the field components to approximate their asymptotic values is

$$\begin{aligned} & Y_2 \sin 2\alpha \gg 1 \\ \text{or} \quad & y \gg \eta_2^{-1} \operatorname{cosec} 2\alpha \end{aligned} \tag{6.58a}$$

This criterion applies when we consider the distance of a station from the actual shore line. If, instead, the station is over the open sea (for instance, an ice-island), the criterion is better stated in terms of the ocean depth H:

$$\begin{aligned} H &\gg \tfrac{1}{2} \sec^2 \alpha \\ h &\gg \tfrac{1}{2} \eta_2^{-1} \sec^2 \alpha \end{aligned} \tag{6.58b}$$

For all values of α to which the theory of this chapter applies, no serious error is incurred by relaxing this condition to

$$h \gg \tfrac{1}{2}\eta_2^{-1}$$

6.2.4 Conditions of Validity of the Solution

Two considerations must be made in using the solutions derived above:

(a) The applicability of the plane-wave technique

(b) The scale size of the assumed geometry.

(a) Applicability of the Plane Wave Technique:

The validity of the plane-wave method used in the previous section must break down eventually, as can be seen from the following consideration. If the angle α is increased from zero, it finally reaches 45°, where N=1. Beyond this value, the only reflection occurring is from the basement; the wave then passes further into medium 2 without returning to the surface. Under this condition our plane-wave solution indicates no further influence of the coastline on the fields. Such a conclusion seems absurd, since we know from Chapter IV that the coast effect certainly exists when $\alpha = 90°$.

It must be remembered, however, that we are not including the effect of the land in this discussion. At a distance of several penetration depths from the shore, the ocean depth for a steeply sloping floor is too great for the electromagnetic wave to "see" the floor, and the effect of the basement becomes negligible.

The apparent anomaly arises from our assumption of plane waves. In Fig. 6.5 we give a schematic outline of the contributions to the total electromagnetic field for an incident field of infinite extent. At any point in the oceanic medium (2) the total field F_2 is composed as follows:

$$F_2 = F_{2\infty} + F_{2r} + F_{2d}$$

where

$F_{2\infty}$ represents the field in the uniform medium (2)

F_{2r} represents the total field resulting from the multiple order reflections at both interfaces

F_{2d} represents the perturbation field produced by scattering at the apex of the oceanic "wedge."

Similarly in the land medium (1), the total field F_1 comprises

$$F_1 = F_{1\infty} + F_{1t} + F_{1d}$$

The $F_{1\infty}$ and F_{1d} contributions are analogous to their counterparts in medium (2), and F_{1t} represents the transmitted field resulting from refraction across the fault plane. The last component will not contribute to the surface field.

At small values of α, the disturbance field F_d will be small (it is non-existent at $\alpha = o°$), but becomes increasingly important as α increases. In the oceanic medium the F_{2r} contribution becomes zero for $\alpha > 45°$ and the entire "coast effect" is caused by F_{2d}. In medium 1, the F_{1d} contribution is responsible for the "coast effect" behavior at all angles, and the influence of the inclined fault will thus be very small on the landward side at low angles of inclination.

It is evident from Ch. IV (Figs. 4.3 and §4.2.3a) that the influence of a vertical fault does not extend beyond about $8\eta^{-1}$. Since we might expect the F_d contribution to be a maximum for $\alpha = 90°$, we can say that the treatment in this chapter should be valid at least beyond a distance of $8\eta_2^{-1}$ in the oceanic medium.

Another approach to the validity of the plane wave solution may be made. The concept of a plane wave is maintained only if the scale of change within the medium is not smaller than the wave length of the wave. Since the wave is specified by

$$\mathrm{Re}(e^{ikz}) = e^{-z/\delta} \cos z/\delta \qquad \delta = \sqrt{2/\mu_o \omega \sigma}$$

the wave length of the wave is given by

$$\lambda = 2\pi\delta \tag{6.59}$$

The plane-wave approach will break down at distances nearer than λ_2 to the apex of the oceanic wedge. We thus restrict our solution to the region

$$y \gtrsim \lambda_2$$

or

$$Y_2 \gtrsim 9$$

These two approaches yield essentially the same condition on the region of validity. As they both yield overestimates of the value of Y_2, we can take the minimum significant value to be $Y_2 = 5$, without seriously affecting the validity.

(b) The Scale Size of the Incline

It is also necessary that the sloping sea floor extend far enough for all possible reflections to occur. We designate the distance by L_c and refer to Fig. 6.6. L_c is therefore the distance from the entry point A of the wave to the point of the last (N^{th}) surface reflection E, with

$$N = \left[\frac{\pi}{2\alpha} - 1\right]$$

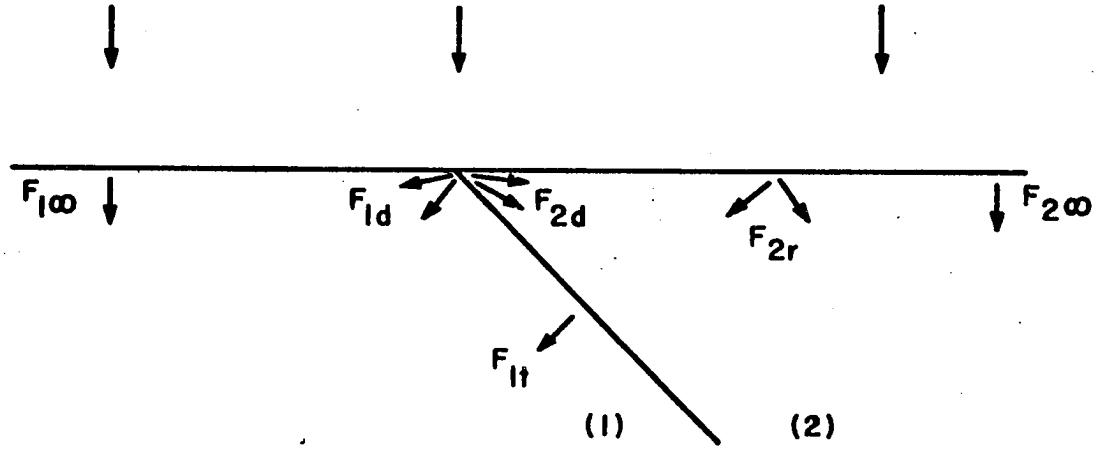

Fig. 6.5 A schematic representation of the contributions to the total electromagnetic field near an inclined fault.

By reference to either Fig. 6.3 or 6.4, we see from the image planes that

$$y_o = y_i \sec N\alpha$$

so that

$$L_c = y_i (\sec N\alpha - 1) = h_i \cot\alpha (\sec N\alpha - 1) \qquad (6.60)$$

Also

$$\frac{L_c}{h_o} = \cos N\alpha \frac{L_c}{h_i} \qquad (6.61)$$

The specification of L_c in terms of the depth h_o is useful if the point E has been selected as an observation point. One then wants to know the distance towards land necessary for the results of §6.2 to apply, and hence the distance over which the slope must be uniform. On the other hand, if the point A represents the start of the incline, we would like to know how far beyond A we must place an observation point in order that all the reflections would be received and the theory of this chapter be valid. Such a question is answered most usefully by specifying L_c in terms of the depth h_i.

In Fig. 6.7, the scale length L_c is shown in terms of both h_i and h_o. The actual curves of (6.60) and (6.61) are saw-toothed in form because of the step-function nature of N. A practical representation would be the curve through the upper limiting points, particularly in the highly "oscillatory" region for small α. The considerations in (a) above also limit the solution to this region.

A simple example will be useful in interpreting Fig. 6.7. Suppose the ocean floor slopes at $\alpha = 3°$. For $\sigma_2 = 3$ mho m^{-1} and $f = 1$ cps,

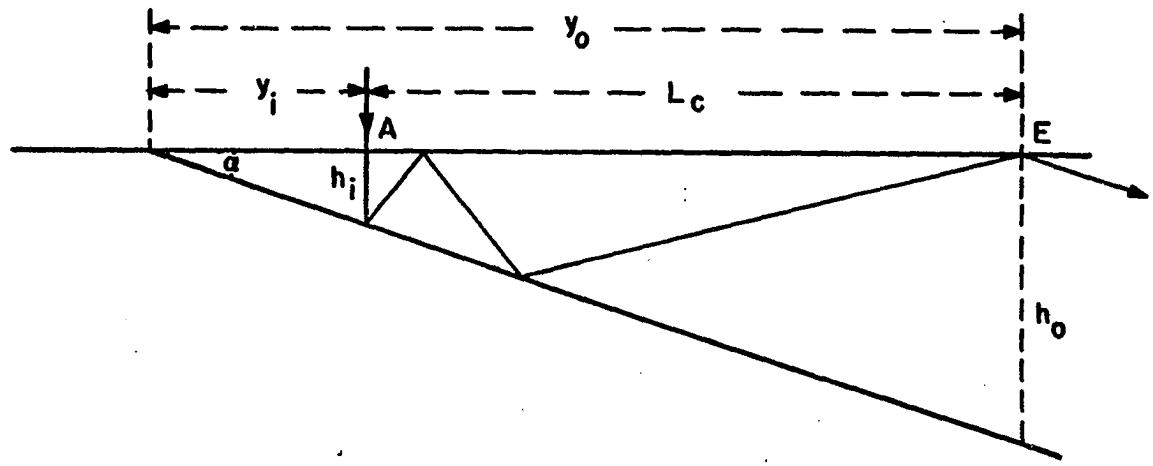

Fig. 6.6 Determination of the scale length L_c.

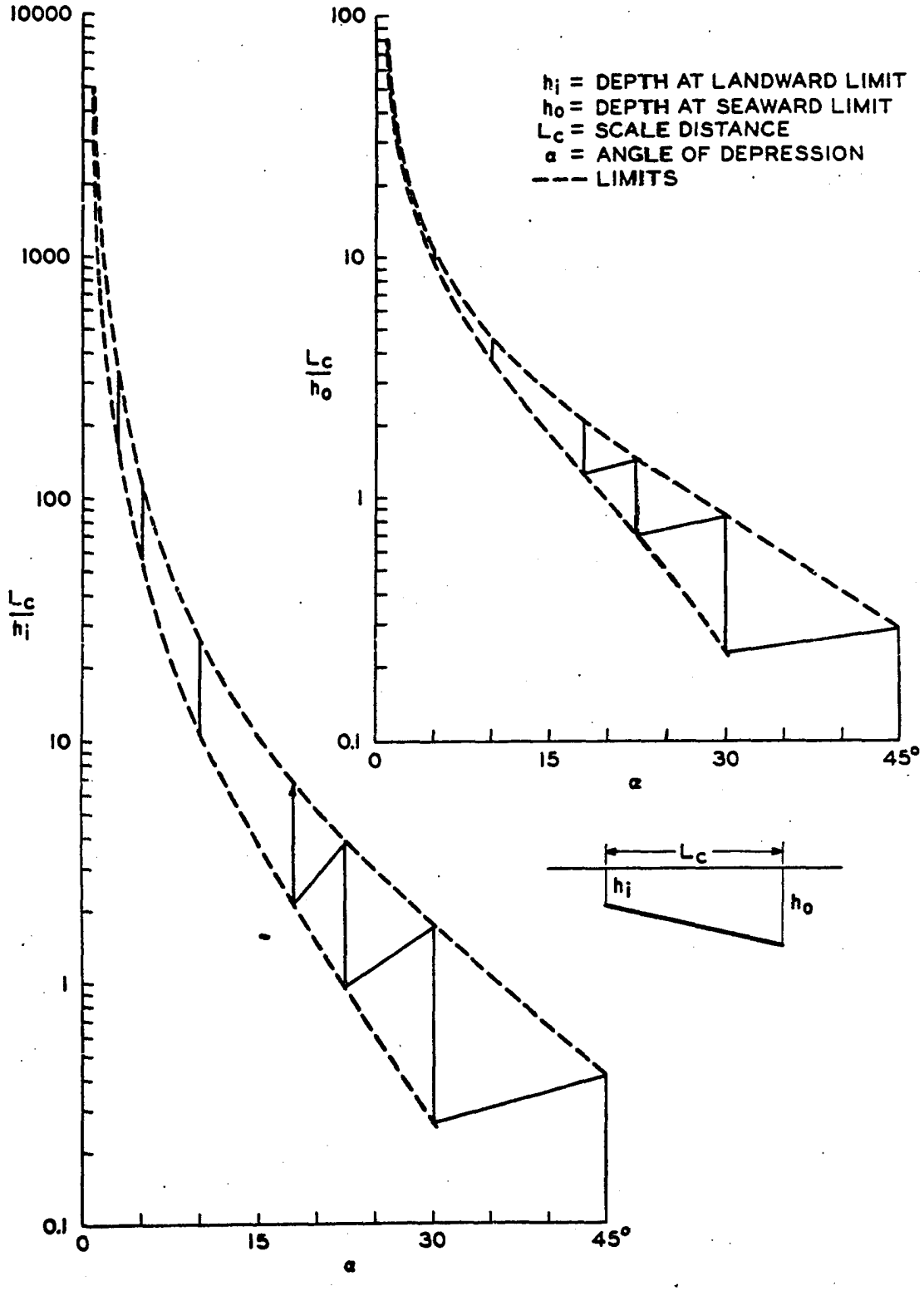

Fig. 6.7 The scale length L_c as a function of the depths h_i and h_o for various angles of inclination α.

we have $\eta_2^{-1} \sim$ 200 m, and our solution will be applicable at any distance from the shoreline beyond about 1000 m. If the observation point (E in Fig. 6.6) is over a depth h_o = 100 m, the 3° slope must be maintained shorewards for a horizontal distance L_c = 1800 m.

The scale distance L_c is not critical, however. At low values of α the number of reflections is very large (29 in the above example), and consequently if the sea is deep the scale distance L_c is enormous (in the above example, if the point in question is A instead of E, L_c is 35 km). However, the distances between the last reflection points become very large (see Fig. 6.4, when α = 10°) and the wave is considerably attenuated by the conducting medium. The effects of these last reflections are insignificant and the actual value of L_c will be very much less than that shown in Fig. 6.7.

The simplest way to determine a representative scale distance in a given case is to plot the ray path on a scale drawing (for instance, as in Fig. 6.4) and determine the next surface reflection point (say the N' - th total reflection) where the path exceeds $5\eta_2^{-1}$. The effective scale distance L_c' is then given by (6.60) with N' replacing N.

To use Fig. 6.4 as an example, if AB = h_i = 200 m, with the above value of η_2^{-1} = 200 m, then the point G is the N' - th reflection. Since N' = 6, then L_c' = 1100 m, as compared with L_c = 5500 m determined from Fig. 6.7.

6.2.5 Computation of the Fields

The relations of Table 6.4 were numerically evaluated with the use of the IBM 7094 and System 360/75 computers at Western Data Processing

Center, University of California, and the IBM 360/40 at the University of Alaska. The program is given in App. 10. The fields were computed for several values of α and ε, including the case considered by Berdichevskii (1961), for which $\alpha = 3°$, $\varepsilon = o$.

6.3 Discussion of Results

In Figs. 6.8(a-d), we present the variation of the field components with distance Y_2 for several values of ε, and $\alpha = 3°$ and $10°$ respectively. The horizontal axes also show the depth H of the basement, given by

$$H = Y_2 \tan \alpha$$

Berdichevskii's values are represented by the limiting curves as $\varepsilon \to o$.

The influence of the sloping basement on all components is quite marked over the region where the depth $H < 3$ (i.e., shallower than about three penetration depths). At shallow depths, the electric fields are enhanced with respect to their asymptotic values, as is the vertical magnetic field H_z. The normal magnetic field H_y increases slightly and then decreases from its asymptotic behavior, as the depth decreases. The effect of the basement slope is less marked for conductivity ratios near unity. At values of $\varepsilon^2 < 10^{-2}$ the fields are nearly independent of ε, and the basement may be assumed non-conducting.

Fig. 6.9 shows the polarization of the electric field with distance, for basement slopes of 3° and 10°, at various conductivity ratios. At shallower basement depths, there is a distinct trend towards linear polarization with a pronounced normal component; the tendency is stronger for greater contrasts in conductivity. As the abscissa of Fig. 6.9 represents distance in units of penetration depth, the behavior with

frequency at a given location over a basement of given slope, can be determined. The linearity and the proportion of the normal component in the polarization ellipse increase at lower frequencies.

The behavior of the electric fields may be explained as follows. At some distance from the coastline, the electric field behaves in a manner qualitatively similar to the field near a vertical fault (cf. Fig. 4.4). As the shore-line is approached, the field polarization changes from circular (over the homogeneous [deep] ocean) to more elliptical. At about one penetration depth ($H \sim 1$) - the value varies with slope α and conductivity ratio ε^2 - the field is oriented parallel to the coast; i.e., the oceanic electric currents are diverted by the relatively non-conducting land. As we approach the shoreline still more closely, however, a "transition region" is traversed. The depth becomes less than the oceanic penetration depth and an appreciable electric field component normal to the coast is evident in the polarization ellipse. On land the field would be oriented normal to the shore (cf. Fig. 4.4); the region of shallow water with sloping base thus provides the transition between electric fields over the land and deep ocean. For the observation distances Y_2 for which our calculations are valid, this transition region is only apparent when $\varepsilon^2 \leq 10^{-2}$; at conductivity ratios nearer to unity, the region would be closer to the shore and the scattering from the actual surface discontinuity would dominate the calculations (Fig. 6.5).

At points within about 10 penetration depths of the shoreline ($Y_2 < 10$), the electric field shows a small anomaly in its variation

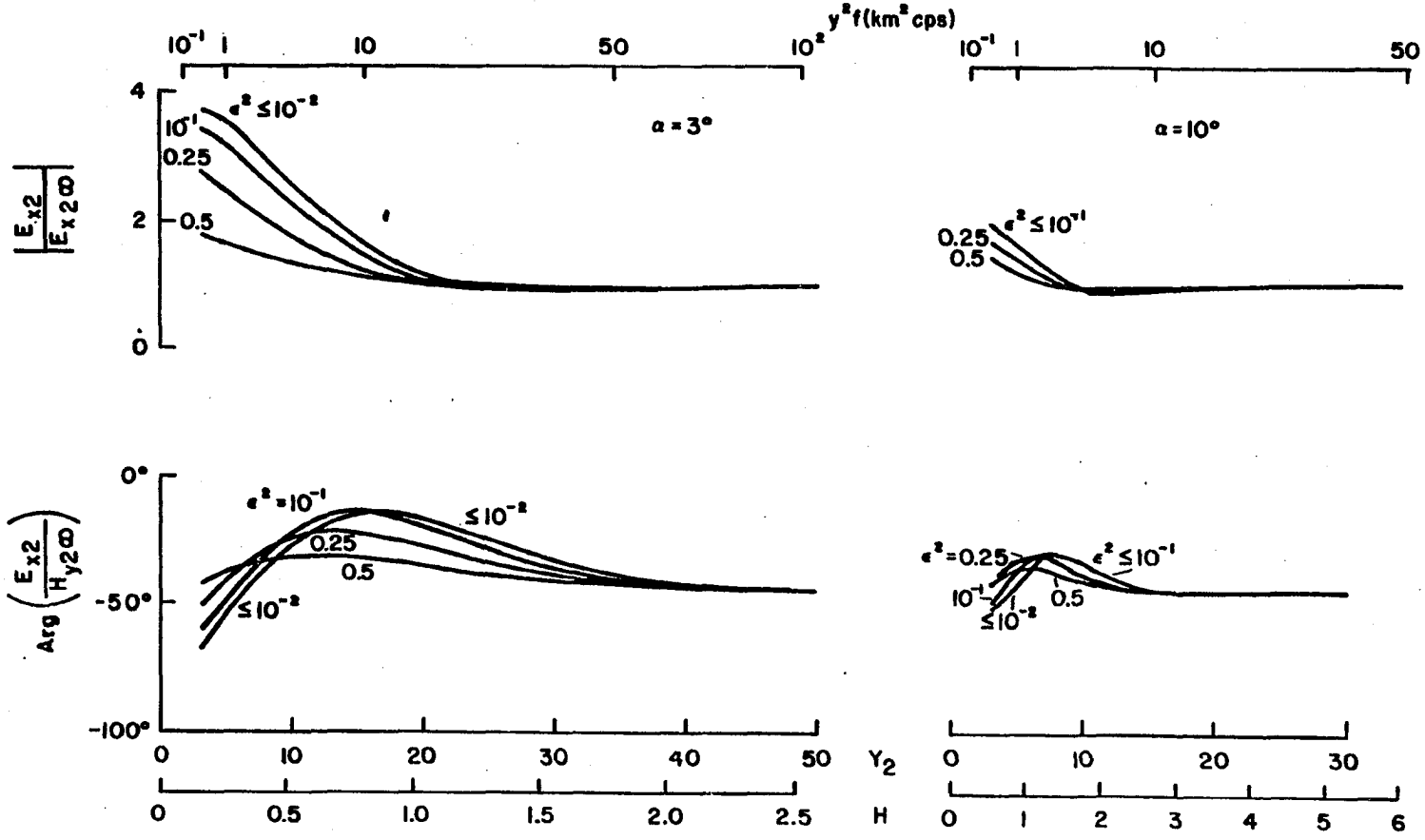

Fig. 6.8 (a) The tangential electric field (E_x) over inclined basements of slope 3^o and 10^o, as functions of distance (Y_2) and conductivity ratio (ϵ^2). Also indicated is the depth H and frequency (y^2f) scales, where y is the distance from the shoreline. The parameters are defined in Table 3.3.

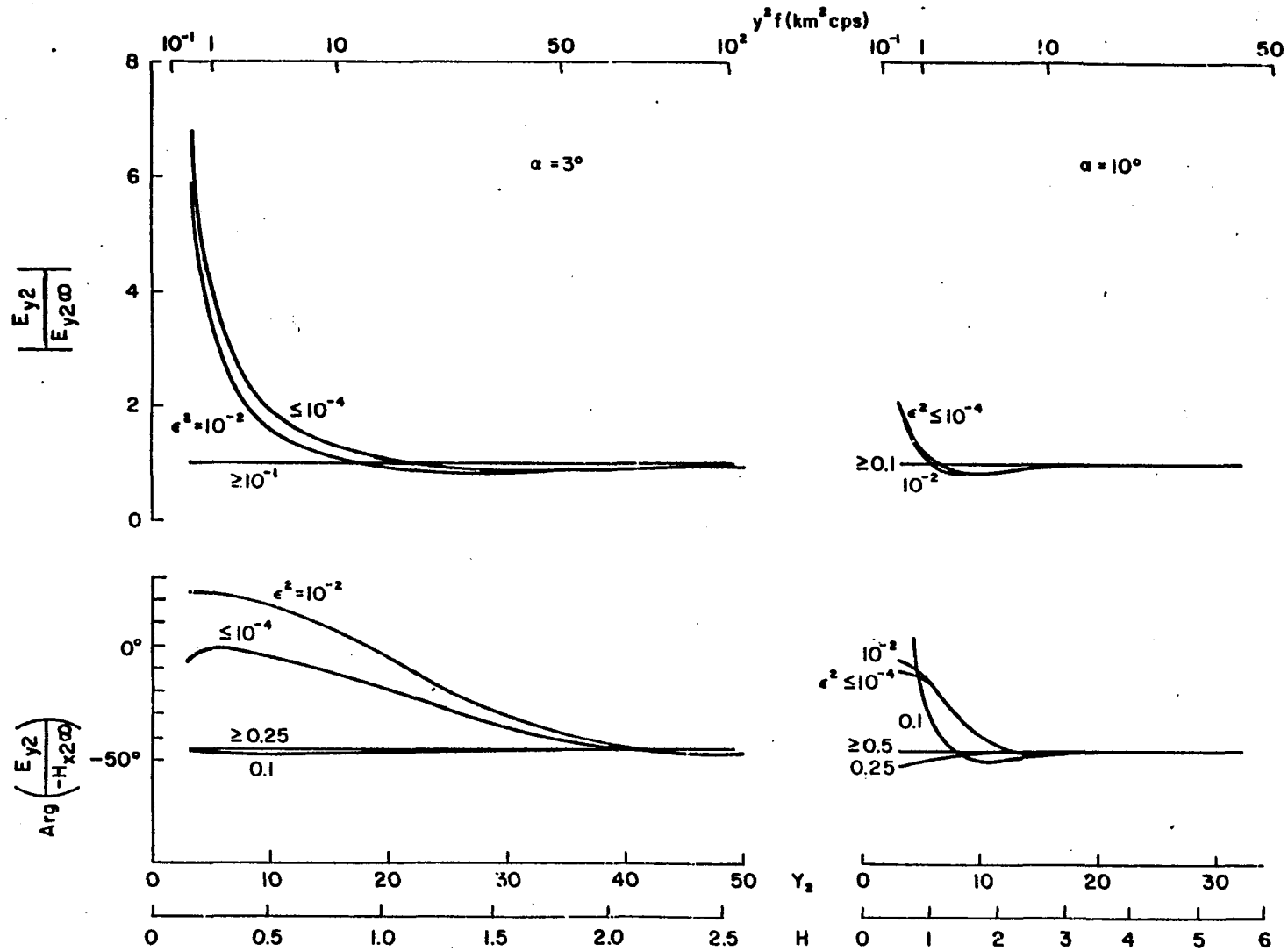

Fig. 6.8 (b) The normal electric field (E_y) over inclined basements of slopes 3^o and 10^o.

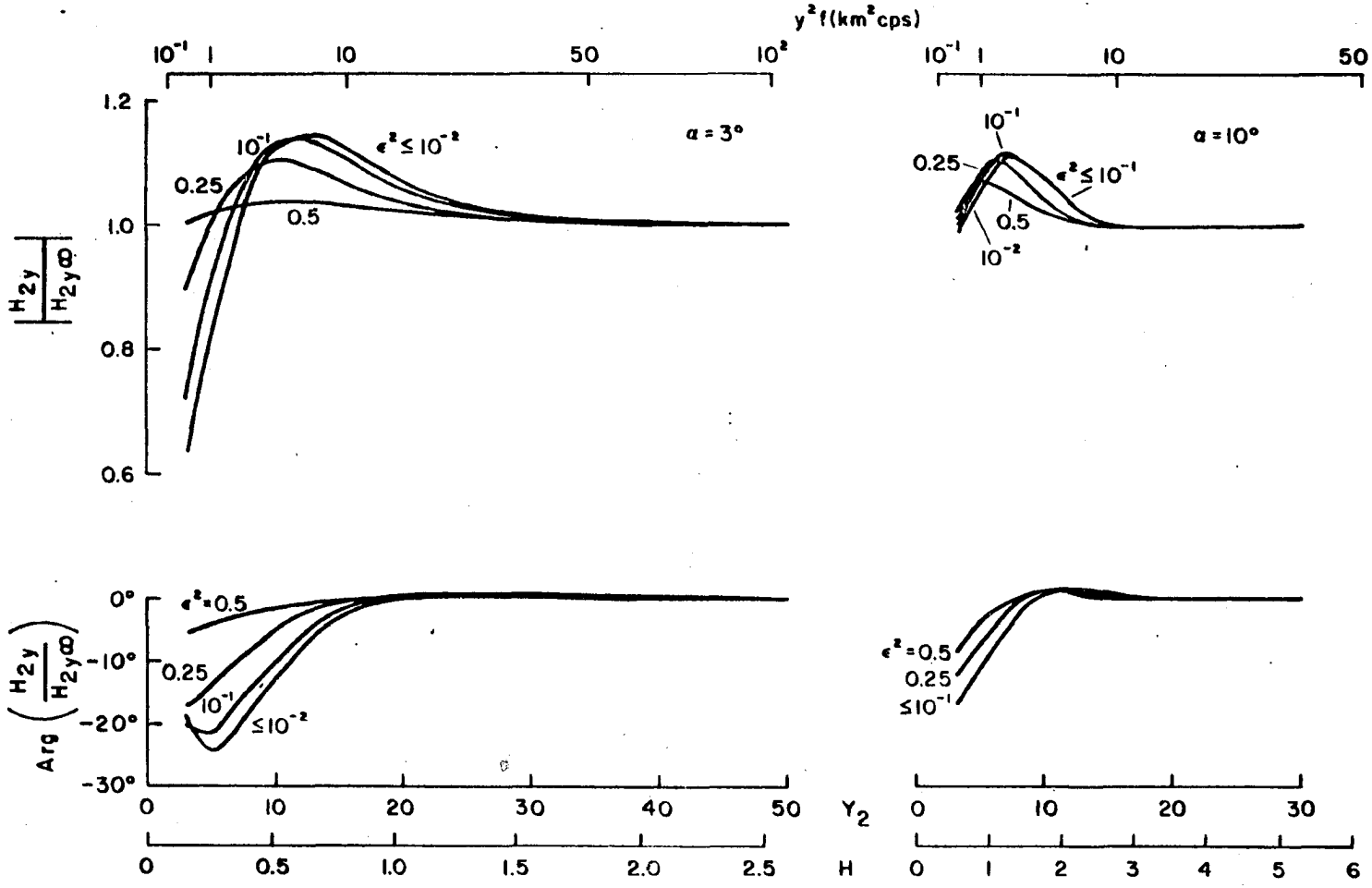

Fig. 6.8 (c) The normal magnetic field (H_y) over inclined basements of slopes 3° and 10°.

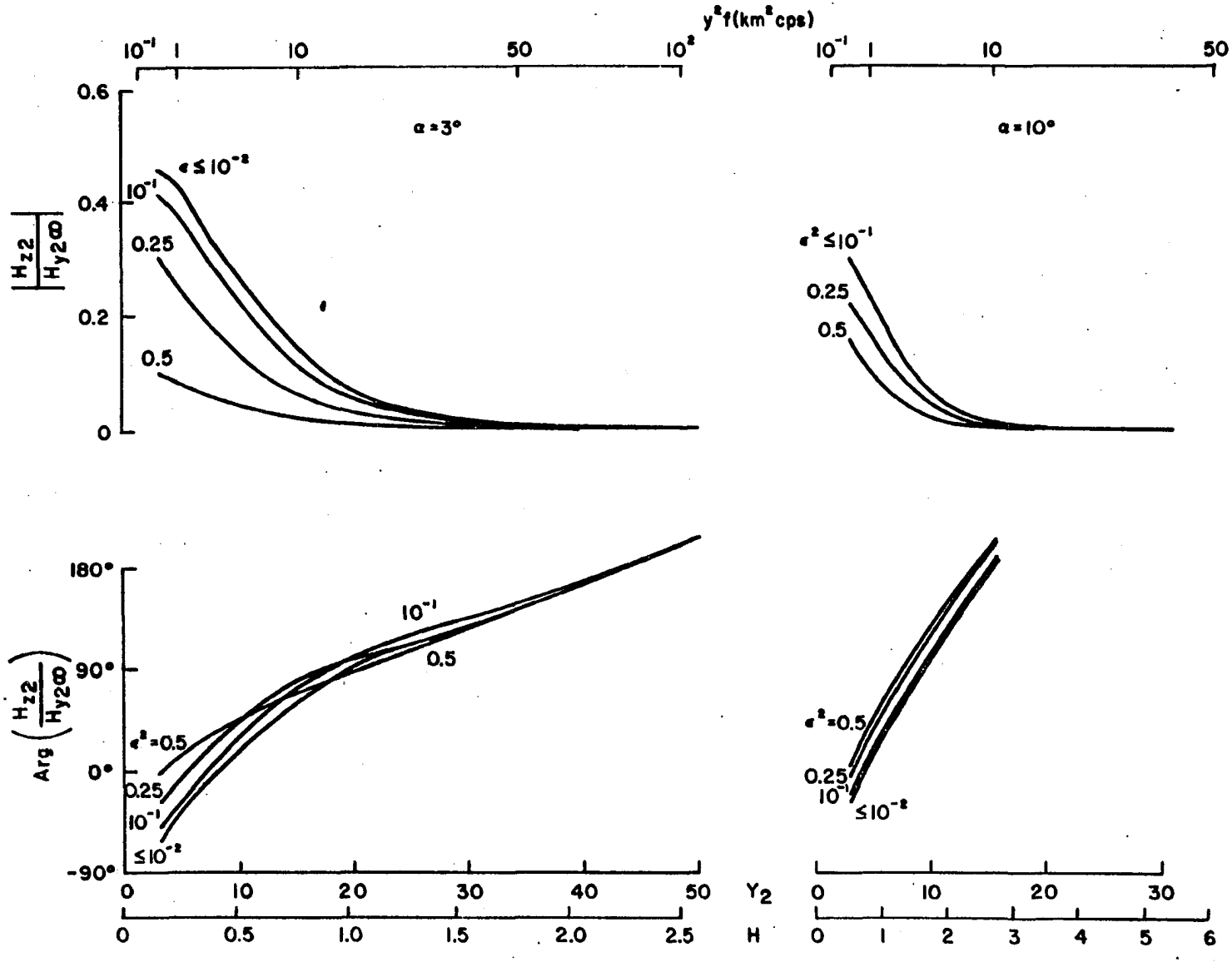

Fig. 6.8 (d) The vertical magnetic field (H_z) over inclined basements of slopes 3° and 10°.

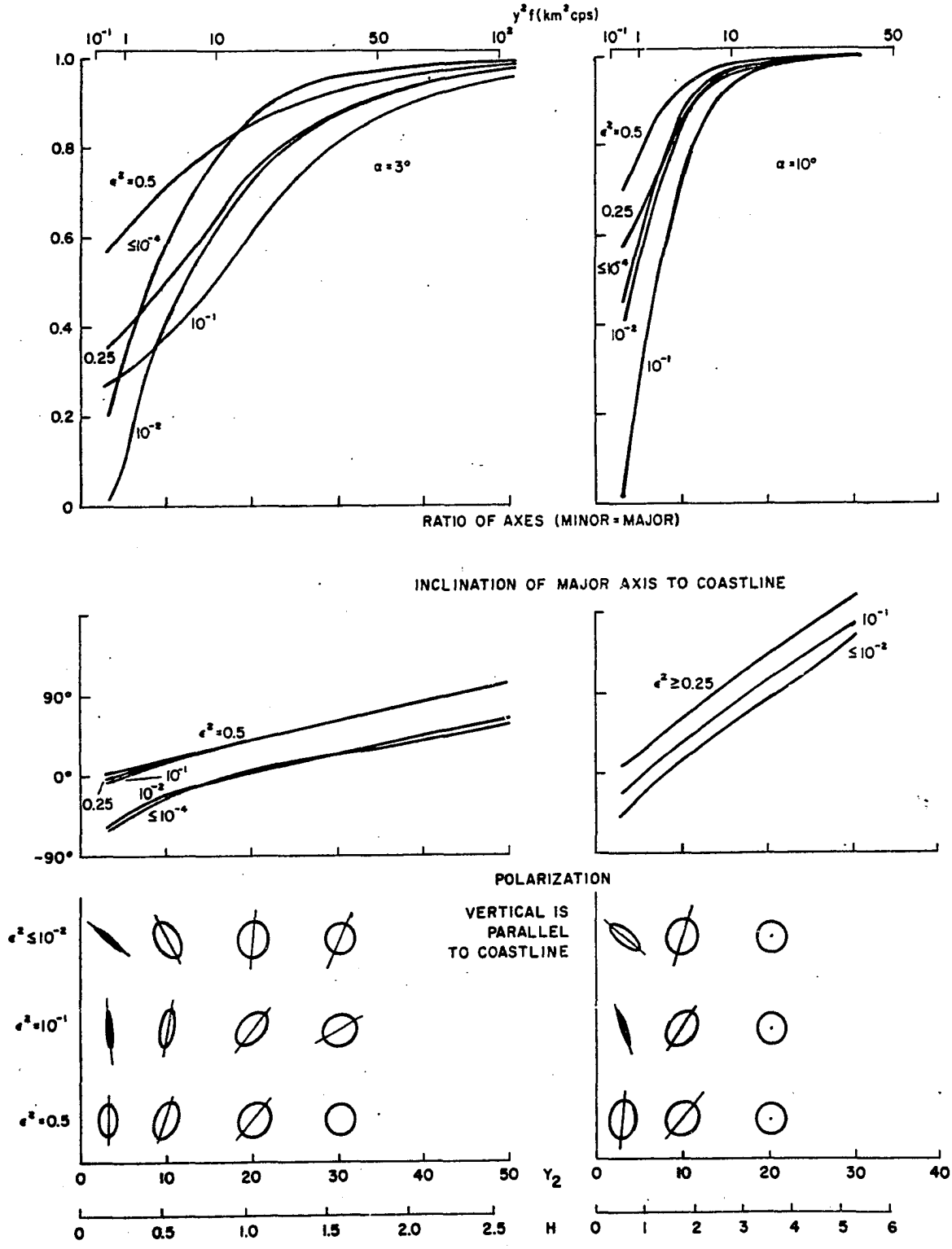

Fig. 6.9 The parameters of the polarization ellipses of the horizontal electric field over inclined basements of slopes 3^{o} and 10^{o}.

with the conductivity. From Fig. 6.9, it is evident that the polarization is more linear for the values of $\varepsilon^2 \sim 10^{-1}$ than for conductivity ratios greater or less than this. This tendency is not so obvious at greater distances from the shore, when the polarization becomes more circular.

Berdichevskii's (1961) results for a non-conducting basement (ε=o) with a 3° slope are given in Fig. (6.10). Our computations are in excellent quantitative agreement, although the lack of a distance scale on his Arg (H_x/H_o) curve prevents a comparison of this quantity. Figures 6.8 a-d may also be interpreted as frequency response curves, with the scale in terms of $y^2 f$ ($km^2 \cdot cps$), as shown at the top of each of the curves. The conductivity of the ocean σ_2 is again assumed to be 3 mho m^{-1} in calculating these values.

Compare the electric field over a sloping basement with that over a horizontal basement. In Fig. (6.11), we have plotted the electric field magnitudes for a horizontal basement and for inclined basements of 1°, 3°, and 10° slopes. The fields are normalized to unity for a field over a uniform medium, and the basement is taken to be non-conducting in all cases. The tangential E_x field is shown; the E_y field at these inclinations is almost identical with the E-field over a horizontal base, at least within the limiting frequencies shown here. The electric field over a non-conducting basement with a horizontal interface is given by eq. (4.58).

The representation as a function of H serves two purposes. If we consider a fixed depth h, then Fig. (6.11) represents frequency

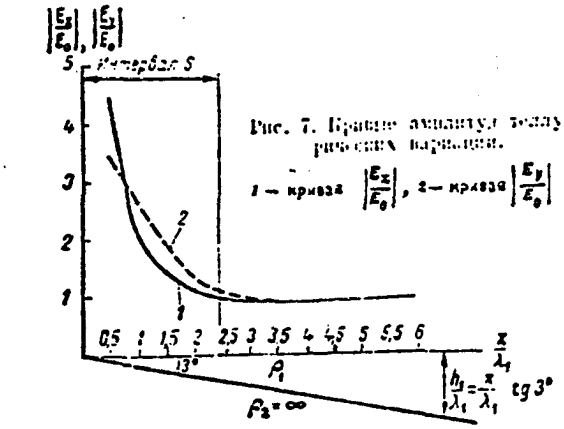

Рис. 7. Кривые амплитуд теллурических вариаций.

1 — кривая $\left|\frac{E_x}{E_0}\right|$, 2 — кривая $\left|\frac{E_y}{E_0}\right|$

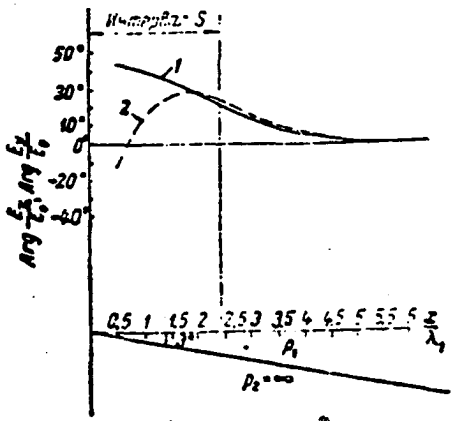

Рис. 9. Кривые фаз теллурических вариаций.

1 — кривая $\operatorname{Arg}\frac{E_x}{E_0}$, 2 — кривая $\operatorname{Arg}\frac{E_y}{E_0}$

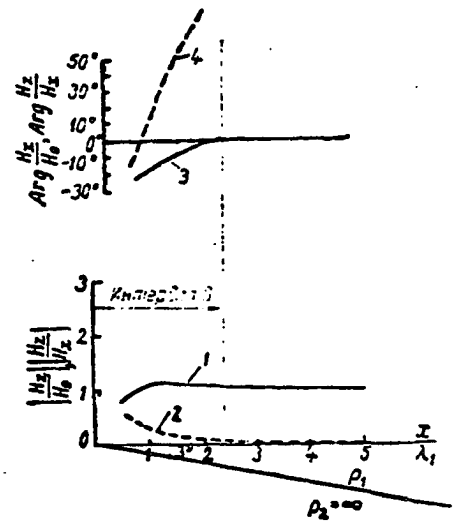

Рис. 10. Кривые амплитуд и фаз магнитных вариаций.

1 — кривая $\left|\frac{H_x}{H_0}\right|$; 2 — кривая $\left|\frac{H_z}{H_x}\right|$; 3 — кривая $\operatorname{Arg}\frac{H_x}{H_0}$; 4 — кривая $\operatorname{Arg}\frac{H_z}{H_x}$

(a)

curves 1: $\frac{E_x}{E_0}$

curves 2: $\frac{E_y}{E_0}$

(b)

curves 1,3: $\frac{H_x}{H_0}$

curves 2,4: $\frac{H_z}{H_0}$

Fig. 6.10 The fields over a non conducting basement inclined at 3°, Berdichevskii (1961). See Fig. (6.1b) for his coordinate system.

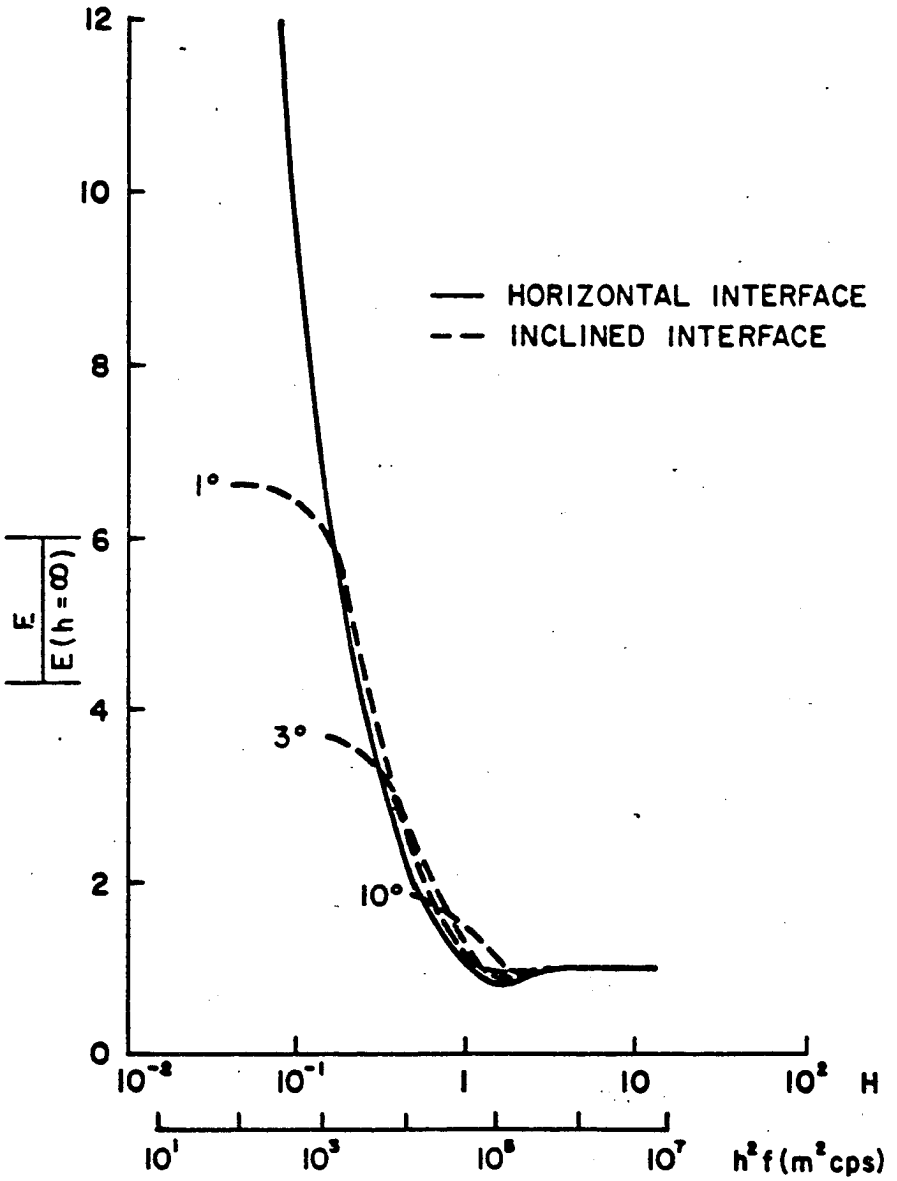

Fig. 6.11 Comparison of the electric fields over a conducting ocean with horizontal or inclined basements, assumed non-conducting. The tangential E_x field over the inclined base is shown; the normal E_y field is indistinguishable from the E-field over a horizontal base.

responses for the E-fields, when the sea floor is inclined at the relevant angles. To assist this interpretation, the abscissa is also scaled in terms of $h^2 f$, where the depth h is measured in meters. The frequency response flattens out at low frequencies, but approaches closely the response of a horizontally layered medium at higher frequencies. Alternatively if we fix the frequency f, the curves show the variation of the electric field as a function of the depth, at each angle α. The low frequency limit is set by the limiting value of Y_2 in Figs. 6.8(a).

As an example, over a sea floor at a depth of 500 m, sloping at 1°, the frequency response for periods longer than about 5 min (at least up to about 1 hr), would be relatively flat. We stress, however, that this is the frequency response of the normalized E field, not of the impedance $|E/H|$. The responses vary in the ratio $\sqrt{T}$, according to (4.58).

6.3.1 Comparison with Observations

Some comparison of the results of this chapter may be made with the observations of Wescott (1967) at Barrow on the Arctic Ocean (see §2.6.2). His station 10 (see Fig. 6.12) was located on the sea ice 2 km from the shore, over a sloping sea bed of depth c. 11 m, and slope 1°. Station 11 was located 3 km from shore over 35 m of water, with a sea floor of similar slope. The slope inshore from the two stations drops to about 0.1°, rising to 2.5° within 150 m of the coast. Wescott estimated the effective conductivity ratio to be about 1:40 ($\epsilon = 0.16$). He found that the electric field at these stations showed a strong polarization component normal to the depth contours.

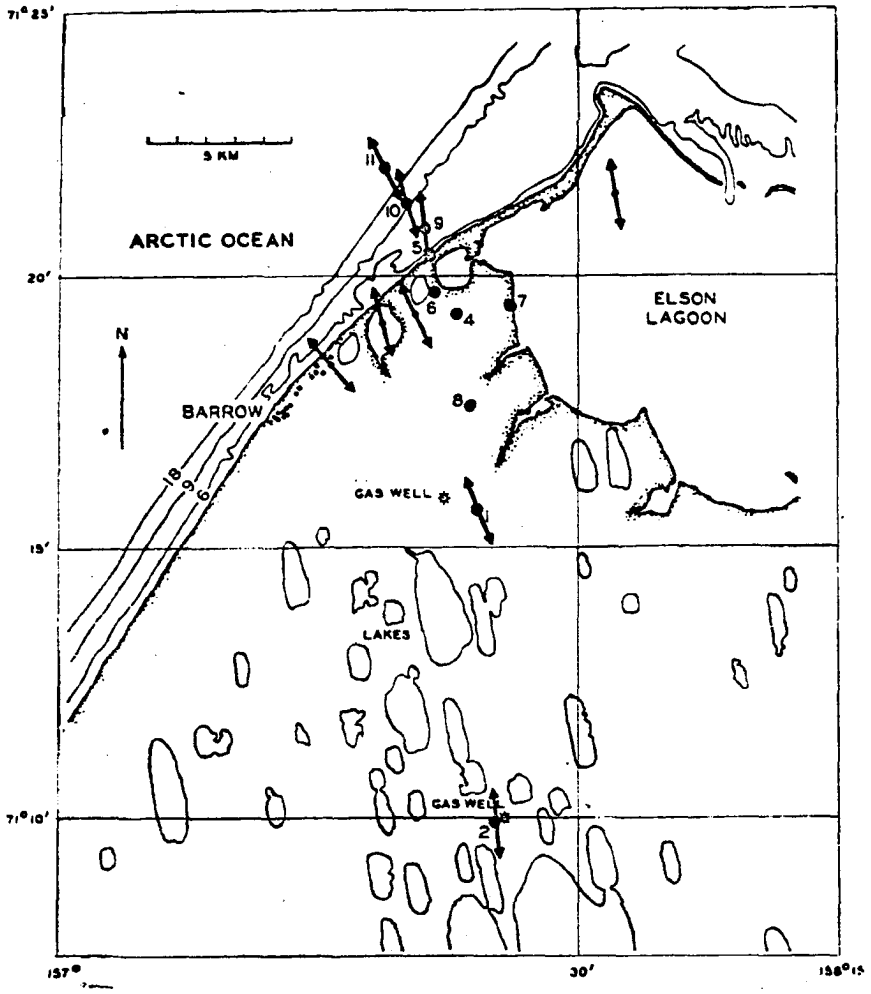

Fig. 2. Map of Barrow, Alaska, area showing numbered temporary variograph stations. Barrow Magnetic Observatory is located at 4. Arrows indicate the long axis of ellipse of polarization of telluric currents. Water depths in meters.

Fig. 6.12 Telluric current polarization near Barrow (Wescott, 1967).

At frequencies greater than about 0.1 cps these sites are distant from the shore by several times the penetration distance η_2^{-1}, and the computations of this chapter may be applicable. However, the changing slope of the sea floor may introduce some complications. Wescott was not able to obtain data at specific frequencies, but instead used the hourly peak-to-peak amplitudes of irregular activity; his data are therefore effective at long periods.

Computation of similar curves to those of Fig. 6.9 for a slope of 1° shows a highly linear polarization inclined at about 60°-75° to the coastline, over depths of $H \sim 0.15$. Wescott's arrows for stations 10 and 11 (Fig. 6.12) indicate major axis inclinations of about 55° and 65° respectively. Although his data are not for specific frequencies, it is known that at Barrow the periods of less than 40 sec are suppressed on the telluric current records. At periods greater than this our calculations are no longer valid within 3 km of the shoreline. However, the results show that there may be a strong normal component in the telluric field over shallow water, where the slope of the sea bed is very gradual. Interpretation of the field behavior at sites closer to the shore line, or at lower frequencies, must await a solution of the inclined fault problem with a greater range of validity than ours.

Wescott's (1967) data at Barrow show a trend in the orientation of the polarization ellipses between 3 and 1 km from the shore line, but his results are complicated by a changing coastal orientation and the difficulty of obtaining information at specific frequencies. His data at least do not contradict the suggestions made in the previous section, but confirmation would require more extensive observations.

Swift and Hessler (1964) found no frequency dependence of the H/E ratio between periods of 1 minute and 1 hour, over an ocean floor of depth 400-450 m, sloping at an angle of 0.5°-1.5°. Point A of Fig. (6.13) shows the area of the observations.

They considered a horizontally layered medium and applied the source theory of Price (1962), but were unable to explain this frequency independence without requiring either a source of thousands of km extent, or an apparent depth of 1 km under station Arlis I (point A).

The flat frequency response of the $|E/H|$ ratio is equivalent to a response of the ratio $|E/E(h=\infty)|$ (used in Fig. 6.11) which is proportional to $\sqrt{T}$; i.e., 1/H. This is the response for a horizontal basement or for the normal E_y field at slopes of 2° or less. At very low angles of inclination (< 0.5°) such a response might be expected in the tangential E_x field, but at greater slopes cannot occur. For a 1° slope, the depth under point A should be at least about 900 m to cause this response.

Much of Swift's and Hessler's data for this site involves the normal E_y component for which a flat frequency response would certainly be expected, even for a slope of 2°. Two observations were also recorded using the E_x component, for which the corresponding theoretical slopes should be $\lesssim$ 0.5°. The sea floor falls about 300 m in 170 km or 0.1°, between Arlis and the Chukchi Shelf, and is therefore well within this range.

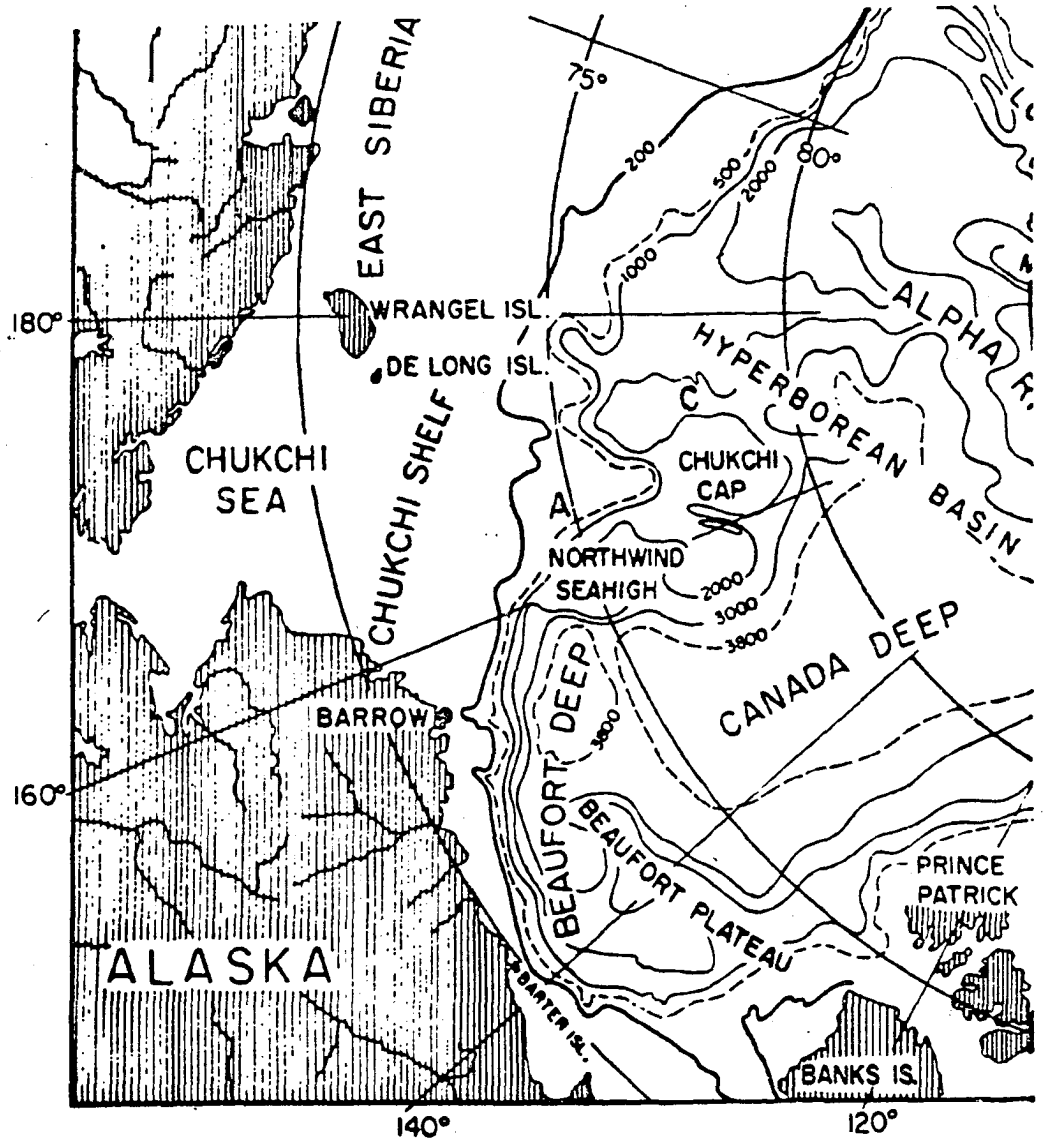

Fig. 9. A chart showing the bottom contours of a section of the Arctic Ocean. The letter *C* denotes the positions of floating ice station Charlie on November 11, 1959, and the letter *A* denotes the position of Arlis on February 20, 1961.

Fig. 6.13 The site (a) of observations by Swift and Hessler (1964). Contours are in meters.

The model is thus consistent with the data of Swift and Hessler, although it cannot explain quantitatively the disparity between actual and effective ocean depths. The sloping basement reduces the effective depth required by a model with a horizontal sea floor, at least at low frequencies; at higher frequencies, there is little difference from the results obtained over a horizontal floor. A smaller difference between the conductivities of ocean and basement would reduce the effective depth of the sea floor still further.

Novysh and Fonarev's (1963, 1966) data pertained to an ocean with depths varying from 80 m to 3 km (see §2.6.1). At the shallower depths we expect a sloping sea floor to exert an influence on the frequency response, but the observations at these depths were made over the East Siberian Sea where the slope is considerably less than 1°.

In their 1966 paper, Novysh and Fonarev present a graph of the dependence of E/H on the depth h, for periods of 6 min. (See Fig. 6.14). The horizontal scale (in km) may be converted to our H by multiplying by 0.26. The Cagniard-Tikhonov theory for a horizontally stratified medium shows good agreement with the results at depths below about 1 km. At shallower depths, however, there is a decrease in the relationship to well below the values resulting from a horizontal sea floor, just as we have calculated in Fig. 6.11. Quantitative comparison cannot be made, however, since our calculations do not extend to the necessary values of α, near 0.1°.

We conclude this comparison with observational results by referring to Berdichevskii's (1961) studies. He found good quantitative

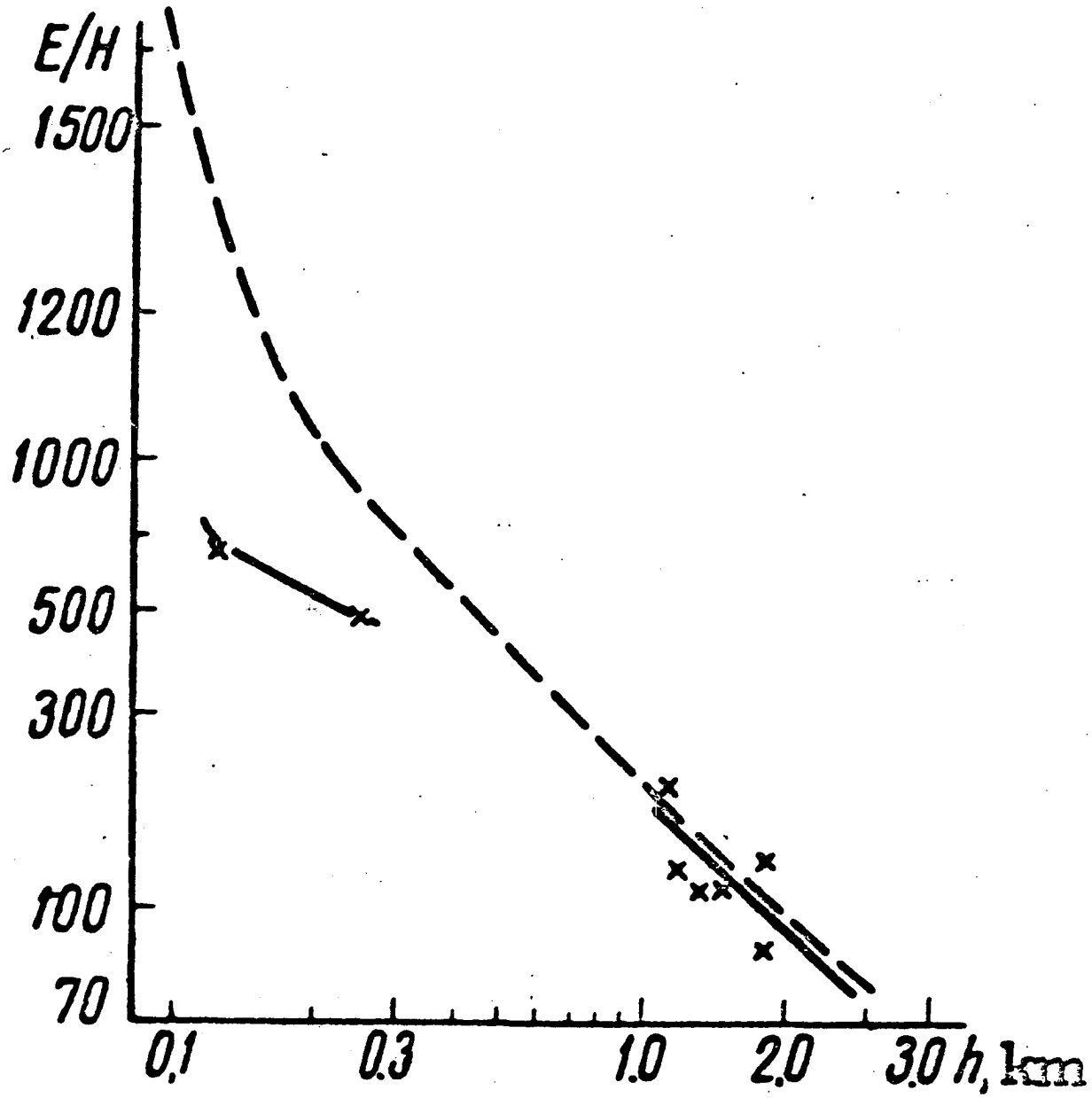

Fig. 6.14 The depth response of the impedance over an ocean at a period of 6 min. The dashed line represents the impedance calculated from the Cagniard-Tikhonov theory for two layers. To convert the scale from h in (km) to H, multiply h by 0.259 (Fonarev, 1966).

agreement between data obtained by geophysical prospectors working in regions with sloping bedding planes, and his calculations for a non-conducting basement (see §2.6.2).

CHAPTER VII

SUMMARY AND CONCLUSIONS

In the preceding chapters several coastal models have been studied to determine the influence of topographical features on the electromagnetic fields at the earth's surface. The frequency of the fields under study has been restricted to the range 10^{-4} to 10^{3} cps, thus avoiding the low frequency contribution from the conducting mantle, and the high frequency contribution from the displacement currents. The frequency range studied includes micropulsations and also the frequencies used by exploration geophysicists in magneto-telluric prospecting.

The results deduced in the preceding chapters have been combined with those of previous investigators to determine how a horizontal ocean floor at various depths influences the electric and magnetic fields near a coastline - the coastal anomaly in these fields constitutes the so-called "coast effect". This term usually refers to the behaviour of the fields near of a continental shoreline, but we have also studied the fields near a narrow promontory of great length, for various ocean depths. Finally we examined the influence of a sloping ocean floor on the fields measured at the ocean surface remote from a coastline such as for instance, on an ice-island. In §5.4 we compared the 'rectangular' models for specific examples. The effects of sloping and horizontal ocean floors were contrasted in §6.3 (Fig. 5.11).

Previous studies have been concerned with only the electric field normal to a fault or coastline; our analysis treats, in addition, the tangential electric field and so enables the polarization of the E-field to be deduced. We have also studied the behaviour of the vertical magnetic field for each model.

The field anomalies calculated for an infinitely deep fault-like shoreline are shown in Figs. 4.3 and 4.4. Over the land the normal electric field is not greatly affected, but the magnitude of the offshore field is suppressed in comparison with the asymptotic field at great distances from the shore. The tangential electric field is modified over both media; it is suppressed over the land and enhanced over the sea. The polarization of the electric field over the land is predominantly normal to the coast, but over the sea it is predominantly parallel; linearity is markedly increased near the shoreline.

The presence of a non-conducting basement at shallow depth (i.e. small in comparison with the penetration depth) enhances the electric fields and causes a more pronounced influence of the shoreline on the electric field tangential to the shore (Fig. 4.3). The coast effect on the normal field, however, is reduced by the presence of a basement. The polarization of the electric field to seawards becomes more linear and is oriented more nearly parallel to the shore in the presence of a basement (Fig. 4.4). The polarization of the field on the land side is not changed so markedly, although it is more nearly normal to the shore line and is more nearly linear.

A basement layer at shallow depth enhances the coast anomaly in the vertical magnetic field, but causes a sharper decrease in the frequency response towards higher frequencies than would be obtained with basements at deeper levels.

If the fields are measured near or on a parallel-sided peninsula of sufficient length that the end effects are negligible, instead of near a "continental" shore line, the surface fields are further modified. The tangential electric field over the land is suppressed and the normal electric field is enhanced. The magnitude of the departure from the fault-like field behaviour near a continental shore line is more pronounced for narrower dykes. The polarization of the electric fields is more linear over a narrow dyke than over a broad one (Figs. 5.5, 5.10). At sea, however, the polarization is significantly dependent on the depth of the sea bed when the dyke is narrow - contrast the behaviour for $Q = \frac{1}{2}\ell\sqrt{\mu_o\omega\sigma_2} = 0.1$ in Figs. 5.5 and 5.10 ($H = h\sqrt{\mu_o\omega\sigma_2} = \infty$ and 0.1 respectively).

The enhancement of the coastal vertical magnetic field is considerably smaller near the shoreline of a narrow dyke than near a continental shore (Fig. 5.9c). If the basement layer is at a shallow depth, however, the coastal enhancement is more pronounced than it is near a deep dyke.

The conditions for the shore line to be 'invisible' to the electromagnetic wave are given in §§4.1.3, 4.2.3, 5.1.3, and 5.2.3. The conditions depend on the geographical structure and the field component under observation; the observer must be at least one, and in

some cases as much as six or more penetration depths distant from the coastline (see Figs. 4.3 and 5.9). Generally the parallel (E_x) component is the more sensitive component of the electric field, and usually the phase of a particular component is more sensitive than the magnitude.

We would expect that a long narrow promontory or island would cause the electromagnetic fields to approximate those of our model, provided the observation point is distant at least five penetration depths from each end. At a frequency of 1 cps, and a conductivity ratio (with respect to the sea) of $\varepsilon^2 = 10^{-2}$, the total length must be 20 km or more; however, the distortion by the 'end effects' from the fields of our model would not be great, even for a total length of 5 km, especially if the phases are not measured.

In most physical situations, the sea floor slopes away from the shoreline at an angle, rather than falling suddenly to a constant depth. The effect of such a geometry on the electromagnetic fields near the coast is difficult to calculate mathematically. However, the influence of an inclined ocean floor at a site remote from a coastline (such as an ice-island) has been determined by extending the method of Berdichevskii (1961). Berdichevskii assumed a non-conducting basement, while we have allowed for finite resistivity.

The electric fields and the vertical magnetic field are enhanced over the shallower depths, but the normal horizontal magnetic component is more complicated (Fig. 6.8). The fields are affected more greatly by smaller inclinations of the sea bed, but the effect becomes less significant as the conductivity ratio ε^2 approaches unity. When the

ratio is smaller than about 10^{-2}, the basement may be treated as non-conducting; this limiting ratio decreases slightly with decreasing slope.

The polarization of the electric field indicates a transition between the strong normal orientation of the land field and the strong tangential orientation of the fields offshore over relatively deep water (cf. Figs. 4.4, 6.9). The gradually sloping sea floor forms a deepening wedge of highly conducting sea and the effective conductivity thus changes from a constant low value on land to a constant high value over deep ocean. The electric field responds to this effective transition in conductivity and its polarization changes gradually across the region, showing a strong normal component close to the shore. The width of the transition is perhaps ten penetration depths being greater for smaller slopes ie. the orientation of the polarization ellipses changes more rapidly with increasing distance over a more steeply sloping sea bed (Fig. 6.9). Observations by Wescott (1967) over the very shallow Arctic Ocean offshore from Barrow, Alaska, demonstrated the inshore portion of this transition: for a distance of about 3 km offshore there is a strong normal component in the polarization. His data were not spectrally resolved, however, and are probably dominated by longer periods than those to which our calculations apply quantitatively.

Swift and Hessler (1964) and Novysh and Fonarev (1966) both compare their observations over the Arctic Ocean with theories assuming horizontal basements. In both cases, over ocean depths of 500 m or less, there is a discrepancy between the calculated and actual depths.

The presence of an inclined sea floor reduces the effective calculated depth; our theory is therefore in qualitative agreement with their observations (compare Figs. 6.11 and 6.14) but exact quantitative comparison cannot be made.

The determination or estimation of the electric and magnetic fields for the topographical models discussed in this work has been possible because of simplifications that have reduced the problems from three to two dimensions. However, the equation governing the fields (eq. 3.3) is a vector partial differential equation, and most of the geometries occurring in nature are also three dimensional (islands, lakes, bays, promontories). The solutions of such boundary problems are very difficult, even numerically. Yet knowledge of the influence of a sharply curving coastline on the fields is important and a method of solution or approximation would be most useful.

Ashour and Chapman (1965) determined the magnetic field about a non-conducting circular island in a conducting ocean. Steady electric current flow would be diverted by the island in the same way as would plane hydrodynamic flow past a circular obstacle. However, their solution does not apply to time-varying fields with the periods studied in this work - e.g., for an island of 10 km, eq. (3.3) indicates the transient term to be negligible for periods longer than about 40 mins. At shorter periods the frequency variation becomes important.

In our treatment of the inclined layer problem we have excluded the coastal region. An extension of the theory to include this region

would be very useful; the approach of Neves (1957) in this respect would have been of more interest had his boundary conditions been more realistic. Likewise the extension of the source theory of Price (1962) to allow for a sloping basement would be valuable in treating problems such as those encountered by Swift and Hessler, and Fonarev and his colleagues.

As an immediate extension from this work, a small item which needs completion is the study of the fields near faults and dykes of intermediate depth. Our calculations of Chapters IV and V were made for H ($= h\sqrt{\mu_o \omega \sigma_2}$) = 0.1, ∞, and the depth and frequency response curves are consequently incomplete. [D'Erceville and Kunetz (1962), and Rankin (1962) have studied the normal (E_y) component of the electric field at various depths, but not the other field components.] The computation would involve the calculation of the relations in Tables 4.5 and 5.4 on a computer, instead of using the shallow layer approximations of Tables 4.5 and 5.5 as we have done.

The approximate boundary condition (iii) of Table 3.2 (see also App. 4) necessarily prevents study of the normal magnetic field at the surface. The variation is probably small, but the restriction must be removed to study its behavior.

BIBLIOGRAPHY

Abramowitz, M., I. A. Stegun. "Handbook of Mathematical Functions." (Nat. Bureau Stand., App. Maths. Ser. 55, USGPO, 1964).

Airey, J. R. "Toroidal Functions and the Complete Elliptic Integrals." Phil. Mag [7], 19, 177-188, 1935.

Akasofu, S. "The Ring Current and the Outer Atmosphere." J. Geophys. Res., 65, 535-543, 1960.

Akasofu, S. "The Main Phase of Magnetic Storm and the Ring Current." Space Sci. Rev., 2(1), 91-135, July, 1963.

Akasofu, S. "Dynamic Morphology of Auroras." Space Sci. Rev., 4(4), 498-540, June, 1965.

Akasofu, S. "The Development of Geomagnetic and Auroral Storms." J. Geomag. Geoelec., 18(2), 109-123, 1966(a).

Akasofu, S. "Electrodynamics of the Magnetosphere: Geomagnetic Storms." Space Sci. Rev., 6(1), 21-143, 1966(b).

Akasofu, S. and S. Chapman. "The Simultaneous Development of the Main Phase (DR) and of Polar Magnetic Storms (DP)." J. Geophys. Res., 68, 3155-3158, 1963(a).

Akasofu, S. and S. Chapman. "The Development of the Main Phase of Magnetic Storms." J. Geophys. Res., 68, 125-129, 1963(b).

Akasofu, S., S. Chapman and A. B. Meinel. "The Aurora." Handbuch der Physik, 49/1, (Geophysics IX/1) 1964.

Andriyenko, D. A. "Results of Determinations of Auroral Heights from Large Scale Photographs Obtained at Tixie Bay." Geom. i Aeron., 5(3), 450-459 (Russ.) 346-352 (Eng.) 1965(a).

Andriyenko, D. A. "Results of Auroral Height Determinations at Tixie Bay in 1964." Geom. i. Aeron., 5(5), 878-883, (Russ.) 684-688 (Eng.) 1965(b).

Anishenko, G. N. "On the Principles of Complex Interpreation of M.T.P. Curves in Areas with Inclined Reference Horizon." Izvestia: Fiz. Zemli., 12, 61-66, 1965. Eng. Trans. Physics of the Earth, 12, 815-818, December, 1965.

Ashour, A. A. "The Induction of Electric Currents in a Uniform Circular Disc." Q. J. Mech. Appl. Maths., 3(1), 119-128, 1950.

Ashour, A. A. "Electromagnetic Induction in Finite Thin Sheets." Q. J. Mech. Appl. Maths., 18(1), 73-86, February, 1965(a).

Ashour, A. A. "The Coastline Effect on Rapid Geomagnetic Variations." Geophys. J.R.A.S., 10(2), 147-162, November 1965(b).

Ashour, A. A. "On the Transformation of Coordinates by Inversion and its Application to Electromagnetic Induction in a Thin Perfectly Conducting Hemispherical Shell." Proc. Lond. Math. Soc., 15(3), 357-376, July, 1965(c).

Ashour, A. A. and S. Chapman. "The Magnetic Field of Electric Currents in an Unbounded Plane Sheet, Uniform Except for a Circular Area of Different Uniform Conductivity." Geophys. J.R.A.S., 10(1), 31-44, 1965.

Ashour, A. A. and A. T. Price. "The Induction of Electric Currents in a Non-Uniform Ionosphere." Proc. Roy. Soc. Lond. (A), 195, 198-224, 1948.

Baird, H. F. "A Preliminary Investigation of Some Features of Four Magnetic Storms Recorded at Seven Magnetic Observatories in the Pacific Ocean Region During 1924." Thesis, Univ. of New Zealand, 1927.

Baños, A. "Dipole Radiation in the Presence of a Conducting Half Space." Pergamon Press, 1965.

Baranskii, L. N. and N. L. Naumenkov. "Observations on Earth Currents at Mirny and Oasis Stations in 1957." Inf. Bull. Sov. Antarctic Exped. No. 14, 74-78, 1959. Eng. Transl. Elsevier, Amsterdam, 1, 120-123, 1964.

Barber, N. F. "The Magnetic Field Produced by Earth Currents Flowing in an Estuary or Sea Channel." M.N.R.A.S. Geophys. Suppl., 5, 258-269, 1948.

Barsukov, O. M. and K. Yu. Zybin. "On the Problem of the Non-Perpendicularity of Vectors of E, H Variations of the Earth's Natural Electromagnetic Field." Communication Concerning Sci. Works in the Field of Geomag. and Aeronomy during 1958-1959. Report compiled by Geomag. and Aeronomy Sect. of Committee on Geodesy and Geophys. of USSR, Acad. Sci., Acad. Sci. Press Moscow, 1960. Eng. Transl. NASA, TT F-60, 28-29, 1961.

Berdichevskii, M. N. "Electrical Surveying by Means of Telluric Currents." Gostoptekhizdat, Moscow, 1960. Eng. Transl. (i) J.E.S. Bradley. Nat. Lending Library for Sci. and Tech., Yorks, U. K. 1963. (ii) G.V. Keller, Q. Colorado School of Mines, 60(1), 1965.

Berdichevskii, M. N. "The Magneto-Telluric Field in a Horizontally Inhomogeneous Medium." App. (Prikladnaya) Geophys. No. 31, 136-164, 1961.

Berdichevskii, M. N., Ye. D. Bryunelli. "Theoretical Premises of Magneto-Telluric Profiling." Bulletin (Izvestia) Acad. Sci. USSR, Geophys. Ser. No. 7, 757-762 (Eng.), 1061-9 (Russ.), 1959.

Berdichevskii, M. N., Ye. D. Bryunelli, A. Ye. Lantsov, O. M. Raspopov. "Using Natural Electromagnetic Variations for Investigation of the Earth's Upper Layers." Problems in Geophysics, Transactions of the Leningrad State University. (Uchenye Zapiski), Physics and Geology Series, 303(13), 49-55, 1962, Eng. Transl. NASA N64, 11484-11499, 10-17, April, 1963.

Bhattacharyya, B. K. "Electromagnetic Induction in a Two-Layered Earth." J. Geophys. Res., 60, 279-288, 1955.

Bhattacharyya, B. K. "The Field on the Earth's Surface Due to a Transient Electromagnetic Disturbance." J. Technol., 1, 151-162, 1956.

Bhattacharyya, B. K. "Electromagnetic Fields of a Transient Magnetic Dipole on the Earth's Surface." Geophys., 24, 89-108, 1959.

Bhattacharyya, B. K. "Electromagnetic Fields of a Vertical Magnetic Dipole Placed Above the Earth's Surface." Geophys., 27, 408-425. June, 1963.

Bomke, H. A. "The Relation of Magnetic Micropulsations to Electric Current and Space-Charge Systems in the Lower Ionosphere." J. Geophys. Res., 67(1), 177-181, 1962.

Bondarenko, A. P. "Relation Between Earth Currents and Geomagnetic Variations." Doklady AN SSSR, 89(3), 443-445, 1953(a).

Bondarenko, A. P. "Electric Field Induced by Vertical Component of Geomagnetic Variations." Doklady AN SSSR, 90(3), 367-370, 1953(b).

Booker, H. G. and C. Clemmow. "Concept of an Angular Spectrum of Plane Waves and its Relation to That of Polar Diagram and Aperture Distribution." Proc. Inst. Elec. Eng. [3], 97(3), 11-17, 1950.

Bostick, F. X. and H. W. Smith. "An Analysis of the Magneto-Telluric Method for Determining Sub-surface Resistivities." Elec. Eng. Lab. Univ. of Texas, Austin, Report No. 120, 1961.

Bostick, F. X. and H. W. Smith. "Investigation of Large Scale Inhomogeneities in the Earth by the Magneto-telluric Method." Proc. I.R.E., 50, 2339-2346, 1962.

Brekhovskikh, L. M. "Waves in Layered Media." Acad. Sci. Press. USSR, 1957. Translated by D. Liebermann, ed. by R. T. Beyer. Acad. Press, 1960.

Bromwich, T. J. I, A. "An Introduction to the Theory of Infinite Series." (MacMillan, London 2nd ed. 1926, repr. 1959).

Bruckshaw, J. "Experiments on Conducting Laminae in Periodic Magnetic Fields." Proc. Phys. Soc., 48, 63-74, 1936.

Bullard, E. C. and H. Gellman. "Homogeneous Dynamos and Terrestrial Magnetism." Phil. Trans. Roy. Soc., A247, 213-278, 1954.

Bullard, E. C., R. G. Mason. "The Magnetic Field Over the Oceans." in "The Sea." Vol. 3. "The Earth Beneath the Sea." Ed. M. N. Hill, (Interscience, N. Y., 1963.).

Byrd, P. F. and M. D. Friedmann. "Handbook of Elliptic Integrals for Engineers and Physicists." Springer, Berlin, 1954.

Cagniard, L. "La Prospection Géophysique." Paris, Presses Universitaires, 1950.

Cagniard, L. "Basic Theory of the Magneto-Telluric Method of Physical Prospecting." Geophysics., 18(3), 605-635, 1953(a).

Cagniard, L. "Principe de la Méthode Magnéto-Tellurique, Nouvelle Méthode de Prospection Géophysique." Ann. Geophys., 9(2), 95-125, 1953(b).

Cagniard, L. "Electricité Tellurique." Handbuch der Physik, 47, 407-469, 1956.

Campbell, W. H. and S. Matsushita. "Auroral Zone Geomagnetic Micropulsations with Periods of 5 to 30 seconds." J. Geophys. Res., 67(2), 555-573, February, 1962.

Cantwell, T. "Detection and Analysis of Low-Frequency Magneto-Telluric Signals." Thesis M.I.T. Cambridge, Massachusetts, 1960.

Carslaw, H. S. "Introduction to the Theory of Fourier Series and Integrals." (3rd Ed. 1930, reprinted Dover, New York).

Chapman, S. "Solar Plasma, Geomagnetism and Aurora." Gordon and Breach, New York, 1964.

Chapman, S. and J. Bartels, "Geomagnetism." (O.U.P. 3rd Ed. 1962), 1940.

Chapman, S. and A. T. Price. "The Electric and Magnetic State of the Interior of the Earth as Inferred from Terrestrial Magnetic Variations". Phil. Trans. Roy. Soc. [A], 229, 427-460, 1930.

Chapman, S. and T. T. Whitehead. "The Influence of Electrically Conducting Material Within the Earth on Various Phenomena of Terrestrial Magnetism." Trans. Camb. Phil. Soc., 22, 463-482, 1923.

Chetaev, D. N. "The Determination of the Anisotropy Coefficient and the Angle of Inclination of a Homogeneous Anisotropic Medium, by Measuring the Impedance of the Natural Electromagnetic Field." Izv. (Bulletin) AN SSSR. Geof. Ser., 4, 617-619 (Russ.), 407-408 (Eng.), 1960.

Chetaev, D. N. "A New Method of Solving Problems of Electrodynamics of Anisotropic Media." Fiz. Zemli, 4, 45-51, 1966.

Clemmow, P. C. "The Plane Wave Spectrum Representation of Electromagnetic Fields." Pergammon, 1966.

Cole, K. D. "Magnetic Storms and Associated Phenomena." Space Sci. Rev., 5(6), 699-770, 1966.

Coode, A. M. "Electric and Magnetic Fields Associated with a Vertical Fault." Thesis. Inst. Earth Sci. Univ. B. C. Vancouver, 1963.

Cornwall, J. M. "Cyclotron Instabilities and Electromagnetic Emission in the Ultra-Low Frequency and Very-Low-Frequency Ranges." J. Geophys. Res., 70(1), 61-69, January, 1965.

Christoffel, D. A., J. A. Jacobs, E. J. Jolley, J. K. Kinnear, J. A. Shand, "The Fraser Delta Experiment of 1960." Pacific Naval Lab., Esquimalt, B. C. Report 61-5, August, 1961.

D'Erceville, I. and G. Kunetz. "The Effect of a Fault on the Earth's Natural Electromagnetic Field." Geophys., 27(5), 651-665, 1962.

de Jager, C. "The Sun as a Source of Interplanetary Plasma." Space Sci. Rev., 1(3), 487-521, 1963.

de Wet, J. M. "Numerical Methods of Solving Electromagnetic Induction Problems with Applications to the Theory of Electric Currents Induced in the Oceans and their Influence on Observed Geomagnetic Variations." Thesis. Univ. Lond., 1949.

de Witt, C., J. Hieblot, A. Lebeau. "Geophysics; The Earth's Environment." (Gordon and Breach, New York, 1963).

Dosso, H. W. "The Magnetic Field at the Surface of a Stratified Flat Conductor in the Field of Plane Waves with Applications to Geophysics." Canad. J. Phys., 40(11), 1583-1592, November, 1962.

Dosso, H. W. "The Electric and Magnetic Fields in a Stratified Flat Conductor for Incident Plane Waves." Canad. J. Phys., 43(5), 898-909, May, 1965.

Dosso, H. W. "A Plane Wave Analogue Model for Studying Electromagnetic Variations." Canad. J. Phys., 44(1), 67-80, January 1966(a).

Dosso, H. W. "A Multi-layer Conducting Earth in the Field of Plane Waves." Canad. J. Phys., 44(1), 81-89, 1966(b).

Dosso, H. W. "Further Results for a Multi-layered Conducting Earth in the Field of Plane Waves." Canad. J. Phys., 44(5), 1197-1199, May, 1966(c).

Dosso, H. W. "Analogue Model Measurements for Electromagnetic Variations Near Vertical Faults and Dykes." Canad. J. Earth Sci., 3(3), 287-304, 1966(d).

Dosso, H. W. "The Electric and Magnetic Fields at the Surface of a Flat Conducting Earth in the Near Field of an Oscillating Line Current." Canad. J. Phys., 44(8), 1923-1932, August, 1966(e).

Dosso, H. W. "Analogue Model Measurements for Electromagnetic Variations near a Coastline." Canad. J. Earth Sci., 3(7), 917-936, December, 1966(f).

Dosso, H. W. and J. E. Locken. "The Resultant Magnetic Field at the Surface of a Flat Conductor for an Incident Plane-Wave." Pacific Naval Lab. Report No. 61-1, February, 1961.

Dougall, J. "The Determination of Green's Function by Means of Spherical Harmonics." Proc. Edinburgh Math. Soc., XVIII, 33-84, 1899-1900.

Duffus, H. J., J. A. Shand and C. S. Wright. "Influence of Geological Features on Very Low Frequency Geomagnetic Fluctuations." Nature, 186(4719), 141-142, April, 1960(a).

Duffus, H. J., J. A. Shand and C. S. Wright. "Fluctuations of the Geomagnetic Field in the Frequency Range 0.02 to 3 cps." Pacific Naval Lab., Esquimalt B.C. Rep. 60-7, July, 1960(b).

Duffus, H. J., J. A. Shand and C. S. Wright. "Short-Range Spatial Coherence of Geomagnetic Micropulsations." Canad. J. Phys., 40 218-225, 1962.

Duffus, H. J., J. A. Shand, C. S. Wright, P. W. Nasmyth and J. A. Jacobs. "Geographical Variations in Geomagnetic Micropulsations." J. Geophys. Res., 64(5), 581-583, May, 1959.

Duffus, H. J., J. K. Kinnear, J. A. Shand and C. S. Wright. "Spatial Variations in Geomagnetic Micropulsations." Canad. J. Phys., 40, 1133-1152, 1962.

Duma, D. P. "Geographical Distribution of Stable Auroral Forms in the Region of Tiksi Bay." IGY Bulletin (of IGY Organizing Committee; Presidium of the Acad. of Sciences for the Ukranian SSR) Kiev, No. 3, 30-33, 1961. Eng. Transl. E. R. Hope; DRB Canada, T403R, November, 1964.

Dwight, H. B. "Table of Integrals and Other Mathematical Data." (MacMillan, New York, 4th ed., 1961).

Elsasser, W. M. "The Earth's Interior and Geomagnetism." Rev. Mod. Phys., 22, 1-35, 1950.

Elsasser, W. M. "Hydromagnetic Dynamo Theory." Rev. Mod. Phys., 28, 135-163, 1956.

Erdélyi, A., W. Magnus, F. Oberhettinger, F. G. Tricomi. The Bateman Manuscript Project: "Tables of Integral Transforms" (TIT: 2 Vols., 1954) "Higher Transcendental Functions" (HTF: 3 Vols., 1953, 1953, 1955), McGraw-Hill, New York.

Fettis, H. E., J. C. Caslin. "Tables of Elliptic Integrals of the First Second, and Third Kind." Aerospace Applied Maths. Res. Labs., Wright-Patterson AFB, Ohio, Rep. ARL 64-232, December, 1964.

Fields, E. C. and C. Greifinger. "Transmission of Hydromagnetic Micropulsations Through the Ionosphere and Low Exosphere." J. Geophys. Res., 70(19), 4885-4899, October, 1965.

Fleming, J. A. "Terrestrial Magnetism and Electricity." 270-307, McGraw-Hill, 1939, 2nd ed., Dover, New York, 1949.

Fletcher, A., J. C. P. Miller, L. Rosenhead, L. J. Comrie. "An Index of Mathematical Tables." 2 Vols. , Addison-Wesley, 2nd ed., 1962.

Fonarev, G. A. "Marine Telluric Currents and Their Relationship to Magnetic Variations." Geomag. i. Aeron., 1(1), 82 (Russ.), 77-80, (Eng.), 1961(a).

Fonarev, G. A. "Variations in Marine Telluric Currents." Geomag. i. Aeron., 1(3), 417-420 (Russ.), 374-377 (Eng.), 1961(b).

Fonarev, G. A. "Some Data on Telluric Currents in the Barents Sea." Geomag. i. Aeron., 1(4), 599 (Russ.), 530-535 (Eng.), 1961(c).

Fonarev, G. A. "Vertical Electric Currents in the Sea." Geomag. i. Aeron., 3(4), 784-785 (Russ.), 636-637 (Eng.), 1963.

Fonarev, G. A. and V. V. Novysh. "Some Results of Telluric Current Measurements at Station North Pole-10 in 1963." Doklady AN SSSR, 160(2), 332-333, 1965, Eng. Trans. Doklady-Geophys. Section 1-2, 1965.

Fonarev, G. A. and V. I. Ivanov. "Magnetic Fields of Telluric Currents in the Sea." Geomag. i. Aeron., 6(3), 544-547, 1966.

Fournier, H. G. "La Spectrographie directionelle magneto-tellurique a Garchy (Nievre)." Ann.de Geophys., 19(2), 138-148, 1963.

Fournier, H. G. "Essai d'un historique des connaissances magneto-telluriques." Institut de Physique du Globe, Faculté des Sciences, Université de Paris, No. 17, September, 1966.

Gaskell, T. F. (ed.) "The Earth's Mantle." (Academic Press, New York) 1967.

Gautschi, W. and W. F. Cahill. "Exponential Integral and Related Functions." in Abramowitz and Stegun (1964), 227-252, 1964.

Gradshteyn, I. S. and I. M. Ryzhik. "Tablitsy Integralov, Summ, Ryadov i Proievedeniy." 4th Ed., Moscow, 1963, prepared by Yu. V. Geronimus and M. Yu. Tseytlin, Eng. Trans. by A. Jeffrey, "Tables of Integrals, Series, and Products." Academic Press, New York, 1965.

Griffiths, D. H. and R. F. King. "Applied Geophysics for Engineers and Geologists." Pergamon Press, London, Commonwealth & International Library, 1965.

Gröbner, W. and N. Hofreiter. "Integraltafel" (2 Vols., Springer, 3rd. ed., 1961).

Hardy, G. H. and M. Riesz. "The General Theory of Dirichlet's Series." Camb. Tract, No. 18, CUP, 1915.

Heirtzler, J. R. "Simultaneous Geomagnetic Measurements on an Island Surface and 1,000 Feet Below." Columbia Univ., Lamont Geological Observ., New York, Tech. Rep. No. 2, CU-2-63, Geology, 1963, see also: Trans. AGU, 46(1), 56, March, 1965.

Hess, W. N. (ed.). "Introduction to Space Science." Gordon and Breach, New York, 1965.

Hess, W. N. and G. D. Mead. "Particles and Fields Research--a Bibliography with Author Index." NASA Rep. X-640-65-37, 1966.

Hess, W. N., G. D. Mead, N. P. Nakada. "Advances in Particles and Fields Present in the Satellite Era." Rev. Geophys., 3(4), 521-570, November, 1965.

Hessler, V. P. "Characteristics of Telluric Currents at Land and Sea-Based Stations." J. Phys. Soc. Jap., 17, Suppl. A-1, 33-34, 1962.

Hessler, V. P. and R. R. Heacock. "Earth Currents at the Auroral Zone." Univ. Alaska Rep. UAG R-133, December, 1962.

Hide, R. "Hydrodynamics of the Earth's Core." In L. H. Ahrens, K. Rankama, S. K. Runcorn, Physics and Chemistry of the Earth, 1, 94-137 (Pergamon Press, 1965).

Hide, R. and P. H. Roberts. "The Origin of the Main Geomagnetic Field." in L. H. Ahrens, F. Press, K. Rankama, S. K. Runcorn, Physics and Chemistry of the Earth, 4, 27-98, (Pergamon Press, London, 1961).

Hill, M. N. and C. S. Mason. "Diurnal Variation of the Earth's Magnetic Field at Sea." Nature, 195(4839), 365-366, July, 1962.

Hines, C. O., I. Paghis, T. R. Hartz, J. A. Fejer. "Physics of the Earth's Atmosphere." (Prentice-Hall, New Jersey, 1965).

Hodgeman, C. D. "Handbook of Physics and Chemistry." 44th Edition, Chem. Rubber Pub. Co., Cleveland, 1963.

Hoffman, A. A. J. and C. W. Horton. "An Analysis of Some Magneto-Telluric Records from Tikhaya Bay USSR." J. Geophys. Res., 71(16), 4047-4052, August, 1966.

Horton, C. W. "Direction of Geomagnetic Fluctuations at Some Soviet Arctic Stations." J. Geomag. Geoelect., 17, 499-505, 1965.

Hutton, R. "The Solar and Lunar Daily Variations of Earth Currents Near the Magnetic Equator." JATP, 24, 673-680, 1962.

IAGA, Berkeley, IUGG, Comptes Rendus, 13th Assembly, Berkeley, August, 1963, Resolution No. 98, pp. 177 and 202.

Ivanov, A. G. "Polar Disturbances in Earth Currents." Doklady AN SSSR, 81(5), 807-810, 1951.

Jackson, J. D. "Classical Electrodynamics." Wiley, New York, 1962.

Jacobs, J. A. "The Earth's Interior." Handbuch der Physik, 47, 364-406, 1965.

Jacobs, J. A., Y. Kato, S. Matsushita, V. Troitskaya. "Classification of Micropulsations." J. Geophys. Res., 69(1), 180-181, January, 1964.

Jacobs, J. A. and K. Sinno. "World-Wide Characteristics of Geomagnetic Micropulsations." Geophys. J. R.A.S., 3, 333-353, 1960.

Jacobs, J. A. and K. O. Westphal. "Geomagnetic Micropulsations." in L. H. Ahrens, F. Press, S. K. Runcorn, Physics and Chemistry of the Earth, 5, 157-224, 1964.

Japanese National Report to 14th Assembly of IAGA, IUGG, J. Geomag. Geoelec. (Japan), 19(3), Suppl. 1-29, 1967.

Jones, F. W. and L. P. Geldart. "Vertical Telluric Currents." Earth and Planet. Sci. Letters, 2(1), 69-74, January 1967.

Kato, Y. "Investigation of the Magnetic Properties of the Rocks Constituting the Earth Crust." 1st Paper, Sci. Rep. Tôhoku Univ. Ser. I, 27(1), 91-100, July, 1938.

Kato, Y. 2nd Report "On the Susceptibility of Rock." Part I, Sci. Rep. Tôhoku Univ. Ser. I, 29(4), 602-628, 1940.

Kato, Y. 3rd Report "On the Susceptibility of Rock." Part II, Sci. Rep. Tôhoku Univ. Ser. I., 29, 629-647, 1941.

Kato, Y. and T. Kikuchi. "On the Phase Difference of Earth Currents Induced by the Changes of the Earth's Magnetic Field." Part I, Sci. Rep. Tôhoku Univ. [5], Geophys., 2, 139-141, 1950(a).

Kato, Y. and T. Kikuchi, "On the Phase Difference of Earth Currents Induced by the Changes of the Earth's Magnetic Field." Part II Sci. Rep. Tôhoku Univ. [5], Geophys., 2, 142-145, 1950(b).

Kato, Y. and K. Yokoto. "Corrected Paper on the Phase Difference of Earth Currents Induced by the Changes of the Earth's Magnetic Field." Sci. Rep. Tôhoku Univ. [5], 5, 41-43, 1953.

Kato, Y. and T. Watanabe. "A Summary of Observational Knowledge of the Geomagnetic Micropulsation." Sci. Rep. Tôhoku Univ. [5], Geophys., 8, 157-185, 1957.

Kertz, W. "Leitungsfähiger Zylinder im Transversalen magnetischen Wechselfeld." Gerlands Beitrage Geophys., 69, 4-28, 1960.

King, J. W. and W. S. Newman. "Solar Terrestrial Physics." (Acad. Press, New York) 1967.

King, R. J. and S. W. Maley. "Model Experiments on Propagation of Ground Waves Across an Abrupt Boundary at Perpendicular Incidence." J. Res. N.B.S., Radio Sci., 69D(10), 1375-1381, October, 1965.

King, R. J. and S. W. Maley. "Model Experiments on Propagation of Ground Waves Across an Abrupt Boundary at Oblique Incidence." J. Res. N.B.S., Radio Sci., 1(1), 111-116, January, 1966.

King, R. J. and W. I. Tsukamoto. "Ground Wave Propagation Across Semi-Infinite Strips and Islands on a Flat Earth." Radio Sci. [New Series], 1(7), 775-788, July, 1966.

Knopp, K. "Theory and Application of Infinite Series." (Blackie, London, 2nd English ed., (1961) of 4th German ed. (1951). Transl. R. C. H. Young).

Kovtun, A. A. "The Magneto-Telluric Investigation of Structures Inhomogeneous in Layers." Izv. (Bulletin) AN SSSR, Geof. Ser. No. 11, 1663-1667, (Russ.), 1085-1087 (Eng.), 1961.

Kunetz, G. and J. Chastenet de Géry. "La Representation Conforme et divers problems de potential." Rev. de l'Inst. Franc. du Petrole Ann. Combust. Liquides, 11(10), 1179-1192, October, 1956.

Kunetz, G. and J. Chastenet de Géry. "Exemples d'application de la Representation Conforme a l'Interpretation du Champ Tellurique." Early Papers and History of the European Assoc. of Exploration Geophysics, Europ. Association of Explor. Geophys., 115-131, 1961.

Lahiri, B. N. and A. T. Price. "Electromagnetic Induction in Non-Uniform Conductors and the Determination of the Conductivity of the Earth from Terrestrial Magnetic Variations." Phil. Trans. Roy. Soc. [A], 237, 509-540, 1939.

Lamb, H. "On Electrical Motions in a Spherical Conductor." Phil. Trans. Roy. Soc. Lond., 174, 519-549, 1883.

Lamb, H. App. to A. Schuster, 1889.

Lambert, A. and B. Caner. "Geomagnetic 'Depth Sounding' and the Coast Effect in Western Canada." Canad. J. Earth Sci., 2(5), 485-509, October, 1965.

Landau, L. and E. Lifshitz. "Electrodynamics of Continuous Media." Moscow, 1959, Eng. Transl. J. B. Sykes, J. S. Bell, Pergamon, 1960.

Latka, R. "Modellrechnungen zur Induktion in Elektrisch leitfahigen Untergrund." Z. f. Geophysik, 32, 512-517, 1966.

Law, P. F. and B. M. Fannin. "Radiation from a Current Filament above a Homogeneous Earth with Application to Micropulsations." J. Geophys. Res., 66(4), 1049-1059, April, 1961.

Lawrie, J. A. "Direction of Geomagnetic Fluctuations Near Coastlines." N. Z. J. Geol. Geoph., 8(5), 869-884, 1965.

Lebedev, N. N. "On an Inversion Formula." Doklady AN SSSR, 52, 655-658, 1946.

Le Galley, D. P. "Space Science." (Wiley, New York) 1963.

Le Galley, D. P. and A. Rosen. "Space Physics." (Wiley, New York) 1964.

Lewin, L. "Dilogarithms and Associated Functions." (MacDonald, London), 1958.

Li, Y. S. "The Problem of the Vertical Fault in Telluric Current Prospecting." Geophysics, 28(3), 479-482, 1963.

Lipskaya, N. V. "On Certain Relationships Between Harmonics of the Periodic Variations of the Terrestrial Electric and Magnetic Fields." Izv. (Bull.) AN SSSRGeof. Ser., 1, 41-47, 1953. Eng. Transl. DRB, T175 R, July, 1955, by E. R. Hope.

Lipskaya, N. V. and V. A. Troitskaya. "Natural Alternating Electromagnetic Fields." Archives Acad. Sci. USSR (Fondy AN SSSR), 1955.

Logn, Ö. "Mapping Nearly Vertical Discontinuities by Earth Resistivities." Geophys., 19(4), 739-760, October, 1954.

Lüst, R. "Interplanetary Plasma." Space Sci. Rev., 1, 522-552, 1963.

McCann, C. and A. T. Price. "Magnetotelluric Measurements at Sea." J. Geophys. Res., 70(14), 3514, July, 1965.

MacDonald, K. L. "Penetration of the Geomagnetic Secular Field Through a Mantle with a Variable Conductivity." J. Geophys. Res., 62(1), 117-141, March, 1957.

Mackin, R. J. and M. Neugebauer, (ed.) "The Solar Wind." (Pergamon, London), 1965.

Madden, T. and P. Nelson. "A Defense of Cagniard's Magnetotelluric Method." Project Rep. ONR NR-371-401 Geophys. Lab., MIT Cambridge, March, 1964.

Malkus, W. V. R. "Precessional Torques as the Cause of Geomagnetism." J. Geophys. Res., 68(10), 2871-2886, May, 1963.

Mann, J. E. "Magnetotelluric Theory of the Sinusoidal Interface." J. Geophys. Res., 69(16), 3517-3524, August, 1964.

Mann, J. E. "The Importance of Anisotropic Conductivity for Magnetotelluric Interpretation." J. Geophys. Res., 70(12), 2940-2942, June, 1964.

Mann, J. E. "A Theoretical Magnetotelluric Problem Exhibiting Effects of Lateral Conductivity Variations and Finite Field Dimensions." J. Geophys. Res., 72(11), 2885-2889, June, 1967.

Mansurov, S. M. "Causes of Local Geomagnetic Variations in the Mirny Region." Information Bulletin, Soviet Antarctic Expedition, No. 2, 37-41, 1958. Eng. Transl. Elsevier Pub. Co. Amsterdam, 1, 82-85, 1964.

Mansurov, S. M. "Certain Peculiarities of a Variable Geomagnetic Field in the Region of Mirny South Pole Observatory." Collected Articles Pertaining to Sections III and IV of the IGY Program (Geomagnetism, Earth Currents, Ionosphere), No. 1, 1959; Eng. Transl. NASA Tech. Trans. F-49, 81-84, January, 1961; also Annals of IGY, 11, 104-106, 1961.

Mason, R. G. "Spatial Dependence of Time-Variations of the Geomagnetic Field on Oahu, Hawaii." Trans. AGU, 44, 40, 1963(a).

Mason, R. G. "Spatial Dependence of Time Variations of the Geomagnetic Field in the Range 24 hrs-3 mins. on Christmas Island." Geophysics Department, Imp. Coll. Sci. Technol. Lond., Rep. No. 63-3, November, 1963(b).

Mason, R. G. "The Equatorial Electrojet in the Central Pacific." Ann. Progr. Rep. Marine Physical Lab., Scripps Inst. of Oceanography, Calif. SIO. Rep. 63-13, May, 1963(c).

Matsushita, S. "On the Notation for Geomagnetic Micropulsations." J. Geophys. Res., 68, 4369-4372, 1963.

Matsushita, S. and W. H. Campbell. "Physics of Geomagnetic Phenomena." Academic Press, New York, 1967.

Mitra, S. K. "The Upper Atmosphere." Calcutta Asiatic Society, (2nd ed.), 1952.

Monteath, G. D. "Application of the Compensation Theorem to Certain Radiation and Propagation Problems." Proc. Inst. Elec. Eng., Part 4, 98, 23-30, 1951.

Nabighian, M. N. "The Theoretical Effect of a Sea Coast on the Distribution of Geomagnetic and Telluric Micropulsations when the Presence of the Bottom is Considered." Trans. AGU, 46(1), 57, March, 1965.

Nadubovich, Yu. A. "Problemy Arktiki i Antarktiki", No. 7, 51, 1961.

Nadubovich, Yu. A. "Influence of the Shore Effect on the Geographic Distribution of Auroral Arcs and Bands as Shown by Observations of the Russian Polar Expedition of 1900-1902." Geomag. i. Aeron., 3(3), 502-513 (Russ.), 409-417 (Eng.), 1963.

Nagata, T., T. Oguti and H. Mackawa. "Model Experiments of Electromagnetic Induction Within the Earth." Bull. Earthquake Res. Inst. Tokyo Univ., 33(4), 561-569, December 1955.

Naidu, P. S. "Telluric Response of Geologic Structures." M. Tech. Thesis, Indian Institute Technol. Kharagpur, Calcutta, 1962.

Naidu, P. S. "Telluric Field and Apparent Resistivity Over an Inclined Normal Fault." Canad. J. Earth Sci., 2(4), 351-360, August, 1965.

Ness, N. F. "Earth's Magnetic Field: A New Look." Science, 151(3714), 1041-1052, March, 1966.

Ness, N. F., K. W. Behannon, S. C. Cantarano, C. S. Scearce. "Observations of the Earth's Magnetic Tail and Neutral Sheet at 510,000 Kilometers by Explorer 33." J. Geophys. Res., 72(3), 927-934, February, 1967.

Ness, N. F., C. S. Scearce, S. C. Cantarano. "Probable Observations of the Geomagnetic Tail at 10^3 Earth Radii by Pioneer 7", J. Geophys. Res., 72(15), 3769-3776, August, 1967.

Neves, A. S. "The Magneto-Telluric Method in Two Dimensional Structures." MIT Ph.D. Thesis, 1957.

Niblett, E. R. and C. Sayn-Wittgenstein. "Variations of Electrical Conductivity with Depth by the Magneto-Telluric Method." Geophys. 25(5), 998-1008, 1960.

Nishida, A. "World-Wide Changes in the Geomagnetic Field." Ph.D. Thesis, Univ. B. C., Vancouver, 1962.

Nishida, A. "Ionospheric Screening Effect in Storm Sudden Commencements." J. Geophys. Res., 69(9), 1861-1874, May 1964.

Novysh, V. V. and G. A. Fonarev. "Telluric Currents in the Arctic Ocean." Geomag. i. Aeron., 3(6), 1141-1143 (Russ.), 919-921 (Eng.), 1963.

Novysh, V. V. and G. A. Fonarev. "Some Results of Electromagnetic Investigations in the Arctic Ocean." Geomag. i. Aeron., 6(2), 406-408 (Russ.), 325-327 (Eng.), 1966.

Obayashi, T. "Geomagnetic Storms and Ionospheric Disturbances." J. Radio. Res. Labs., 6(26), 373-514, 1959.

Obayashi, T. "The Streaming of Solar Flare Particles and Plasma Into Interplanetary Space." Space Sci. Rev., 3, 78-108, 1964.

Odishaw, H. "Research in Geophysics." Vol. 1, (MIT Press), 1964.

Osborne, D. G. "Equatorial Electrojet in Ghana." Nature, 193, 567-568, 1962.

Ohshio, M. "Solar Flare Effect on Geomagnetic Variation." J. Radio. Res. Labs., 11(58), 377-491, November, 1964.

Pagurova, V. I. "Tablitsy Integro-eksponentsial'noi funktsii $E_\nu(x) = \int_1^\infty e^{-xu}u^{-\nu}du$." Akad. Nauk, Moscow, Eng. Transl. D. G. Fry: "Tables of the Exponential Integral...." Pergamon Press, London, 1961.

Panofsky, W. K. H. and M. Phillips. "Classical Electricity and Magnetism." Addison-Wesley, Massachusetts, 1955.

Parasnis, D. S. "Long Horizontal Cylindrical Ore Body at Arbitrary Depth in the Field of Two Linear Current Electrodes." Geophys. Prospecting, 12(4), 457-487, 1964(a).

Parasnis, D. S. "The Electric Potential and Apparent Resistivity due to a Pair of Long Line Electrodes in the Presence of a Vertical Outcropping Vein." Z. f. Geophysik, 30(6), 263-274, 1964(b).

Parker, E. N. "Dynamics of the Geomagnetic Storm." Space Sci. Rev., 1, 62-99, 1962(a).

Parker, E. N. "Interplanetary Dynamical Processes." (Interscience, New York), 1962(b)

Parker, E. N. "Dynamical Theory of the Solar Wind." Space Sci. Rev., 4, 666-708, 1965.

Parkinson, W. D. "Directions of Rapid Geomagnetic Fluctuations." Geophys.. J.R.A.S., 2(1), 1-14, March, 1959.

Parkinson, W. D. "The Influence of Continents and Oceans on Geomagnetic Variations." Geophys. J.R.A.S., 6(4), 441-449, June, 1962(a).

Parkinson, W. D. "Magnetic Variation Over the Oceans." Geomagnetica, (Lisbon), 97-108, 1962(b).

Parkinson, W. D. "Terrella Model Experiment", Progress Report, 1962, Aust. Bureau Min. Res., Geol. Geophys. Record, 1963(102), 8 pp.

Parkinson, W. D. "Conductivity Anomalies in Australia and the Ocean Effect." J. Geomag. Geoelec., Japan, 15(4), 222-226, 1964.

Phillips, E. G. "Functions of a Complex Variable." (Oliver and Boyd, Edinburgh, 7th ed., 1951, reprinted 1954).

Piddington, J. H. "Geomagnetic Storms, Auroras, and Associated Effects." Space Sci. Rev., 3, 726-780, 1964.

Ponomarev, Ye. A. "The Nature of the Geomagnetic Coast Effect." Acad. Sci. USSR, Section III of IGY Committee, No. 4, Geomag. Disturbances, Moscow, Acad. of Sciences Press, 35-41, 1960; Eng. Transl. (i) E. R. Hope DRB, Can., T 382 R, February, 1963. (ii) NASA TT-F-105, 43-53, December, 1963.

Ponomarev, Ye. A. and I. A. Rudenko. "Observations on the Positions and Orientation of Auroral Arcs." (Collection of IGY papers), No. 11 90-97, Kiev, Schevchenko University, 1963. Eng. Transl. E. R. Hope, DRB, Canada, T403 R, November, 1964.

Price, A. T. "The Induction of Electric Currents in Non-Uniform Thin Sheets and Shells." Q. J. Mech. App. Maths., 2(3), 283-310, 1949.

Price, A. T. "Electromagnetic Induction in a Semi-Infinite Conductor with a Plane Boundary." Q. J. Mech. App. Maths, 3(4), 385-410, 1950.

Price, A. T. "The Theory of Magneto-telluric Methods When the Source Field is Considered." J. Geophys. Res., 67(5), 1907-1918, May, 1962.

Price, A. T. "A Note on the Interpretation of Magnetic Variations and Magneto-telluric Data." J. Geom. Geoelec., 15(4), 241, 1964.

Price, A. T. "Effects of Induced Earth Currents on Low Frequency Electro-magnetic Oscillations." Radio Science, J. Res. NBS, 69D(8), 1161-1168, August, 1965.

Quon, C. "Electromagnetic Fields of Elevated Dipoles on a Two-layered Earth." M. Sc. Thesis, Univ. of Alb., Edmonton, 1963.

Rankin, D. "The Magneto-Telluric Effect on a Dike." Geophysics, 27(5), 666-676, October, 1962.

Rankin, D., G. D. Garland and K. Vozoff. "An Analog Model for the Magneto-telluric Effect." J. Geophys. Res., 70(8), 1939-1945, April, 1965.

Redding, J. L. "Diurnal Variation of Telluric Currents Near the Magnetic Equator." J. Atm. Terr. Phys., 29(3), 297-305, March, 1967.

Rikitake, T. "Electromagnetic Induction Within the Earth and Its Relation to the Electrical State of the Earth's Interior." Part I (1), Bull. Earthquake Res. Inst., Tokyo Univ., 28(1/2), 45-100, 1950(a).

Rikitake, T. "Electromagnetic Induction Within the Earth and Its Relation to the Electrical State of the Earth's Interior." Part I (2), Bull. Earthquake Res. Inst., Tokyo Univ., 28(3/4), 219-262, 1950(b).

Rikitake, T. "Electromagnetic Induction Within the Earth and Its Relation to the Electrical State of the Earth's Interior." Part II, Bull. Earthquake Res. Inst., Tokyo Univ., 28(3/4), 263-283, 1950(c).

Rikitake, T. "Electromagnetic Induction Within the Earth and Its Relation to the Electrical State of the Earth's Interior." Part III, Bull. Earthquake Res. Inst., Tokyo Univ., 29(1), 61-69, 1951(a).

Rikitake, T. "Changes in Earth Currents and Their Relation to the Electrical State of the Earth's Crust." Bull. Earthquake Res. Inst. Tokyo Univ., 29(2), 271-276, 1951(b).

Rikitake, T. "Electromagnetic Induction Within the Earth and Its Relation to the Electrical State of the Earth's Interior." Bull. Earthquake Res. Inst. Tokyo Univ. Part IV, 29, 539-547, 1951(c).

Rikitake, T. "Anomaly of Geomagnetic Variations in Japan." Geophys. J.R.A.S., 2, 276-287, 1959.

Rikitake, T. "Electromagnetic Induction in a Hemispherical Ocean by Sq." J. Geomag. Geoelect (Japan), 11(3), 65-79, 1960.

Rikitake, T. "The Effect of the Ocean on Rapid Geomagnetic Changes." Geophys. J.R.A.S., 5(1), 1-15, May, 1961(a).

Rikitake, T. "Sq and the Ocean." J. Geophys. Res., 66, 3245-3254, 1961(b).

Rikitake, T. Supplement to Paper "Sq and Ocean." J. Geophys. Res., 67(6), 2588-2591, June, 1962.

Rikitake, T. "Outline of the Anomaly of Geomagnetic Variations in Japan." J. Geom. Geoelec. (Japan), 15(4), 181-184, 1964(a).

Rikitake, T. "Electromagnetic Induction in a Perfectly Conducting Plate with a Circular Hole." J. Geomag. Geoelec. (Japan), 16(1), 31-36, 1964(b).

Rikitake, T. "Electromagnetic Induction in a Semi-Infinite Conductor Having an Undulating Surface." Bull. Earthquake Res. Inst., Tokyo Univ., 43(1), 161-166, March, 1965.

Rikitake, T. "Electromagnetism and the Earth's Interior." Developments In Solid Earth Geophysics, Amsterdam, Elsevier Pub. Co., 1966.

Rikitake, T. and K. Whitham. "Interpretation of the Alert Anomaly in Geomagnetic Variations." Canad. J. Earth. Sci., 1(1), 35-62, August, 1964.

Rikitake, T. and I. Yokoyama. "The Anomalous Behavior of Geomagnetic Variations of Short Period in Japan and Its Relation to the Subterranean Structure." Bull. Earthquake Res. Inst., Tokyo Univ., 33(3), 297-331, 1955.

Roden, R. B. "The Effect of an Ocean on Magnetic Diurnal Variations." Geophys. J.R.A.S., 8(4), 375-388, May, 1964.

Rokityanskii, I. I. "On the Application of the Magnetotelluric Method to Anisotropic and Inhomogeneous Masses." Izvestiya (Bull.) AN SSSR, Geof. Ser., 11, 1607-1613 (Russ.), 1050-1053 (Eng.), November, 1961.

Rokityanskii, I. I. "The Shore Effect in Variations of the Earth's Magnetic Field." Izvestiya (Bull.) AN SSSR (Geophys. Ser.) No. 12, 1214-1222 (Russ.), 1101-1105 (Eng.), December, 1963.

Rokityanskii, I. I., P. K. Senko, S. M. Mansurov, J. K. Kalinan and G. A. Fonarev. "The Coast Effect in the Variation of the Earth's Electromagnetic Field." Geomag. Geoelec. (Japan), 15(4), 271-274, 1964.

Rooney, W. J. "Earth Currents" in "Physics of the Earth" Vol. 8; ed. J. A. Fleming, "Terrestrial Magnetism and Electricity." Chapter 6, McGraw-Hill, 1939.

Runcorn, S. K. "The Magnetism of the Earth's Body." Handbuch der Physik, 47, 498-533, 1956.

Saito, T. "Statistical Studies of Three Types of Geomagnetic Continuous Pulsations." Sci. Rep. Tôhoku Univ. [5], Geophys., 14(3), 81-106, 1962.

Samsonov, V. P. and N. S. Zaretskiy. "The Azimuthal and Geographical Distribution of Auroral Rays Revealed by Data for the Yakutsk Network of Stations." Geomag. i. Aeron., 3, 246-251 (Russ.), 198-202 (Eng.), 1963.

Schelkunoff, S. A. "Electromagnetic Fields." Blaisdell Publishing Company, New York, 1963.

Schlak, G. A. and J. R. Wait. "Electromagnetic Wave Propagation over a Non-parallel Stratified Conducting Medium." Canad. J. Phys., 45(12), 3697-3720, December, 1967.

Schmucker, U. "Erdmagnetische Tiefensondierung in Deutschland 1957/9 Magnetogramme und erste Auswertung." Abh. d. Akad. d. Wissenschaften in Göttingen, Math-Phys. Klasse, Beitrage z. Internationalen Geophysikalischen Jahr, 5, 1959.

Schmucker, U. "Anomalies of Geomagnetic Variations in the Southwestern United States." J. Geomag. Geoelec. (Japan), 15(4), 193-221, 1964.

Scholte, J. G. and J. Veldkamp. "Geomagnetic and Geoelectric Variations." J. Atmos. Terr. Phys., 6, 33-45, 1955.

Schuster, A. "The Diurnal Variation of Terrestrial Magnetism." Phil. Trans. Roy. Soc. Lond., 180, 467-518, 1889; with Appendix by H. Lamb: "On the Currents Induced in a Spherical Conductor by Variation of an External Magnetic Potential."

Sen'ko, P. K. "Unusual Magnetic Variations in the Mirny Region." Information Bulletin Sov. Ant. Exp. No. 1, 81-82, 1958. Eng. Transl. Elsevier Publ. Co. Amsterdam, 1, 52-53, 1964.

Sen'ko, P. K. "Coastal Effect in Magnetic Variations." Inf. Bull. Sov. Ant. Exp. No. 4, 61-65, 1959. Eng. Transl., Elsevier Pub. Co. Amsterdam, 1, 203-206, 1964.

Shand, J. A. "On the Suitability of Arctic Sea Ice as a Platform for Measuring Electromagnetic Background at Micropulsation and Extremely Low Frequencies." Pacific Naval Lab. Report, Esquimalt, B. C. 64-7, August, 1964.

Shand, J. A., C. S. Wright and H. J. Duffus. "A Study of the Distribution of Geomagnetic Micropulsations." Report 59-15, Pacific Naval Labs. Esquimalt, B. C., November 1959.

Sheinman, S. M. "Uses of Telluric Current Fields and Long-Distance Radio Stations in Geological Mapping." Trans. (Trudy) All-Union Inst. of Methods and Techniques of Prospecting, Gostoptekhizdat, Moscow, 1958.

Shuleykin, V. V., Doklady AN SSSR, 119(2), 257 (Russ.), 1958.

Shuleykin, V. V. "More Concerning Eddy Currents in the Ocean." Doklady AN SSSR, 134(6), 1343-1346 (Russ.), 1960. Eng. Transl. Doklady-Geophysics Section, 988-9.

Skey, H. F. "Christchurch Magnetic Observatory Report for the Year 1926-27." Records of the Survey of N. Z., 4:42, 1928.

Slichter, L. B. "An Electromagnetic Interpretation Problem in Geophysics." Geophysics, 16(3), 431-449, 1951.

Smith, H. W., L. D. Provazek, F. X. Bostick. "Directional Properties and Phase Relations of the Magneto-telluric Fields at Austin, Texas." J. Geophys. Res., 66, 879-887, 1961.

Smythe, W. R. "Static and Dynamic Electricity.", McGraw-Hill, New York, 1950.

Sommerfeld, A. "Electrodynamics." Academic Press, 1948, (Eng. Transl.) 1952.

Srivastava, S. P. "Method of Interpretation of Magneto-telluric Data When Source Field is Considered." J. Geophys. Res., 70(4), 945-954, February, 1965(a).

Srivastava, S. P. "Theory of the Magneto-telluric Method for Non-Uniform Conductors." J. Geomag. Geoelec., 17(3/4), 507-515, 1965(b).

Srivastava, S. P. "Theory of the Magnetotelluric Method for a Spherical Conductor." Geophys. J.R.A.S., 11(4), 373-388, November, 1966.

Srivastava, S. P. and J. A. Jacobs. "Determination of the Resistivity Distribution at Meanook, Alberta, Canada, by the Magneto-telluric Method." J. Geomag. Geoelec., 15, 280-288, 1964.

Srivastava, S. P., J. L. Douglass, S. H. Ward. "Magneto-telluric and Telluric Methods in Central Alberta." Geophysics, 28, 426-446, 1963.

Stratton, J. A. "Electromagnetic Theory." McGraw Hill, New York, 1941.

Sugiura, M. and S. Chapman. "The Average Morphology of Geomagnetic Storms With Sudden Commencement." Abh. Akad. Wiss. Gottingen, Math-Phys. Klasse, Sonderheft, Nr. 4, 1960.

Swift, D. W. and V. P. Hessler. "A Comparison of Telluric Current and Magnetic Field Observations in the Arctic Ocean." J. Geophys. Res., 69(9), 1883-1893, May, 1964.

Swift, D. W. and E. M. Wescott. "The Effect of Small Islands on Telluric Currents." J. Geophys. Res., 69(19), 4149-4154, October, 1964.

Tepley, L. "Recent Investigations of Hydromagnetic Emissions, Part I. Experimental Observations." J. Geomag. Geoelec., 18(2), 227-256, 1966.

Thomas, B. D., T. G. Thompson, C. L. Utterback. "The Electrical Conductivity of Sea Water." J. Cons. Int. Explor. Mer., 9, 28-35, 1934. See also American Inst. Physics Handbook, pp. 2-118, -120, McGraw Hill, New York, 1957.

Tikhonov, A. N. "Determination of the Electric Characteristics of Deep Layers of the Earth's Crust." Doklady AN SSSR, 73(2), 295-297, 1950. Eng. Transl. DRB, Canada (E. R. Hope), T43R and also: T175R, July, 1955, pps. 1-5.

Tikhonov, A. N. and N. V. Lipskaya. "Variations in the Earth's Electric Field." Doklady AN SSSR, 87(4), 547-550, 1952. Eng. Transl. DRB, Canada (E. R. Hope), T43R and also T175R, July 1955, pp. 6-11.

Tikhonov, A. N. and D. N. Shakhsuvarov. "The Possibility of the Use of the Impedance of the Earth's Natural Electromagnetic Field for Studying its Upper Layers." Izv. (Bull.) AN SSSR Ser. geofiz. No. 4, 410-418, 1956. Eng. Transl. OTS-TT62-18527, 1962.

Tralli, N. "Classical Electromagnetic Theory." McGraw Hill, New York, 1963.

Tranter, C. J. "Integral Transforms in Mathematical Physics." (Methuen, London, 2nd ed., 1956).

Troitskaya, V. A. "Short Period Oscillatory Distribution in the Terrestrial Magnetic Field," Doklady AN SSSR, 91(2), 241-244, 1953(a).

Troitskaya, V. A. "Two Oscillatory Modes of the Terrestrial Magnetic Fields and their Diurnal GMT Cycle." Doklady AN SSSR, 93(2), 261-264, 1953. Eng. Trans. E. R. Hope, DRB, Canada, T174R, 1955, with additional comments.

Troitskaya, V. A. "Rapid Variations of the Electromagnetic Field of the Earth." in H. Odishaw: Research in Geophysics, 1, MIT Press, 1964.

Utzmann, R. and B. Favre. "The Effect of the Limited Length of the Structures on the Telluric Field." Rev. Inst. Franc. du Petrole, 12, 135-144, 1957.

van Bemmelen, W. "The Starting Impulse of Magnetic Disturbances." Proc. Amsterdam Acad., 773-782, 1908.

van Wijngaarden, I. A. "Polylogarithms: I Numerical Values." Comp. Dept., Mathematisch Centrum, Amsterdam Rep. R24, 1954.

Van'yan, L. L. "Electromagnetic Depth Sounding." Plenum Press, New York, 1967 (selected and translated by G. V. Keller).

Van'yan, L. L. and B. Ye. Marderfeld. "Influence of Local Geoelectric Conditions on the Sudden Commencement of Magnetic Storms." Geomag. i. Aeron., 6(1), 163-164 (Russ.), 128-129 (Eng.), 1966.

Vinogradov, P. A. "The Measurement of the Vertical Component of the Earth's Electric Field in Lake Baikal." Izv. (Bull.) AN SSSR Ser. Geofiz. No. 1, 83-86, (Russ.), 47-48 (Eng.), 1959.

Vinogradov, P. A. "Some Characteristics of pc Pulsations, as Revealed by Observations in Different Media and at Different Depths." Report to the 1st All Union Conf. on IGY Results, Moscow, 1963.

Vladimirov, N. P. "The Feasibility of Using the Earth's Natural Electromagnetic Field for Geological Surveying." Izv. (Bull.) AN SSSR, Geoph. Ser. No. 1, 139-141 (Eng.), 1960.

Vladimirov, N. P. and V. A. An. "A Method of Processing Magnetotelluric Oscillograms." Izv. (Bull.) AN SSSR, Geophys. Ser., No. 11, 1649-1654 (Eng.), 1961.

Vladimirov, N. P. and M. V. Kolmakov. "The Resolving Power of the Magnetotelluric Method." Izv. (Bull.) AN SSSR Geoph. Ser. No. 11, 1598-1600 (Eng.), 1960.

Vladimirov, N. P. and N. N. Nikiforova. "On the Interpretation of Magnetotelluric Sounding Curves." Izv. (Bull.) AN SSSR, Geoph. Ser. No. 1, 111-113 (Eng.), 1961.

Vozoff, K., R. M. Ellis, M. D. Burke. "Telluric Currents and their Use in Petroleum Exploration." Bull. Am. Assoc. of Petroleum Geologists, 48(12), 1890-1901, December, 1964.

Wait, J. R. "Magnetic Dipole over a Horizontally Stratified Earth." Can. J. Phys., 29, 577-592, 1951.

Wait, J. R. "On the Relation Between Telluric Currents and the Earth's Magnetic Field." Geophysics, 19(2), 281-289, April, 1954(a).

Wait, J. R. "The Fields of a Line Source of Current Over a Stratified Conductor." App. Sci. Res., [Sec. B], 3, 279-292, 1954(b).

Wait, J. R. "Transmission and Reflection of Electromagnetic Waves in the Presence of Stratified Media." J. Res. N.B.S., 61, 205-232, September, 1958.

Wait, J. R. "Electromagnetic Radiation from Cylindrical Structures." Pergamon Press, London, 1959.

Wait, J. R. "Some Solutions for Electromagnetic Problems Involving Spheroidal, Spherical, and Cylindrical Bodies." J. Res. N.B.S., 64B(1), 15-32, January/March, 1960.

Wait, J. R. "Theory of Magneto-telluric Fields." J. Res., Nat. Bur. of Standards, Radio Propagation, 66D(5), 509-541, September/October, 1962(a).

Wait, J. R. "Electromagnetic Waves." Pergamon Press, London, 1962(b).

Wait, J. R. "Oblique Propagation of Groundwaves Across a Coastline, Part I." J. Res. Nat. Bur. Stand., D. Radio Propagation, 67D(6), 617-624, December, 1963.

Wait, J. R. and W. J. Surtees. "Impedance of a Top-Loaded Antenna of Arbitrary Length over a Circular Grounded Screen." J. App. Phys., 25(5), 553-555, May, 1954.

Ward, S. H., H. F. Morrison. "Discussion of Paper by A. A. J. Hoffman and C. W. Horton." J. Geophys. Res., 71(16), 4053-4054, August, 1966.

Weaver, J. T. "The Magnetic Field at the Surface in the Near Field of an Alternating Line Current with Applications to Geomagnetic Micropulsations." Pacific Naval Lab. Rep. No. 61-6, October, 1961, Esquimalt, Canada.

Weaver, J. T. "The Electromagnetic Field Within a Discontinuous Conductor with Reference to Geomagnetic Micropulsations near a Coastline." Can. J. Phys., 41(3), 484-495, March, 1963(a).

Weaver, J. T. "A Discussion of the 'Fault' and 'Dike' Problems in Magnetotelluric Theory." Geophysics, 28(3), 487-490, June, 1963(b).

Weaver, J. T. "Electro-magnetic Induction in a Two-layered Earth." Pacific Naval Lab., Esquimalt, B. C., Canada, Rep. 64-1, May, 1964(a).

Weaver, J. T. "On The Separation of Local Geomagnetic Field Into External and Internal Parts." Z. f. Geophys., 30(1), 29-36, 1964(b).

Wentworth, R. C. "Recent Investigations of Hydromagnetic Emissions, Part II, Theoretical Interpretations." J. Geomag. Geoelec., 18(2), 257-274, 1966.

Wescott, E. M. "The Effect of Topography and Geology on Telluric Currents." Thesis, University of Alaska, 1960.

Wescott, E. M. "Coastal Effects in Magnetic and Telluric Current Variations Near a Complex Land, Shelving Seawater Boundary." J. Geophys. Res., 72(7), 1959-1969, April, 1967.

Wescott, E. M. and V. P. Hessler. "The Effects of Topography and Geology on Telluric Currents." J. Geophys. Res., 67(12), 4813-4823, November, 1962.

Whitham, K. and F. Anderson. "Magneto-Telluric Experiments in Northern Ellesmere Island." Geophys. J.R.A.S., 10(3), 317-345, December, 1965.

Yoshimatsu, T. "Universal Earth Currents and their Local Characteristics." Memoirs of the Kakioka Magn. Observatory, Supp. Vol. 1, Kakioka, Japan, May, 1957.

Yukutake, T. "Attenuation of Geomagnetic Secular Variation Through the Conducting Mantle of the Earth." Bull. Earthquake Res. Inst., Tokyo Univ., 37, 13-32, 1959.

Yungul, S. H. "Telluric Sounding--A Magneto-telluric Method Without Magnetic Measurements." Geophys., 31(1), 185-191, February, 1966.

Zhigalov, L. N. "Some Features of the Variations of the Geomagnetic Vertical Component in the Arctic Ocean." Geomagnetic Disturbances: a Collection of Articles Relating to Sections III of the IGY Program, Acad. Sci. Press, Moscow, 1960. Eng. Transl. E. R. Hope; DRB, Ottawa, T358R, 1961, and NASA TT-F-105, December, 1963, 36-42.

Appendix 1: The Polarization of the Electric Vector

In Chapters IV, V, and VI, the E_x, E_y and H_z field components were derived with respect to the surface values of the horizontal magnetic field components H_x and H_y. No relation was assumed between these magnetic field components. To study the behavior of the total horizontal electric vector at the surface, we must in some way compare the two components E_x and E_y. Some assumption must therefore be made concerning the relative behavior of the surface H_x and H_y fields.

Let us write:

$$E_x = R_x e^{i\phi_x} \cdot Ae^{-i\omega t} \quad \text{where } H_y \Big|_{z=0} = A$$

$$E_y = -R_y e^{i\phi_y} Be^{-i\omega t} \quad \text{where } H_x \Big|_{z=0} = -B \qquad \text{(A1.1)}$$

Here A and B are treated as constants.

The horizontal H-wave then has the form

$$\underset{\sim}{H} = (H_x \hat{\underset{\sim}{\varepsilon}}_x + H_y \hat{\underset{\sim}{\varepsilon}}_y) e^{-i\omega t} = (-B\hat{\underset{\sim}{\varepsilon}}_x + A\hat{\underset{\sim}{\varepsilon}}_y) e^{-i\omega t} \qquad \text{(A1.2)}$$

and there will be some phase relation between A and B; in general the wave will be elliptically polarized. Two special cases are evident:

(i) when A and B are in phase, the H-wave is linearly polarized at an angle θ with the $\hat{\underset{\sim}{\varepsilon}}_x$ axis, with

$$\tan\theta = \frac{A}{-B}$$

$$\text{and magnitude: } H = \sqrt{A^2 + B^2}$$

(ii) when A and B are equal in magnitude but out of phase by 90^{o} ($A = \pm iB$), the H-wave is circularly polarized, either left or right handedly.

Assume that the H-wave at the surface is circularly polarized, say left(right)-handedly (remembering that $H_x = -B$). Then from (ii), we have,

$$A = \underset{(\mp)}{} iB = H_o \text{ , say}$$

so that from (A1.2):

$$\underset{\sim}{H} = -H_o (\hat{\varepsilon}_{\sim x} \underset{(-)}{+} i\hat{\varepsilon}_{\sim y})\, e^{-i\omega t}$$

Using (A1.1), the E-field components are:

$$\left.\begin{aligned} E_x &= -R_x\, e^{i(\phi_x + \frac{\pi}{2})}\, H_o\, e^{-i\omega t} \\ E_y &= \underset{(+)}{-R}\, e^{i\phi_y} \cdot H_o e^{-i\omega t} \end{aligned}\right\} \qquad \text{(A1.3)}$$

so that the surface E-wave is given by:

$$\underset{\sim}{E} = E_x \hat{\varepsilon}_{\sim x} + E_y \hat{\varepsilon}_{\sim y} = -\left(H_o R_x e^{i(\phi_x + \frac{\pi}{2})}\, \hat{\varepsilon}_{\sim x} \underset{(-)}{+} R_y\, e^{i\phi_y}\, \hat{\varepsilon}_{\sim y}\right) e^{-i\omega t}$$

which, in general, represents elliptic polarization.

To determine the ellipse parameters in terms of the R's and ϕ's, we use the more convenient notation suggested by Jackson (1962, §7.2); we write:*

$$\hat{\varepsilon}_{\sim \pm} = \frac{1}{\sqrt{2}} (\hat{\varepsilon}_{\sim x} \pm i\, \hat{\varepsilon}_{\sim y})$$

---

*The reason behind this substitution is that instead of forming our total $\underset{\sim}{E}$-vector from two linearly polarized waves of complementary phase, a pair of oppositely polarized circular waves has been used; the the superposition in general still gives an elliptically polarized, complex, resultant vector.

as complex orthogonal vectors, so that the $\underset{\sim}{E}$-vector is:

$$\underset{\sim}{E} = (E_+ \hat{\underset{\sim}{\xi}}_+ + E_- \hat{\underset{\sim}{\xi}}_-)\, e^{-i\omega t}$$

where:

$$E_\pm = \frac{1}{\sqrt{2}} (E_x \pm iE_y)$$

$$\text{i.e. } E_\pm = -\frac{H_o}{\sqrt{2}} \left\{ R_x e^{i(\phi_x + \frac{\pi}{2})} \pm (\mp) R_y e^{i(\phi_y + \frac{\pi}{2})} \right\} \qquad \text{(A1.4)}$$

Now let

$$\frac{E_-}{E_+} = \rho e^{i\psi} \qquad \text{(A1.5)}$$

Then the ratio of minor axis to major axis for the polarization ellipse is given by

$$\mu = \frac{|1-\rho|}{1+\rho}, \qquad \text{(A1.6)}$$

and the major axis is inclined at angle $\frac{1}{2}\psi$ to the $\hat{\underset{\sim}{\xi}}_x$ - axis.

The geometry is shown in Fig. (A1.1)

Thus from (A1.4) and (A1.5):

$$\rho e^{i\psi} = \frac{R_x e^{i\phi_x} \mp R_y e^{i\phi_y}}{R_x e^{i\phi_x} \pm R_y e^{i\phi_y}}$$

$$= \frac{1-\gamma^2 \pm i\, 2\gamma \sin(\phi_x - \phi_y)}{1+\gamma^2 \pm 2\gamma \cos(\phi_x - \phi_y)}$$

where $\gamma = \frac{R_y}{R_x}$

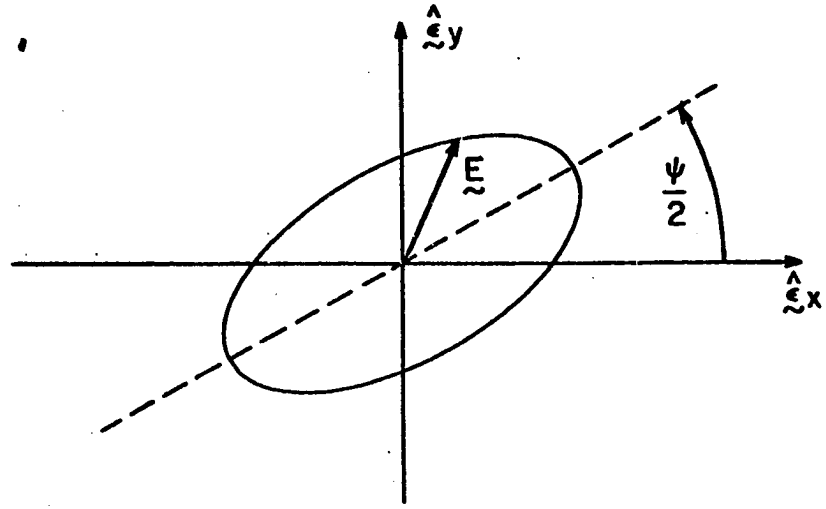

Fig. A1.1 Representation of the surface electric field by a polarization ellipse.

Immediately we have the relations:

$$\left.\begin{aligned} \rho &= \frac{\sqrt{(1-\gamma^2)^2 + 4\gamma^2 \sin^2(\phi_x - \phi_y)}}{1+\gamma^2 \underset{(-)}{+} 2\gamma \cos(\phi_x - \phi_y)} \\ \tan\psi &= \frac{\underset{(-)}{+} 2\gamma \sin(\phi_x - \phi_y)}{1-\gamma^2} \end{aligned}\right\} \quad (A1.7)$$

Equations (A1.6) and (A1.7) specify the characteristics of the polarization ellipse for the surface $\underset{\sim}{E}$-vector when the surface $\underset{\sim}{H}$-wave is circularly polarized. The upper sign represents a left-handed polarization of both H and E waves and the lower (parenthetical) sign represents a right-handed polarization. For convenience in further discussion we consider the left-hand case; the right-hand case is simply obtained by a mirror-reflection of the ellipse about the $\hat{\underset{\sim}{\varepsilon}}_x$-axis.

For clarity let us summarize the various special cases which may arise from relations (A1.6) and (A1.7).

Case (i): Circular Polarization: (Fig. A1.2a)

Conditions: $\gamma=1$; $\phi_x - \phi_y = o, \pm\pi, \pm 2\pi$

Result: $\rho = o, \mu=1$, ψ indeterminate,

Case (ii): Linear Polarization: (Fig. A1.2b)

Conditions: $\phi_x - \phi_y = (n\pi - \frac{\pi}{2})$; $n=0, \pm1, +2$

Result: $\rho=1$; $\mu=0$; $\tan\psi = (-1)^{n+1} \frac{2\gamma}{1-\gamma^2}$

Special Cases:

(a) $\gamma=1$ $\quad \psi/2 = \begin{cases} +45^o & \text{if } n=0, 2 \\ -45^o & \text{if } n= \pm1 \end{cases}$ (Fig. A1.2c)

This represents linear polarization at $\pm 45^{o}$

(b)

$$\gamma = \begin{cases} 0 \\ \infty \end{cases} ; \psi/2 = \begin{cases} 0^{o} : \text{polarization } // \text{ x-axis (strike)} \\ 90^{o} : \text{polarization } \perp \text{ x-axis (strike)} \end{cases} \quad \text{(Fig. A1.2d)}$$

independent of $(\phi_x - \phi_y)$

Case (iii): Elliptic Polarization at Special Angles:

(a) Conditions: $\gamma=1$; $\phi_x - \phi_y \neq n\frac{\pi}{2}$ (Fig. A1.2c)

Results: $\rho = |\tan \tfrac{1}{2}(\phi_x - \phi_y)|$; $\mu = |\cot \tfrac{1}{2}(|\phi_x - \phi_y| + \frac{\pi}{2})|$

$$\frac{\psi}{2} = \begin{cases} +\frac{\pi}{4} & \text{if } |\phi_x - \phi_y| \in (0,\pi) \text{ or } (-2\pi,-\pi) \\ -\frac{\pi}{4} & \text{if } |\phi_x - \phi_y| \in (-\pi,0) \text{ or } (\pi,2\pi) \end{cases}$$

This represents elliptic polarization at $\pm 45^{o}$.

(b) Conditions: $\phi_x - \phi_y = n\pi$, $n=0, \pm1, \pm2$; $\gamma \neq 0, 1, \infty$

Results: $$\rho = \begin{cases} \frac{|1-\gamma|}{1+\gamma} & \text{if } n=0, \pm2 \\ \frac{1+\gamma}{|1-\gamma|} & \text{if } n=\pm1 \end{cases} \quad \text{(Fig. A1.2f)}$$

$\mu = \gamma$; $\frac{\psi}{2} = 0^{o}$ if $\gamma < 1$

$\mu = 1/\gamma$; $\frac{\psi}{2} = \pm 90^{o}$ if $\gamma > 1$

This represents elliptic polarization // to the $\hat{\varepsilon}_{v_x}$ axis (strike)

or $\perp$ to the $\hat{\varepsilon}_{v_x}$ axis (strike)

Case (iv): General Elliptic Polarization:

The general case, when none of the conditions in the above three special cases occur, is illustrated by Fig. (A1.1) - an ellipse, ratio $\frac{|1-\rho|}{1+\rho}$ inclination $\frac{1}{2}\psi$.

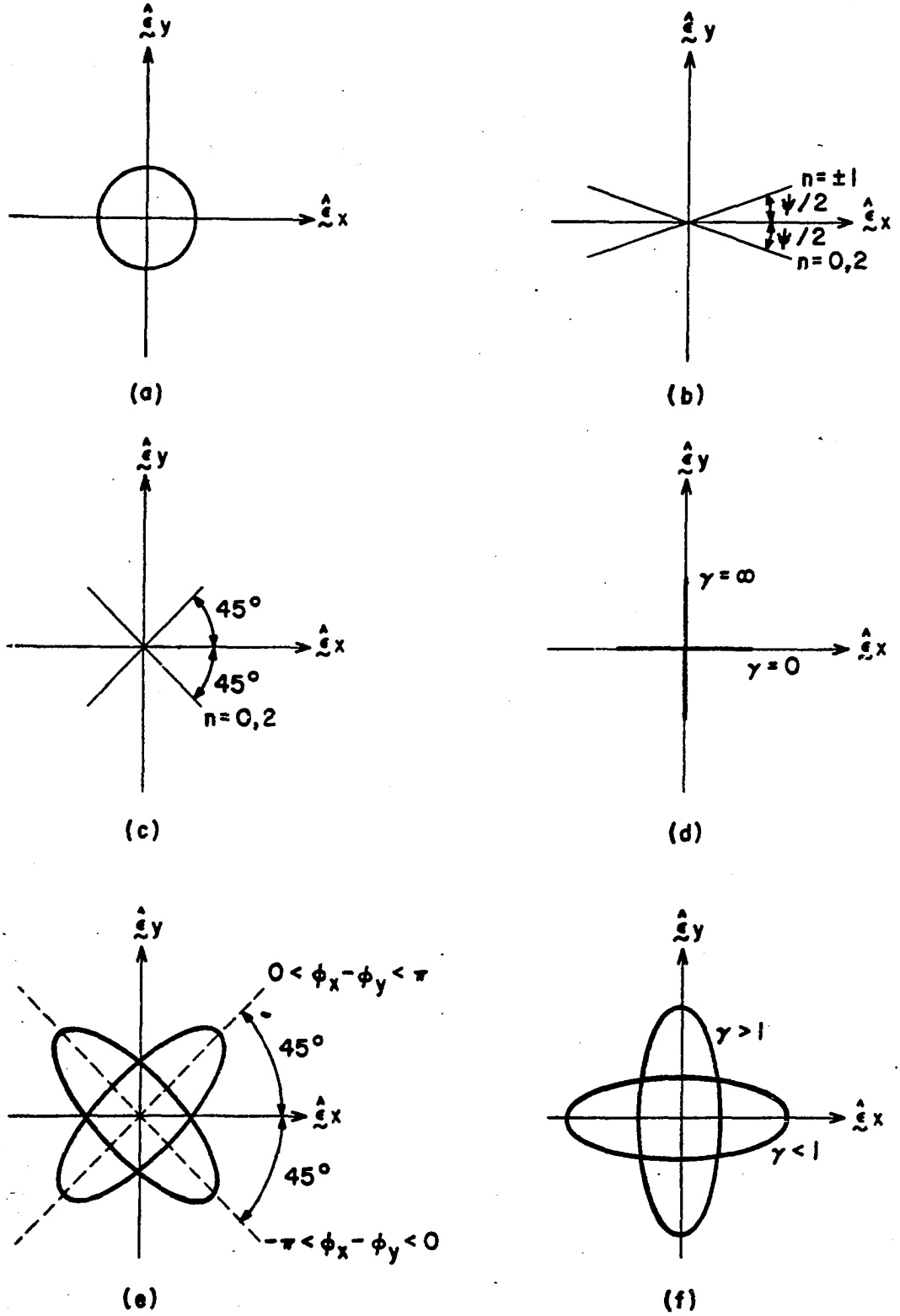

Fig. A1.2 Special polarization conditions of the surface electric field under the conditions described in the text.

Appendix 2: The Derivation of the Surface Electric Fields Over an Infinitely Deep Fault

(a) Parallel Electric Field E_x

The surface electric field E_x is given by eq. (4.8) of Table 4.2, for both media. As the field is continuous across the interface $y_i=o$, it is irrelevant which of these expressions is used. We may write

$$\sqrt{\frac{\sigma_2}{\mu_o\omega}}\,\frac{E_x(o,o)}{A} = \sqrt{-i} + \frac{2i}{\pi}\int_o^\infty \left\{ \frac{1}{u^2-i} - \frac{1}{\sqrt{(u^2-i\varepsilon^2)\,(u^2-i)}} \right\} du$$

But from App. 3 we have

$$I_o = \int_o^\infty \frac{du}{u^2-i} = \frac{\sqrt{i}\,\pi}{2}$$

Thus we have only to evaluate

$$I_1 = \int_o^\infty \frac{du}{\sqrt{(u^2-i\varepsilon^2)\,(u^2-i)}}$$

The substitution $u = \sqrt{-i}\;x$ gives

$$I_1 = \frac{1}{\sqrt{-i}} \int_o^\infty \frac{dx}{\sqrt{(x^2+\varepsilon^2)\,(x^2+1)}} \qquad \text{(A2.1)}$$

This integral is well-known and may be found in many tables [Byrd and Friedman, 1954, 222.00; Gröbner and Hofreiter, 1961, II, 223.11: Gradshteyn and Ryzhik, 1963, 1965, 3.152(1)]:

$$I_1 = \frac{1}{\sqrt{-i}} \; K\left(\sqrt{1-\varepsilon^2}\right) \qquad \text{(A2.2)}$$

where K(k) is the complete elliptic integral of the 1st kind, whose argument is the modulus $k = \sqrt{1-\varepsilon^2}$. It may also be written as

$$K(k) = F\left(\frac{\pi}{2}, k\right)$$

where $F(\alpha,k)$ specifies the incomplete elliptical integral:

$$F(\alpha,k) = \int_0^{\infty} \frac{d\phi}{\sqrt{1-k^2 \sin^2 \phi}}$$

Then

$$\sqrt{\frac{\sigma_2}{\mu_o \omega}} \; \frac{E_x(o,o)}{A} = \sqrt{-i} + \frac{2i}{\pi} (I_o - I_1) = \sqrt{-i} \; \frac{2}{\pi} K\left(\sqrt{1-\varepsilon^2}\right) \qquad \text{(A2.3)}$$

This relation is used in §4.1.3.

(b) Normal Electric Field E_y

Equation (4.9) of Table 4.2 specifies the surface E_y-field for each medium. The field is discontinuous across the interface Y_i=o so that each expression must be treated in turn. The more complicated denominator causes difficulties in evaluating the expression, and even so the final expressions obtained are much more involved than those for the tangential E_x field over the interface.

(i) Oceanic E_y (o,o) field

The integral term involved in (4.9b) at Y_2=o is

$$I = \int_0^\infty \frac{u^2}{\sqrt{u^2-i\varepsilon^2}\ (u^2-i)\left\{\sqrt{u^2-i\varepsilon^2} + \varepsilon^2\sqrt{u^2-i}\right\}}\,du \qquad (A2.4)$$

If the integrand is multiplied throughout by $\left[\sqrt{u^2-i\varepsilon^2} - \varepsilon^2\sqrt{u^2-i}\right]$, and the substitution

$$\delta^2 = \frac{\varepsilon^2}{1+\varepsilon^2}$$

made, this integral may be reduced to

$$I = \frac{1}{1-\varepsilon^4}\int_0^\infty \left\{\frac{1+\varepsilon^2}{u^2-i} - \frac{\varepsilon^2}{u^2-i\delta^2} - \frac{\varepsilon^2}{\sqrt{(u^2-i\varepsilon^2)\ (u^2-i)}} - \frac{i\varepsilon^2\delta^2}{(u^2-i\delta^2)\sqrt{(u^2-i\varepsilon^2)(u^2-i)}}\right\}du$$

$$= \frac{1}{1-\varepsilon^4}\left\{(1+\varepsilon^2)\ I_o - \varepsilon^2 I_{o1} - \varepsilon^2 I_1 - i\varepsilon^2\delta^2\ I_2\right\}$$

The integrals involved here are all known except I_2:

$$I_o = \int_0^\infty \frac{du}{u^2-i} = \sqrt{i}\ \frac{\pi}{2} \qquad \text{by App. 5}$$

$$I_{o1} = \int_0^\infty \frac{du}{u^2-i\delta^2} = \frac{\sqrt{i}}{\delta}\frac{\pi}{2} \qquad \text{by App. 5}$$

$$I_1 = \int_0^\infty \frac{du}{\sqrt{(u^2-i\varepsilon^2)\ (u^2-i)}} = \sqrt{i}\ K(k); \qquad k^2 = 1-\varepsilon^2, \text{ by A2.2 of part (a) above.}$$

The last integral I_2 may be evaluated to a close approximation as follows:

$$I_2 = \int_0^\infty \frac{du}{(u^2-i\delta^2)\sqrt{(u^2-i\varepsilon^2)\,(u^2-i)}}$$

Let $u = \sqrt{-i}\,x$; then

$$I_2 = -\sqrt{-i}\int_0^\infty \frac{dx}{(x^2+\delta^2)\sqrt{(x^2+\varepsilon^2)\,(x^2+1)}}$$

This does not appear to be known in closed form. However the error in assuming $\delta^2 \approx \varepsilon^2$ when $\varepsilon^2 \ll 1$ is very small (1% in δ^2, for $\varepsilon=0.1$). If this approximation is made, the integral takes the following form (Byrd and Friedman, 1954, 222.05):

$$I_2 \approx -\sqrt{-i}\int_0^\infty \frac{dx}{(x^2+\varepsilon^2)\sqrt{(x^2+\varepsilon^2)\,(x^2+1)}} = -\sqrt{-i}\int_0^{u_1} sd^2(u)\,du$$

where $am(u_1) = \frac{\pi}{2}$ and $u_1 = K(k) = F(\frac{\pi}{2}, k)$, $k^2=1-\varepsilon^2$, and sd(u) represents the ratio sn(u)/dn(u) of the Jacobian elliptic functions. This may be evaluated in closed form (Byrd and Friedman, 1954, 318.02):

$$I_2 \approx \frac{\sqrt{-i}}{\varepsilon^2(1-\varepsilon^2)}\left\{\varepsilon^2\,K(k) - E(k) + (1-\varepsilon^2)\,sn(u_1)\,cd(u_1)\right\}$$

where $E(k) = E(\frac{\pi}{2}, k)$ is the complete elliptic integral of the 2nd kind, with

$$E(\alpha,k) = \int_0^\alpha \sqrt{1-k^2\sin^2\theta}\;d\theta$$

specifying the incomplete elliptic integral.

The Jacobian elliptic functions with argument $u_1=K$ reduce to: (Byrd and Friedman, 1954, 122.02)

$$sn(u_1) = 1;\ cn(u_1) = o;\ dn(u_1) = \varepsilon;\ cd(u_1) = cn(u_1)/dn(u_1) = 0$$

so that I_2 may be written:

$$I_2 \approx \frac{\sqrt{-i}}{\varepsilon^2(1-\varepsilon^2)} \left\{\varepsilon^2 K(k) - E(k)\right\} \tag{A2.5}$$

Combining all of these expressions we may write the total integral as

$$I \approx \frac{1}{1-\varepsilon^4} \left\{\sqrt{i}\,\frac{\pi}{2}\,(1+\varepsilon^2-\varepsilon\sqrt{1+\varepsilon^2}) - \sqrt{i}\,\varepsilon^2\,\frac{1+\varepsilon^2-\varepsilon^4}{1-\varepsilon^4}\,K(k) + \frac{\sqrt{i}\varepsilon^2}{1-\varepsilon^4}\,E(k)\right\}$$

Substituting this in relation (4.9b), we have

$$\sqrt{\frac{\sigma_2}{\mu_o\omega}}\,\frac{E_{y2}}{B} = \sqrt{-i} + \frac{2i}{\pi}\,(1-\varepsilon^2)\,I$$

so that

$$\sqrt{\frac{\sigma_2}{\mu_o\omega}}\,\frac{E_{y2}(o,o)}{B} \approx \sqrt{-i}\,\delta\left\{1 + \frac{2}{\pi}\,\frac{\delta}{1-\varepsilon^4}\left[(1+\varepsilon^2-\varepsilon^4)\,K(k) - E(k)\right]\right\};\ \varepsilon^2<<1 \tag{A2.6}$$

(ii) Land E_y (o,o) field:

The integral in (4.9a) at $Y_1 = 0$ is

$$I = \int_o^\infty \frac{u^2}{(u^2-i\varepsilon^2)\sqrt{(u^2-i)}\left[\sqrt{u^2-i\varepsilon^2} + \varepsilon^2\sqrt{u^2-i}\right]}\,du \tag{A2.7}$$

Treating this in the same manner as the previous integral (A2.6), it may be reduced to

$$I = \frac{1}{1-\varepsilon^4} \int_0^\infty \left\{ \frac{1}{u^2-i\delta^2} - \frac{1+\varepsilon^2}{u^2-i\varepsilon^2} + \frac{1}{\sqrt{(u^2-i\varepsilon^2)\,(u^2-i)}} + \frac{i\delta^2}{(u^2-i\delta^2)\sqrt{u^2-i\varepsilon^2}\,\sqrt{u^2-i}} \right\} du$$

$$= \frac{1}{1-\varepsilon^4} \left\{ I_{o1} - (1+\varepsilon^2)\, I_{o2} + I_1 + i\delta^2\, I_2 \right\}$$

Most of the integrals involved in this also occurred in the evaluation above, the only different one being:

$$I_{o2} = \int_0^\infty \frac{du}{u^2-i\varepsilon^2} = \frac{\sqrt{i}}{\varepsilon}\,\frac{\pi}{2}$$

With the same condition ($\varepsilon^2 << 1$) previously imposed on I_2, we may write:

$$I \underset{\sim}{\approx} \frac{\sqrt{i}}{1-\varepsilon^4} \left\{ -\frac{\pi}{2}\,\frac{1+\varepsilon^2-\sqrt{1+\varepsilon^2}}{\varepsilon} + \frac{1+\varepsilon^2-\varepsilon^4}{1-\varepsilon^4}\,K(k) - \frac{E(k)}{1-\varepsilon^4} \right\}$$

Substituting in (4.9a):

$$\sqrt{\frac{\sigma_1}{\mu_o\omega}}\,\frac{E_{y1}}{B} = \sqrt{-i} - \frac{2i}{\pi}\,\varepsilon\,(1-\varepsilon^2)\, I$$

Then

$$\sqrt{\frac{\sigma_1}{\mu_o\omega}}\,\frac{E_{y1}(o,o)}{B} \underset{\sim}{\approx} \frac{\sqrt{-i}}{\sqrt{1+\varepsilon^2}} \left\{ 1 + \frac{2}{\pi}\,\frac{\delta}{1-\varepsilon^4}\,[(1+\varepsilon^2-\varepsilon^4)\,K(k) - E(k)] \right\};\ \varepsilon^2 << 1 \qquad \text{(A2.8)}$$

Relations (A2.6) and (A2.8) are used in §4.1.3.

Appendix 3: Evaluation of Series

$$\text{(a)} \quad \sum_{\xi=1}^{\infty} \frac{\cos \alpha\xi}{(\frac{\pi}{h})^2 \xi^2 - i\eta^2}, \qquad \alpha = \frac{\pi z}{h} \tag{A3.1}$$

We may simplify the notation by writing:

$$S = \sum_{\xi=1}^{\infty} \frac{\cos \alpha\xi}{\xi^2 - i\beta^2}$$

where $\beta = \frac{h}{\pi}\eta$ and the series (A3.1) is given by $(\frac{h}{\pi})^2 S$.

Since all the parameters are real, the series S is both absolutely and uniformly convergent (this may be established by comparison with $\Sigma\, \xi^{-2}$ and Weierstrass' M-test respectively (Knopp, 1951). The following reduction can thus be made:

$$S = \frac{1}{2\sqrt{i}\beta} \left[\sum_{\xi=1}^{\infty} \frac{\cos \alpha\xi}{\xi - \sqrt{i}\beta} - \sum_{\xi=1}^{\infty} \frac{\cos \alpha\xi}{\xi + \sqrt{i}\beta} \right] = \frac{1}{2\sqrt{i}\beta} (S_- + S_+)$$

Here S_+ and S_- are both uniformly (but not absolutely) convergent, by Dirichlet's test provided $\alpha \neq 2m\pi$, m=0, 1, 2, ... (Knopp, 1951).

Then S_+ may be written:

$$S_+ = \sum_{\xi=1}^{\infty} \frac{\cos \alpha\xi}{\xi + \sqrt{i}\beta} = - \sum_{-\infty}^{-1} \frac{\cos \alpha\xi}{\xi - \sqrt{i}\beta}$$

and we can also write

$$S = \frac{1}{2\sqrt{i}\beta} \left\{ \sum_{-\infty}^{\infty} \frac{\cos \alpha\xi}{\xi - \sqrt{i}\beta} + \frac{1}{\sqrt{i}\beta} \right\} \qquad \beta \neq 0$$

The value of

$$S_1 = \sum_{\xi=-\infty}^{\infty} \frac{\cos \alpha\xi}{\xi - \sqrt{i}\beta}$$

is known for a term a(=$\sqrt{i}\beta$ here) unrestricted in the complex domain, provided that a≠0 or a real integer (Bromwich, 1926, §125). Then substituting for α and β:

$$S_1 = -\pi \frac{\cos \sqrt{i}\eta(h-z)}{\sin \sqrt{i}\eta h}$$

Substituting for S_1 we obtain S, and hence:

$$\sum_{\xi=1}^{\infty} \frac{\cos \frac{\pi z}{h} \xi}{(\frac{\pi}{h})^2 \xi^2 - i\eta^2} = \frac{1}{2i\eta^2} \left\{ 1 - \sqrt{i}\, h\eta \frac{\cos \sqrt{i}\eta(h-z)}{\sin \sqrt{i}\eta h} \right\} \qquad \text{(A3.2)}$$

where $0 \leq z \leq h$ and $\eta \neq 0$.

This relation is employed as eq. (4.28).

(b) $$\sum_{\xi=1}^{\infty} \frac{\xi \sin \alpha\xi}{(\frac{\pi}{h})^2 \xi^2 - i\eta^2} \; ; \qquad \alpha = \frac{\pi}{h} z \qquad \text{(A3.3)}$$

This series is uniformly convergent, provided $\alpha \neq 2m\pi$, m=0, 1, 2, ..., since it satisfies the Dirichlet conditions (Knopp, 1951, §199). It may thus be treated as the derived series corresponding to (A3.2), the derivative being taken with respect to either z or α.

Thus we have that

$$\sum_{\xi=1}^{\infty} \frac{\xi \sin \frac{\pi}{h} z\xi}{(\frac{\pi}{h})^2 \xi^2 - i\eta^2} = \frac{h^2}{2\pi} \frac{\sin \sqrt{i}\eta(h-z)}{\sin \sqrt{i}\eta h} \qquad \text{(A3.4)}$$

and this is the relation used as eq. (4.39).

Appendix 4: The Derivation of the Fields in a Double-layered Half-Space

We assume the geometry of Fig. A4.1, with a uniform medium of conductivity σ_2 and depth h, underlain by an infinitely deep medium of conductivity σ_3 and separated by a plane horizontal interface. The electromagnetic field is incident normally, in the z-direction. Let us consider the $\underset{\sim}{E}$-field. Since it is symmetrical in the horizontal directions and varies only with z, it satisfies a scalar Helmholtz equation (3.3) in the form

$$\left(\frac{d^2}{dz^2} + i\eta^2\right) E = 0, \qquad \eta^2 = \mu_o \omega \sigma \tag{A4.1}$$

The solutions in regions 2 and 3 must be of the forms:

$$E_2 = a_2 e^{-\sqrt{-i}\eta_2 z} + b_2 e^{\sqrt{i}\eta_2 z}$$

$$E_3 = a_3 e^{-\sqrt{-i}\eta_3 z} \tag{A4.2}$$

The continuity of E and H (or dE/dz) at the interface z=h, and the relations assumed in (iii) of Table 3.2, viz.:

$$\frac{dE}{dz} = i\omega\mu_o A \qquad \text{at } z=0$$

allow the three coefficients to be determined and (A4.2) becomes:

$$E_2 = \frac{i\mu_o \omega A}{\Delta} \left\{\cosh \sqrt{-i}\eta_2(h-z) + (\eta_3/\eta_2) \sinh \sqrt{-i}\eta_2(h-z)\right\}$$

$$E_3 = 2 \frac{i\mu_o \omega A}{\Delta} e^{-\sqrt{-i}\eta_3(z-h)} \tag{A4.3}$$

$$\Delta = -\sqrt{-i}\eta_2 \left\{\sinh \sqrt{-i}\eta_2 h + (\eta_3/\eta_2) \cosh \sqrt{-i}\eta_2 h\right\}$$

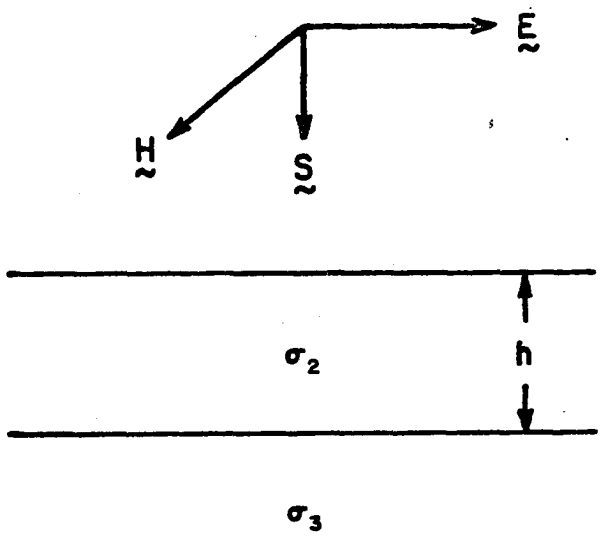

Fig. A4.1 A double-layered half-space with horizontal interfaces.

In the special case in which we are interested, $\sigma_3=0$ and

$$E_2 = \sqrt{i}\ \frac{\mu_o \omega A}{\eta_2}\ \frac{\cos \sqrt{i}\eta_2(h-z)}{\sin \sqrt{i}\eta_2 h} \tag{A4.4}$$

The orthogonal magnetic field is then given by Maxwell's equation in the form:

$$H = \frac{1}{i\mu_o\omega}\ \frac{dE}{dz}$$

Then

$$H_2 = A\ \frac{\sin \sqrt{i}\eta_2(h-z)}{\sin \sqrt{i}\eta_2 h} \tag{A4.5}$$

Relations (A4.4) and (A4.5) are the expressions for the asympototic fields in a bi-layered medium at great distances from the discontinuities discussed in §§4.2 and 5.2.

Appendix 5: Evaluation of Integrals:

$$(a)\ I(z) = \int_0^\infty \frac{\cos \xi z}{\xi^2 - i\eta_i^2}\, d\xi \qquad (A5.1)$$

This infinite integral converges absolutely, by the comparison test. For convenience write: $x = \xi/\eta_i$; $y = \eta_i z$

$$\text{Then } I = \frac{1}{\eta_i} \int_0^\infty \frac{\cos xy}{x^2 - i}\, dx$$

Since the integrand is even, we may write this as:

$$I = \frac{1}{2\eta_i} \int_{-\infty}^\infty \frac{\frac{1}{2}(e^{ixy} + e^{-ixy})}{x^2 - i}\, dx$$

$$\text{Write} \qquad I_{1,2}(y) = \int_{-\infty}^\infty \frac{e^{\pm ixy}}{x^2 - i}\, dx$$

$$\text{with } I = \frac{1}{4\eta_i}(I_1 + I_2)$$

To evaluate these, consider

$$I_1 = \int_{C_1} \frac{e^{+iwy}}{w^2 - i}\, dw \quad ; \quad I_2 = \int_{C_2} \frac{e^{-iwy}}{w^2 - i}\, dw$$

where the contours C_1 and C_2 are depicted in Figs. A5.1 (a) and (b) respectively. They are semicircles in the positive and negative half planes respectively, of radii R beyond the singularities in the respective upper and lower half planes, at $w = \pm\sqrt{i}$.

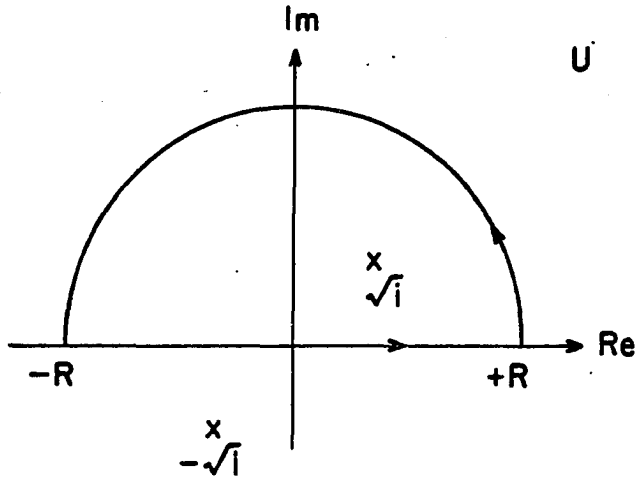

(a) CONTOUR C_1

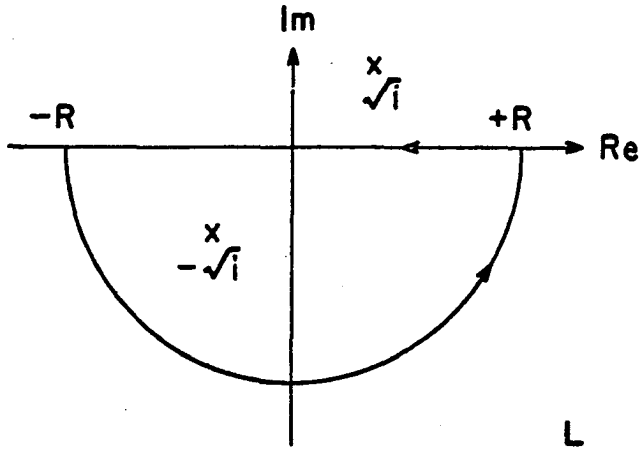

(b) CONTOUR C_2

Fig. A5.1 Contours for the evaluation of the complex integrals.

The integrands satisfy the requirements of (i) Cauchy's Residue Theorem and also of (ii) Jordan's Lemma, so that the integrals may be evaluated from the residues; the contributions from the semi-circular arcs vanish in the limit as $R \to \infty$, leaving the required integrals I_1 and I_2. (See, for instance, Phillips, 1954).

$$I_1 = \int_{-\infty}^{\infty} \frac{e^{ixy}}{x^2 - i}\, dx = 2\pi i \quad \text{(Residue in U)}$$

$$I_2 = \int_{-\infty}^{\infty} \frac{e^{-ixy}}{x^2 - i}\, dx = -2\pi i \quad \text{(Residue in L)}$$

Residue in U at singularity $w = +\sqrt{i}$

$$= \frac{e^{+iy\sqrt{i}}}{2\sqrt{i}}$$

Residue in L at singularity $w = -\sqrt{i}$

$$= -\frac{e^{+iy\sqrt{i}}}{2\sqrt{i}}$$

Thus $I_1 = \pi\sqrt{i}\, e^{-\sqrt{-i}\, y}$, $\mathrm{Re}\sqrt{-i} > 0$

$$I_2 = \pi\sqrt{i}\, e^{-\sqrt{-i}\, y}$$

So $I(z) = \frac{\sqrt{i}}{2\eta_i}\, e^{-\sqrt{-i}\, \eta_1 z}$ where $\mathrm{Re}\sqrt{-i} > 0$ or $\sqrt{-i} = -i\sqrt{i}$ (A5.2)

This is the relation used in §5.1.2(a) as equation (5.8)

(b) $$I(z) = \int_0^{\infty} \frac{\xi \sin \xi z}{\xi^2 - i\eta_i^2}\, d\xi \qquad \text{(A5.3)}$$

This integral may be evaluated as in (a) above. Alternatively we note that, since ξ and z are real and $\eta_i \neq 0$, the integrand in (A5.1) is a continuous function of both ξ and z in $[o,\infty)$, and has a continuous z-derivative there. The integral (A5.1) is thus convergent, and we may differentiate under the integral sign with respect to z, provided the integral in (A5.3) can be shown uniformly convergent on any fixed arbitrary interval of z in $[o,\infty)$. The derived integral will be the value of (A5.3) (see Carslaw, 1921).

The integral (A5.3) is uniformly convergent by Dirichlet's test. We may thus write

$$I(z) = \int_o^\infty \frac{\xi \sin \xi z}{\xi^2 - i\eta_i^2}\, d\xi = -\frac{\partial}{\partial z}\int_o^\infty \frac{\cos \xi z}{\xi^2 - i\eta_i^2}\, d\xi = -\frac{\partial}{\partial z}\left[\frac{\sqrt{i}\,\pi}{2\eta_i} e^{-\sqrt{-i}\,\eta_1 z}\right]$$

$$\text{or } I(z) = -\frac{\sqrt{i}\,\pi}{2\eta_i} \cdot (-\sqrt{-i}\,\eta_i)\; e^{-\sqrt{-i}\,\eta_i z}$$

$$\text{or } I(z) = \frac{\pi}{2}\; e^{-\sqrt{-i}\,\eta_i z} \qquad \text{(A5.4)}$$

This relation is used in §5.1.2(b) as equation (5.16).

Appendix 6: Reduction of the Complex Integrands to Real and Imaginary Parts

The integrals of Table (5.2) may be considered as special cases of two particular types, depending on whether they refer to Region 1 or Region 2. These general forms are:

$$\text{Region 1:} \int_0^\infty \frac{u^n \, \text{hyp}\left[Q(Y+1)\sqrt{u^2-i\varepsilon^2}\right]}{\sqrt{u^2-i}\;\;(u^2-i\varepsilon^2)^{m_1}\,D_j}\,du \qquad \text{(A6.1)}$$

$$\text{Region 2:} \int_0^\infty \frac{u^n\, e^{-QY\sqrt{u^2-i}}\sinh\left[Q\sqrt{u^2-i\varepsilon^2}\right]}{(u^2-i)^{m_2}\sqrt{u^2-i\varepsilon^2}\;\cdot D_j}\,du \qquad \text{(A6.2)}$$

Here 'hyp' refers to either hyperbolic function 'sinh' or 'cosh', and the D_j are given by

$$\left.\begin{aligned} D_1 &= \sqrt{u^2-i\varepsilon^2}\;\;\sinh\left[Q\sqrt{u^2-i\varepsilon^2}\right] + \sqrt{u^2-i}\;\;\cosh\left[Q\sqrt{u^2-i\varepsilon^2}\right] \\ D_2 &= \sqrt{u^2-i\varepsilon^2}\;\;\sinh\left[Q\sqrt{u^2-i\varepsilon^2}\right] + \varepsilon^2\sqrt{u^2-i}\;\;\cosh\left[Q\sqrt{u^2-i\varepsilon^2}\right] \end{aligned}\right\} \qquad \text{(A6.3)}$$

The values of the indices n, m_1, m_2 and subscript i are given in Table A6.1.

Table A6.1

Values of the Indices in the Integrand Expressions

n	m_1	m_2	j	Relation
0	1	1	1	E_x
	½	½	1	H_z
2	1	1	2	E_y

Denote: $\sqrt{u^2-i\varepsilon^2} = (\alpha_{11} + i\beta_{11})/\sqrt{2}$ $\qquad$ $\sqrt{u^2-i} = (\alpha_{22} + i\beta_{22})/\sqrt{2}$

where $\alpha_{11} = [(u^4 + \varepsilon^4)^{\frac{1}{2}} + u^2]^{\frac{1}{2}}$ $\qquad$ $\beta_{11} = -[(u^4 + \varepsilon^4)^{\frac{1}{2}} - u^2]^{\frac{1}{2}}$

$\alpha_{22} = [(u^4 + 1)^{\frac{1}{2}} + u^2]^{\frac{1}{2}}$ $\qquad$ $\beta_{22} = -[(u^4 + 1)^{\frac{1}{2}} - u^2]^{\frac{1}{2}}$

Also let

$$(u^2 - i\varepsilon^2)\sqrt{u^2-i} = (\alpha_{11} + i\beta_{11})^2 (\alpha_{22} - i\beta_{22})/2\sqrt{2} = (p_1 + iq_1)/2\sqrt{2}$$

$$(u^2 - i)\sqrt{u^2-i\varepsilon^2} = (\alpha_{11} + i\beta_{11})(\alpha_{22} + i\beta_{22})^2/2\sqrt{2} = (p_2 + iq_2)/2\sqrt{2}$$

$$\sqrt{(u^2-i)(u^2-i\varepsilon^2)} = (\alpha_{11} + i\beta_{11})(\alpha_{22} + i\beta_{22})/2 = (p_3 + iq_3)/2$$

where:

$$p_1 = \alpha_{22}(\alpha_{11}^2 - \beta_{11}^2) - 2\,\alpha_{11}\,\beta_{11}\beta_{22}$$

$$q_1 = 2\alpha_{11}\,\alpha_{22}\beta_{11} + \beta_{22}\,(\alpha_{11}^2 - \beta_{11}^2)$$

$$p_2 = \alpha_{11}(\alpha_{22}^2 - \beta_{22}^2) - 2\,\alpha_{22}\,\beta_{11}\,\beta_{22}$$

$$q_2 = 2\alpha_{11}\,\alpha_{22}\,\beta_{22} + \beta_{11}(\alpha_{22}^2 - \beta_{22}^2)$$

$$p_3 = \alpha_{11}\,\alpha_{22} - \beta_{11}\,\beta_{22}$$

$$q_3 = \alpha_{11}\,\beta_{22} + \alpha_{22}\,\beta_{11}$$

Now let $\alpha_i = Q\alpha_{ii}/\sqrt{2}$; $\beta_i = Q\beta_{ii}/\sqrt{2}$ for i = 1,2.

We have also

$$\text{hyp}\left[Q(Y+1)\sqrt{u_2-i\varepsilon^2}\right]$$

$$= \text{hyp}\left[(Y+1)(\alpha_1 + i\beta_1)\right]$$

$$= \tfrac{1}{2}\, e^{(Y+1)\alpha_1}\left[e^{i\beta_1(Y+1)} \pm e^{-2\alpha_1(Y+1)}\, e^{-i\beta_1(Y+1)}\right]$$

where the + refers to 'cosh', the - to 'sinh'.

Then

$$\cosh\left[Q(Y+1)\sqrt{u^2-i\varepsilon^2}\right] = e^{(Y+1)\alpha_1}(n_1 + it_1)$$

$$\sinh\left[Q(Y+1)\sqrt{u^2-i\varepsilon^2}\right] = e^{(Y+1)\alpha_1}(n_3 + it_3)$$

$$e^{-QY\sqrt{u^2-i}}\sinh Q\sqrt{u^2-i\varepsilon^2} = e^{\alpha_1}(n_2 - it_2)$$

If we also designate

$$\text{snhm } x = \tfrac{1}{2}(1 - e^{-2x}) = e^{-x}\sinh x$$

$$\text{cshm } x = \tfrac{1}{2}(1 + e^{-2x}) = e^{-x}\cosh x$$

then we may write:

$$n_1 = \text{cshm } \alpha_1(Y+1)\cos\beta_1(Y+1)$$

$$t_1 = \text{snhm } \alpha_1(Y+1)\sin\beta_1(Y+1)$$

$$n_2 = \text{snhm } \alpha_1(Y+1)\cos\beta_1\cos Y\beta_2 + \text{cshm } \alpha_1(Y+1)\sin\beta_1\sin Y\beta_2$$

$$t_2 = \text{cshm } \alpha_1(Y+1)\sin\beta_1\cos Y\beta_2 - \text{snhm } \alpha_1(Y+1)\cos\beta_1\sin Y\beta_2$$

$$n_3 = \text{snhm } \alpha_1(Y+1)\cos\beta_1(Y+1)$$

$$t_3 = \text{cshm } \alpha_1(Y+1)\sin\beta_1(Y+1)$$

The initial exponential factors are removed in the hyperbolic expressions since α_1 (proportional to Q and, approximately, to u) can become extremely large for large values of Q and/or u. Nevertheless there is a cancellation of large factors between the numerator and denominator (D_1) hyperbolic expressions. Initial removal avoids overflow in the machine computations.

Similarly we may write

$$D_1 = e^{\alpha_1} (r_1 + i\, s_1)/\sqrt{2}$$

$$D_2 = e^{\alpha_1} (r_2 + i\, s_2)/\sqrt{2}$$

where:

$$r_1 = \alpha_{11} \operatorname{snhm} \alpha_1 \cos \beta_1 - \beta_{11} \operatorname{cshm} \alpha_1 \sin \beta_1 + \\ + \alpha_{22} \operatorname{cshm} \alpha_1 \cos \beta_1 - \beta_{22} \operatorname{snhm} \alpha_1 \sin \beta_1$$

$$s_1 = \beta_{11} \operatorname{snhm} \alpha_1 \cos \beta_1 + \alpha_{11} \operatorname{cshm} \alpha_1 \sin \beta_1 + \\ + \beta_{22} \operatorname{cshm} \alpha_1 \cos \beta_1 + \alpha_{22} \operatorname{snhm} \alpha_1 \sin \beta_1$$

$$r_2 = \alpha_{11} \operatorname{snhm} \alpha_1 \cos \beta_1 - \beta_{11} \operatorname{cshm} \alpha_1 \sin \beta_1 + \\ + \varepsilon^2 \alpha_{22} \operatorname{cshm} \alpha_1 \cos \beta_1 - \varepsilon^2 \beta_{22} \operatorname{snhm} \alpha_1 \sin \beta_1$$

$$s_2 = \beta_{11} \operatorname{snhm} \alpha_1 \cos \beta_1 + \alpha_{11} \operatorname{cshm} \alpha_1 \sin \beta_1 + \\ + \varepsilon^2 \beta_{22} \operatorname{cshm} \alpha_1 \cos \beta_1 + \varepsilon^2 \alpha_{22} \operatorname{snhm} \alpha_1 \sin \beta_1$$

In the six expressions of Table 5.2, there are five different denominators occurring in the integrands. These may be written as

$$\frac{1}{2\sqrt{2}} (p_1 + iq_1) D_1 = \frac{e^{\alpha_1}}{4} (\ell_1 + im_1)$$

$$\frac{1}{2\sqrt{2}} (p_2 + iq_2) D_1 = \frac{e^{\alpha_1}}{4} (\ell_2 + im_2)$$

$$\frac{1}{2\sqrt{2}} (p_3 + iq_3) D_2 = \frac{e^{\alpha_1}}{4} (\ell_3 + im_3)$$

$$\frac{1}{2\sqrt{2}} (p_4 + iq_4) D_2 = \frac{e^{\alpha_1}}{4} (\ell_4 + im_4)$$

$$\frac{1}{2} (p_5 + iq_5) D_1 = \frac{1}{2\sqrt{2}} e^{\alpha_1} (\ell_5 + im_5)$$

The last of these expressions occurs in both of the relations (5.27). We may thus write out the ℓ_i, m_i in terms of p_i, q_i, r_j, s_j:

$$\ell_1 = p_1 r_1 - q_1 s_1 \quad ; \quad m_1 = q_1 r_1 + p_1 s_1$$

$$\ell_2 = p_2 r_1 - q_2 s_1 \quad ; \quad m_2 = q_2 r_1 + p_2 s_1$$

$$\ell_3 = p_1 r_2 - q_1 s_2 \quad ; \quad m_3 = q_1 r_2 + p_1 s_2$$

$$\ell_4 = p_2 r_2 - q_2 s_2 \quad ; \quad m_4 = q_2 r_2 + p_2 s_2$$

$$\ell_5 = p_3 r_1 - q_3 s_1 \quad ; \quad m_5 = q_3 r_1 + p_3 s_1$$

The integrands of Table 5.2, represented by (A6.1) and (A6.2), may therefore be resolved into real and imaginary parts, involving only the ℓ_i, m_i and a preliminary real factor. We represent these integrands by F(L,M), where L = 1,2,3 designate E_x, E_y, H_z respectively, and M = 1,2 designate the real and imaginary parts of region 1, M = 3,4, the real and imaginary parts of region 2. This nomenclature is used because of its convenience in the computer calculations.

The integrands F(L,M) are given in Table A6.2.

The relations specified in Table A6.2 may be used to express the real and imaginary parts of the expressions in Table 5.2. These are specified as relations (A6.4 - A6.9) in Table A6.3.

Table A6.2

The Real and Imaginary Parts of the Integrands of the Field Component Expressions in Table 5.2

Field Component	Part	Label		Expressions
E_{x1}	Real	F(1,1)	=	$4\, e^{Y\alpha_1} \dfrac{n_1\ell_1 + m_1 t_1}{\ell_1^2 + m_1^2}$
	Imaginary	F(1,2)	=	$4\, e^{Y\alpha_1} \dfrac{\ell_1 t_1 - m_1 n_1}{\ell_1^2 + m_1^2}$
E_{x2}	Real	F(1,3)	=	$4\, e^{-Y\alpha_2} \dfrac{n_2\ell_2 + m_2 t_2}{\ell_2^2 + m_2^2}$
	Imaginary	F(1,4)	=	$4\, e^{-Y\alpha_2} \dfrac{\ell_2 t_2 - m_2 n_2}{\ell_2^2 + m_2^2}$
E_{y1}	Real	F(2,1)	=	$4\, u^2\, e^{Y\alpha_1} \dfrac{n_1\ell_3 + m_3 t_1}{\ell_3^2 + m_3^2}$
	Imaginary	F(2,2)	=	$4\, u^2\, e^{Y\alpha_1} \dfrac{\ell_3 t_1 - m_3 n_1}{\ell_3^2 + m_3^2}$
E_{y2}	Real	F(2,3)	=	$4\, u^2\, e^{-Y\alpha_2} \dfrac{\ell_4 n_2 + m_4 t_2}{\ell_4^2 + m_4^2}$
	Imaginary	F(2,4)	=	$4\, u^2\, e^{-Y\alpha_2} \dfrac{\ell_4 t_2 - m_4 n_2}{\ell_4^2 + m_4^2}$
H_{z1}	Real	F(3,1)	=	$2\sqrt{2}\, e^{Y\alpha_1} \dfrac{n_3\ell_5 + m_5 t_3}{\ell_5^2 + m_5^2}$
	Imaginary	F(3,2)	=	$2\sqrt{2}\, e^{Y\alpha_1} \dfrac{\ell_5 t_3 - m_5 n_3}{\ell_5^2 + m_5^2}$
H_{z2}	Real	F(3,3)	=	$2\sqrt{2}\, e^{-Y\alpha_2} \dfrac{n_2\ell_5 + m_5 t_2}{\ell_5^2 + m_5^2}$
	Imaginary	F(3,4)	=	$2\sqrt{2}\, e^{-Y\alpha_2} \dfrac{\ell_5 t_2 - m_5 n_2}{\ell_5^2 + m_5^2}$

Table A6.3

The Real and Imaginary Parts of the Complete Field Expressions in Table 5.2

Field Component		Part		
$\frac{1}{\mu_o \omega^{\frac{1}{2}} \ell}$	$\frac{Ex_1}{A}$	Real	$\frac{1}{\sqrt{2}\, Q\varepsilon} + \frac{2}{\pi} \frac{1-\varepsilon^2}{Q} \int_0^\infty F(1,1)\, du$	(A6.4)
		Imaginary	$-\frac{1}{\sqrt{2}\, Q\varepsilon} + \frac{2}{\pi} \frac{1-\varepsilon^2}{Q} \int_0^\infty F(1,2)\, du$	
$\frac{1}{\mu_o \omega^{\frac{1}{2}} \ell}$	$\frac{Ex_2}{A}$	Real	$\frac{1}{\sqrt{2}\, Q} - \frac{2}{\pi} \frac{1-\varepsilon^2}{Q} \int_0^\infty F(1,3)\, du$	(A6.5)
		Imaginary	$-\frac{1}{\sqrt{2}\, Q} - \frac{2}{\pi} \frac{1-\varepsilon^2}{Q} \int_0^\infty F(1,4)\, du$	
$-\frac{1}{\mu_o \omega^{\frac{1}{2}} \ell}$	$\frac{Ey_1}{B}$	Real	$-\frac{1}{\sqrt{2}\, Q\varepsilon} - \frac{2}{\pi} \frac{1-\varepsilon^2}{Q} \int_0^\infty F(2,2)\, du$	(A6.6)
		Imaginary	$\frac{1}{\sqrt{2}\, Q\varepsilon} + \frac{2}{\pi} \frac{1-\varepsilon^2}{Q} \int_0^\infty F(2,1)\, du$	
$-\frac{1}{\mu_o \omega^{\frac{1}{2}} \ell}$ q	$\frac{Ey_2}{B}$	Real	$-\frac{1}{\sqrt{2}\, Q} + \frac{2}{\pi} \frac{1-\varepsilon^2}{Q} \int_0^\infty F(2,4)\, du$	(A6.7)
		Imaginary	$\frac{1}{\sqrt{2}\, Q} - \frac{2}{\pi} \frac{1-\varepsilon^2}{Q} \int_0^\infty F(2,3)\, du$	
	$\frac{Hz_1}{A}$	Real	$-\frac{2}{\pi}(1-\varepsilon^2) \int_0^\infty F(3,2)\, du$	(A6.8)
		Imaginary	$\frac{2}{\pi}(1-\varepsilon^2) \int_0^\infty F(3,1)\, du$	
	$\frac{Hz_2}{A}$	Real	$-\frac{2}{\pi}(1-\varepsilon^2) \int_0^\infty F(3,4)\, du$	(A6.9)
		Imaginary	$\frac{2}{\pi}(1-\varepsilon^2) \int_0^\infty F(3,3)\, du$	

Appendix 7: The Asymptotic Expansion of the Complex Integrands in Table 5.2 for Large Values of u:

Asymptotic expansions to lowest order of the integrands of all of the expressions in Table 5.2 (when $\varepsilon/u << 1$ and consequently also $1/u << 1$) may be made very easily by employing binomial expansions of the radicals and their hyperbolic functions. Unfortunately, however, it is necessary to go considerably beyond the lowest order expansions for useful purposes in the ranges where the integrands are still large enough to be involved in the computations. This involves an enormous amount of exceedingly tedious algebra which we will only outline.

If we write $f = \frac{\varepsilon}{u} << 1$

then $(u^2 - i\,\varepsilon^2)^{\frac{1}{2}} \approx u\,(1 - \frac{1}{2}\,if^2)$

$$\text{hyp}\,(u^2 - i\varepsilon^2)^{\frac{1}{2}}\alpha \approx \tfrac{1}{2}\,e^{\alpha u}\,\text{cis}\,(-\tfrac{1}{2}\alpha u f^2) \pm \tfrac{1}{2}\,e^{-\alpha u}\,\text{cis}\,(+\tfrac{1}{2}\alpha u f^2)$$

where 'hyp' represents a hyperbolic function cosh (+ sign on r.h.s.) or sinh (- sign on r.h.s.), and 'cis' represents 'cos + i sin'. When the arguments of the 'cis' are very small, these can be further expanded by Taylor series. The expansion places a requirement on the value of α, a function of Q and Y. It is also useful to define a further parameter:

$$\delta = \frac{1-\varepsilon^2}{1+\varepsilon^2}$$

always slightly smaller than unity. Only the terms involving the two lowest orders were retained in the calculation of the expansions for

each of the real and imaginary parts; however, it is found that the lowest order term (which we term the zeroth order) is in all cases purely real, while the next term is purely imaginary. Thus to obtain an expansion of both real and imaginary parts to an order greater than the lowest, it is necessary to consider three orders of terms in any particular field component expression. It is this behavior that causes the enormous amount of algebraic manipulation necessary to obtain the relatively simple final expressions.

The expressions for the E_x and H_z integrands of Table 5.2 present no difficulty. In the E_y expression the denominator involves the term D_2 instead of D_1, the difference being a quite innocent looking ϵ^2 before the second term of its formula. This ϵ^2 results in the expansions involving series in δ, which, although convergent, complicate the expression of even the zeroth order terms. These series, however, can all be summed in closed form and are basically special cases of one of the following two series:

$$\sum_{n=0}^{\infty} a^n (x+\gamma+2\beta n)^2 e^{-\alpha(x+2n)} = \frac{(x+\gamma)^2 e^{-\alpha x}}{1-ae^{-2\alpha}} + \frac{4a\beta(x+\gamma+\beta) e^{-\alpha(x+2)}}{(1-ae^{-2\alpha})^2} + \frac{8a^2\beta^2 e^{-\alpha(x+4)}}{(1-ae^{-2\alpha})^3} \tag{A7.1}$$

$$\sum_{n=0}^{\infty} a^n (x+\gamma+2\beta n) e^{-\alpha(x+2n)} = \frac{(x+\gamma)e^{-\alpha x}}{1-ae^{-2\alpha}} + \frac{2a\beta e^{-\alpha(x+2)}}{(1-ae^{-2\alpha})^2}$$

These series are summed to the terms on the right, in App. 8, under the conditions: $u \gg \text{Max}(1, QY)$ in region 2

or $u \gg \text{Max}(1, Q\epsilon^2)$ in region 1,

and for the E_y expressions we also need $Qu \gtrsim 1$.

The asymptotic expansions of the integrands F(L,M) for large u, are given in Table A7.1.

The convergence of such complicated series would be difficult to establish; suffice it to say that at large u the terms themselves tend to zero very strongly and we might reasonably expect the series to converge, at least for realistic values of the other parameters.

For sufficiently large values of u, the higher order terms will certainly be smaller than the lower order terms, for any fixed set of the other parameters. Assuming that the series may be approximated sufficiently closely by such an expansion, and that it can be integrated term-by-term, we note that the integration beyond some u = a reduces to a series of terms in

$$\int_a^\infty \frac{e^{-pQu}}{(Qu)^n}\, d(Qu) \qquad (A7.2)$$

The expressions for E_y are readily reduced to series in these terms; in fact the series (A7.1) are series in such integrands, n being 2,3,4, in the 0th, 1st, and 2nd order terms respectively.

The change of variable Qu = ax reduces the expression(A7.2) to

$$\frac{1}{a^{n-1}} \int_1^\infty \frac{e^{-pax}}{x^n}\, dx;$$

These integrals are the well-known generalized exponential integrals (for further information and tables see Gautschi and Cahill, 1964; Fletcher, et al, 1962, Pagurova, 1961):

$$\frac{1}{a^{n-1}} E_n(pa)$$

The $E_n(pa)$ diverge at $pa = 0$, for $n = 0, 1$ (which are not involved here), but otherwise converge. We thus have further indication of the convergence behavior of the integrals of Table 5.2 in the extreme range of the integration variable u.

Table A7.1

Asymptotic Expansions of Integrands with Respect to the Integration Variable u

(a) Terms in E_x

Integrand	0th Order	1st Order	2nd Order
Region 1: $\alpha \le \lvert y\rvert < \frac{1}{2}t$:			
Real: $\frac{1}{\rho^3} F(1,1)$	$\approx \frac{1}{2}\left(\frac{e^{-Qu\lvert Y\rvert} + e^{-Qu.\overline{2-\lvert Y\rvert}}}{(Qu)^4}\right)$		$-\frac{(Q\epsilon)^4}{16}\left(\frac{Y^2 e^{-Qu\lvert Y\rvert} + (2-\lvert Y\rvert)^2 e^{-Qu.\overline{2-\lvert Y\rvert}}}{(Qu)^6}\right)$
Imaginary: $\frac{1}{\rho^3} F(1,2)$	$\approx$	$\left(\frac{(Q\epsilon)^2}{4}\frac{\lvert Y\rvert e^{-Qu\lvert Y\rvert} + (2-\lvert Y\rvert)\, e^{-Qu.\overline{2-\lvert Y\rvert}}}{(Qu)^5}\right)$	$+\frac{Q^2}{8}\frac{(3+5\epsilon^2)\left(e^{-Qu\lvert Y\rvert} + e^{-Qu.\overline{2-\lvert Y\rvert}}\right) + (1-\epsilon^2)\left(e^{-Qu.\overline{2+\lvert Y\rvert}} + e^{-Qu.\overline{4-\lvert Y\rvert}}\right)}{(Qu)^6}$
Region 2: $\lvert y\rvert > \frac{1}{2}t$			
Real: $\frac{1}{\rho^3} F(1,3)$	$\approx \frac{1}{2}\left(\frac{e^{-QuY} - e^{-Qu.\overline{Y+2}}}{(Qu)^4}\right)$		$-\frac{Q^4}{16}\left(\frac{Y^2 e^{-QuY} - (Y+2\epsilon^2)^2 e^{-Qu.\overline{Y+2}}}{(Qu)^6}\right)$
Imaginary: $\frac{1}{\rho^3} F(1,4)$	$\approx$	$\frac{Q^2}{4}\left(\frac{Ye^{-QuY} - (Y+2\epsilon^2)\, e^{-Qu.\overline{Y+2}}}{(Qu)^5}\right)$	$+\frac{Q^2}{8}\frac{(5+3\epsilon^2)\left(e^{-QuY} - e^{-Qu.\overline{Y+2}}\right) + (1-\epsilon^2)\left(e^{-Qu.\overline{Y+2}} - e^{-Qu.\overline{Y+4}}\right)}{(Qu)^6}$

Table A7.1 (cont'd)

Asymptotic Expansions of Integrands with Respect to the Integration Variable u

(b) Terms in Ey

Integrand	0th Order	1st Order	2nd Order
Region 1: $o<\|y\|<\frac{1}{2}t$:			
Real $\frac{1}{Q}F(2,1)$ $\sim$	$\frac{1}{(1+\varepsilon^2)(Qu)^2}\,\frac{e^{-Qu\|Y\|}+e^{-Qu.\overline{2-\|Y\|}}}{1-\delta e^{-2Qu}}$	$-\frac{(Q\varepsilon)^4}{8(1+\varepsilon^2)(Qu)^4}\,\frac{Y^2e^{-Qu\|Y\|}+(2-\|Y\|)^2e^{-Qu.\overline{2-\|Y\|}}}{1-\delta e^{-2Qu}}+4\delta\,\frac{(\|Y\|+1)e^{-Qu.\overline{\|Y\|+2}}+2(3-\|Y\|)e^{-Qu.\overline{4-\|Y\|}}}{(1-\delta e^{-2Qu})^2}+$ $+8\delta^2\,\frac{e^{-Qu.\overline{\|Y\|+4}}+e^{-Qu.\overline{6-\|Y\|}}}{(1-\delta e^{-2Qu})^3}$	
Imaginary: $\frac{1}{Q}F(2,2)$ $\sim$	$\frac{(Q\varepsilon)^2}{2(1+\varepsilon^2)(Qu)^3}\,\frac{\|Y\|e^{-Qu\|Y\|}+(2-\|Y\|)e^{-Qu.\overline{2-\|Y\|}}}{1-\delta e^{-2Qu}}+$ $+2\delta\,\frac{e^{-Qu.\overline{\|Y\|+2}}+e^{-Qu.\overline{4-\|Y\|}}}{(1-\delta e^{-2Qu})^2}$	$+\frac{(Q\varepsilon)^2}{(1+\varepsilon^2)^2(Qu)^4}\left(e^{-Qu\|Y\|}+e^{-Qu.\overline{2-\|Y\|}}\right)+\frac{Q^2(1+2\varepsilon^2)}{2(1+\varepsilon^2)(Qu)^4}\cdot\frac{e^{-Qu\|Y\|}+e^{-Qu.\overline{2-\|Y\|}}}{1-\delta e^{-2Qu}}$	
Region 2: $\|y\|>\frac{1}{2}t$:			
Real: $\frac{1}{Q}F(2,3)$ $\sim$	$\frac{1}{(1+\varepsilon^2)(Qu)^2}\,\frac{e^{-QuY}+e^{-Qu.\overline{Y+2}}}{1-\delta e^{-2Qu}}$	$-\frac{Q^4}{8(1+\varepsilon^2)(Qu)^4}\,\frac{Y^2e^{-QuY}+(Y+2\varepsilon^2)e^{-Qu.\overline{Y+2}}}{1-\delta e^{-2Qu}}+4\delta\,\frac{(Y+\varepsilon^2)e^{-Qu.\overline{Y+2}}+(Y+3\varepsilon^2)e^{-Qu.\overline{Y+4}}}{(1-\delta e^{-2Qu})^2}+$ $+8\varepsilon^4\delta^2\,\frac{e^{-Qu.\overline{Y+4}}+e^{-Qu.\overline{Y+6}}}{(1-\delta e^{-2Qu})^3}$	
Imaginary: $\frac{1}{Q}F(3.4)$ $\sim$	$\frac{Q^2}{2(1+\varepsilon^2)(Qu)^3}\,\frac{Ye^{-QuY}+(Y+2\varepsilon^2)e^{-Qu.\overline{Y+2}}}{1-\delta e^{-2Qu}}+$ $+2\varepsilon^2\delta\,\frac{e^{-QuY+2}+e^{-Qu.\overline{Y+4}}}{(1-\delta e^{-2Qu})^2}$	$+\frac{Q^2}{(1+\varepsilon^2)^2(Qu)^4}\left(e^{-Qu}+e^{-Qu.\overline{Y+2}}\right)+\frac{Q^2(2+\varepsilon^2)}{2(1+\varepsilon^2)(Qu)^4}\cdot\frac{e^{-QuY}+e^{-Qu.\overline{Y+2}}}{1-\delta e^{-2Qu}}$	

Table A7.1 (cont'd)

Asymptotic Expansions of Integrands with Respect to the Integration Variable u

(c) Terms in H_2

Integrand	0th Order	1st Order	2nd Order
Region 1: $0 \le \lvert y\rvert < \frac{1}{2}\varepsilon$:			
Real: $\frac{1}{Q^2}F(3,1) \sim$	$\frac{1}{2}\left(\frac{e^{-Qu\lvert Y\rvert} - e^{-Qu.\overline{2-\lvert Y\rvert}}}{(Qu)^3}\right)$		$-\frac{(Q\varepsilon)^4}{16}\left(\frac{Y^2 e^{-Qu\lvert Y\rvert} - (2-\lvert Y\rvert)^2\, e^{-Qu.\overline{2-\lvert Y\rvert}}}{(Qu)^5}\right)$
Imaginary: $\frac{1}{Q^2}F(3,2) \sim$		$\frac{(Q\varepsilon)^2}{4}\left(\frac{\lvert Y\rvert e^{-Qu\lvert Y\rvert} - (2-\lvert Y\rvert)\, e^{-Qu.\overline{2-\lvert Y\rvert}}}{(Qu)^4}\right)$	$+\frac{Q^2(1+\varepsilon^2)}{8}\left(\frac{3(e^{-Qu.\lvert Y\rvert} - e^{-Qu.\overline{2-\lvert Y\rvert}}) + \delta(e^{-Qu.\overline{2+\lvert Y\rvert}} - e^{-Qu.\overline{4-\lvert Y\rvert}})}{(Qu)^5}\right)$
Region 2: $\lvert y\rvert > \frac{1}{2}\varepsilon$:			
Real: $\frac{1}{Q^2}F(3,3) \sim$	$\frac{1}{2}\left(\frac{e^{-QuY} - e^{-Qu.\overline{Y+2}}}{(Qu)^3}\right)$		$-\frac{Q^4}{16}\left(\frac{Y^2 e^{-QuY} - (Y-2\varepsilon^2)\, e^{-Qu.\overline{Y+2}}}{(Qu)^5}\right)$
Imaginary: $\frac{1}{Q^2}F(3,4) \sim$		$\frac{Q^2}{4}\left(\frac{Ye^{-QuY} - (Y+2\varepsilon^2)\, e^{-Qu.\overline{Y+2}}}{(Qu)^4}\right)$	$+\frac{Q^2(1+\varepsilon^2)}{8}\left(\frac{3(e^{-QuY} - e^{-Qu.\overline{Y+2}}) + \delta(e^{Qu.\overline{Y+2}} - e^{-Qu.\overline{Y+4}})}{(Qu)^5}\right)$

Appendix 8: Summation of the Series Occurring in the Asymptotic Expansions

In Appendix 7, the series

$$S_1 = \sum_{n=0}^{\infty} a^n (x+\gamma+2\beta n)^2 \; e^{-\alpha(x+2n)}$$

$$S_2 = \sum_{n=0}^{\infty} a^n (x+\gamma+2\beta n) \; e^{-\alpha(x+2n)}$$

were mentioned. The constants a and α are both positive; x and γ are of either sign. Actually $a = \delta < 1$.

Now the series $\sum_{n=0}^{\infty} n^r \mu^n$, $r \geq o$, $o \leq \mu \leq 1$

are well-known, being special cases of the Dirichlet Series (Hardy and Riesz, 1915), and converge uniformly for all r and μ in the above domains. Since uniformly convergent series may be linearly combined to give further uniformly convergent series, (see for instance, Knopp, 1951), the series designated S_1 and S_2 above are also uniformly convergent. They may be written in the form:

$$S_1 = \beta^2 \, e^{-\frac{\alpha}{\beta}((\beta-1)x-\gamma)} \sum_{n=0}^{\infty} a^n \left(\frac{x+\gamma}{\beta} + 2n\right)^2 e^{-\alpha\left(\frac{x+\gamma}{\beta} + 2n\right)}$$

$$S_2 = \beta \, e^{-\frac{\alpha}{\beta}((\beta-1)x-\gamma)} \sum_{n=0}^{\infty} a^n \left(\frac{x+\gamma}{\beta} + 2n\right) e^{-\alpha\left(\frac{x+\gamma}{\beta} + 2n\right)}$$

Now let us consider the series:

$$S = \sum_{n=0}^{\infty} a^n \, e^{-\alpha\left(\frac{x+\gamma}{\beta} + 2n\right)} = e^{-\alpha\frac{x+\gamma}{\beta}} \sum_{n=0}^{\infty} (ae^{-2\alpha})^n$$

which is a form of the geometric series (we have specified $a < 1$ already).

Its derived series (with respect to α) are

$$S' = -\sum_{n=0}^{\infty} a^n \left(\frac{x+\gamma}{\beta} + 2n\right) e^{-\alpha\left(\frac{x+\gamma}{\beta} + 2n\right)}$$

$$S'' = \sum_{n=0}^{\infty} a^n \left(\frac{x+\gamma}{\beta} + 2n\right)^2 e^{-\alpha\left(\frac{x+\gamma}{\beta} + 2n\right)}$$

Apart from constant factors, these are the series involved in S_1 and S_2, which we already know are uniformly convergent. We may therefore write:

$$S_1 = \beta^2 e^{-\frac{\alpha}{\beta}((\beta-1)x-\gamma)} \frac{d^2S}{d\alpha^2}$$

$$S_2 = -\beta e^{-\frac{\alpha}{\beta}((\beta-1)x-\gamma)} \frac{dS}{d\alpha}$$

The geometric series S has the sum:

$$S = \frac{e^{-\alpha\frac{x+\gamma}{\beta}}}{1-ae^{-2\alpha}}$$

so that the derivatives are

$$\frac{dS}{d\alpha} = -\left(\frac{x+\gamma}{\beta} + \frac{2ae^{-2\alpha}}{1-ae^{-2\alpha}}\right) \frac{e^{-\alpha\frac{x+\gamma}{\beta}}}{1-ae^{-2\alpha}}$$

$$\frac{d^2S}{d\alpha^2} = \left(\frac{4ae^{-2\alpha}}{1-ae^{-2\alpha}} + \frac{4a^2e^{-4\alpha}}{(1-ae^{-2\alpha})^2}\right) \frac{e^{-\alpha\frac{x+\gamma}{\beta}}}{(1-ae^{-2\alpha})} + \left(\frac{x+\gamma}{\beta} + \frac{2ae^{-2\alpha}}{1-ae^{-2\alpha}}\right)^2 \frac{e^{-\alpha\frac{x+\gamma}{\beta}}}{1-ae^{-2\alpha}}$$

The expressions (A7.1) then immediately follow from S_1 and S_2:

$$S_1 = (x+\gamma)^2 \frac{e^{-\alpha x}}{1-ae^{-2\alpha}} + \frac{4a\beta e^{-\alpha(x+2)}}{(1-ae^{-2\alpha})^2} (x+\gamma+\beta) + \frac{8a^2\beta^2 e^{-\alpha(x+4)}}{(1-ae^{-2\alpha})^3}$$

$$S_2 = (x+\gamma) \frac{e^{-\alpha x}}{1-ae^{-2\alpha}} + \frac{2a\beta e^{-\alpha(x+2)}}{(1-ae^{-2\alpha})^2}$$

Appendix 9. The Computer Program for the Numerical Evaluation of the Fields near an Infinitely Deep Dyke.

In § 5.1.4, the behaviour of the integrands of the expressions in Table 5.2 was briefly mentioned. We saw that the integration could best be carried out by considering several ranges of the variable u, and integrating these separately. It was most convenient to integrate all the expressions on any one range simultaneously, since most of the parametric equations had to be calculated anyway. The total integrals were finally evaluated by summing the sub-integrals from all ranges. The eventual decrease to very minute values of the integrands, together with the known convergence of the integrals, enabled the $u \to \infty$ limit to be replaced with $u = 100$. In most cases, however, the integration cut-off was defined by computer underflow limitations long before this value was reached.

The total number of integration ranges needed was entirely dependent on the value of ϵ. The basic ranges selected were those in Table A9.1, the range number being the parameter used in the computer programming to label the particular range in use.

Table A9.1

Basic Integration Ranges

Range No. J1	u_{max}
1	Point u=0
2	10^{-4}
3	10^{-3}
4	10^{-2}
5	0.3
6	2.0
7	10.0
8	100

For a given value of ε not all of these subdivisions would necessarily be used. For larger values of ε, the subdivisions corresponding to the lower values of J1 would be combined to give one range. At lower values of ε however, it would be necessary to use all the subdivisions. Suppose that ε was within the limits $10^{-n} \leq \varepsilon < 10^{-(n-1)}$. The subdivisions necessary in u would then be $[0,10^{-n}]$, $(10^{-n}, 10^{-(n-1)}]$;.....for $n \leq 4$, subject to the values of u_{max} corresponding to J1 = 5,6.

We clarify this with an example: suppose we have $\varepsilon = 10^{-2}$, so that n = 2. The appropriate integration ranges are then:

$[0,10^{-2}]$;$(10^{-2}, 0.3]$; (0.3,2.0]; (2.0, 10.0]; (10,100] where the square brackets indicate the inclusion of the range limits.

We now define some of the parameters used in the program. Table A9.1 indicates that there were eight ranges of integration possible in the program, and at least five were used no matter what the value of ε. Within each integration range the value of the integration variable u varied from a minimum to a maximum and each range was subdivided into a number of intervals for use in the numerical integration procedure. The following parameters specify these quantities in the program.

NR1: defines the <u>total</u> number of integration ranges used in the whole integration. Its value depends on ε and varies between 5 and 8.

J1: specifies the number of a particular range, on an absolute basis. It ranges from 1 to 8 and is independent of ε.

N(J1): defines the number of integration <u>intervals</u> within the J1'th range.

UMAX(J1): specifies the maximum value of the integration variable u in the J1'th range. UMAX(1) = 0; UMAX(8) = 100.

UMIN(J1): specifies the minimum value of the integration variable u in the J1'th range. UMIN(1) = 0; UMIN(8) = 10.

J11: specifies a particular range, varying contiguously between 1 and NR1, without jumps when any of the middle J1 values are omitted.

These parameters are shown schematically in Fig. A9.1, for the example given above, where $\varepsilon = 10^{-2}$.

There are five input cards necessary for the program used here, the first card selects the number of values of the parameters ε, Q, Y to be used, and specifies whether Y is positive or negative (ie, outside or within the dyke). Card 2 specifies N(J1), the number of intervals in each of the eight ranges J1, card 3 defines UMAX(J1) for each range, and cards 4 and 5 specify the values of Y in each region. The values of ε, Q are built into the program, and may not be arbitrarily selected.

The following program is written in FORTRAN II, the data cards specify $\varepsilon = 0.5, 10^{-1}$. It carries out the following steps:

(i) specifies the total range number NR1 according to the selected value of ε;

(ii) designates the particular ranges of u needed for this value of ε;

(iii) performs the integration over each of these ranges, using the input data to define both the total number of integration points within each range, and the maximum value of u in the range;

(iv) calculates the sum of the integrations over all the ranges, to give the complete integral;

(v) computes the real and imaginary parts of all the fields, and converts to polar form;

(vi) determines the polarization characteristics of the electric field.

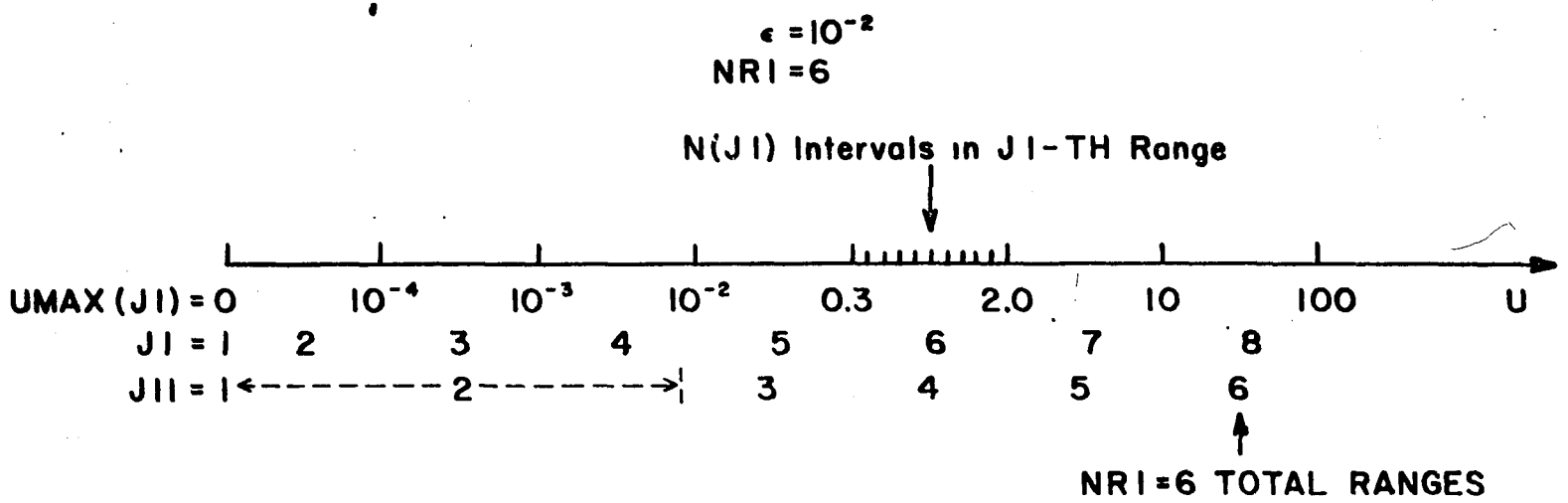

Fig. A9.1 Schematic representation of the numerical integration parameters used in the computer program.

The controls placed on the calculation are:

(i) because the integrands decay to zero rapidly at large u, the computation has a maximum value of u = 100 imposed.

(ii) if the exponential term $e^{-\alpha_j |Y|}$ becomes too small for the computer's underflow limitation, the value of the integrand is taken as zero for the rest of the range and in all succeeding ranges. (The α_j are defined in App. 6, and Table A6.2 indicates the use of the above exponential).

(iii) the terms β_{11} and β_{22} (see App. 6) are calculated in a subroutine from a series expansion, whenever $u \geq 5e$ or $u \geq 5$ respectively.

(iv) ratios of hyperbolic functions are modified to avoid large numbers which essentially cancel out (see App. 6).

```
C
C       WAVE COMPONENT EVALUATION AT SURFACE NEAR OCEANIC RIDGE
C       MKS UNITS AND EXP(-IWT) TIME DEPENDENCE
C
        DIMENSION N(8),UMIN(8),UMAX(8),SOD1(3,4),SEV1(3,4),F(3,4),F0(3,4),
       1FMAX(3,4),FMIN(3,4),TINT(3,4),TRE(3,2),TIM(3,2),
       2PHASE(3,2),XMAG(3,2),IP(8),
       3 Y1(7),Y2(10)
C       INPUT CARD 1 CONTAINS THE FOLLOWING PARAMETERS
C       IP(1) SPECIFIES START OF EP DO LOOP BY DEFINING I10
C       IP(2),IP(3)SPECIFY THE LIMITS OF Q,TO FACILITATE ANY VALUES OF Q
C       IP(4),IP(5)SPECIFY THE NO. OF Y1,Y2 VALUES READ IN
C       IP(6),IP(7) SPECIFY RANGES OF Y
C       IE. 01,01 = Y1 ONLY,02,02 = Y2 ONLY,01,02 = BOTH Y1 AND Y2
C       IP(8) SPECIFIES END OF EP DO LOOP BY DEFINING I20
        READ INPUT TAPE 5,1012,(IP(K10),K10=1,8)
        READ INPUT TAPE 5,1007,(N(I12),I12=1,8)
        READ INPUT TAPE 5,1008,(UMAX(I13),I13=1,8)
        I51=IP(4)
        I52=IP(5)
        READ INPUT TAPE 5,1009,(Y1(I5),I5=1,I51)
        READ INPUT TAPE 5,1010,(Y2(I6),I6=1,I52)
 1012 FORMAT(8I2)
 1007 FORMAT(8I3)
 1008 FORMAT(F3.1,7E6.5)
 1009 FORMAT(7 F4.1)
 1010 FORMAT(10 F4.1)
        RAD=57.295780
C       DOUBLE PRECISION PRELIMINARY SETTINGS
D       A2=0.
D       U=0.
D       G1=0.
D       G2=0.
D       EP=0.
```

```
D       A4=0.
D       AD=1.
        WRITE OUTPUT TAPE 6,1011
 1011 FORMAT(1H1,18X,55HWAVE COMPONENT EVALUATION AT SURFACE NEAR OCEANI
     1C RIDGE/25X,39HMKS UNITS AND EXP(-IWT) TIME DEPENDENCE//12X,65HNEG
     2ATIVE Y SPECIFY VALUES OVER LAND,MEASURED FROM SHORE TO CENTRE/12X
     3,61HPOSITIVE Y SPECIFY VALUES OVER OCEAN,MEASURED AWAY FROM SHORE/
     4//////4X,2HEP,7X,1HQ,8X,1HY,15X,2HEX,20X,2HEY,20X,2HHZ/25X,3(4X,19
     5HMAGNITUDE     PHASE),5X,18HRATIO  INCLINATION)
C
C       PARAMETER LOOPS AND DEFINITIONS
C
C       PARAMETERS USED BELOW MEAN AS FOLLOWS
C       N(J1)=NO.OF INTERVALS IN RANGE J1
C       UMAX(J1)=MAXIMUM U FOR RANGE J1
C       UMIN(J1)=MINIMUM U FOR RANGE J1
C       NR1=TOTAL NO.OF RANGES BEING CONSIDERED FOR THIS PARTICULAR EP
C
C       EP SPECIFICATION
        I10=IP(1)
        I20=IP(8)
        DO 601 I1=I10,I20
        IF(I1-1)111,111,110
  111   EP=0.5
        NR1=5
        GO TO 112
  110   EP=10.**(-I1+1)
        NR1=I1+3
  112   A3=EP**4
        A14=.63366198*(1.-EP*EP)
C       Q SPECIFICATION
        KP1=IP(2)
        KP2=IP(3)
        DO 601 I2=KP1,KP2
```

```
      Q=10.**(I2-3)
C     BASIC PARAMETERS
      A1=.70710678*Q
      A7=4./(Q**3)
      A9=2./(Q*A1)
      A12=1./(Q*1.4142136)
      A13=A12/EP
      A15=Q*Q*A14
      WRITE OUTPUT TAPE 6,2101,EP,Q
 2101 FORMAT(1X,1PE8.0,1X,E8.0)
C     Y SPECIFICATION
      I41=IP(6)
      I42=IP(7)
      DO 601 I4=I41,I42
      GO TO(800,801),I4
C     I3=NO.OF Y VALUES BEING CONSIDERED
C     REGION 1
  800 I3=IP(4)
      M1=1
      M2=2
      GO TO 802
C     REGION 2
  801 I3=IP(5)
      M1=3
      M2=4
  802 DO 601 I7=1,I3
      GO TO(803,804),I4
  803 Y=Y1(I7)
      GO TO 1098
  804 Y=Y2(I7)
C     PRELIMINARY VALUES FOR INTEGRAL SUMMATION
 1098 DO 805 L=1,3
      DO 805 M=M1,M2
  805 TINT(L,M)=0.
```

```
C
C       DO LOOP DEFINING ALL RANGES FOR PARTICULAR EP
C
C       NOTE- J11 HAS MAXIMUM OF NR1
C             J1 HAS MAXIMUM OF 8
C
        KK=0
        DO 602 J11=1,NR1
        IF(J11-1)1,1,2
    1   J1=J11
        GO TO 6
    2   NR2=NR1-4
        GO TO(3,4,5,1),NR2
    3   J1=J11+3
        GO TO 6
    4   J1=J11+2
        GO TO 6
    5   J1=J11+1
    6   N1=N(J1)
C       SPECIFY VALUE OF UMIN
C       CASE 1,U=0,OR IN SECOND RANGE
        IF(J11-2)7,7,8
    7   UMIN(J1)=0.
        GO TO 1102
C       CASE 2,U NOT = 0,AND NOT IN SECOND RANGE
    8   UMIN(J1)=UMAX(J1-1)
C       KK DEFINED =1 IN INTEGRAND CALCULATION IF EXP(-Y α_j) TOO SMALL
 1102   IF(KK)10,10,603
C       INCREMENT OF INTEGRATION H
   10   DN1=N1
        H=(UMAX(J1)-UMIN(J1))/DN1
        H1=.33333333*H
        PRELIMINARY VALUES
        U=UMIN(J1)
```

```
      DO 9 L=1,3
      DO 9 M=M1,M2
      SOD1(L,M)=0.
    9 SEV1(L,M)=0.
C
C     DO LOOP FOR INTEGRANDS FOR EACH U
C
      DO 120 J2=1,N1
  531 U=U+H
C
C     CALCULATION OF INTEGRANDS
C     PARAMETER CALCULATION
C     PARAMETERS COMMON TO ALL INTEGRANDS
      IF(KK)34,34,23
   34 A2=U**4
      A4=U*U
      A5=SQRTF(A2+A3)
D     A6=SQRTF(A2+1.)
      A8=4.*A4/Q
      AL11=SQRTF(A5+A4)
      AL1=A1*AL11
      IF(U)26,26,25
   26 BT11=-EP
      GO TO 188
   25 G1=EP/U
      IF(G1-0.2)19,19,18
D  19 CALL BETA(U,EP,BT)
      BT11=-BT
      GO TO 188
   18 IF(G1-1.0)27,27,28
D  27 BT11=-U*SQRTF(SQRTF(1.+G1**4)-1.)
      GO TO 188
   28 G2=U/EP
D     BT11=-EP*SQRTF(SQRTF(1.+G2**4)-G2*G2)
```

```
  188 BT1=A1*BT11
      AL22=SQRTF(A6+A4)
      AL2=A1*AL22
      GO TO(501,502),I4
  501 IF(Y*AL1+88.)507,507,503
  502 IF(Y*AL2-88.)503,507,507
  507 KK=1
      GO TO 23
  503 IF(U)189,189,190
  189 BT22=-1.
      GO TO 191
  190 IF(U-5.)16,15,15
   15 CALL BETA(U,AD,BT)
      BT22=-BT
      GO TO 191
   16 BT22=-SQRTF(A6-A4)
  191 BT2=A1*BT22
      B1=2.*AL11*AL22
      B2=2.*BT11*BT22
      P3=0.5*(B1-B2)
      Q3=AL11*BT22+AL22*BT11
      IF(2.*AL1-88.)200,201,201
  200 CALL HYPM(AL1,SNHM,CSHM)
      C1=SNHM
      C2=CSHM
      GO TO 202
  201 C1=0.5
      C2=0.5
  202 C3=SINF(BT1)
      C4=COSF(BT1)
      C5=C1*C4
      C6=C2*C3
      C7=C2*C4
      C8=C1*C3
      C9=AL11*C5-BT11*C6
      C10=AL22*C7-BT22*C8
```

```
      C11=BT11*C5+AL11*C6
      C12=BT22*C7+AL22*C8
      R1=C9+C10
      S1=C11+C12
      R2=C9+EP*EP*C10
      S2=C11+EP*EP*C12
      EL5=P3*R1-Q3*S1
      EM5=Q3*R1+P3*S1
      W5=EL5*EL5+EM5*EM5
      W6=A9/W5
C     PARAMETERS PECULIAR TO EACH REGION
      GO TO(21,22),I4
C     REGION TWO PARAMETERS
   22 B6=AL22*AL22
      B7=BT22*BT22
      B8=B6-B7
      P2=AL11*B8-AL22*B2
      Q2=BT22*B1+BT11*B8
      D8=Y*BT2
      D9=COSF(D8)
      D10=SINF(D8)
      EN2=D9*C5+D10*C6
      T2=D9*C6-D10*C5
      EL2=P2*R1-Q2*S1
      EM2=Q2*R1+P2*S1
      EL4=P2*R2-Q2*S2
      EM4=Q2*R2+P2*S2
      W2=EL2*EL2+EM2*EM2
      W4=EL4*EL4+EM4*EM4
      W20=Y*AL2
      W21=EXPF(-W20)
      W22=(A7/W2)*W21
      W23=(A8/W4)*W21
      W24=W6*W21
```

```
      GO TO 23
C     REGION ONE PARAMETERS
   21 R3=AL11*AL11
      R4=BT11*BT11
      B5=B3-B4
      P1=AL22*B5-AL11*B2
      Q1=BT11*B1+BT22*B5
      D1=Y+1.
      D2=D1*AL1
      D3=D1*BT1
      IF(2.*D2-88.)203,204,204
  203 CALL HYPM(D2,SNHM,CSHM)
      D4=CSHM
      D5=SNHM
      GO TO 205
  204 D4=0.5
      D5=0.5
  205 D6=COSF(D3)
      D7=SINF(D3)
      EN1=D4*D6
      T1=D5*D7
      EL1=P1*R1-Q1*S1
      EM1=Q1*R1+P1*S1
      EN3=D5*D6
      T3=D4*D7
      EL3=P1*R2-Q1*S2
      EM3=Q1*R2+P1*S2
      W1=EL1*EL1+EM1*EM1
      W3=EL3*EL3+EM3*EM3
      W10=-Y*AL1
      W11=EXPF(-W10)
      W12=(A7/W1)*W11
      W13=(A8/W3)*W11
      W14=W6*W11
```

```
C       SPECIFICATION OF INTEGRAND TYPE
C       SPECIFICATION OF INTEGRAND REGION
   23 DO 120 L=1,3
      DO 120 M=M1,M2
      KK1=KK+1
      GO TO(509,508),KK1
  508 F(L,M)=0.
      GO TO 30
C       CALCULATION OF INTEGRANDS
  509 GO TO(41,42),I4
C       REGION TWO INTEGRANDS
   42 GO TO(75,85,95),L
   75 GO TO(96,96,77,78),M
   77 F(1,3)=W22*(EN2*EL2+EM2*T2)
      GO TO 30
   78 F(1,4)=W22*(EL2*T2-EM2*EN2)
      GO TO 30
   85 GO TO(96,96,87,88),M
   87 F(2,3)=W23*(EN2*EL4+EM4*T2)
      GO TO 30
   88 F(2,4)=W23*(EL4*T2-EM4*EN2)
      GO TO 30
   95 GO TO(96,96,97,98),M
   96 WRITE OUTPUT TAPE 6,100
      GO TO 30
   97 F(3,3)=W24*(EN2*EL5+EM5*T2)
      GO TO 30
   98 F(3,4)=W24*(EL5*T2-EM5*EN2)
      GO TO 30
  100 FORMAT(1X,5HERROR)
C       REGION ONE INTEGRANDS
   41 GO TO(70,80,90),L
   70 GO TO (71,72,96,96),M
   71 F(1,1)=W12*(EN1*EL1+EM1*T1)
```

```
      GO TO 30
   72 F(1,2)=W12*(EL1*T1-EM1*EN1)
      GO TO 30
   80 GO TO(81,82,96,96),M
   81 F(2,1)=W13*(EN1*EL3+EM3*T1)
      GO TO 30
   82 F(2,2)=W13*(EL3*T1-EM3*EN1)
      GO TO 30
   90 GO TO(91,92,96,96),M
   91 F(3,1)=W14*(EN3*EL5+EM5*T3)
      GO TO 30
   92 F(3,2)=W14*(EL5*T3-EM5*EN3)
C     END INTEGRANDS CALCULATION
C
C     ORDINATE LABELLING FOR SIMPSONS INTEGRATION FORMULA
C
   30 IF(J11-1)43,43,44
   43 F0(L,M)=F(L,M)
      GO TO 20
   44 IF(J2-N1)45,46,46
   46 FMAX(L,M)=F(L,M)
      GO TO 20
   45 IF(J11-2)47,47,48
   47 FMIN(L,M)=F0(L,M)
      GO TO 49
   48 FMIN(L,M)=FMAX(L,M)
   49 TT1=(-1.)**J2
      IF(TT1)50,51,51
   50 SOD1(L,M)=SOD1(L,M)+F(L,M)
      GO TO 20
   51 SEV1(L,M)=SEV1(L,M)+F(L,M)
   20 ZZZ=0.
  120 CONTINUE
C
```

```
C       SIMPSONS RULE INTEGRALS FOR EACH RANGE
C
        IF(J11-1)603,603,534
  534   DO 600 L=1,3
        DO 600 M=M1,M2
        FR=FMIN(L,M)+FMAX(L,M)
        SINT1=H1*(FR+2.*SEV1(L,M)+4.*SOD1(L,M))
        TINT(L,M)=TINT(L,M)+SINT1
  600   ZZZ=0.
  603   CONTINUE
  602   CONTINUE
C
C       REAL AND IMAGINARY PARTS OF EACH COMPONENT
C
        GO TO(701,702),I4
C       REGION 1
  701   TRE(1,1)=A13+A15*TINT(1,1)
        TIM(1,1)=-A13+A15*TINT(1,2)
        TRE(2,1)=-A13-A14*TINT(2,2)
        TIM(2,1)=A13+A14*TINT(2,1)
        TRE(3,1)=-A15*TINT(3,2)
        TIM(3,1)=A15*TINT(3,1)
        GO TO 710
C       REGION 2
  702   TRE(1,2)=A12-A15*TINT(1,3)
        TIM(1,2)=-A12-A15*TINT(1,4)
        TRE(2,2)=-A12+A14*TINT(2,4)
        TIM(2,2)=A12-A14*TINT(2,3)
        TRE(3,2)=-A15*TINT(3,4)
        TIM(3,2)=A15*TINT(3,3)
C       CONVERSION TO POLAR COORDINATES
  710   DO 703 L=1,3
        VX=TRE(L,I4)
        VY=TIM(L,I4)
```

```
      XMAG(L,I4)=RANGE(VX,VY)
      PHASE(L,I4)=RAD*ARG(VY,VX)
  703 CONTINUE
C     SPECIFICATION OF POLARIZATION OF TOTAL E COMPONENT
C     (ASSUMING A=B IN HORIZONTAL H COMPONENT AT Z=0)
      GG1=XMAG(1,I4)
      GG2=XMAG(2,I4)
      PHI=(PHASE(2,I4)-PHASE(1,I4))*.01745329
      CALL POLZN(GG1,GG2,PHI,RATIO,XINC)
      GO TO(704,705),I4
  704 WRITE OUTPUT TAPE 6,1704,Y,(XMAG(L,1),PHASE(L,1),L=1,3),RATIO,
     1XINC
      GO TO 706
  705 WRITE OUTPUT TAPE 6,1704,Y,(XMAG(L,2),PHASE(L,2),L=1,3),RATIO,
     2XINC
 1704 FORMAT(21X,F5.1,3(2X,  E12.5,2X,  F6.1),3X,F9.6,3X,F6.1)
  706 CONTINUE
  601 CONTINUE
      CALL EXIT
      END
      SUBROUTINE BETA(U,XX,BT)
D     RT2IN=.7071067811865 48
D     C10=.078125
D     C11=.0546875
D     C12=.0205078125
D     A10=XX/U
D     A11=XX*A10*RT2IN
      DO 400 LL=1,5
      LL1=4*LL
      AA=LL1
      BB=AA*(LOGF(XX)-LOGF(U))
      IF(BB+88.)402,402,401
D 402 AB=0.
      GO TO 403
```

```
D 401 AB=A10**LL1
  403 GO TO(404,405,406,407,408),LL
D 404 A12=AB
      GO TO 400
D 405 A13=AB
      GO TO 400
D 406 A14=AB
      GO TO 400
D 407 A15=AB
      GO TO 400
D 408 A16=AB
  400 CONTINUE
D     BT=A11*SQRTF(1.-.25*A12+.125*A13-C10*A14+C11*A15-C12*A16)
D     RETURN
      END
      SUB ROUTINE HYPM(X,SNHM,CSHM)
      EX=EXPF(-2.*X)
      SNHM=0.5*(1.-EX)
      CSHM=0.5*(1.+EX)
      RETURN
      END
      FUNCTION RANGE(X,Y)
C     COMPUTATION OF MAGNITUDE OF Z=X+IY WITH REDUCED CHANCE OF
C     UNDERFLOW OR OVERFLOW
      T0=1.0E-19
      IF(ABSF(X)-ABSF(Y))2,2,1
    1 T1=X
      T2=Y/T1
      GO TO 3
    2 T1=Y
      T2=X/T1
    3 IF(ABSF(T2)-T0)4,4,5
    4 RANGE=ABSF(T1)
      GO TO 6
```

```
     5 RANGE=ABSF(T1)*SQRTF(1.+T2*T2)
     6 RETURN
       END
       FUNCTION ARG(Y,X)
C      COMPUTATION OF ARTAN(Y/X) WITHIN (-PI,+PI)
C      DEFINE ARTAN 0/0 =0.
C      RESULT =0.OR PI IF Y=0.
       PI=3.1415927
       IF(Y)5,1,5
     1 IF(X)2,3,3
     2 ARG=PI
       GO TO 30
     3 ARG=0.
       GO TO 30
C      RESULT = -PI/2 OR +PI/2 IF ABS(Y/X) GREATER THAN 10**F,WHERE
C      F IS MACHINES LIMITING EXPONENT
C      TRICK.IF X+Y=Y ON COMPUTER,THEN Y IS MUCH GREATER THAN X
     5 IF((Y+X)-Y)10,6,10
C      SET SIGN OF RESULT = SIGN OF Y
     6 IF(Y)7,7,8
     7 ARG=-1.5707963
       GO TO 30
     8 ARG=1.5707963
       GO TO 30
    10 ARG=ATANF(Y/X)
C      RESULT IN  1ST OR 4TH QUADRANT IF X GREATER THAN 0
       IF(X)11,11,30
C      RESULT IN 2ND OR 3RD QUADRANT IF X LESS THAN 0
    11 IF(Y)12,12,13
    12 ARG=ARG-PI
       GO TO 30
    13 ARG=ARG+PI
    30 RETURN
       END
```

```
C
C       DETERMINE POLARIZATION OF ELECTRIC FIELD
C
        SUBROUTINE POLZN (GG1,GG2,PHI,RATIO,XINC)
C       DETERMINES RATIO OF AXES AND INCLINATION OF MAJOR AXIS TO POSITIVE
C       X DIRECTION FOR POLARIZATION ELLIPSE OF E COMPONENTS
C       RATIO = MINOR AXIS/MAJOR AXIS
C       G=GAMMA
C
C       IF G=INFINITY,THEN RATIO=0,XINC=90,LINEAR POLARIZATION AT 90
C       (LINEAR POLARIZATION ALSO OCCURS FOR G=0,AT ANGLE 0
C               AND FOR DEL=+OR-90,+OR-270,AT ANGLE=XINC)
C
        PI2=0.63661977
        DEL=-PHI
        IF((GG1+GG2)-GG2)1,2,1
    2   RATIO=0.
        XINC=90.
        GO TO 14
    1   G=GG2/GG1
        G2=G*G
C
C       WHEN G=1,AND DEL=0,+OR-180,+OR-360,THEN RATIO=1,AND
C       XINC INDETERMINATE...CIRCULAR POLARIZATION,XINC=999
C       WHEN G=1,AND DEL=+OR-90,+OR-270,THEN RATIO=0,AND
C            XINC=+45 IF DEL=-90 OR +270
C                 -45 IF DEL=+90 OR -270
C
C       USE G*G AS CRITERION
        IF(G2-1.)3,4,3
    4   ADEL=DEL*PI2
        DO 100 ND=1,9
        DN=ND
        IF(ABS(ADEL+5.-DN)-1.E-05)6,6,60
```

```
   60 IF(ADEL+5.-DN)5,6,100
    6 GO TO(7,8,7,9,7,8,7,9,7),ND
C
C      CIRCULAR POLARIZATION
    7 RATIO=1.
      XINC=999.
      GO TO 14
C
C      LINEAR POLARIZATION AT -45
    8 RATIO=0.
      XINC=-45.
      GO TO 14
C
C      LINEAR POLARIZATION AT +45
    9 RATIO=0.
      XINC=+45.
      GO TO 14
C
C      WHEN G=1,DEL NOT=+OR- N*PI/2,THEN ELLIPTIC POLARIZATION AT +OR-45
C      NOTE..STILL NEED RATIO CALCULATION
C
    5 GO TO(3,11,11,12,12,11,11,12,12),ND
C
C      DEL=(-360,-180)OR(0,180),THEN POLARIZATION AT +45
   11 XINC=+45.
      GO TO 13
C
C      DEL=(-180,0)OR(180,360),THEN POLARIZATION AT -45
   12 XINC=-45.
      GO TO 13
  100 CONTINUE
C
C      NON SPECIAL DENOMINATORS
    3 VX=1.-G2
```

```
      VY=2.*G*SIN(DEL)
      XINC=ATAN2(VY,VX)*28.647690
   13 R=(SQRT((1.-G2)**2+4.*G2*((SIN(DEL))**2)))/(1.+G2+2.*G*COS(DEL))
      RATIO=ABS((1.-R)/(1.+R))
   14 RETURN
      END
```

```
*      DATA
01010607100102O2
0010160320320640320640320
0.0.1E-03.1E-02.1E-01.3E-00.2E+01.1E+02.1E+03
-1.0-0.7-0.5-0.3-0.2-0.1-0.0
00.000.100.200.300.500.701.002.005.010.0
```

Appendix 10. The Computer Program for the Numerical Evaluation of the Fields Near an Inclined Fault.

The program uses four input cards, specifying the conductivity ratio ($FF=\epsilon^2$), angle of inclination α in degrees (=ALP), and the distance Y_2(=YY). The first card specifies the number of values of each parameter used as input on cards 2 to 4.

The program itself is a straightforward calculation of the relations of Table 6.4, with subroutines to determine (a) the coefficients a_p, b_p (AB), (b) D_E and D_H in case (i) (FLSA) and case (ii) (FGSA) of Table 6.4 and (c) the polarization of the electric field (POLZN) by the method described in App. 1.

The program is written in FORTRAN IV, making use of the complex arithmetic facility of this language. The only difference from the equations of Table 6.4 is that the $\sqrt{-i}$ factor of the E_x and E_y relations is omitted (essentially absorbing it onto the left hand side of these relations). The phases thus represent Arg (E/E_∞), instead of Arg $(E_j/H_{k\infty})$ as calculated for the other models of this study. This computational difference has been adjusted in plotting the results in Figs. 6.8 - 6.9.

The limiting cases, as ϵ becomes very small, were checked by recomputing the calculations of Berdichevskii (1961), with $\epsilon = 0$. The values of the coefficients a_p, b_p are assigned in statement 4 of the main program, when $F = \epsilon^2 = 0$. This short-cuts the computation by avoiding the subroutines AB, FLSA, and FGSA.

```
C
C       FIELD COMPONENTS OVER INCLINED OCEAN BED
C       MKS UNITS AND EXP(-IWT) TIME DEPENDENCE
C
        DIMENSION FF(10),ALP(10),YY(20),XMAG(4),PHASE(4)
        COMPLEX Z,Z1,S1,S2,S3,E1,EY,EY1,EY2,AP,BP,FX(4),DX
        COMMON F,ALPHA,Z,P,SA,AP,BP
C       INPUT CARD 1 SPECIFIES LIMITS TO NUMBERS OF FF,ALP,YY VALUES USED
C       INPUT CARD 2 CONTAINS RATIOS OF CONDUCTIVITY,FF
C       INPUT CARD 3 CONTAINS ANGLES OF INCLINATION ,ALPHA,IN DEGREES
C       INPUT CARD 4 CONTAINS DISTANCES FROM SURFACE CONJUNCTION,YY,
C                      IN UNITS PROPORTIONAL TO PENETRATION DEPTH
        READ(1,500)NF,NA,NY
        READ(1,501)(FF(J1),J1=1,NF)
        READ(1,502)(ALP(J2),J2=1,NA)
        READ(1,503)(YY(J3),J3=1,NY)
C
        WRITE(3,1001)
C
C       LOOPS SPECIFYING SUCCESSIVE VALUES OF F,ALPHA,Y RESPECTIVELY
C
        DO 101 JF=1,NF
        F=FF(JF)
        DO 101 JA=1,NA
        ALPHA=ALP(JA)*.017453292
        WRITE(3,1002)F,ALP(JA)
        DO 101 JY=1,NY
        Y=YY(JY)
C
C       PRELIMINARY CONSTANTS, VARIABLES
C
        Z=(0.0,1.0)
        Z1=(.70710678,-.70710678)
        PI2=1.5707963
```

```
      RAD=57.295780
      SA=SIN(ALPHA)
      N=(90./ALP(JA))-1.
C
CC    TEST N EVEN OR ODD
C
      IF(MOD(N,2))1,1,2
C     N EVEN.GO TO 1
C     N ODD. GO TO 2
    1 M=N/2
      GO TO 3
    2 M=(N-1)/2
    3 S1=(0.0,0.0)
      S2=(0.0,0.0)
      S3=(0.0,0.0)
C
CC    SUMMATION LOOP
C
      DO 100 M1=1,M
      P=M1
      P2=P*P
      A1=2.*P*ALPHA
      A2=2.*A1
      B1=COS(A1)
      B2=SIN(A2)
      B3=SIN(A1)
      E1=CEXP(-Z*A1*P)
      EY=CEXP(-Z1*B3*Y)
      EY1=E1*B2*EY
      EY2=B1*EY
C
CC    DETERMINE COEFFICIENTS
C
      IF(F)4,4,5
```

```
    4 AP=(-1.)**M1
      BP=CEXP(-2.*Z*P2*ALPHA)
      GO TO 6
    5 CALL AB
C
C       CALCULATE SUMS
C
    6 S1=S1+BP*E1*EY2
      S2=S2+((-1.)**M1)*AP*EY2
      S3=S3+BP*EY1
  100 CONTINUE
C
C       CALCULATE FIELD COMPONENTS
C
      FX(1)=1.+2.*S1
      FX(2)=1.+2.*S2
      FX(3)=1.-Z*S3
      FX(4)=-S3
C
C       CALCULATE MAGNITUDE,PHASE OF EACH COMPONENT
C
      DO 10 I=1,4
      DX=FX(I)
      XMAG(I)=CABS(DX)
      PHASE(I)=ATAN2(AIMAG(DX),REAL(DX))*RAD
   10 CONTINUE
C
C       CALCULATE POLARIZATION ELLIPSE OF ELECTRIC FIELD
C       RATIO=MINOR AXIS/MAJOR AXIS
C       XINC =INCLINATION OF MAJOR AXIS TO X-AXIS
C       GG1=EX
C       GG2=EY
C       PHI=PHASE(EY)-PHASE(EX) IN RADIANS
C
```

```
      GG1=XMAG(1)
      GG2=XMAG(2)
      PHI=(PHASE(2)-PHASE(1))*.017453292
      CALL POLZN(GG1,GG2,PHI,RATIO,XINC)
      WRITE(3,1000)Y,(XMAG(I),PHASE(I),I=1,4),RATIO,XINC
  101 CONTINUE
 1001 FORMAT(1H1,28X,54HSURFACE FIELD COMPONENTS OVER OCEAN WITH INCLINE
     1D BASE/35X,39HMKS UNITS AND EXP(-IWT) TIME DEPENDENCE///////1X,17H
     2RT.COND. SLOPE  Y,13X,2HEX,19X,2HEY,19X,2HHY,19X,2HHZ,11X,4HAXES,3
     3X,4HINCL/2X,5HRATIO,3X,5HALPHA,4X,4(7X,3HMAG,6X,5HPHASE),4X,5HRATI
     40,2X,5HANGLE)
 1000 FORMAT(14X,F6.2,4(3X,E10.3,2X,F6.1),3X,F6.3,1X,F6.1)
 1002 FORMAT(2X,E8.1,1X,F4.0)
  500 FORMAT(3I2)
  501 FORMAT(10E8.1)
  502 FORMAT(10F5.1)
  503 FORMAT(16F5.1)
      END
C
C     CALCULATION OF COEFFICIENTS A(P),B(P)
C
      SUBROUTINE AB
      COMPLEX Z,DH,DE,AP,BP
      COMMON F,ALPHA,Z,P,SA,AP,BP
      F2=F*F
      NP=P
C
C     PRELIMINARIES FOR D MULTIPLICATION
C
      AP=(1.0,0.0)
      BP=(1.0,0.0)
C
C     CALCULATE EACH D PRIOR TO MULTIPLICATION
C
```

```
      DO 100 NS=1,NP
C
C     DIRECT TO CALL FOR D,DEPENDING ON F/SIN(ALPHA)
C
      IF(F-SA)1,1,2
    1 CALL FLSA(NS,F2,DE,DH)
      GO TO 3
    2 CALL FGSA(NS,F2,DE,DH)
    3 AP=AP*DH
      BP=BP*DE
  100 CONTINUE
      RETURN
      END
C
C     CALCULATION OF DE,DH WHEN F LESS THAN SIN(ALPHA) OR SIN(2S-1)ALPHA
C
      SUBROUTINE FLSA(NS,F2,DE,DH)
      COMPLEX DH,DE,Z
      COMMON F,ALPHA,Z
      S=NS
      SA2=(2.*S-1.)*ALPHA
      T=SIN(SA2)
      T2=COS(SA2)
      X=(SQRT(T*T-F2))/(F*T2)
      X2=(X*X)+1.
      DH=(-1.+2./X2)-(Z*2.*X/X2)
      V=F/T
      PHI=ATAN2(T*SQRT(1.-V*V),T2)
      DE=CEXP(-2.*Z*PHI)
      RETURN
      END
C
C     CALCULATION OF DE,DH WHEN F GREATER THAN SIN(ALPHA)
C
```

```
      SUBROUTINE FGSA(NS,F2,DE,DH)
      COMPLEX Z,DE,DH
      COMMON F,ALPHA,Z
      S=NS
      SA2=(2.*S-1.)*ALPHA
      T=SIN(SA2)
      T2=COS(SA2)
C     TEST SIZES OF F AND SIN(2S-1)ALPHA
      IF(F-T)1,1,2
    1 CALL FLSA(NS,F2,DE,DH)
      GO TO 3
    2 X=(SQRT(F2-T*T))/(F*T2)
      DH=-1.+2./(1.+X)
      V=F/T
      TF=(T/T2)*SQRT(V*V-1.)
      DE=-1.+2./(1.+TF)
    3 RETURN
      END
```

```
C
C       DETERMINE POLARIZATION OF ELECTRIC FIELD
C
        SUBROUTINE POLZN (GG1,GG2,PHI,RATIO,XINC)
C       DETERMINES RATIO OF AXES AND INCLINATION OF MAJOR AXIS TO POSITIVE
C       X DIRECTION FOR POLARIZATION ELLIPSE OF E COMPONENTS
C       RATIO = MINOR AXIS/MAJOR AXIS
C       G=GAMMA
C
C       IF G=INFINITY,THEN RATIO=0,XINC=90,LINEAR POLARIZATION AT 90
C       (LINEAR POLARIZATION ALSO OCCURS FOR G=0,AT ANGLE 0
C               AND FOR DEL=+OR-90,+OR-270,AT ANGLE=XINC)
C
        PI2=0.63661977
        DEL=-PHI
        IF((GG1+GG2)-GG2)1,2,1
    2   RATIO=0.
        XINC=90.
        GO TO 14
    1   G=GG2/GG1
        G2=G*G
C
C       WHEN G=1,AND DEL=0,+OR-180,+OR-360,THEN RATIO=1,AND
C       XINC INDETERMINATE...CIRCULAR POLARIZATION,XINC=999
C       WHEN G=1,AND DEL=+OR-90,+OR-270,THEN RATIO=0,AND
C            XINC=+45 IF DEL=-90 OR +270
C                 -45 IF DEL=+90 OR -270
C
C       USE G*G AS CRITERION
        IF(G2-1.)3,4,3
    4   ADEL=DEL*PI2
        DO 100 ND=1,9
        DN=ND
        IF(ABS(ADEL+5.-DN)-1.E-05)6,6,60
```

```
   60 IF(ADEL+5.-DN)5,6,100
    6 GO TO(7,8,7,9,7,8,7,9,7),ND
C
C      CIRCULAR POLARIZATION
    7 RATIO=1.
      XINC=999.
      GO TO 14
C
C      LINEAR POLARIZATION AT -45
    8 RATIO=0.
      XINC=-45.
      GO TO 14
C
C      LINEAR POLARIZATION AT +45
    9 RATIO=0.
      XINC=+45.
      GO TO 14
C
C      WHEN G=1,DEL NOT=+OR- N*PI/2,THEN ELLIPTIC POLARIZATION AT +OR-45
C      NOTE..STILL NEED RATIO CALCULATION
C
    5 GO TO(3,11,11,12,12,11,11,12,12),ND
C
C      DEL=(-360,-180)OR(0,180),THEN POLARIZATION AT +45
   11 XINC=+45.
      GO TO 13
C
C      DEL=(-180,0)OR(180,360),THEN POLARIZATION AT -45
   12 XINC=-45.
      GO TO 13
  100 CONTINUE
C
C      NON SPECIAL DENOMINATORS
    3 VX=1.-G2
```

```
      VY=2.*G*SIN(DEL)
      XINC=ATAN2(VY,VX)*28.647690
   13 R=(SQRT((1.-G2)**2+4.*G2*((SIN(DEL))**2)))/(1.+G2+2.*G*COS(DEL))
      RATIO=ABS((1.-R)/(1.+R))
   14 RETURN
      END
```